1975

The electronic spectra of organic mixed crystals, azulene and the azaazulenes

Francis Patrick Burke
Iowa State University

The electronic spectra of organic mixed crystals: Azulene and the azaazulenes

by

Francis Patrick Burke

A Dissertation Submitted to the
Graduate Faculty in Partial Fulfillment of
The Requirements of the Degree of
DOCTOR OF PHILOSOPHY

Department: Chemistry
Major: Physical Chemistry

Approved:

Signature was redacted for privacy.

In Charge of Major Work

Signature was redacted for privacy.

For the Major Department

For the Graduate College

Iowa State University
Ames, Iowa

1975

TABLE OF CONTENTS

LIST OF TABLES

LIST OF FIGURES

PART I. THE ELECTRONIC SPECTRA OF 1,3-DIAZAAZULENE AND 2-PHENYL-1,3-DIAZAAZULENE

INTRODUCTION

The impetus for studying the electronic spectroscopy of the nitrogen heterocycles of azulene, the azaazulenes, derives from the unusual radiative and vibronic absorption properties of the parent, azulene. As early as 1955,[1] it was recognized that azulene violates Kasha's rule[2] by fluorescing readily from its second excited singlet state (S_2). Later work by Sidman and McClure[3] who obtained the low temperature mixed crystal spectrum of azulene in naphthalene, demonstrated two other important features of azulene's electronic states. First, they observed that the absorption spectrum of S_2 exhibits band widths which are less than those of the first excited singlet (S_1), in contrast to the usual situation in which the higher excited states of aromatic molecules exhibit diffuse absorption spectra. Secondly, they recognized that, while the analysis of the first absorption system is relatively straight forward in terms of progressions and combinations of vibrational fundamentals, the second absorption system is remarkably complex. In fact, of the 150 S_2 absorption bands which they report, only 40 are assigned with confidence. The subsequent literature on azulene is extensive, but the interpretations[4-8] of the above mentioned phenomena are predicted on a weak vibronic interaction between the 7000Å (S_1) and 3500Å (S_2) states, and a strong vibronic interaction between S_2 and the higher excited states.

The question of the nature and strength of vibronic interactions among azulene's electronic states is an important one. Lacey[9] and Lacey et al.[10] have made the most detailed study of azulene to date and have elucidated a number of important coupling mechanisms for azulene's 3500Å state. Three of these are of principal interest and are discussed below: intensity borrowing, moving levels, and vibronic Fermi resonance. The last two are both manifest through changes in vibronic frequencies between the ground and excited states, and through a medium dependence of the vibronic energies. Their importance in the azulene 3500Å spectrum may very well derive from the first, intensity borrowing. That is, as much as eighty percent of the intensity of the 3500Å transition is the result of vibronic coupling, an induced oscillator strength of 0.04.[9] Not only is this a large percentage of the total oscillator strength, but the absolute magnitude is characteristic of a moderately strong transition. It is reasonable to assume that whatever vibronic effects are responsible for the complexity of the azulene spectra are present in other molecules, but to a sufficiently lesser degree that they are usually ignored. It is the dominant status of these effects in the azulene spectra that make it such an important and interesting molecule.

In this context we undertook the study of the electronic spectra of the nitrogen heterocycles of azulene, the azaazulenes. The work to be reported in this thesis is mainly

concerned with two of diazaazulenes (cycloheptimidazoles): 1,3-diazaazulene (Figure 1) and 2-phenyl-1,3-diazaazulene. To understand the rationale behind a study of the azaazulenes it is necessary to consider the excited states of azulene, and the kinetic parameters[11,12] which define the decay routes of these states (Figure 1). The usual explanation of the azulene phenomena asserts that the weak vibronic interaction between S_2 and S_1 leads to a radiative lifetime of S_2 comparable to its nonradiative decay rate, making S_2 capable of fluorescence. The nonradiative depletion of S_1 is quite fast, resulting in the observed low quantum yield of fluorescence from S_1. The object of obtaining the electronic spectra of the diazaazulenes was to observe the effect of an $n\pi^*$ state, presumably lying between the S_1 and S_2 $\pi\pi^*$ states of azulene, on the vibronic interactions and radiative properties of those states. Previous studies of $n\pi^*$ transitions[13-15] had shown them to be weak, certain of them low lying in energy, and with the ability to couple quite effectively with the $\pi\pi^*$ states. In addition they did not in general appear to effect major alterations in the $\pi\pi^*$ transition energies. The inclusion of a new electronic state between S_1 and S_2 of azulene might lead to a fast nonradiative decay of S_2 and a consequent decrease in the quantum yield of fluorescence. In addition, the S_1 and S_2 absorption spectra would be interesting to compare to those of azulene in terms of changes in the vibronic effects. A further listing of these preliminary

assumptions concerning the electronic spectra of the azaazulenes is not germane, since the work reported below will show that while correlations between azulene and the azaazulenes exist, it is those features which set them apart which have proven to be the most interesting.

The research reported in this thesis has been divided into three parts, the first of which concerns inself with the analysis of the electronic and vibrational spectra of the two diazaazulenes studied. Absorption and emission spectra are presented for these molecules in a variety of crystal hosts, and attention is directed toward assignment of the electronic state spatial symmetries and intensities, and of the fundamental vibrational frequencies in the ground and excited states. The effects of vibronic coupling in these spectra will be described, particularly in regard to the change in vibrational frequencies between the ground and excited states. Wherever possible, quantitative information concerning spectral parameters will be presented. In particular, an attempt will be made to provide accurate band intensity data. The two pieces of raw data that a spectrum provides are band positions and band intensities, and too often in reading the literature one discovers that highly precise transition energies are tabulated with intensities given as "weak", "medium" or "strong".

The second part of this thesis will contain the results of the electric field (Stark) spectra of diazaazulene in two

mixed crystal hosts, naphthalene and quinazoline. The Stark spectra of a guest molecule in a mixed crystal allow one to calculate the change in dipole moment between the ground state and those excited states exhibiting sharp line vibronic spectra. These results will show that the dipole moment of a vibronically coupled excited state differs measurably from that presumed within the Condon approximation.

In the third part of this thesis, we will consider the effects of the quadratic electron-phonon coupling in molecular mixed crystals. That is, an absorption or emission band of a molecular impurity has a finite band width, which is the sum of two contributions. The first is an inhomogeneous (Gaussian) component arising from minute variations of the guest substitution, and the second is the homogeneous (Lorentzian) lifetime broadening. At low temperatures (4.2°K), the contribution of the inhomogeneous broadening is usually dominant. Typical band widths of sharp vibronic spectra are 1-3 cm^{-1}, and the lifetime contribution for a state with a radiative lifetime of 10^{-9} sec is .005 cm^{-1}. If the temperature of the mixed crystal is increased an additional (nonlifetime) homogeneous broadening mechanism becomes important, accompanied by a shift in transition energy. In the low temperature limit, where thermal population of the molecular vibrational levels is negligible, these phenomena are the result of the interaction between the electronic

transition and the motion of the lattice. This effect, the quadratic electron-phonon coupling, has been investigated for a number of inorganic mixed crystal systems[16-18] but not previously for molecular mixed crystals. Results are presented which describe the dependence of the electron-phonon coupling on the final vibron level of the transition, the analogy of the gas phase vibrational-rotational coupling. Results are also presented for a system which exhibits twelve energetically inequivalent guest substitution sites[19] to determine the effect of the lattice site on the quadratic electron-phonon coupling.

EXPERIMENTAL

Sample Preparation and Crystal Growth

Typical guest concentrations in mixed crystals are on the order of 10^{-4}-10^{-3} mole/mole, and the host purity must be correspondingly high. For this reason, considerable effort in the sample preparation is directed toward purifying the host material. By far the most ubiquitous technique is zone-refining, and the hosts p-terphenyl, biphenyl, dibenzyl and p-dichlorobenzene, were all purified in this manner. Naphthalene was purified by fusion with potassium followed by vacuum sublimation and zone-refining. This process was carried out in an apparatus specially designed so that the naphthalene was never exposed to the atmosphere. Quinazoline was purified by repeated vacuum sublimations (at least three). All of these host materials were obtained from Aldrich Chemicals.

Purification of all guest material was accomplished by vacuum sublimation. 1,3-Diazaazulene was synthesized by the method of Nozoe and coworkers.[20] 2-Phenyl-1,3-diazaazulene and 2-phenylmonoazaazulene were the gift of Dr. Yukichi Kishida, Sankyo Co. Ltd., Tokyo. Azulene was obtained commercially from Aldrich Chemicals.

Mixed crystals were grown under vacuum from the melt in a Bridgman furnace. The sample material was melted into a glass tube symmetrically constricted so that a seed crystal could be formed at the bottom. When a stable liquid-solid

junction had formed, the crystal tube was lowered through a temperature gradient, with crystal growth occurring vertically up the tube. In this manner mixed crystal ingots one centimeter in diameter and two to three centimeters long were obtained. Guest concentrations were adjusted in the range 10^{-3} to 10^{-4} mole/mole so that a crystal section of two to three millimeter thickness would yield absorption bands with an optical density of about 0.5.

The melt grown ingots were removed from the crystal growth tubes and ab and bc' sections cut from them. The faces were identified conoscopically[21] using the optical crystallographic data of Winchell.[22] Since, with the possible exception of quinazoline, these host materials all exhibit monoclinic unit cells, only the ab and bc' faces are suitable for polarization measurements. In the case of quinazoline, for which a crystal structure has not been determined, melt grown ingots exhibited a prominent cleavage plane parallel to the direction of growth. Examination of this section under the polarizing microscope gave extinction directions parallel and perpendicular to the growth direction. These directions were given the appellations "z" and "x", respectively. The mutually perpendicular direction was called "y", and their convention has been maintained throughout this thesis. The spectra of quinazoline host crystals reported in this thesis were taken using the xz and yz faces.

The utility of the mixed crystal technique lies in the fact that the orientation of the host, and consequently guest molecule axes is known with respect to some laboratory frame of reference. This is predicted on an assumption of perfect guest-host substitution, an assumption which has been justified for many systems. The orientation of the host (guest) molecular axes is usually tabulated as the projection which they make on the unit cell axes. For the host crystals used in this work, these are the projections of the long (L), medium(M) and normal (N) axes on the a, b, and c' unit cell directions. These values, which are usually called the squared direction cosines, are given below.

Naphthalene[23,24]

	L	M	N
a	0.192	0.103	0.705
b	0.044	0.760	0.196
c'	0.764	0.137	0.099

p-Terphenyl[25,26]

	L	M	N
a	.088	.286	.629
b	0	.690	.310
c'	.912	.024	.061

Dibenzyl[19,27,28]

	L	M	N
a	.503	.274	.230
b	.058	.664	.275
c'	.438	.063	.497

Biphenyl[29,30]

	L	M	N
a	.092	.265	.638
b	0	.702	.299
c'	.908	.030	.063

p-Dichlorobenzene[31]

	L	M	N
a	.62	.19	.18
b	.37	.36	.26
c'	.01	.44	.56

The definitions of long, medium and normal axes for these host materials, with the exception of dibenzyl, are intuitively obvious. For dibenzyl, the long axis was taken to be parallel to a line from the connected ring carbon through the ring carbon para to it.

A few comments about the use of direction cosines in predicting polarization ratios seem germane. For the mixed

crystal system azulene/naphthalene, for example, the lowest energy absorption is the 7000Å $^1B_1 \leftarrow {}^1A_1$ transition. This transition is therefore polarized along the short (M) axis of the azulene molecule, and the naphthalene direction cosines predict the intensity ratio I_b/I_c, = 5.5 for the a_1 vibronic components. Small and Kusserow[32] have made careful intensity measurements of this transition, and the observed intensity ratio is several times greater than that calculated from the direction cosines. This discrepancy between observed and calculated polarization ratios, qualitatively correct but quantitatively inaccurate, is the rule rather than the exception with mixed crystal spectra. The factors which account for it have never been carefully elucidated, but no doubt include experimental uncertainties in the preparation of a specific crystallographic face, and location of the crystal axes during the experiment. More subtle effects, such as crystal defects and local strain may also be of major importance. The occurrence of nonuniformly polarized multiplet origins presents ample evidence of local effects.[19]

Cryostats

Spectra which were recorded photoelectrically were taken with the sample mounted in an Andonian metal dewar, model MHD-3L-30N, with the 0-7MH throttling system. With this system, the sample was cooled by the boil-off of liquid helium, the level of which can be kept just below the sample.

The sample temperature could be varied by adjusting the helium throttling rate in conjunction with a 20 Ω heater mounted below the sample chamber, which warmed the helium gas before entry into the sample chamber. The temperature, between 4.2 and 30°K, was measured using a Cryo-Cal CR500 germanium resistance thermometer (S/N 484), with a precision within 0.1°K.

For spectra recorded photographically, a double nested liquid nitrogen-liquid helium dewar with quartz tail section was used. This dewar is commercially available from Pope, part number 30053. For these spectra, the sample was directly immersed in the liquid helium. The same dewar was used for the Stark spectra, but with a modified dewar top, fitted with Stupakoff feed-throughs, rated at 17 KV. These were used for the high voltage leads, while the ground wires were run through the sample support rod, to insure electrical insulation. The experimental details of the Stark set-up are given in a later section.

Spectrometers and Light Sources

The choice of a spectrometer or spectrograph for a particular spectroscopic experiment usually involves a compromise of the resolving power desired and the mode of detection to be used. Where absolute or relative intensities of spectral components are the object, in the case of polarized spectra, for example, the photoelectric mode of detection is

most desirable. However, to obtain adequate signal-to-noise ratios, a faster spectral instrument is necessary; that is, one with a shorter focal length and resultant loss of resolution. For the work reported here, a 1-m Jarrell-Ash Czerny-Turner spectrograph, model 75-150, was used, operated in the photoelectric mode, whenever higher resolution could be sacrificed. The grating used was Jarrell-Ash, number 980-43-20-22, blazed for 5000Å in first order, and which gave a resolution of 0.11Å in first order, when used with the 1-m spectrograph. Detection was accomplished by use of either an EMI 9558 QB or an EMI 6256 B photomultiplier tube, the output of which was displayed on a strip chart recorder.

For the determination of band position, spectra were recorded photographically using a 3.4 m Jarrell-Ash Ebert Spectrograph, model 70-000, with a grating blazed for 5000Å in first order. This instrument has a reciprocal linear dispersion of 5.1Å/mm, compared to 8.2Å/mm for the 1 m instrument. Kodak 103a-0 or 103a-F photographic plates were used to record the spectra, and the plates were subsequently analyzed using a Jarrell-Ash model 23-500 scanning microdensitometer. The spectra were calibrated with the emission spectrum of an iron-neon hollow cathode lamp.

The Stark experiments have as their object the measurement of small differences between the splittings of various bands in the spectrum. To obtain the requisite precision and accuracy in these measurements, the Stark spectra were

recorded photographically on a 3.4 M Jarrell-Ash Ebert spectrograph with a Harrison grating blazed for 60,000Å in first order. At 4500Å in 13th order (the first absorption system of diazaazulene) the instrument has a reciprocal linear dispersion of 0.34Å/mm. Separation of orders was achieved using a Jarrell-Ash monochromator, model 82-410, with a band width of 50 cm^{-1} at half the transmission peak height.

A McPherson 0.3 m scanning monochromator, model 218, was used as a preset monochromator in the photo-excitation experiment performed on the diazaazulene and phenyldiaza-azulene fluorescence and phosphorescence system. This instrument was also used (with photoelectric detection) as a spectrometer on various occasions to record absorption and emission spectra. The 0.3 m spectrometer with grating blazed for 5000Å in first order, exhibits 0.6Å resolution with an effective aperature ratio of f/5.3. This increased speed, compared to f/8.3 for the 1 m Jarrell-Ash spectrometer, made the McPherson spectrometer useful for detection of weak luminescences which could subsequently be photographed at higher resolution on another instrument.

Two kinds of light sources are common in optical spectroscopic experimentation: continuum sources for measurement of absorption spectra, and excitation sources for emission spectra. The continuum sources used in the work

reported here included a 450 W Xenon arc lamp, 150 W tungsten-iodide filament lamp, and a 30/60 W deuterium lamp. Excitation sources included high and low pressure mercury arc lamps.

THEORY

It is a familiar concept that, for molecules with a point group symmetry other than C_1 or O_h, the absorption or emission of radiant energy is an anisotropic process. Specifically, for molecules with symmetry, the dipole moment operator $\underset{\sim}{d}_e$ can be related to the symmetry axes of the molecule. The intensity of an electronic transition is proportional to the square of the transition moment integral, $\underset{\sim}{M}_{if}$, dotted with the electric vector, $\underset{\sim}{\mu}$, of the absorbed or emitted light,

$$I_{if} \propto |\underset{\sim}{\mu} \cdot \langle \psi_f | \underset{\sim}{d}_e | \psi_i \rangle|^2 \qquad (1)$$

where ψ_i and ψ_f are the wavefunctions for the initial and final transition states. In what follows, we employ the Born-Oppenheimer (adiabatic) approximation to write the molecular wavefunctions (ψ_i and ψ_f) as a product of an electronic and a vibrational wavefunction. The former, $\phi(r,q)$, depends functionally upon the electronic coordinates, r, and parametrically on the nuclear coordinates, q. The vibrational wavefunctions x(q) depend on the coordinates q and the electronic state quantum number. The adiabatic product wavefunctions, $\phi \cdot x$ are not, however, diagonal with respect to the nuclear kinetic energy operator. Because we will be considering the spin allowed transitions, the spin functions will not be included in the ensuing treatment.

With the adiabatic approximation, Equation 1 can be written as

$$I_{f\beta,io} \propto |\underset{\sim}{\mu}\cdot\langle\phi_f x_{f\beta}|\underset{\sim}{d}_e|\phi_i x_{io}\rangle|^2 \qquad (2)$$

for the transition $f\beta \leftarrow io$ which in our experiments always originates from the zero point vibrational sublevel of the initial electronic state. The integration in Equation 2 is over both nuclear and electronic coordinates.

The first level of approximation in evaluating the integral in Equation 2 is the crude adiabatic approximation in which we assume that the electronic wavefunctions ϕ_i are eigenvectors of the electronic hamiltonian H_o, where the subscript o implies that the hamiltonian and wavefunctions are evaluated at the equilibrium nuclear geometry. Then, with

$$H_o\,\phi_i^o = E_i^o\,\phi_i^o, \qquad (3)$$

Equation 2 becomes

$$I_{f\beta,io} \propto |\underset{\sim}{\mu}\cdot\langle\phi_f^o|\underset{\sim}{d}|\phi_i^o\rangle\langle x_{f\beta}|x_{io}\rangle|^2 \qquad (4)$$

The symmetry of the molecule requires that the integrals in Equation 4 will vanish if their integrands do not contain the totally symmetric representation of the molecular point group. Since, for those molecules to be considered in this thesis, the initial vibrational sublevel is the zero point level, x_{io} will belong to the totally symmetric representation, requiring that the final vibrational level also be totally

symmetric. The requirement on the electronic integral is that the direct product of the symmetry representations of the two electronic wavefunctions transform like one of the axial vectors of the molecule (x, y or z), that is, one of the components of the dipole moment operator. The transitions considered in this thesis have the ground electronic state as either the initial state (absorption) or the final state (fluorescence), and for the closed shell ground state molecules considered here, the ground state electronic wavefunction belongs to the totally symmetric representation of the molecular point group. Then the electronic integral in Equation 4 will "pick out" that component of the dipole moment operator which belongs to the same symmetry representation as the excited state electronic wavefunction. The polarization vector of the absorbed or emitted light must lie along the same direction as this dipole operator component for the product $\underset{\sim}{\mu} \cdot \underset{\sim}{d}$ to be nonzero. Therefore, measurement of the polarized absorption or emission intensity ratios for an oriented molecule will allow the determination of the spatial symmetry of the excited state electronic wavefunction. The mixed crystal, of course, provides the requisite molecular orientation.

The crude adiabatic approximation has a certain applicibility in explaining the absorption or emission spectra of a molecule, but fails to account for the intensity of transitions to nontotally symmetric vibrational levels in the

final electronic state. Electronic transitions are also observed which are forbidden in the crude adiabatic approximation. Perhaps the best known example of this is the near ultraviolet absorption system of benzene, which has been shown to be the forbidden $^1B_{2u} \leftarrow {}^1A_{1g}$ transition (point group D_{6h}).[33] The observation of forbidden vibrational levels built on allowed electronic transitions is also well documented.[34,3] To account for these phenomena it is necessary to consider the mixing of the crude adiabatic electronic states through the nuclear motion, the vibronic coupling. The formalism of Herzberg and Teller[35] has been widely applied in this context.

In the Herzberg-Teller vibronic coupling theory, the electronic hamiltonian is expanded in terms of the ground state normal coordinates of the molecule

$$H = H_0 + \sum_a \left(\frac{\partial H}{\partial q_a}\right)_0 q_a + \frac{1}{2} \sum_{a,b} \left(\frac{\partial^2 H}{\partial q_a \partial q_b}\right)_0 q_a q_b + \cdots$$

$$= H_0 + \sum_a A_a q_a + \sum_{a,b} B_{a,b} q_a q_b + \cdots$$

$$= H_0 + H'(q) \qquad (5)$$

where the subscript zero indicates evaluation at the equilibrium nuclear geometry. H_0 is, of course, the crude adiabatic hamiltonian, which has as its eigenvectors the ϕ_i^o's. Using them as a basis set we can write the Herzberg-Teller wavefunctions in terms of the perturbation $H'(q)$.

Neglecting the quadratic and higher order terms,

$$\phi_f^{HT} = \phi_f^0 + \sum_j \sum_a \frac{\langle \phi_f^0 | A_a q_a | \phi_j^0 \rangle}{E_f^0 - E_j^0} \phi_j^0 \tag{6}$$

For simplicity, we consider the case of one coupling state ϕ_j^0 and one coupling mode q_a. Then Equation 6 becomes

$$\phi_f^{HT} = \phi_f^0 + \frac{A_a^{f,j}}{E_f^0 - E_j^0} q_a \phi_j^0 \tag{7}$$

Substituting this into Equation 2 we obtain

$$I_{fa,io} \propto |\underset{\sim}{\mu} \cdot \{ \langle \phi_i^0 | \underset{\sim}{d} | \phi_f^0 \rangle \langle x_{fa} | x_{io} \rangle + \frac{A_a^{fj}}{E_f^0 - E_j^0} \langle \phi_j^0 | d | \phi_i^0 \rangle \langle x_{fa} | q_a | x_{io} \rangle \}|^2$$

$$= |\underset{\sim}{\mu} \cdot \{ \underset{\sim}{M}_{if}^0 \langle x_{fa} | x_{io} \rangle + \alpha_{fj}^a \underset{\sim}{M}_{ij}^0 \langle x_{fa} | q_a | x_{io} \rangle \}|^2 \tag{8}$$

The first term in Equation 8 is the crude adiabatic transition moment. The second term describes the intensity of the transition fa←io induced by coupling of the state ϕ_f^0 to the state ϕ_j^0. α_{fj}^a is the linear Herzberg-Teller vibronic coupling coefficient.

Two features of Equation 8 are of particular importance. First, for states ϕ_j and ϕ_i of the appropriate symmetry, the vibronic coupling term will induce intensity into transitions to nontotally symmetric vibrational levels x_{fa}, since q_a belongs to the same symmetry rep as x_{fa}. Secondly, although

$\underline{M}_{if}^{0}$ may be zero by symmetry, intensity can be induced into the dipole forbidden transition through the nontotally symmetric vibronic modes. In terms of the oscillator strengths of the coupled states, the coefficients α_{fj}^{a} are given by

$$\sum_{a} \alpha_{fj}^{a} = \frac{f_{f}^{in} E_{j}^{0}}{f_{j} E_{f}^{0}(E_{f}^{0}-E_{j}^{0})^{2}} \qquad (9)$$

where f_{f}^{in} is the intensity induced by coupling to state ϕ_{j}^{0}.

In addition to its role in intensity borrowing, the concept of vibronic coupling may be applied to perturbations of the excited state vibrational frequencies. We begin with the hamiltonian of Equation 5, and write the correction to the excited state electronic energy

$$E_{i}(Q) = E_{i}^{0} + \sum_{a} \alpha_{ii}^{a} q_{a} + \frac{1}{2} \sum_{ab} \beta_{ii}^{ab} q_{a} q_{b} + \sum_{jab} \frac{\alpha_{ij}^{a} \alpha_{ij}^{b}}{E_{i}^{0}-E_{j}^{0}} q_{a} q_{b} \qquad (10)$$

where $\beta_{ii}^{ab} = \left\langle \phi_{i}^{0} \middle| \frac{\partial^{2} H}{\partial q_{a} \partial q_{b}} \middle| \phi_{i}^{0} \right\rangle$. For one coupling mode q_{a} and one coupling state ϕ_{j}^{0} the excited state vibronic energies are

$$E_{i,a} = E_{i}^{0} + \alpha_{ii}^{a} \langle x_{ia} | q_{a} | x_{ia} \rangle + \left\{ \frac{1}{2} \beta_{ii}^{aa} + \frac{(\alpha_{ij}^{a})^{2}}{E_{i}^{0}-E_{j}^{0}} \right\} \langle x_{ia} | q_{a}^{2} | x_{ia} \rangle \qquad \ldots. \quad (11)$$

Now, q_a can be written as a function of the raising and lowering operators

$$q_a = (\hbar/2w_a)^{1/2}(a^+ + a^-)$$

where

$$a^+|n_a\rangle = (n_a+1)^{1/2}|n_a+1\rangle$$

$$a^-|n_a\rangle = (n_a)^{1/2}|n_a-1\rangle$$

where $|n_a\rangle$ is the vibrational wave function for n quanta of vibrational mode a excited. Within the harmonic approximation, Equation 11 then becomes

$$E_{i,a} = E_i^0 + \{\frac{1}{2}\beta_{ii}^{aa} + \frac{(\alpha_{ij}^a)^2}{E_i^0 - E_j^0}\}\frac{\hbar}{2w_a}(2n_a + 1) \quad . \qquad (12)$$

We are primarily concerned with the frequencies of the excited state fundamentals (n_a=1) in terms of their separations (Δw) from the excited state zero point level. From Equation 11 we obtain

$$\Delta w_a = \frac{\hbar}{2w_a}\{\frac{1}{2}\beta_{ii}^{aa} + \frac{(\alpha_{ij}^a)^2}{E_i^0 - E_j^0}\} \times 2 \quad . \qquad (13)$$

The diagonal quadratic term β_{ii}^{aa} and the off-diagonal terms which we neglected in writing Equation 11 are important in the mixing of the ground state normal coordinates in the excited state, the Duschinsky effect.[36-38] This will be considered in more detail in a later section. The importance of Equation 13 lies in the term $2\alpha^2/\Delta E$, which describes the

dependence of the excited state vibronic frequencies on their coupling to other electronic states, and on the energy gap between the states. Lacey[9] and Lacey and coworkers[10] have used this approach to explain the medium dependence of vibronic frequencies in azulene's S_2 absorption spectrum, although their derivation errs by failing to account for the adiabaticity of the vibronic wavefunctions. The important feature is the $^1/\Delta E$ dependence of the coupling term in Equation 13, implying that a change in the energy gap between coupled electronic states in different host media will lead to a medium dependence of the frequencies of vibronically active modes.

RESULTS AND DISCUSSION, 1,3-DIAZAAZULENE

At 4.2°K, the absorption spectrum of 1,3-diazaazulene in naphthalene commences with a band at 22154 cm^{-1} (4500Å) which, from its intensity and location in the spectrum is assigned as the origin of lowest energy electric dipole allowed transition (see below for confirmation of this assignment). The polarized ab and bc' absorption spectra of the 1,3-diazaazulene in naphthalene 4500Å transition are shown in Figures 3 and 4, respectively, and the polarization of the origin band in these spectra, uniformly along the b crystallographic direction, allows identification of the transition as $^1B_1 \leftarrow {}^1A_1(\pi\pi^*)$, analogous to the lowest energy transition of azulene. The integrated absorption spectrum of a room temperature solution of diazaazulene in benzene gives a value of f = 0.009 for the oscillator strength of this transition, identical to that reported for the 7000Å transition of azulene.[34] It is tempting, then, to describe the diazaazulene 4500Å transition as "the azulene 7000Å transition blue shifted by some 8000 cm^{-1}". Lending credence to this description are the facts that the transitions appear to share similar orbital parentages, and the net intensities of the transitions are the same. However, as will become apparent, the similarities between these two transitions are largely limited to these, and more important are the differences between the azulene 7000Å and diazaazulene 4500Å spectra. The most

dramatic of these is that the 4500Å state is, in fact, the fluorescent state of diazaazulene. Phosphorescence is also observed, originating at 5200Å. The absorption spectrum is seen to exhibit complex vibronic coupling, through both the a_1 and b_1 vibronic modes, which manifests itself not only in intensity stealing but also in a medium dependence of the vibronic band positions. There is also a distinct lack of mirror symmetry between the absorption and fluorescence spectra, again indicative of strong vibronic interactions. Since the spectra can be best understood by considering the similarities and differences among the spectra in the various hosts used, a general description of the electronic spectra of diazaazulene in the three hosts naphthalene, quinazoline and p-dichlorobenzene will be given first, followed by a detailed analysis of the spectra.

The $^1B_1 \leftarrow {}^1A_1$ Absorption of 1,3-Diazaazulene

Naphthalene host

The origin of the lowest energy absorption of diazaazulene in naphthalene occurs at 22154 cm^{-1} and as is obvious from Figures 3 and 4 is uniformly polarized along b for both the ab and bc' faces of the naphthalene host. The polarization ratios of the origin band, measured from these spectra are $I_b/I_a = 2.3$, $I_b/I_{c'} \sim 20$. The quantitative agreement between these values and the oriented gas ratios for naphthalene is

not good, but the error is fortuitous since the large polarization ratio on the bc' face effectively separates the a_1 and b_1 vibronic components, facilitating the analyses of the spectra. Absorption spectra taken on certain other diazaazulene/naphthalene crystals (Figure 5) exhibit polarization ratios much closer to the oriented gas ratios, certainly within the expected tolerances for polarized mixed crystal spectra, and we are confident in our assignment of the 4500Å transition as $^1B_1 \leftarrow {}^1A_1 (\pi\pi^*)$. The positions and analyses of the absorption bands of the bc' polarized spectrum of diazaazulene/naphthalene are given in Tables 1 and 2. From group theoretical considerations, it is easily determined that diazaazulene has 15 a_1 and 14 b_1 vibrational frequencies. Of the a_1 frequencies, 11 are associated with skeletal distortion, and of the b_1 frequencies, 8 are skeletal distortions. The remaining vibrational modes are predominantly C-H stretching motions. The identification of the b_1 fundamentals was facilitated by the unique polarization of the bc' face, and by the surprising efficiency of the b_1 modes in forming combinations with the a_1 fundamentals. The identification of the a_1 fundamentals is a more difficult problem, since an a_1 band which gains its intensity through vibronic coupling will not in general form progressions. The observation of bands at frequencies corresponding to the overtones of a band is a confirmatory test of the assignment of that band as a vibronic

fundamental. The 539 and 575 cm^{-1} bands in the b polarized spectrum of diazaazulene/naphthalene (Figure 3) are exemplary of this problem. The overtones of these bands are not observed, though they would fall in spectrally congested regions, and this may obscure them. However, the 575 band is not seen in combination with, say, the 678 cm^{-1} mode, or with many of the other progression forming modes. In Table 1, a number of bands have been assigned as combinations in the 539 and 575 cm^{-1} modes. In a number of these instances, other assignments are possible, so that the evidence that the 539 and 575 modes are active in forming vibronic progression is less than convincing. The intensity of the 539 and 575 cm^{-1} bands, and their location in the spectrum preclude their assignment as overtones or combinations of other fundamentals. Therefore, they must either be assigned as a_1 fundamentals or discounted as impurity absorption bands. Other evidence makes the assignment of these bands as a_1 fundamentals the favored choice. Their polarization ratios are consistent with the other a_1 bands in the spectrum, as are their band widths at 4.2°K. In addition, the phonon wing-bands built on the 539 and 575 bands exhibit a structure similar to that of the other a_1 components. To add weight to these arguments, absorption spectra were taken using two crystals of 1,3-diazaazulene/naphthalene. One was grown from the melt using a diazaazulene sample which had intentionally been allowed to

undergo considerable decomposition. The other crystal was an ab face which had been grown by cosublimation of purified diazaazulene and naphthalene. The polarizations and the intensities of the 539 and 575 bands relative to the origin were the same in the absorption spectra of the two crystals.

p-Dichlorobenzene host

The use of p-dichlorobenzene as a host crystal for diazaazulene was of limited success because of the only slight solubility of diazaazulene. It was, however, possible to obtain unpolarized absorption and emission spectra using a section of melt grown crystal which did show the presence of the diazaazulene guest. The absorption spectrum of this section is given in Figure 6, and the band position in Table 4. The origin of this absorption occurs at 22192 cm^{-1}, a shift of only 38 cm^{-1} from the origin in the naphthalene host. The magnitude of this shift is not unusual for mixed crystal spectra. The vibronic band positions are very similar to those in naphthalene host, but with a two important differences. The bands at 539 and 575 cm^{-1} in naphthalene host are missing, but two new absorption peaks are observed at 357 and 664 cm^{-1}. Two other bands, at 761 and 956 cm^{-1} in naphthalene, appear to undergo smaller shifts to 719 and 914 cm^{-1}, respectively. To speak of shifts in vibronic band positions is less than precise, since the changes in the molecule's force constants which result in differing vibronic

structure in various hosts produce changes in the normal coordinates which define those vibrations. However, because many of the vibrational modes are largely unaffected by changing the host material, correlations between the perturbed modes are useful in comparing the spectra. The b_1 vibronic modes are all found at very much the same position in both the naphthalene and dichlorobenzene hosts.

Quinazoline host

The polarized absorption spectrum of the xz face of diazaazulene in quinazoline is shown in Figure 7, and the band positions are given in Tables 5 and 6. The origin of the transition (at 22540 cm^{-1}) and its a_1 vibronic components are strongly polarized along the z direction. However, the b_1 bands exhibit comparable intensity in both polarizations. Polarized absorption measurements of the yz face gave $I_z/I_y \sim 2$. The similarities between the xz and yz polarized spectra of diazaazulene/quinazoline and the bc' and ab spectra of diazaazulene/naphthalene, respectively, are evident. The vibronic fundamentals assigned from these spectra are given in Table 3. The absence of a_1 absorption peaks in the 500-600 cm^{-1} region, and the occurrence of two new peaks at 384 and 660 cm^{-1} is additional evidence of a medium dependence of the 539, 575 bands of diazaazulene/naphthalene. The b_1 vibronic frequencies are, again, essentially unchanged from their values in naphthalene host. On the basis of this

evidence the 539 and 575 bands in naphthalene host are assigned as a_1 vibronic fundamentals. It is also suggested that the 357, 664 bands in dichlorobenzene host and the 384, 660 bands in quinazoline host are a result of the "motion" of the 539, 575 bands to these positions. An analysis of some other complexities of the spectra lends credence to this identification of the 539, 575 bands as moving levels.

In Table 3 are listed, for naphthalene host, fourteen absorption bands which from their intensities and/or locations might be assigned as a_1 vibronic fundamentals. Since diazaazulene has only eleven a_1 fundamentals (excluding the 4 CH modes at 3100 cm^{-1}), three of these bands must be spurious. Two bands, at 1068 and 1680 cm^{-1} are not observed in either dichlorobenzene or quinazoline hosts, and attention is focused on these.

The 1068 band is not assigned as a combination in any of the a_1 fundamentals. If it were an a_1 fundamental, it should be observed in the other hosts either at 1068, or moved to some new position. Yet there is no "new" band near enough to 1068 in either dichlorobenzene or quinazoline hosts to allow for this possibility. As noted above, the overtone of the 539 band is not observed at 1078 cm^{-1}, twice the fundamental frequency. There are, however, two strong a_1 fundamentals, at 1096 and 1104 cm^{-1}. These vibrational modes, in Fermi resonance with a two quantum mode at 1078 cm^{-1} would greatly intensify the band, and result in its shift to

lower energy. Since it could resonate with both the higher frequency modes similtaneously, the intensity of the band might be deceptively large. In addition, when the 539 band moves, in the other hosts, to lower frequency, its overtone would lose its proximity to the resonant modes, and the overtone absorption band would be greatly diminished in intensity. This type of resonant interaction has been explored by Lacey[9] in his analysis of azulene's 3500Å absorption. The model calculations yielded intensities in the two quantum modes which are entirely consistent with what is proposed here for the 1068 mode. The 1068 mode is, therefore, assigned as the overtone of the 539 a_1 fundamental. Our ability to make this identification reflects an important feature of the diazaazulene 4500Å absorption. Azulene's 3500Å absorption is a model case of vibronic effects run rampant, resulting in a degree of complexity which severely hinders the kind of qualitative judgments necessary in the analysis of vibronic spectra. The diazaazulene spectrum, while still manifesting these vibronic effects, does so in a sufficiently limited fashion that the analysis may proceed with considerably less confusion, and a concomitant increase in our confidence. The analysis of the 1680 cm^{-1} absorption band is a good case in point.

The 1680 cm^{-1} band in the absorption spectrum of diazaazulene/naphthalene (Figure 4) is of sufficient intensity to merit its consideration as an a_1 fundamental. However,

since the highest energy ground state a_1 fundamental is at 1597 cm^{-1} (vide infra), this assignment is questionable. Also, the 1680 band is not observed in either dichlorobenzene or quinazoline hosts. This strongly suggests the possibility that the 1680 band is somehow involved with the moving levels, and it is possible to assign the 1680 band as the combination (575 + 1104). In quinazoline and dichlorobenzene the 575 band is moved to 660 and 644 cm^{-1}, respectively, while the 1104 band is found essentially unperturbed at 1103 and 1109 cm^{-1}. If the assignment of the 1680 band is correct, one would expect to find absorption bands at 1768 cm^{-1} in quinazoline and 1753 cm^{-1} in dichlorobenzene. In fact, these bands are observed and establish the assignment of the 1680 band of diazaazulene/naphthalene. The intensities of the 1768 and 1753 bands are consistent with that of the 1680 band, and there is no band near 1760 in naphthalene host which cannot be convincingly assigned.

The $^1B_1 \rightarrow {}^1A_1$ Fluorescence of 1,3-Diazaazulene

The fluorescence of 1,3-diazaazulene originates from its lowest excited singlet state, in contrast to azulene, which emits from its second excited singlet. The diazaazulene emission is sufficiently strong that no difficulty is encountered in recording the fluorescence using standard dc photoelectric detection. Fluorescence spectra have been obtained using three host crystals, naphthalene,

p-dichlorobenzene and quinazoline, and the band positions are reported in Tables 7, 8 and 9, respectively. These ground state vibrational frequencies exhibit none of the medium dependence characterized above for the absorption spectra, and the correlation of the fluorescence fundamentals is given in Table 10. Table 10 also gives the IR and Raman frequencies of diazaazulene. The IR spectra were taken at room temperature with the diazaazulene in a KBr pellet. The Raman spectra were taken with the sample in a "Displex" cryogenic refrigerator, and the sample at a temperature of 20°K. Figures 8 and 9 show the ab and bc' polarized fluorescence spectra of diazaazulene/naphthalene. The fluorescence spectra with dichlorobenzene and quinazoline host are nearly identical to that in naphthalene host, and they are reproduced in Figures 10 and 11.

The fluorescence is dominated, in all media, by an a_1 vibronic fundamental at ca. 922 cm^{-1}, which has about one-half the intensity of the origin band. (In viewing Figures 8 and 9 it should be recalled that the origin band is largely reabsorbed, and a comparison of intensities is better made by considering the phonon wing-bands.) This is most obvious in the diazaazulene/quinazoline fluorescence spectrum of Figure 10. Progressions and combinations are observed for most of the a_1 and b_1 modes. The only assignment problem involves the weak bands at 952, 1228 and 1541 cm^{-1} in naphthalene host.

Diazaazulene should have eleven totally symmetry vibrational fundamentals with frequencies between 300 and ca. 1700 cm^{-1}. Table 10 lists twelve frequencies in this region which are likely candidates for assignment as fundamentals. Based on the coincidence of IR or Raman frequencies or observation of progressions, all but the 952, 1228 and 1541 bands are assigned with confidence as a_1 fundamentals. There are IR absorptions in the 1230 and 1540 cm^{-1} regions, but the symmetries of the IR frequencies are not known, making correlations questionable. Although the 952, 1228 and 1541 bands are all very weak, so that progressions and combinations are not likely to be observed, there are several possible assignments of combinations in all three modes listed in Tables 7-9. In short, there is little spectral evidence to allow identification of two of these bands as fundamentals to the exclusion of the third. None of these three bands is identifiable as a progression or combination in a known a_1 mode, suggesting that the one which is not a fundamental gains its intensity through Fermi resonance.[26]

In an effort to solve the assignment problem, and to provide additional insight into the ground-state vibrational structure, an attempt was made to calculate the ground state frequencies and normal coordinates. The vibrational secular equation was solved using the program of Pinter and Orr[39] who in turn follow the algorithm of Schactschneider.[40,41]

This method involves refinement of an initial set of force constants to fit the calculated to the observed vibrational frequencies. In this instance the force constants were employed as a generalized valence force field. The results obtained were less than satisfactory. The initial force field was necessarily crude, particularly in regard to the carbon-nitrogen stretching and bending force constants. It is also necessary, in this approach, to somewhat arbitrarily restrain certain force constant values lest, in the presence of a local minimum, the refinements tend to enhance or diminish them beyond the limits of the physically reasonable. In spite of such obstacles, the calculation did reproduce the main features of the spectrum, but not in such a way that would allow confident assignment of the 952, 1228 and 1541 cm^{-1} bands. At this point their identities remain enigmatic.

The fluorescence is a long spectrum, and the positions of some 150 bands have been measured from photomultiplier tracings of photographed spectra. The assignment of these bands is moderately complete, and there are none of the striking enigmas posed by the absorption spectra. There are undoubtedly a number of Fermi resonances occurring, especially at higher frequencies, which account for the large number of bands. The most obvious occurs at 700 cm^{-1}, with the overtone of the 349 b_1 band interacting with a prominent a_1 fundamental at about 696 cm^{-1}.

The Phosphorescence Spectra of 1,3-Diazaazulene

1,3-Diazaazulene has a phosphorescent triplet state at 5200Å. Its spectrum has been obtained in naphthalene, p-dichlorobenzene, and quinazoline hosts. The polarized ab and bc' phosphorescence spectra of diazaazulene/naphthalene are shown in Figures 12 and 13 and the band positions are listed in Table 11. Unpolarized phosphorescence spectra in dichlorobenzene and quinazoline hosts are given in Figures 14 and 15 and Tables 12 and 13, respectively.

The polarized phosphorescence spectra are not particularly instructive in characterizing the triplet state or the ground state vibronic modes. The spectra are depolarized, with $I_a \sim I_b$ and $I_b/I_c \sim 1.5$ for the origin band. The polarization ratios of the strongest spectral bands, along with a correlation of frequencies among the three hosts is given in Table 14.

The polarizations of the spectra depend upon the nature of the spin-orbit coupling through which the transition gains intensity. To determine the spatial symmetry of the triplet state, it is necessary to remove the degeneracy of the three magnetic substates by placing the molecule in a magnetic field. The phosphorescence bands are then split into three components, corresponding to the three magnetic quantum numbers m = 1, ±1. When the molecule is prepared as a mixed crystal guest, its orientation with respect to the external

magnetic field is known. The relative intensities of the three bands depend upon the particular spin orbit coupling route involved, and therefore upon the spatial symmetry of the coupling states.[42] As a result, varying the direction of the magnetic field, i.e., along the three crystallographic axes, will produce three sets of intensity ratios which may determine the triplet state symmetry, the symmetry of the state to which it spin-orbit couples, and the magnetic sub-state responsible for coupling. The results are not necessarily unambiguous, since for a molecule of C_{2v} symmetry, there are two coupling routes which will give the same intensity ratios and two unique ones. The Zeeman experiment has been performed for the phosphorescence origin band of diazaazulene/naphthalene and fortunately, the ambiguity cited above is not encountered. The results are consistent with the assignment of the triplet state as $^3A_1(\pi\pi^*)$, and with the short axis spin state being the active one. These results are tentative, since the experiment was not repeated, nor was it extended to bands other than the origin. There is, however, some theoretical rationale for this assignment. Pariser[43] has calculated the electronic states of azulene, and finds a gap of roughly 12000 cm^{-1} between the lowest excited A_1 triplet and singlet states, but a gap of only 2000 cm^{-1} between the lowest singlet and triplet B_1 states. If these gaps are maintained in

diazaazulene (an admittedly tenuous assumption) the blue shift of the B_1 states could leave the $^3A_1$ as the lowest triplet state. The possibility that the triplet state might be an $n\pi^*$ state has been excluded by the measurement of the zero field splitting parameters and lifetime of the phosphorescence.[44,45]

The vibronic structure of the diazaazulene phosphorescence does not lend itself to easy analysis. The position of the bands in wavenumbers are the ground state vibrational frequencies, and, therefore, the a_1 and b_1 modes can be identified by comparison with the fluorescence spectra. However, only six a_1 and one b_1 fundamental can be assigned in this manner, and the remaining bands must be a_2 or b_2 fundamentals. The symmetry of diazaazulene requires it to have four a_2 and five b_2 fundamentals, and there are nine unassigned frequencies in Table 14. This may be fortuitous, and there is no way to distinguish the a_2 from the b_2 vibronic frequencies on the basis of their polarizations. The infrared spectrum provides some information, since the a_2 vibrational modes are not IR active. All of the symmetries are allowed in Raman transitions. The IR and Raman frequencies which do not correspond to a_1 or b_1 ground state frequencies are listed in Table 14. On the basis of these spectra, the 770, 970, 1390 and 1510 cm^{-1} bands are assigned as b_2 ground state fundamentals, and the 941 and 1276 bands as a_2 fundamentals. The IR scan did not extend below 600 cm^{-1}, so assignment of

the 323, 424 and 579 bands (naphthalene host frequencies) is not possible. Aside from these three bands, and an ambiguity noted above in the fluorescence assignments, Tables 10 and 14 provide a complete listing of the a_1, a_2 and b_2 ground state frequency assignments of diazaazulene. Of the b_1 frequencies, six of the eight have been assigned.

The Second Excited Singlet State of 1,3-Diazaazulene

The solution spectrum of 1,3-diazaazulene in cyclohexane (Figure 16) exhibits an absorption, the onset of which occurs at about 3300Å, and which has an oscillator strength of f = 0.1. There are four prominent absorption maxima, the first occurring at 31800 cm^{-1} (ε = 3100), with the other three displaced from it by 754 cm^{-1} (ε = 5500), 1457 cm^{-1} (ε = 5000) and 2271 cm^{-1} (ε = 4800). The intensity and location of this transition suggest a correlation to the second transition of azulene, the 3500Å $^1A_1 \leftarrow {}^1A_1$ absorption, which also has an oscillator strength of f = 0.1 (Figure 17). A blue shift of the diazaazulene spectrum from that of azulene might be expected in light of the large blue shift of the lowest excited singlet. The mixed crystal spectra, however, belie this assumption.

Of the three mixed crystal hosts used for diazaazulene, quinazoline, with an absorption cut-off at about 3700Å, was not suitable for observing guest absorption spectra above

the lowest excited singlet state. Nor was the dichlorobenzene adequate, since as noted earlier, the lack of diazaazulene solubility in that host made it necessary to use a disoriented sample, precluding polarized measurements. The characterization of S_2 was, therefore, primarily dependent upon the use of naphthalene host.

The polarized ab and bc' absorption spectra of the second excited singlet state of diazaazulene/naphthalene are shown in Figure 18. A remarkable feature of these spectra is that their onsets occur at about 3650Å, 27400 cm^{-1}. This represents a shift of some 3000 cm^{-1} to the red of the position of the second absorption system observed in the solution spectrum. In addition, the spectra are polarized along the b crystallographic axis of both the ab and bc' faces, although two of the four absorption maxima observed in the ab spectra are a-polarized. This suggests the assignment of the second excited singlet state of diazaazulene as $^1B_1(\pi\pi^*)$ and not A_1, the spatial symmetry of azulene's second excited singlet state. This is unexpected, but several arguments favor the identification of the 3650Å state of diazaazulene/naphthalene with the 3300Å absorption observed in the solution spectra. First is a consideration of the general absorption contour of the spectrum. A comparison of the mixed crystal and solution spectra reveals that each exhibits four absorption maxima, with the weakest one lying at lowest energy, followed by

the strongest peak, and two of intermediate intensity. Second, and more important, the separations of these peaks are nearly identical for the mixed crystal and solution spectra. The first two bands are separated by 750 cm^{-1}, and from the polarization results, each of these has an absorption built on it at a separation of 1440 cm^{-1}. This, in turn, suggests that the portion of the mixed crystal spectrum which is a-polarized corresponds to vibronically induced absorption into nontotally symmetric vibrational levels built on the second excited singlet state. The alternative hypothesis would suggest that the a-polarized absorption corresponds to an overlapping $^1B_2(n\pi^*)$ state, thus its out-of-plane polarization would be observed in absorption along a. This is unlikely because of the obvious intensity of the a-polarized absorption. If we estimate its intensity at one-half of the total intensity of the 3550Å absorption, that would correspond to an oscillator strength of 0.050. This is an order of magnitude larger than the usual oscillator strength of an allowed $n\pi^*$ transition. The intensity and 1440 cm^{-1} vibrational spacing of the a-polarized absorption lead us to conclude that it is nontotally symmetric vibronic structure built on the $^1B_1(\pi\pi^*)$ second excited singlet state of diazaazulene.

To further explicate this matter we turn our attention to a consideration of higher energy absorption in the spectrum of

diazaazulene/p-dichlorobenzene. In this host, no diazaazulene absorption is observed until the onset of a strong broad absorption at 3380Å (29600 cm^{-1}). This is, of course, much closer to the onset of the second absorption in the solution spectra, than to the diazaazulene 3650Å absorption. Again, the absorption spectrum (Figure 19) reveals four absorption maxima, at 30490 cm^{-1}, 31250 cm^{-1}, 32010 cm^{-1} and 33190 cm^{-1}. The separations are 760 cm^{-1}, 1520 cm^{-1} and 2700 cm^{-1}. Except for the last value, these separations are essentially the same as those found for both the solution and naphthalene host spectra. Also, the intensity distribution of the spectrum in dichlorobenzene is similar to that found in the other two media. The question of why the S_2 absorption of diazaazulene/naphthalene in red shifted relative to both the cyclohexane solutions and dichlorobenzene host spectra is answered in part by recalling the nature of the diazaazulene/dichlorobenzene melange. As noted above, this is not a true mixed crystal, since the diazaazulene did not dissolve into the bulk of the solid. Instead, some was trapped near the top of the melt grown ingot in a (probably) highly inhomogeneous solid solution. It is not unlikely, therefore, that the intermolecular forces which cause the red shift of S_2 in naphthalene host are absent in both the cyclohexane solution and dichlorobenzene host spectra.

The higher electronic states of diazaazulene lie above the absorption cut-off's of all the mixed crystal hosts, so no polarization data is available to assist in assigning the symmetries of these states. However, reasonable conjectures can be made. Following the 3300Å state, the next absorption system of diazaazulene in a moderately intense state which has its onset at about 2850Å. This state is nearly masked by the fourth absorption, which has its onset at about 2600Å, and an oscillator strength of f = 0.8. It is possible that this intense state is analogous to S_4 is azulene, and is assigned as $^1A_1$. The 2800Å state is also assumed to be $^1A_1$. There is no evidence of $n\pi^*$ absorption in any of the diaza-azulene spectra, although it is unlikely that a weak absorption would be observed above 30000 cm^{-1}, among the intense $\pi\pi^*$ absorption. In summary, the $\pi\pi^*$ states of diazaazulene are assigned as: 4500Å, $^1B_1$, f = 0.009; 3200Å (3650Å in naphthalene host), $^1B_1$, f = 0.1; 2800Å, $^1A_1$, f $\sim$ 0.1; 2600Å, $^1A_1$, f = 0.8.

With the assignment of the excited state symmetries, it is possible to determine the vibronic coupling routes responsible for the nontotally symmetric vibronic coupling in the 4500Å state. Since the 4500Å state has B_1 spatial symmetry, the b_1 vibrational modes can gain intensity by coupling to an A_1 state. Two candidates present themselves. The 38500 cm^{-1} and 35700 cm^{-1} states, separated from the 4500Å state by 16000 cm^{-1} and 13000 cm^{-1}, respectively.

The total b_1 intensity of the 4500Å state has been determined by measuring the optical densities of the a_1 and b_1 vibronic fundamentals, and has been found to be f = 0.0013, or about 15 percent of total intensity of the transition. The results are nearly identical for the spectra in both naphthalene and dichlorobenzene hosts, and the results are listed in Tables 15 and 16. The Herzberg-Teller coefficients for S_1-S_4 coupling fall between 200 and 500 cm^{-1}, and these magnitudes are quite reasonable.[32] The total vibronic coupling energy is about 2300 cm^{-1}. The coupling coefficients for S_1-S_3 coupling are over twice as large, and it is likely that S_1-S_4 coupling is primarily responsible for the b_1 vibronic activity in diazaazulene's 4500Å state. However, the S_1-S_3 coupling coefficients are not unreasonably large, and it may be that both S_3 and S_4 provide intensity to the 4500Å state.

The totally symmetric vibronic activity is more difficult to deal with quantitatively, since it is not generally possible to distinguish Condon from Herzberg-Teller intensity. The intensity distribution of the spectrum provides some clue, since a combination of two Herzberg-Teller bands is not expected to carry significant intensity, nor is the overtone of a vibronically induced mode. Therefore, a spectrum exhibiting a large degree of vibronic coupling would be expected to be short, in the extreme case limited to only the fundamentals. On the other hand, bands which gain their intensity through Franck-Condon factors would exhibit

progressions and the resulting spectrum would be long. The latter appears to be the case for the diazaazulene 4500Å absorption. In particular, the nontotally symmetric absorption is a long spectrum, with numerous combinations of the a_1 and b_1 modes, Table 2. The b_1 modes must gain their intensity through vibronic coupling. Therefore, an a_1 fundamental capable of forming a combination with a b_1 mode must gain at least some of its intensity through its Franck-Condon factor. Conspicuously absent in combination with the b_1 modes are the 539 and 575 cm^{-1} bands. These are the modes which exhibit the strong medium dependence described above and their lack of combination with the b_1 modes is consistent with the assertion that they are vibronically active. While it is not possible to determine how much of their intensities is vibronically induced, it is possible to place an upper limit on their coupling coefficients by assuming that their entire intensities are induced. The coupling state is the $^1B_1(\pi\pi^*)$ state at 3650Å in naphthalene host, and at 3375Å in dichlorobenzene. This state has an intensity of f = 0.1, and the coupling coefficients are calculated to be 440 cm^{-1} for the 539 band and 520 cm^{-1} for the 575 band. In dichlorobenzene host, these bands are shifted to 357 and 644 cm^{-1}, and the coupling coefficients are determined to be 600 and 820 cm^{-1}, respectively. The quantitative agreement between these two sets of coupling coefficients is not especially good, but it is improbable that the 539, 575 bands comprise

the entire a_1 coupling intensity, and in the different hosts a redistribution of the vibronic activity may occur. This is clearly the case for the b_1 modes, where the total vibronic intensity in the two hosts is almost identical, but the relative intensities of the individual bands vary.

No attempt has been made to determine the vibronic coupling parameters for diazaazulene/quinazoline for two reasons. First, the observed intensity of a transition depends upon the projection which its transition dipole makes on the polarization vector of the absorbed light. For the bc' face of naphthalene host, the long and short molecular axes, along which the b_1 and a_1 vibronic transition moments are aligned, make nearly equal projection on the c' and b crystallographic axes, respectively.[23,24] Therefore, measurement of the a_1 vibronic intensities in the b polarization, and of the b_1 intensities in the c' polarizations will give the correct relative intensities of all the bands. In dichlorobenzene host, the diazaazulene molecules are assumed to have been randomly oriented, so that the unpolarized absorption spectrum yields the correct relative intensities. For quinazoline host, however, the molecular orientations are not known and the distinct polarization of the absorption, Figure 7, precludes the possibility of random orientation. Therefore, it is not possible to determine the projections of the a_1 or b_1 components on the crystallographic faces, and

the intensities of the a_1 components relative to the b_1 cannot be determined. Secondly, because of the low absorption cut-off of quinazoline, the location of S_2 cannot be determined. The remarkable mobility of this state in going from naphthalene to dichlorobenzene host makes its location in quinazoline host quite uncertain.

RESULTS AND DISCUSSION, PHENYLDIAZAAZULENE

In mixed crystal spectroscopy it is desirable to obtain the spectra of a particular guest in a number of different host materials. In this way one may hope to isolate those spectral features which owe their existence to the particular host, thereby obtaining as nearly as possible the electronic spectrum of the "unperturbed" guest. It is also useful to obtain spectra of similar guest molecules. Isotopic substitutions (when available) are a particular favorite, because of the similarity of the spectra in a sequence of isotopically related molecules. In the realm of vibrational calculations, for example, a surfeit of frequencies from isotopically related (often, deuterated) molecules is used to better refine an otherwise under-determined force field, with a concomitant increase in one's confidence in the calculated normal modes.[39-41]

The comparison of the electronic spectra of substituted molecules is not necessarily so straight-forward, particularly when the substituent may be expected to significantly alter the electronic properties of the parent molecule. The treatment of biphenyl[46] as a substituted benzene would involve, at the least, some philosophical difficulties. The original hypothesis of this research, that azaazulenes might exhibit electronic properties similar to those of the parent azulene, is a singularly pertinent example.

In this section the electronic spectra of 2-phenyl-1,3-diazaazulene are presented, and the features of these spectra correlated with those of 1,3-diazaazulene. The spectra were obtained in these media: methyl-cyclohexane solution, and biphenyl and dibenzyl mixed crystals.

The room temperature solution spectrum of phenyldiaza-azulene is shown in Figure 20. The lowest absorption system has its onset at 4550Å, and has a maximum extinction coefficient of 1300. The oscillator strength is calculated to be f = 0.013. This value is comparable to that found for the lowest excited singlet state of 1,3-diazaazulene. The location and intensity of this transition strongly suggest a correlation with the lowest excited singlet state of diaza-azulene, and, as will be shown, the mixed crystal spectra confirm this.

The second absorption system of phenyldiazaazulene in methylcyclohexane has its onset at about 3850Å. The oscillator strength of this transition is calculated to be f = 0.40. This transition is, therefore, about four times as intense as S_2 of diazaazulene, and its solution spectrum shifted some 4000 cm^{-1} to the red of the diazaazulene solution spectrum. It is also worth noting, at this point, that the shape of the phenyldiazaazulene S_2 absorption differs considerably from that of the diazaazulene S_2 absorption (Figure 16), in that the first absorption maximum in the spectrum is the most intense. A detailed analysis of the

phenyldiazaazulene absorption spectra will be presented along with a consideration of the S_1 absorption spectra.

The Excited Electronic States of 2-Phenyl-1,3-diazaazulene

The lowest energy absorption system of phenyldiazaazulene in dibenzyl commences, at 4.2°K, with a band at 21312 cm^{-1} which is the first of four site origins. By far the most intense occurs at 21908 cm^{-1}, and is denoted as O_4 in Figures 21 and 22, the ab and bc' polarized absorption spectra of the 4500Å absorption. The positions of the vibronic bands in these spectra are denoted by their displacements in wavenumbers from O_4. Subsequent reference to the origin band will be to O_4, since the other multiplets are too weak for vibronic structure built on them to be observed.

The measurement of the polarized ratios of O_4 in Figures 21 and 22 reveals that the totally symmetric components of the 4500Å absorptions are polarized along the b crystallographic axis of dibenzyl for both the ab and bc' faces. The polarization ratios are $I_b/I_a = 1.7$ and $I_b/I_{c'} = 4.8$. A comparison of these values with the oriented gas ratios for dibenzyl leads to the assignment of the state as $^1B_1(\pi\pi^*)$, the same spatial symmetry as the 4500Å state of 1,3-diazaazulene.

The analysis of the a-polarized absorption spectrum is given in Table 17. The spectrum is dominated by a totally

symmetric fundamental at 262 cm^{-1}, which carries one-half of the intensity of the origin band. A band is observed at 527 cm^{-1}, very nearly the position of the overtone of the 262 band. A band is also observed at 788 cm^{-1}, which is the supposed position of the second overtone of the 262 fundamental. It is interesting to use the intensities of these bands to determine their assignments and, if they do in fact form a progression, to calculate the shift in the origin of the 262 vibration upon excitation. Assuming that a band "a" gains the whole of its intensity through its Franck-Condon factor, we may write that its intensity is proportional to

$$|M_{o_1}\langle 0_a|i'_a\rangle \prod_{i\neq a}^{3N-6} \langle 0_i|0'_i\rangle|^2$$

where the primed vibrational wavefunctions are expressed in terms of the excited state normal coordinates $Q'(i_a=0,1,2...)$. The ground state normal coordinates are Q". The ratio of the "a" band intensity to that of the origin is simply

$$I_a/I_{oo} = |\langle 0_a|1'_a\rangle/\langle 0_a|0'_a\rangle|^2$$

and for the overtones

$$I_{2a}/I_{o,o} = |\langle 0_a|2'_a\rangle/\langle 0_a|0'_a\rangle|^2$$

$$I_{3a}/I_{o,o} = |\langle 0_a|3'_a\rangle/\langle 0_a|0'_a\rangle|^2, \text{ etc.}$$

For the 262 band these values are (relative to the origin band) $I_{0,0}/I_{0,0} = 1$, $I_{262}/I_{0,0} = .54$, $I_{527}/I_{0,0} = .17$, $I_{788}/I_{0,0} = .02$.

It is now possible to compare these values with tabulated, calculated values for Franck-Condon factors.[47,48,49] These tables are arranged in terms of two dimensionless parameters δ and D where

$$\delta = \sqrt{w''/w'} \quad \text{and} \quad D = (Q'-Q'')\sqrt{w''/h}$$

and w'' and w' are the ground and excited state fundamental frequencies. The 262 mode is observed in the phenyldiaza-azulene fluorescence spectrum (vide infra) at 277 cm^{-1}, giving a value for δ of 1.03, or essentially unity. Then, for $\delta = 1$ and D = 1.0 the tabulation gives the following values for the intensity ratios relative to the origin: 0.500, 0.125 and 0.021. The equivalence of these values to those determined from the experimental intensities is evident. The phases cannot, of course, be determined experimentally, since only the square of the Franck-Condon factor is measured. The value of D = 1.0 then allows calculation of the origin shift upon excitation as $(Q'-Q'') = 0.678\ amu^{1/2}-a_o$, where a_o is the Bohr radius. The determination of this parameter is restricted to those instances in which an excited state mode carries sufficient intensity to make observation of higher overtones possible. In addition, the correlation of ground and excited state frequencies must be good enough to allow determination of the parameter δ. The assumption inherent in the calculation of the origin shift is that the ground and excited state normal coordinates are, indeed,

related by a simple translation of the origin (Q'-Q"). That is, it does not account for the possible rotation of normal coordinates in the excited state, the Duschinsky mixing.[36-38] For cases like that treated above, where the frequency shift upon excitation is very small, and the intensity of the mode is equivalent in the ground and excited state, (i.e., mirror symmetry exists between the absorption and fluorescence spectra) this assumption is likely valid. The equality of the observed and calculated intensity ratios out to the second overtone of the fundamental, largely substantiates this. In addition, one may calculate the Franck-Condon factor using the ground state intensities. If, in fact, the Duschinsky mixing is negligible, and $\delta \sim 1$, the ground state should give the same values for the intensity ratios and for the origin shift as the excited state intensities. These values have been calculated for the 277 band in the phenyldiazaazulene fluorescence spectrum, and are 0.54 and 0.17. As a result of this analysis, it is possible to assign the 527 cm^{-1} band with certainty as the overtone of the 262 cm^{-1} mode. The 3 cm^{-1} error in the position of the overtone is not surprising, since the band widths of this system are on the order of 10 cm^{-1}, making the location of the band center somewhat uncertain. In addition, it has been demonstrated that the 262 band is strongly Franck-Condon allowed, and that the normal coordinate

defining it is related to a similar mode in the ground state by a simple translation of the origin of the vibrational potential.

Apart from the 262 band, the most intense absorption in the phenyldiazaazulene/dibenzyl 4500Å spectrum occurs in the region 1100 cm^{-1} from the origin. Three fundamentals appear to comprise the intensity in this region: an a_1 band at 1111 cm^{-1} and two b_1 bands at 1060 and 1096 cm^{-1}. All form strong combinations with the 262 mode. b_1 modes are also observed at 1176, 1244, 1277 and 1461 cm^{-1}, in addition to low frequency modes at 450 and 557 cm^{-1}. It is an important feature of this spectrum that the vibronic intensity, apart from the 262 and 1111 bands, is mostly due to the nontotally symmetric vibronic modes. This is a significant departure from the case of the diazaazulene 4500Å absorption, in which the a_1 vibronic intensity is clearly dominant. In another departure from the diazaazulene 4500Å absorption spectra, there is little evidence of totally-symmetric vibronic coupling in the phenyldiazaazulene spectra. All of the a_1 fundamentals are observed in combination with the 262 band, and with intensities very close to those predicted in the Condon approximation. No combinations are observed with modes other than the 262 mode, except for 1111 + 450. This is not surprising since the a_1 vibronic structure, with the exception of the 262 and 1111 modes, is very weak, and the

widths of all the bands in the spectrum are large. The result is that the spectrum becomes very broad above about 1800 cm^{-1} from the origin, and measuring band positions in this region is not possible.

In Table 18, the oscillator strengths for the origin band and the vibronic fundamentals of phenyldiazaazulene/dibenzyl are given. From these values it is determined that the non-totally symmetric component of the phenyldiazaazulene absorption has an oscillator strength of 3.1×10^{-3}, or about 24% of the total oscillator strength of the transition. Since the spatial symmetry of S_1 is B_1, the b_1 vibronic modes must gain their intensity through coupling to an A_1 excited state, or through ground state coupling. The relatively large energy gap between the ground state and S_1 makes the latter coupling mechanism unlikely. To decide on a coupling mechanism it is necessary to know the intensities and locations of the A_1 excited states.

The solution spectrum, Figure 20, exhibits a strong absorption, f = 0.4, originating at 3800Å. A weaker absorption originating at 3100Å is followed by a strong absorption, f = 0.8, which has its maximum at 2550Å. Only the 3800Å system lies below the mixed crystal cut off of dibenzyl host, and its ab and bc' absorption spectra are given in Figure 23. The spectra show the same four absorption maxima for the ab and bc' faces. These are polarized strongly along a of the ab face, but are slightly more intense along b of the bc'

face. That these polarizations are anomalous is obvious from a comparison of the observed intensity ratios with the oriented gas ratios. None of the three allowed excited state symmetries would yield $I_a >> I_b$ and $I_b > I_{c'}$. To interpret these results, then, requires some intuitive judgment. The 3800Å absorption intensity, f = 0.4, is far too large for an $n\pi^*$ state, and the direction cosines for a normal axis transition are at the most complete variance with the observed intensity ratios. That is, a normal axis transition should have $I_b > I_a$, $I_{c'} > I_b$. Secondly, the 3800Å absorption is polarized differently than the 4500Å state, which has B_1 spatial symmetry. Although the observed polarization ratios for the 4500Å state are less than the oriented gas ratios by a factor of two, this discrepancy is reproducible, as is that in the S_2 polarization ratios, suggesting a disorientation of the guest molecules in dibenzyl host. The most plausible explanation of these phenomena leads to the assignment of S_2 as $^1A_1(\pi\pi^*)$. To buttress this analysis, the 3800Å absorption system of phenyldiazaazulene/dibenzyl is graced with a touch of serendipity. An ubiguitous impurity in dibenzyl is stilbene(1,2-diphenylethene). Dyck and McClure[50] have studied the mixed crystal spectrum of stilbene in dibenzyl and have concluded that the 3300Å state of stilbene is long axis polarized. The stilbene absorption can be seen at the high energy side of the phenyldiazaazulene/dibenzyl spectra in

Figure 23. The polarization ratios have been measured and yield $I_a/I_b = 1.50$, $I_b/I_{c'} = 1.10$. The geometry of stilbene is sufficiently similar to that of phenyldiazaazulene to make a case for the proposition that the nearly quantitative agreement of the stilbene and phenyldiazaazulene polarization ratios supports the assignment of S_2 of phenyldiazaazulene as A_1 in spatial symmetry.

The assignment of S_2 of phenyldiazaazulene as A_1 is a particularly illuminating feature in the study of the electronic states of azulene and the azaazulenes. The second excited singlet state of 1,3-diazaazulene has B_1 spatial symmetry, while the 3500Å $^1A_1$ state of azulene has an intensity of f = 0.10. The location and intensity of the 3800Å state of phenyldiazaazulene therefore represent both an intensification and substantial red shift of this absorption system, relative to the two "parent" molecules. The 4500Å state, however, has the intensity, location and symmetry of the lowest excited singlet of diazaazulene. The symmetries of the weak ($f \sim 0.1$) 3100Å and very strong ($f \sim .8$) 2800Å states of phenyldiazaazulene are not experimentally determinable. If an anology to azulene is possible, the most plausible analysis would assign the 3100Å state as $^1B_1$ and the 2800Å state as $^1A_1$. In addition, diazaazulene has an excited B_1 state (f = 0.1) which in solution has its absorption onset at 3200Å, and which may correspond to the phenyldiazaazulene 3100Å state.

To summarize, the excited singlet states of 2-phenyl-1,3-diazaazulene are assigned as follows: $^1B_1(1)$, 21908 cm^{-1}, f = 0.013; $^1A_1(2)$, 26300 cm^{-1}, f = 0.4; $^1B_1(2)$, 32000 cm^{-1}, f $\sim$ .1; $^1A_1(3)$, 36000 cm^{-1}, f $\sim$ 0.8.

With these assignments of the higher excited states, it is now possible to propose a vibronic coupling mechanism by which the b_1 vibronic modes in the S_1 absorption gain their intensity. Two possible coupling states exist, the 3800Å and 2800Å $^1A_1$ absorptions. The latter (S_4) is separated from S_1 by 13000 cm^{-1}, while the S_1-S_2 energy gap is only 4400 cm^{-1}. However, the intensity of the 3800Å state is larger by a factor of two. The calculated vibronic coupling coefficients are given in Table 18, for both possible coupling states. Those values calculated for the 3800Å state as the coupling state are smaller by a factor of three than those calculated for the 2800Å state, and on the basis of their relative magnitudes, it is most likely that the 3800Å state is primarily responsible for the b_1 vibronic coupling of the 4500Å state. However, the calculated vibronic coefficients for S_1-S_4 coupling are not especially large, and it may well be that at least part of the b_1 vibronic intensity is gained through S_1-S_4 coupling. An excellent basis for comparison is Small and Kusserow's analysis of the nontotally symmetric vibronic activity of azulene's 7000Å state.[32] They find that the most probable mechanism involves coupling of S_1 to the

intense A_1 state at 34000 cm^{-1}, and calculate coupling coefficients on the order of 100 to 300 cm^{-1}, with a maximum of 750 cm^{-1}. The values of the phenyldiazaazulene coupling coefficients for both S_1-S_2 and S_1-S_4 coupling are within this range. This may account for the fact that the induced b_1 oscillator strength of phenyldiazaazulene ($f^i \sim 3.1 \times 10^{-3}$) is larger than that of diazaazulene's 4500Å transition ($f^i_{b_1} \sim 1.3 \times 10^{-3}$). As reported above, the second excited state of diazaazulene has B_1 spatial symmetry, and there is no evidence of an A_1 state below the relatively weak absorption at 2800Å. This is followed by an intense absorption (f = 0.76) at 2600Å which is most likely analogous to the S_4 $^1A_1$ state of both azulene and phenyldiazaazulene. It is also considered to be the state responsible for the b_1 vibronic activity of diazaazulene's 4500Å state. The S_4 state of phenyldiazaazulene has both the intensity and location of S_4 of diazaazulene, but the phenyldiazaazulene system has an additional moderately intense A_1 state (S_2) lying relatively close to S_1, and which is responsible for the increase in the b_1 vibronic intensity relative to that of diazaazulene's 4500Å state.

The only other host found for phenyldiazaazulene was biphenyl. Unfortunately, the spectra in this host are very broad, with 100 cm^{-1} band widths in the 4500Å absorption system. The polarizations confirm the assignment of the 4500Å state as $^1B_1$, with $I_b/I_a \sim 1.8$. There is a strong a polarized

absorption, $I_a/I_b = 1.6$, some 1100 cm^{-1} from the origin region, which corresponds to the 1060 and 1096 b_1 fundamentals measured in a dibenzyl host. A broad, intense absorption originates at 3900Å, with $I_a/I_b \sim 1.5$, and most certainly correlates with the 3800Å $^1A_1$ state of phenyldiazaazulene/dibenzyl.

The $^1B_1 \rightarrow {}^1A_1$ 4500Å Fluorescence of Phenyldiazaazulene/Dibenzyl

The phenyldiazaazulene fluorescence spectrum is shown in Figure 24, and the band positions and assignments are given in Table 19. Aside from the 277 and 658 bands, there is no obvious correlation of ground and excited state vibronic frequencies. A total of eight a_1 and two b_1 vibronic fundamentals have been assigned, and the correlation of these with the ground state frequencies of diazaazulene is quite good, Table 20. The reduction in frequency of the 405 mode of diazaazulene to 277 cm^{-1} for phenyldiazaazulene is a mass effect of the phenyl substitution. Two other modes may also be sensitive to this phenyl substitution, the 957 and either 1425 of 1391 bands. The assignment of the 952 band as an a_1 fundamental of diazaazulene is not solidly established (vide supra), so that the 957 band may correlate with one of the bands in the 1200 cm^{-1} region of the diazaazulene spectrum. Either the 1391 of 1425 band may correlate with the 1407 mode of diazaazulene, and the other with the 1597 band. The

importance of the phenyl substitution in determining a vibrational frequency depends upon the extent to which the motion of a particular mode couples with the diazaazulene-phenyl bond, and this is not known without a determination of the normal coordinates. As with diazaazulene, an attempt was made to calculate the ground state normal coordinates, but the results, comparing the calculated and observed frequencies, were not good enough to inspire confidence in the calculated normal modes.

The fluorescence spectrum does not present any assignment problems, and essentially all of the observed bands can be analyzed in terms of combinations and progressions of the a_1 fundamentals. The only two b_1 fundamentals observed, at 1027 and 1131 cm^{-1}, are very weak. As mentioned above. the correlation between the ground state frequencies of diazaazulene and of phenyldiazaazulene is very good. However, as in the case of diazaazulene, the correlation between the ground and excited state frequencies of phenyldiazaazulene is poor. The 277 band in fluorescence is mirrored by the 262 band in absorption, and the bands at 658 and 1425 cm^{-1} in fluorescence have their counterparts in the absorption spectrum. There are no other obvious correlations.

The Phosphorescence Spectrum of Phenyldiazaazulene/Dibenzyl

2-Phenyl-1,3-diazaazulene/dibenzyl phosphoresces from a triplet state at 5930Å, the origin occurring at 16853 cm^{-1}. The spectrum is shown in Figure 25 and the band positions and assignments in Table 21. The origin band in phosphorescence is by far the strongest in the spectrum, carrying about 70% of the entire transition intensity. For that reason, two traces of the phosphorescence spectrum have been included in Figure 25. In the upper trace the origin has been amplified off scale to facilitate observation of the vibrational band positions. In the lower trace, the origin is on scale, and the scan includes the 194, 263 and 421 cm^{-1} bands to demonstrate the relative intensity of origin.

The analysis of the phosphorscence spectrum, Table 21, was aided in part by a comparison with the fluorescence spectrum, allowing assignment of the bands at 661, 959, 1397 and 1590 cm^{-1} as a_1 fundamentals. Several other tentative assignments are made in Table 21, but the lack of other hosts for phenyldiazaazulene makes firm assignments impossible.

The phenyldiazaazulene phosphorescence, at 16850 cm^{-1}, is red shifted some 2200 cm^{-1} relative to the diazaazulene phosphorescence. The S_1, ($^1B_1$) absorptions of both molecules lie within a few hundred wavenumbers of each other at 4500Å,

but the first excited state of A_1 spatial symmetry undergoes a large red shift in the phenyldiazaazulene spectrum. These results are consistent with the Zeeman results on the diazaazulene phosphorescence origin, described above, which lead to the assignment of the triplet as $^3A_1(\pi\pi^*)$.

An interesting corollary to the question of the triplet state assignment is provided by a selective excitation experiment performed using the phenyldiazaazulene/dibenzyl and the diazaazulene/naphthalene systems. In this experiment, the fluorescence to phosphorescence intensities were measured as a function of the wavelengths of the exciting light. The experiment was performed by passing the light from a 500 W high pressure mercury lamp through a monochromator with a 20Å band pass, set at the various emission maxima of the mercury spectrum: 3020, 3122, 3342, 3655, 4045 and 4360Å. The first two of these lie above the naphthalene cut off, and the first three above the dibenzyl cut off. The intensities of the phosphorescence and fluorescence origin bands, and several prominent vibronic bands were measured at each of these excitation wavelengths. The following results were obtained.

For the diazaazulene/naphthalene system, the ratio of phosphorscence to fluorescence intensity was essentially unchanged by varying the exciting wavelength. The average deviation in the ratios was about 10%.

The phosphorescence to fluorescence intensity ratios of phenyldiazaazulene for the three exciting lines to higher energy of the dibenzyl absorption edge were equivalent. However, for excitation at 3650Å, within the 3800Å $^1A_1$ state of phenyldiazaazulene, the phosphorescence was enhanced by a factor of more than two, relative to the fluorescence. For excitation at 4045 and 4300Å, this was nearly reversed, and the fluorescence intensity was increased by a factor of about 1.7; relative to the phosphorescence. These results lead to the conclusion that intersystem crossing from S_2 ($^1A_1$) of phenyldiazaazulene into the triplet manifold may account for a significant portion of the phosphorescence. At the same time, intersystem crossing out of S_1 is shown to be a less favored process. A plausible explanation of the diazaazulene results is that internal conversion of S_1 ($^1B_1$) to S_1 is the favored relaxation route. Aside from its implications concerning radiationless transitions in the azaazulenes, the photoselection experiment on phenyl-diazaazulene/dibenzyl does provide a very attractive visual effect. The change in color of the emitted light, from purple at an exciting wavelength of 3000Å to deep red at 3650Å and finally a pale translucent blue at 4300Å is dramatic.

The Breakdown of Mirror Symmetry Between Fluorescence and Absorption

Within the Condon approximation, the probability of a transition from the zero point level of the ground state to an excited electronic state vibrational level is given by

$$I_{0,0}^{1,n_a} \alpha |\langle \psi_0 | \underset{\sim}{d} | \psi_1 \rangle \langle x_0 | x'_{n_a} \rangle|^2 \qquad (1)$$

when n quanta of vibrational mode a are excited in the upper electronic state. The corresponding transition is fluorescence has an intensity

$$I_{0,n_a}^{1,0} \alpha |\langle \psi_0 | \underset{\sim}{d} | \psi_1 \rangle \langle x_{n_a} | x'_0 \rangle|^2 \qquad (2)$$

If the ground and excited state nuclear configurations are sufficiently similar, so that the vibrational wavefunctions in the ground and excited state are the same, then the expressions above predict that the absorption spectrum (extending to higher energy) will be mirrored by the fluorescence spectrum (extending to lower energy) with the reflection plane at the origin band position. Two papers of historical importance are Strickler and Berg[51] and Birks and Dyson.[52] These workers expand on the theoretical basis described above to provide a means of comparing the fluorescence and absorption intensities of a molecule, and provide considerable experimental evidence that the mirror symmetry relationship is generally valid for condensed

aromatics. Birks and Dyson have also looked at the absorption and fluorescence of diphenyl polyenes, and found that the mirror symmetry relationship does not hold as well for those systems which, presumably, lack the rigidity to maintain the ground state geometry upon excitation.

The azaazulenes exhibit a significant departure from the assumption of mirror symmetry in the spectra of condensed aromatics. Eslinger[19] has observed these dissimilarities between the absorption and fluorescence spectra of the mono-azaazulenes, and this thesis has presented similar evidence for the diazaazulenes. A comparison of the bc' absorption and fluorescence spectra of diazaazulene/naphthalene, Figures 4 and 9 respectively, clearly demonstrates this. The band positions and intensities of the fundamentals are listed in Table 22. There are two possible a_1 correlations between the absorption and fluorescence spectra which would exemplify mirror symmetry: the 405 and 386 bands and the 696 and 678 bands. There are other bands which might be correlated on the basis of frequency, but the intensities are grossly different. For example, the 922, 870 cm^{-1} ground state modes might be correlated with the excited state frequencies, 904, 876 cm^{-1}. However, the two ground state bands are the strongest in the fluorescence spectrum while the excited state bands are two of the weakest fundamental absorptions. Another disturbing feature of these correlations is that there is no a_1 fluorescence in the 539, 575 band region, in which a

considerable amount of the absorption intensity is concentrated. The assignment of these modes as vibronic fundamentals and their marked medium dependence, were discussed in a previous section. That is, their frequencies change to 357 and 644 cm^{-1} in dichlorobenzene host and 384 and 660 cm^{-1} in quinazoline host. There are, then, two aspects of the problem of breakdown of mirror symmetry in electronic spectra. The first is the lack of correlation between absorption and fluorescence in a single medium. The second is the medium dependence of vibronic band positions and intensities within the absorption spectrum of a system, the fluorescence spectrum of which is <u>not</u> medium dependent.

The question of medium dependence of Herzberg-Teller vibronic bands was discussed in the Theory section, in light of the theory of moving levels. It was shown that the expression for the vibrational frequency of a vibronically active mode in the excited state, relative to the unperturbed ground state mode is

$$\Delta w = -\left(\frac{\hbar}{2w_a}\right) \frac{2(\alpha^a_{ij})^2}{\Delta E_{ij}} , \qquad (3)$$

when α^a_{ij} is the H-T vibronic coupling coefficient, and ΔE_{ij} is the energy gap between the two coupled states. It should be recalled that this expression neglects the quadratic contributions by assuming that their change in going from the

ground to excited state is negligible. The 539 and 575 bands have vibronic coupling energies of 440 and 520 cm^{-1} (Table 15), and substitution of these values into the frequency shift expression gives $\Delta\nu(575) = 100\ cm^{-1}$, $\Delta\nu(539) = 70\ cm^{-1}$. For the absorption spectrum in dichlorobenzene host, where $\Delta E = 8000\ cm^{-1}$, as compared to $5000\ cm^{-1}$ in naphthalene host, the shift values for the 357 and 644 bands are $130\ cm^{-1}$ and $140\ cm^{-1}$, respectively, using the coupling parameter given in Table 16. If instead, one assumes that the coupling parameters remain the same upon going from one host to the other, the shift values in dichlorobenzene host are reduced to $40\ cm^{-1}$ and $60\ cm^{-1}$. The problem is obviously plagued by a cyclical redundancy. The coupling coefficients are calculated in terms of the vibronic band intensity and the energy gap between the coupled states. However, in using the frequency shift equation one might wish to assume that the coupling strength remains the same, and explain the medium dependence of the vibronic band positions in terms of a change in the energy gap between the coupled states. This is the approach which Lacey, McCoy and Ross[10] take in explaining the shift in intensity of azulene from $1500\ cm^{-1}$ in the fluorescence spectrum to $1000\ cm^{-1}$ in the absorption.

In any case, the calculated shift values suggest that the excited state frequencies may be depressed by up to several hundred wavenumbers from the ground state frequencies. The difficulty in obtaining precise, quantitative results is

largely one of determining how much intensity is actually induced by a particular vibronically active mode. For the sake of argument, however, it is assumed that moderately large shifts can occur. If it is further assumed that 25% of the diazaazulene 4500Å a_1 absorption is vibronically induced, the total frequency shift is about 300 cm^{-1}. This is clearly insufficient to explain the lack of mirror symmetry between the ground and excited state frequencies. If, for example, the 539, 575 absorption fundamentals are correlated with the nearest fluorescence fundamentals, the 870, 922 bands, the total frequency shift is nearly 700 cm^{-1}, or twice that available under the generous assumption that one-quarter of the 4500Å absorption intensity is vibronically induced. These results make a strong case for the conclusion that the effect of frequency shifts of vibronically active levels is not sufficient to explain the lack of correlation between the ground and excited state frequencies of diazaazulene. It should not be inferred from this that the moving levels theory does not have its application in the spectra of other molecules. In the azulene 3500Å spectrum, for example, the amount of induced intensity is probably an order of magnitude greater than in the diazaazulene 4500Å absorption, while the energy gaps between coupled states are equivalent. Therefore, the effect of vibronic coupling in altering excited state frequencies would be similarly enhanced.

Although insufficient to explain the lack of mirror symmetry between the fluorescence and absorption spectra of diazaazulene's 4500Å state, the idea of vibronically perturbed excited state frequencies may be applied to the problem of the medium dependence of the vibronic band positions in the 300-700 cm^{-1} region of the absorption spectrum. It is quite clear from Table 3 that there is excellent correlation among the absorption spectra in the three hosts (naphthalene (N), dichlorobenzene (D) and quinazoline (Q)) except in the region between 300 and 700 cm^{-1}, and it is apparent that the 539, 575 bands in (N) correlate with the 357, 644 bands in (D) and the 384, 660 bands in (Q). There are several pertinent observations:

1) The energy gap between coupled states in (N) host is 5000 cm^{-1}, but is 8000 cm^{-1} in (D). This value is not known for (Q).
2) The total intensities of the two bands (oscillator strengths x 10^4) are 13.5 (N), 13.9 (D), 13.3 (Q), and these are equivalent to within experimental accuracy.
3) The relative intensities of the two bands within a particular host are I_{575}/I_{539} = 1.4 (N), I_{644}/I_{357} = 1.9 (D), I_{660}/I_{384} = 6 (Q).
4) The vibronic coupling coefficients are calculated to be C(539) = 440 cm^{-1},

$C(575) = 520\ cm^{-1}$, $C(357) = 600\ cm^{-1}$ and $C(644) = 820\ cm^{-1}$. Because the energy gap is not known, these values could not be calculated for quinazoline host.

5) Using these values for the coupling parameters and the energy gaps, the frequency shifts are calculated to be: $\Delta\nu(539) = 70\ cm^{-1}$, $\Delta\nu(575) = 100\ cm^{-1}$, $\Delta\nu(357) = 130\ cm^{-1}$, $\Delta\nu(644) = 140\ cm^{-1}$.

One interpretation of these data is as follows. Upon going from naphthalene to dichlorobenzene host, both the 539 and 575 bands are shifted to lower energy. Because it is the more strongly active mode, the 575 band undergoes a larger shift and the two bands are brought into near resonance at about $500\ cm^{-1}$. The interactions of these two modes then causes them to split apart, one moving to higher energy, the other lower energy. The situation is apparently much the same in quinazoline host as in dichlorobenzene, suggesting that the energy gap in quinazoline host is also near $8000\ cm^{-1}$. This interpretation is necessarily qualitative, and depends on rough estimates of the various interaction parameters. It gleans support from the fact that only two relatively close lying vibronic modes demonstrate this medium dependence. Moreover, while their frequencies and relative intensities change markedly between hosts, the <u>total</u> absorption intensity

of the two bands remains the same. In addition, while the frequencies of the other excited state modes are unchanged from one host to another, their intensities do differ, but in such a way that the total transition energy is relatively unchanged (cf. Tables 15 and 16). These results can be explained in terms of the Duschinsky effect, the rotation of ground state normal modes in the excited state, to produce a set of excited state normal coordinates which differ from the ground state normal modes by more than a simple translation of the origin.[36] This problem has been considered by Small,[37] who determines the excited state vibronic energies to be

$$\varepsilon_1(Q) = \varepsilon_1(0) + \sum_a V_{11}^a Q_a + \frac{1}{2} \sum_{a,b} V_{11}^{ab} Q_a Q_b + \sum_{a,b} V_{12}^a V_{12}^b Q_a Q_b / \Delta E_{1,2} \quad (4)$$

for an electronic state ψ_1 coupled to an electronic state ψ_2, and where the Q's are ground state normal coordinates. The V's are the Herzberg-Teller vibronic coupling coefficients, where, for example

$$V_{12}^a = \langle \psi_1(0) | (\frac{\partial H}{\partial Q_a})_0 | \psi_2(0) \rangle$$
$$V_{11}^{a,b} = \langle \psi_1(0) | (\partial^2 H / \partial Q_a \partial Q_b)_0 | \psi_1(0) \rangle \quad (5)$$

There are, then, two quadratic off-diagonal terms which can mix the ground state frequencies in the excited state, only one of which is dependent upon the energy gap between the

coupled electronic zero-order states. The coupling parameters in this term V^{a}_{12}, V^{b}_{12} are simply the linear Herzberg-Teller vibronic coupling coefficients, which are relatively large for the 539, 575 bands of diazaazulene/naphthalene. The other term, $V^{a,b}_{11}$, is not active in intensity borrowing, since it does not couple two excited states. Moreover, it does not depend upon the energy gap between the coupled states, and ΔE is apparently the active agent in the medium dependence of the 539, 575 bands.

The following is then postulated to explain the breakdown of mirror symmetry and the medium dependence of diazaazulene's 4500Å absorption.

1) The 539, 575 bands are the only a_1 modes which induce significant vibronic activity. They are therefore shifted down from their ground state positions by the diagonal "moving level" effect of Equation 3. Their frequencies are also altered by Duschinsky mixing with each other through the $(V^{a}_{12}\ V^{b}_{12}/\Delta E)$ term of Equation 4, and possibly with mixing with the other a_1 modes through the $V^{a,b}_{11}$ term. Because they are vibronically active modes, their frequencies are dependent upon ΔE, and therefore their frequencies are medium dependent.

2) Many of the other ground state fundamentals are mixed in the excited state through the $V_{11}^{a,b}$ term of Equation 4. Therefore, their frequencies and intensities cannot be correlated with the ground state frequencies. Some of the ground state normal modes do not undergo mixing. For example, the 405 and 696 fluorescence bands almost certainly correlate with the 386, 678 excited state modes. However, since none of these modes is active in intensity borrowing, their mixing is <u>independent</u> of the energy gap between S_1 and S_2, and their frequencies are independent of the medium.

3) For the vibronically active modes, there are two possible contributions to the Duschinsky mixing: the interstate coupling (V_{12}) and the intrastate coupling (V_{11}). Their relative magnitudes and algebraic signs are a matter of conjecture. It is possible that the interplay between these two terms, for vibronically active modes, could create a situation of constructive-destructive interference, making their apparent importance in determining the excited state

frequencies less than obvious. While one might estimate the interstate coupling from the experimental coupling coefficients, the magnitude of the intrastate mixing is not obtainable from experiment.

The Electronic States of Azulene and the Azaazulenes

As noted in the Introduction, the initial impetus of this work was to provide some insight into the azulene problem. As the preceding pages demonstrate, the azaazulenes provide sufficient problems in their own right, and the emphasis of this thesis has been on understanding the electronic and vibrational properties of the diazaazulenes. It seems appropriate, at this point, to comment briefly on the larger question of correlations and comparisons among azulene and the azaazulenes. Figure 26 is a graphical tabulation of the locations, intensities and symmetry assignments of two azulenes and four azaazulenes. The intensities are given as oscillator strengths, and are estimated in the cases of those states which strongly overlap. All of the intensity values in Figure 26 were calculated by this author, except in the case of azulene for which these intensities are well-known.[9] These solution spectra are all reproduced in this thesis: diazaazulene, Figure 16; azulene, Figure 17; phenyldiazaazulene, Figure 20; phenylazulene, Figure 27; chloromonoazaazulene, Figure 28;

and phenylmonoazaazulene, Figure 29. The locations of the states are estimates of the origin band position, taken preferably from mixed crystal spectra, but from solution spectra where necessary.

The symmetry assignments for diazaazulene and phenyldiazaazulene have been established in this thesis. Those for azulene are from Lacey.[9] Eslinger[19] has established the symmetry of the lowest state of the monoazaazulenes as $^1B_1$, although the lack of the C_{2v} symmetry among the monoazaazulenes makes the question of symmetry assignments somewhat nebulous. The phenylazulene spectra were taken by Small.[53]

The symmetry assignments of the lowest $\pi\pi^*$ state as $^1B_1$, and of S_4 as $^1A_1$ are certain for all six molecules. The correlations among the intensities are particularly convincing. The assignments of the second and third excited singlets of the monoazaazulenes are this author's reassessment of Eslinger's polarization results,[19] and are supported by the solution spectra. In the S_2 region of the chloroazaazulene absorption spectrum (Figure 28) there is a relatively weak peak at 28500 cm^{-1}, denoted as B, followed by an intense peak at 29600 cm^{-1} (A). The spectrum of phenylazaazulene (Figure 29) shows an intense absorption at 26400 cm^{-1} (A), which is not preceded by the weak peak found in the chloroazaazulene spectrum. Both spectra exhibit a second strong absorption

at 31000 cm^{-1} in the chloroazaazulene spectrum (A'), and at 27300 in the phenylazaazulene spectrum (A'). It is apparent that these strong absorption peaks, separated by 1400 cm^{-1} for both molecules, are part of the same absorption system, which undergoes a red shift upon phenyl substitution. There are two other peaks which also belong to this state (A" and A'"). The remaining absorption peaks are relatively unchanged by the phenyl substitution, so that the phenylazaazulene spectrum has a peak at 28500 cm^{-1}, which correlates with (B) of the chloroazaazulene spectrum. This tendency toward red shift of the A_1 states, along with intensification of the transition, is similar to that observed for the diazaazulenes. The B_1 states are relatively unaffected, if anything shifting slightly to the blue. In light of these assignments of the azaazulene states, a comparison of the azulene and phenylazulene spectra presents an interesting observation. The azulene spectrum (Figure 17) commences with a weak band at 28400 cm^{-1}, followed by an intense peak at 29400 cm^{-1}, and a second moderately intense peak at 30700 cm^{-1}. The phenylazulene spectrum, however, begins with a strong absorption at 25700 cm^{-1}, followed by a second intense peak at 26900 cm^{-1}. There is a third, weaker absorption maximum at 28200 cm^{-1}. The parallel between this situation and that of the monoazaazulenes is striking, and would lead to the conclusion that there is a B_1 state near or, in fact, <u>below</u>

the 3500Å A_1 state of azulene. The fact that the 3500Å state is $^1A_1$ is well established from mixed crystal spectra, and there is no evidence of B_1 absorption in the region. However, it should be recalled that the A_1 absorption system exhibits extremely narrow line widths in the mixed crystal at 4.2°K (on the order of a wavenumber). A broad B_1 absorption system in the region would have a maximum optical density of only a few percent of that of the sharp A_1 absorption, and might well be lost in the background, even though its integrated intensity is comparable to that of the A_1 transition. The experimental evidence for this assignment is less than adequate, and is presented here with that firmly in mind. The assignments in Figure 26 are the best possible on the basis of the present evidence, but obviously present an incomplete picture of the azaazulenes' excited states. For instance, no $n\pi^*$ states have been assigned, although it is likely that they lie within the manifold of states shown in Figure 26. The prospect of this detection is unlikely since they must overlap the intense $\pi\pi^*$ states in the region.

CONCLUSIONS

The electronic absorption and luminescence spectra of 1,3-diazaazulene and 2-phenyl-1,3-diazaazulene in mixed crystals have been obtained. Analyses of the spectra have led to assignment of the excited electronic state spatial symmetries and of ground and excited state vibrational fundamental frequencies. Particular attention has been paid to the medium dependence of vibrational bands in the S_1 absorption system of diazaazulene, and to the breakdown of mirror symmetry between the absorption and fluorescence spectra. In addition an attempt has been made to correlate the excited states of azulene and the azaazulenes.

The stated goal of the study of the electronic spectra of the azaazulenes was to provide some insight into the azulene problem. It has become apparent that the azaazulenes are sufficiently different from azulene that this objective cannot be completely satisfied. However, there is considerable evidence that the azaazulenes, particularly diazaazulene, exhibit in a limited fashion, those features of the azulene spectra which make its analysis so complex. The various manifestations of vibronic coupling, including intensity borrowing, moving levels, vibronic resonances, and Duschinsky mixing, which have been invoked to explain the vibrational structure of azulene's S_2 absorption, have been identified above for diazaazulene. The importance of the diazaazulene

spectra lies in the considerably lesser extent to which these effects occur. For example, the 539, 575 bands in diazaazulene's S_1 absorption spectrum appear to be a model case of a two-level vibronically active system, a useful approximation in considering vibronic effects. As the subsequent two parts of this thesis will demonstrate, the well defined nature of the 539, 575 bands makes them a useful tool for investigating the dependence of two spectral phenomena, the Stark effect and the electron-phonon coupling, on the final vibron level of a transition.

The electronic spectroscopy of diazaazulene and phenyldiazaazulene in mixed crystals may be considered to be completed, in terms of S_0 and S_1 vibrational frequencies and some of the higher electronic state spatial symmetries. Although other host materials might be found for the diazaazulenes, it is unlikely that their spectra will provide any significant additional insights. Further Zeeman studies of the phosphorescence spectrum, to confirm the assignment of the phosphorscent triplet as $^3A_1$, would be of value. Determination of the ground and excited state normal coordinates and force fields would be a first step toward a more complete understanding of the manifestation of the Duschinsky effect in mirror symmetry breakdown. Work is in progress to determine the Duschinsky mixing in isotopically related molecules,[54,55] and hopefully these results may lead to its extension to the azaazulenes.

PART II. STARK SPECTRA OF 1,3-DIAZAAZULENE MIXED CRYSTALS

INTRODUCTION

The use of electric field splitting of lines in the optical spectra of molecular crystals was first reported by Hochstrasser and Noe[56] as a method for determining excited state dipole moments of polyatomic molecules. Since then, the technique has been applied to a number of neat and mixed crystals, and many of these results are summarized by Hochstrasser.[57] We have previously reported the Stark spectra of 1,3-diazaazulene in naphthalene,[58] and determined the ground and excited state dipole moments to be: $\mu(S_0) = +2.98 \pm 0.01$ D; $\mu(S_1) = +1.18 \pm 0.05$ D; $\mu(T_1) = +1.88 \pm 0.07$ D. The positive sign indicates that the dipole points toward the 2-position of diazaazulene. A surprising feature of these results is that, while the dipole moment change upon excitation to S_1 is 1.80 D for the origin band and the vibronic fundamentals at 386, 678, 876 and 956 cm^{-1}, the value calculated for the 539 and 575 cm^{-1} bands is 1.98 D. The difference is well outside of experimental error. This led us to consider under what condition the Stark spectrum of a mixed crystal guest should depend upon the final vibronic level of the transition. It also suggested a pertinent experiment. The 539, 575 bands in naphthalene host were correlated with the 384, 660 bands in quinazoline host. If these correlations are correct, we might expect to observe a similar vibron level dependence of the Stark spectrum of the 384, 660 bands of diazaazulene in quinazoline.

In its simplest form, neglecting the possible effects of vibronic excitation, the theory of Stark splitting in molecular mixed crystals is as follows.[57] Suppose that an electric field is impressed across a crystal, such that it lies either parallel or perpendicular to one of the symmetry axes of the crystal. Then the axes of the molecules related by that symmetry axis will make the same squared projections ($\cos^2\theta$) on the electric field. If those molecules possess permanent dipole moments, the cosine of the angle between the electric field and that dipole may be positive or negative. In the event that the product $\underset{\sim}{E}\cdot\underset{\sim}{\mu}_1 = |\underset{\sim}{E}||\underset{\sim}{\mu}_1| \cos\theta$ is positive this interaction is attractive, and the molecules have their energy lowered by the field. For those molecules for which $\cos\theta < 0$, the interaction is repulsive, and the molecular energies are increased. The same situation occurs in the excited state, and leads to a separation of the excited state energies of $2|\underset{\sim}{E}||\underset{\sim}{\mu}_2| \cos\theta$. The spectral manifestation of this is a splitting of the absorption or emission bands given by

$$\Delta w \propto 2|E \cos\theta \ (\underset{\sim}{\mu}_1 - \underset{\sim}{\mu}_2)| \qquad (1)$$

where E is the magnitude of the electric field at the molecular site. Therefore, by measuring the splitting of spectral bands of a crystal in an electric field, one may determine the <u>magnitude</u> of the change in dipole monent upon excitation. Under some conditions, it is possible to make a

reasonable assumption concerning the direction of the dipole change, and, with a knowledge of the ground state dipole moment, determine the excited state dipole moment. Such was the case with the diazaazulene/naphthalene results, for which it was argued that it is reasonable to assume that charge flows from the five- to the seven-membered ring upon excitation, reducing the dipole moment from 2.98 D in the ground state to 1.18 D in the first excited singlet state.[58]

θ, in Equation 1, is the angle that the permanent dipole of the molecule makes with the electric field. Since the electric field is to be directed parallel or perpendicular to a crystallographic axis, $\cos\theta$ is simply the appropriate direction cosine of the host crystal. Finally, E is the magnitude of the electric field at the guest molecule. In a molecular crystal this differs from the applied field because of the local effects due to induced dipoles of the host molecules. Hochstrasser[59] has shown that the local field E_L is, to a good approximation, related to the applied field E_A by

$$E_L = E_A[(\varepsilon_i+2)/3] \qquad (2)$$

where ε_i is the dielectric constant of the crystal in the field direction. Taking these factors, and the appropriate conversion constants into account, the Stark splitting for a monoclinic host crystal is given by

$$\Delta w_i(cm^{-1}) = 0.560\ (\varepsilon_i+2)E_A G_i |\Delta\mu|\ (debye) \qquad (3)$$

where the subscript i labels the field direction, and G_i = $2\cos\theta_i$. E_A is in units of 10^5 V/cm.

EXPERIMENTAL

The Stark spectra of diazaazulene/naphthalene were taken in Lin's lab, and the experimental details of that determination are given in reference 58. The ground state dipole moment was measured in this lab, using the heterodyne beat method and apparatus of Vandenbroucke, et al.[60]

For the Stark spectra of diazaazulene/quinazoline, mixed crystals of 10^{-3} mole/mole concentration were grown from the melt in a Bridgman furnace, and sections parallel and perpendicular to the cleavage plane were cut from this ingot. Since the crystal structure and optical properties of quinazoline are not known, it was necessary to proceed by trial and error to obtain a face that exhibited the splitting requisite for accurate Stark measurements. The face finally chosen was the xy face, as defined in the Experimental section of the first part of this thesis. The long axis of the diazaazulene molecule appears to be nearly perpendicular to the face, since no splitting was observed for the other two faces. That is, the dipole moment of diazaazulene is directed along the long axis, so that the splitting is proportional to the projection that the electric field makes on the long axis. The crystals were polished to flatness, and mounted between quartz optical flats which had been coated with tin oxide. The DC potential was supplied by a Sorensen model 1030-20 high voltage power supply (30 KV, 20 ma maximum). The

applied field strength was measured using a high voltage probe (Fluke, Model 80F-15) with a ratio accuracy of ±0.05% and a digital voltmeter (Keithley Model 168) with an accuracy of 0.1%. Crystal thicknesses were measured with a micrometer, and are accurate to within 0.5%.

The band splittings were determined by fitting the observed band profiles to a sum of two Lorentzians. Experience has shown that, while a band profile may exhibit significant Gaussian character, this is most severely manifest at large distances from the band center, where a Lorentzian profile decreases less rapidly than a Gaussian. Nearer the band center, the Gaussian and Lorentzian band shapes are nearly identical. For this reason only the experimental band profile above half peak height was used in the fitting procedure. The diazaazulene/quinazoline spectra were photographed in 13th order on a Jarrell-Ash Ebert spectrograph with a grating blazed for 57000Å in first order. This gave a reciprocal linear dispersion of 0.34Å/mm in 13th order. The spectra were then recorded on a strip chart using a scanning microdensitometer. In this way it was possible to make band intensity vs position measurements in tenth- to quarter-wavenumber increments, so that up to 40 experimental points were obtained for each fitting procedure. In addition, at the higher voltages, where the two Stark components were essentially resolved, the splitting could be measured directly

by estimating the band centers of the two peaks. The agreement between the curve fit and direct measurement data was excellent. The slopes of the splitting vs voltage lines were calculated by a linear least-squares fit, and the quality of the least-squares fit was checked by calculation of the standard deviation and by observing the effect of sequential weightings of the (o-voltage, o-splitting) point on the calculated slope. That is, in the absence of an applied field the spectral lines are not split and therefore the splitting vs voltage line should intercept at the origin. To test this the least-squares fit was performed first excluding the origin, then weighting it by a factor of one and then two. For the five band splittings reported here, the largest deviation occurred for the 384 band, for which the calculated slope varied by about four percent over the three weightings. For the other bands the deviations were less than one percent.

RESULTS

The Stark splittings of five absorption bands ((0,0), 372, 384, 660, 734 cm^{-1}) in the diazaazulene/quinazoline 4500Å transition were measured, and their slopes are given in Table 23. The spectral region including these five bands is shown in Figure 30, and the splitting vs voltage curves are shown in Figures 31-35. The origin and 372 and 734 bands exhibit the same Stark splittings to within experimental uncertainty. The slopes of the 384 and 660 band splitting are three to four percent less than those of the other bands, and this difference is outside of experimental error. It should be emphasized that the actual calculation of the change in dipole involves considerable uncertainty, through measurement of the crystal thickness and applied field, and the assumptions concerning the relationship of the applied to the local field. A reasonable estimate of this error is on the order of two to five percent. However, these difficulties are not pertinent to the relative magnitudes of the slopes given in Table 23, since all of the data were taken using the same crystal, under identical experimental conditions. The only uncertainty that remains is in measuring the splittings, and the small standard deviations of the slopes make a strong case for the accuracy of these determinations. To provide a measure of the magnitude of the dependence of the excited state dipole on the vibron level, the values of $|\Delta\mu|$ are given in Table 23,

assuming that the change in dipole of the origin band is the same in quinazoline as in naphthalene host. This is probably a bad assumption, certainly an unfounded one, and serves only to illustrate the magnitude of the effect in a convenient unit, debyes.

These results confirm that the 384, 660 bands in quinazoline host exhibit the same kind of vibron level dependent dipole moments as the 539, 575 bands in naphthalene host, and substantiate the correlation of these two sets of bands. At the time of this writing, Stark measurements are being made in this laboratory on the azulene/naphthalene 3500Å transition, for which strong vibronic coupling is observed. Preliminary results indicate that this system also exhibits vibron level dependent dipole moments.

THEORY AND DISCUSSION

The object of this section is to provide a theoretical basis for understanding the above results. It is not possible, in the absence of detailed vibrational and electronic wavefunctions to calculate the interaction matrix elements which will be derived. However, model calculations, using experimentally justifiable parameters, will be performed to underscore the applicibility of the theory. The basic premise is this. In writing an electronic wavefunction for a vibronically perturbed state one mixes in some character of the coupled state through the normal coordinates of the perturbed state. If these vibronically coupled wavefunctions are to be used to calculate transition dipole moments, they should also be used to calculate permanent dipole moments. The dipole moment of the state of interest will then depend, to some extent, upon the dipole moment of the state to which it couples. In general terms this can be expressed as follows. Assume we have two excited zeroth order states ϕ_1^0 and ϕ_2^0 which are coupled through the vibrational normal modes Q of ϕ_1^0. Then the vibronic wavefunction for ϕ_1 is given by

$$\phi_1 = \phi_1^0 + A(Q)\,\phi_2^0 \qquad (1)$$

where A(Q) is a collection of the appropriate vibronic coupling matrix elements. If $\underset{\sim}{d}$ is the dipole moment operator,

the dipole moment of a vibronic level $x_{1,\alpha}$ in electronic state ϕ_1 is given by

$$\underset{\sim}{\mu}_{1,\alpha} = \langle(\phi_1^0 + A(Q)\phi_2^0)x_{1,\alpha}|\underset{\sim}{d}|(\phi_1^0 + A(Q)\phi_2^0)x_{1,\alpha}\rangle \tag{2a}$$

$$\underset{\sim}{\mu}_{1,\alpha} = \langle\phi_1^0|\underset{\sim}{d}|\phi_1^0\rangle\langle x_{1,\alpha}|x_{1,\alpha}\rangle + 2\langle\phi_1^0|\underset{\sim}{d}|\phi_2^0\rangle\langle x_{1,\alpha}|A(Q)|x_{1,\alpha}\rangle + \langle\phi_2^0|\underset{\sim}{d}|\phi_2^0\rangle\langle x_{1,\alpha}|A(Q)^2|x_{1,\alpha}\rangle \tag{2b}$$

$$\underset{\sim}{\mu}_{1,\alpha} = \underset{\sim}{\mu}_1^0 + 2\,\underset{\sim}{M}_{1,2}^0\langle x_{1,\alpha}|A(Q)|x_{1,\alpha}\rangle + \underset{\sim}{\mu}_2^0\langle x_{1,\alpha}|A(Q)^2|x_{1,\alpha}\rangle \tag{3a}$$

In Equation 2, the dipole moment operator $\underset{\sim}{d}$ is the sum of the electronic and nuclear dipole moment operators, $\underset{\sim}{d}_e + \underset{\sim}{d}_N$. In writing Equation 3, the assumption has been made that the nuclear dipole moment provides only a constant contribution to the Condon dipole moments. That is, it is not considered to make a contribution to the vibron level dependence of the total dipole moment. To show this, we expand the nuclear dipole moment operator in terms of the vibrational normal coordinates

$$\underset{\sim}{d}_N = \underset{\sim}{d}_N^0 + \sum_a \left(\frac{\partial \underset{\sim}{d}_N}{\partial Q_a}\right)_0 Q_a \tag{3b}$$

Higher order derivatives are zero, since the nuclear dipole moment operator has a linear dependence on the normal

coordinates. Then the nuclear contribution (μ_N) to the molecular dipole moment is

$$\underset{\sim}{\mu}_N = \underset{\sim}{d}_N{}^0 \langle \Psi_{1\alpha} | \Psi_{1\alpha} \rangle + \sum_a \left(\frac{\partial \underset{\sim}{d}_N}{\partial Q_a}\right)_0 \langle \Psi_{1\alpha} | Q_a | \Psi_{1\alpha} \rangle \qquad (3c)$$

$$= \underset{\sim}{\mu}_N{}^0 + \sum_a \left(\frac{\partial \underset{\sim}{d}_N}{\partial Q_a}\right)_0 \langle x_{1,\alpha}\, A(Q) | Q_a | x_{1,\alpha}\, A(Q) \rangle \qquad (3d)$$

where $\Psi_{1,\alpha}$ is the adiabatic wavefunction of Equations 2. In the harmonic approximation, only even powers of Q will make the integrand in Equation 3d nonzero. Since the lowest dependence of A(Q) on Q is linear, (vide infra), the lowest even power of Q in Equation 3d is the quartic. We consider the quartic contribution to be negligible.

Two observations are made concerning Equation 3a. First, the vibronic dipole moment of state ϕ_1 depends on the permanent dipole moment of the state to which it couples, and upon the intensity of a transition between these two states. Secondly, in the harmonic approximation only those terms in A(Q) which are of even powers in the normal coordinate Q_α will contribute to the vibronic dipole moment. Limiting the perturbation to the harmonic terms, only $Q_\alpha{}^2$ will contribute, and Equation 3 may be written as

$$\underset{\sim}{\mu}^e_{1,\alpha} = \underset{\sim}{\mu}_1{}^0 + (2\, \underset{\sim}{M}_{1,2}\, A^\alpha_{1,2} + \underset{\sim}{\mu}_2{}^0\, B^\alpha_{1,2}) \frac{\hbar}{2w_\alpha} (2v_\alpha + 1) \qquad (4)$$

where v_α is the number of quanta of Q_α excited, and w_α is the fundamental frequency. $A^\alpha_{1,2}$ and $B^\alpha_{1,2}$ are the appropriate vibronic coupling matrix elements. The importance of Equation 4 is that it shows that there will be a vibronic dipole moment contribution to the <u>zero</u> vibron level of state ϕ_1. Also, while equation 4 has been written for a single vibronic level Q_α, the complete expression would consist of summation over all vibronically active modes and coupling states. The derivation of $A^\alpha_{1,2}$ and $B^\alpha_{1,2}$ is somewhat tedious, but straightforward. The electronic hamiltonian is expanded in the excited state normal coordinates to give the perturbation

$$H' = \sum_a \left(\frac{\partial H}{\partial Q_a}\right)_0 Q_a + \frac{1}{2} \sum_{a,b} \left(\frac{\partial^2 H}{\partial Q_a \partial Q_b}\right) Q_a Q_b \qquad (5)$$

The excited state wavefunction ϕ_1 is then corrected to second order, and terms higher than quadratic are neglected. The result, for one coupling, state $\phi_2{}^0$, is

$$\underset{\sim}{\mu}_1 - \underset{\sim}{\mu}_1{}^0 = \sum_a \frac{\hbar}{2w_a} (2v_a+1)\left\{\frac{(\alpha^a_{12})^2}{\Delta E^2_{1,2}} \underset{\sim}{\mu}_2{}^0 - 2\left(\frac{\beta^a_{1,2}}{\Delta E_{1,2}} + \frac{\alpha^a_{12}(\alpha^a_{11} - \alpha^a_{22})}{\Delta E^3_{1,2}}\right) \underset{\sim}{M}^0_{1,2}\right\}$$

... (6)

where $\alpha^a_{1,2} = \langle \phi_1{}^0 | (\frac{\partial H}{\partial Q_a})_0 | \phi_2{}^0 \rangle$

$\beta^a_{1,2} = \langle \phi_1{}^0 | \frac{\partial^2 H}{\partial Q_a{}^2})_0 | \phi_2{}^0 \rangle$

$\Delta E_{1,2} = |E^o_1 - E^o_2|$

Before considering the implications of this result, we will estimate its magnitude with vibronic coupling parameters taken from the diazaazulene/naphthalene 4500Å spectrum (Table 15). For w = 575 cm^{-1}, $(\hbar/2w)^{1/2}$ = .324 amu - $a_o{}^2$. From Table 15, $\alpha^a_{12}\langle 0|Q|1\rangle$ = 500 cm^{-1}, so let $\alpha^a_{12} \sim 1500$ cm^{-1} $amu^{-1/2}$ $a_o{}^{-1}$, and let $\underset{\sim}{\mu}^o_2$ = 2 Debye. Then, for the first term in Equation 6, we obtain, for $\Delta E = 5000$ cm^{-1}.

$$(\hbar/2w_a)(2\nu_a+1)(\frac{\alpha^a_{12}}{\Delta E_{1,2}})^2 \underset{\sim}{\mu}_2{}^0 = (.02)(2\nu_a+1) \text{ debye} \qquad (7)$$

The term in $\underset{\sim}{M}^c_{1,2}$ is harder to estimate, since the transition intensity between the excited states is not known, nor are the quadratic coupling coefficients $\beta^a_{1,2}$. However, if we assume $\beta \sim \alpha/10$, and $\underset{\sim}{M}^o_{1,2} \sim 2$ debyes (an oscillator strength of about 0.3) we obtain the result that

$$2\,\hbar/2w_a\,(2\nu_a+1)\,\frac{\beta^a_{1,2}}{\Delta E_{1,2}}\,\underset{\sim}{M}^o_{1,2} = (0.01)(2\nu_a+1) \text{ debye} \qquad (8)$$

Finally, we can evaluate the terms $\alpha_{12}(\alpha_{11}-\alpha_{22})$ by noting the $(\alpha_{11}-\alpha_{22})$ is the displacement of the potential minimum along Q between states ϕ_1 and ϕ_2.[47] In terms of the dimensionless constant $D = (Q_a'-Q_a'')(w/\hbar)^{1/2}$

$$|\alpha_{11}-\alpha_{22}|(\hbar/2w)^{1/2} = 2^{-1/2}\ w\ D \tag{9}$$

substituting this into Equation 10 we obtain

$$2(\hbar/2w)^{1/2}\ (2v_a+1)\ \frac{\alpha_{12}}{\Delta E_{1,2}^2}\ \ 2^{-1/2}\ w_a\ D\ \underset{\sim}{M}^{o}_{1,2} =$$

$$(0.03)\ D\ (2v_a+1)\ \text{debye} \tag{10}$$

For transitions from the <u>ground</u> state to the excited state, D has a maximum value of about 1.[47,48,49] Therefore, Equation 10 may be expected to provide a significant contribution to the vibronic Stark splitting when the displacement of normal coordinates between the two coupled states is large.

The values of two of the parameters used in evaluating Equations 7-10, $\underset{\sim}{M}^{o}_{1,2}$ and D, are not readily available from experiment, and estimates of their importance in induced dipole moments are consequently hindered. The value of D = 1 is an upper limit of sorts. The value of 2 debyes for $\underset{\sim}{M}_{1,2}$ is a less obvious choice, and it may in fact be considerably

less. Pariser[43] has calculated the $T_j(B_1) \leftarrow T_1(B_1)$ oscillator strengths for azulene, and gives a value of 0.01 for the oscillator strength of the $^3B_1(2) \leftarrow ^3B_1(1)$ absorption. This corresponds to a dipole length of 0.07 debye. Under the assumption that the oscillator strength should not be significantly different for the singlet-singlet transition, Small and Kusserow[32] use this value in an investigation of vibronic effects in azulene's lowest excited singlet state. A value of $\underset{\sim}{M}_{1,2}$ this small would render the contribution of Equations 8-10 negligible in the induced dipole moment. It will be argued below that, because of the medium dependence of the induced dipole moment, the cumulative contribution of terms in $\underset{\sim}{M}_{1,2}$ must be significant.

Equation 6 is strictly valid only within the harmonic approximation, since we have neglected the linear terms under the assumption that $\langle v|Q|v\rangle = 0$. To take the anharmonicity into account we need to correct the vibrational wavefunctions through the third order correction to the electronic energy. For one coupling state ϕ_2^0 and one coupling mode Q

$$E_1^{(3)} = \left(\frac{\alpha_{12}}{\Delta E_{12}}\right)^2 (\alpha_{22}-\alpha_{11})Q^3 \qquad (11)$$

$$= A_{1,2}\, Q^3$$

such that

$$|v^{ah}\rangle = |v^{h}\rangle + A_{12}\frac{\langle v|Q^3|v+1\rangle}{\hbar w_f}|v+1\rangle$$

$$+ A_{12}\frac{\langle v|Q^3|v-1\rangle}{\hbar w_f}|v-1\rangle \qquad (12)$$

where w_f is the frequency of the coupling mode. Then

$$\langle v^{ah}|Q^3|v^{ah}\rangle = 6\left(\frac{\alpha_{12}}{\Delta E_{12}}\right)^2\left(\frac{\hbar}{2w}\right)^{3/2}\frac{\alpha_{22}-\alpha_{11}}{\hbar w_f}$$

$$\{(v+1)^2 + v^2\} \qquad (13)$$

but $(\hbar/2w)^{1/2}(\alpha_{22}-\alpha_{11}) = 2^{-1/2}\,\bar{w}\,D$

so

$$\langle v^{ah}|Q^3|v^{ah}\rangle = \sqrt{18}\left(\frac{\alpha_{12}}{\Delta E_{12}}\right)^2\frac{\hbar}{2w}D\,((v+1)^2 + v^2) \qquad (14)$$

Substituting this into the linear term in Equation 3

$$\underset{\sim}{\mu}_{\ell}^{ah} = \underset{\sim}{M}^{o}_{1,2}\left(\frac{\alpha_{1,2}}{\Delta E_{1,2}}\right)^3\sqrt{18}\,D\,(\hbar/2w)^{3/2}\,((v+1)^2 + v^2) \qquad (15)$$

using the values of these parameters used above, we obtain

$$\underset{\sim}{\mu}_{\ell}^{ah} = 7.3\times10^{-3}\,D\,((v+1)^2 + v^2)\ \text{debye} \qquad (16)$$

or, for v=1, D=1

$$\underset{\sim}{\mu}_{\ell}^{ah} = 0.036 \text{ debye} .$$

Therefore, the anharmonicity, for large D, may comprise a substantial portion of the induced dipole moment. In writing Equation 15 we have adhered to the assumption that only one excited state ψ_2^0 couples to our state of interest, ψ_1^0. For other coupling states, Equation 15 would be a sum over the appropriate terms. An interesting feature of Equation 15 is that its dependence on the vibrational quantum number is considerably different from that found for the harmonic terms. Therefore, for equal values of the coupling coefficients, the harmonic terms will make a greater contribution to the zero point level dipole moment than will the anharmonic terms.

Having provided justification for the importance of vibronically induced dipole moments, attention is now turned toward an examination of the implications of Equations 6 and 15. The terms in these expressions depend upon one of two vector quantities, and for diazaazulene's totally symmetric coupling, both, $\underset{\sim}{\mu}_2$ and $\underset{\sim}{M}^{o}_{1,2}$, are directed along the long axis of the molecule (the C_2 rotation axis). However, the phase of $\underset{\sim}{M}^{o}_{1,2}$ is not known, so that it may add either constructively or destructively to $\underset{\sim}{\mu}_2^0$. If in fact they do add destructively, and are of the same magnitude, than the observed induced

dipole moment might be considerably less than either of the two individual terms. An interesting consequence is that the vibronic dipole moments could exhibit a medium dependence similar to that described above for the frequencies of vibronically active modes (the moving levels theory). That is, the various terms in Equations 6 and 15 have different dependences on the energy gap between the coupled states, and therefore a change in the energy gap will alter the relative magnitudes of the terms in $\underset{\sim}{M}^{o}_{1,2}$ and $\underset{\sim}{\mu}^{o}_{1,2}$. This may well be the case for the diazaazulene Stark spectra, for which the splittings of the vibronically induced modes in naphthalene host are 10% greater than that of the origin, while in quinazoline host their splittings are 5% less than the origin band splitting. Other effects, such as a change in $\underset{\sim}{M}^{o}_{1,2}$, may also be determining factors in the medium dependence of the Stark splitting. The fact that we do observe this medium dependence indicates that the terms in $\underset{\sim}{M}^{o}_{1,2}$ are of the same magnitude as those in $\underset{\sim}{\mu}^{o}_{2}$, since the terms in $\underset{\sim}{\mu}^{o}_{2}$ can make only a positive contribution to the dipole moment change.

An important feature of Equations 6 and 15 is that they show that the dipole moment of the zero-point level of an electronic state will have a vibronically induced component if there are vibronically active modes built upon it. For diazaazulene, with its large permanent dipole moment, the

percentage of induced dipole is small. However, for a molecule like phenanthrene, with an S_1 dipole moment of 0.3 debye,[57] and for which nearly half of its intensity is vibronically induced[30] the induced dipole moment may be considerably more important.

CONCLUSIONS

As noted above, the theory presented here is a necessarily qualitative basis for understanding the phenomenon of vibron level dependent dipole moments. We have intentionally excluded the possibility of more than one coupling electronic state to make the evaluation of the vibronic coupling parameters tractable. The theory as presented is then sufficient to explain the diazaazulene Stark spectra in terms of vibronically induced dipole moments. Unfortunately, the diazaazulene results comprise a limited body of data. In particular, they exclude Stark measurements on nontotally symmetric (b_1) vibronic bands. This is a necessary evil with the experimental set up used, since the b_1 bands are polarized along the long axis of the molecule. However, for Stark splittings large enough to make accurate comparisons of the splittings of various bands, that crystal face must be used which exhibits the smallest projection of the long axis. The b_1 components are not observed for spectra of this face. The work in progress in this lab on the vibronic Stark spectra of azulene's 3500Å $^1A_1$ state may circumvent this problem, since the b_1 components are polarized along the short axis in that spectrum. Hopefully, future work on the Stark spectra of polyatomic molecules will be extended to include the splittings of bands other than the origin band. Data on other vibronically active and inactive systems would be very

useful in assessing the importance of vibronically induced dipole moments.

PART III. ELECTRON-PHONON COUPLING IN MOLECULAR MIXED CRYSTALS

INTRODUCTION

The manifestations of the electron-phonon interaction in the electronic spectra of impurity ions or molecules in a host medium include low frequency phonon structure and the thermal broadening and shift of the impurity zero-phonon bands. Because one is concerned with an impurity transition the symmetry considerations for the electron-phonon interaction derive from the group of the impurity site. Thus, in molecular systems, for example, where the impurity site group contains only the identity element, all the system phonons may couple with the electronic transition. Such is the case for the molecular systems we consider. The situation, therefore, is quite different from that for an exciton transition of the crystal where the reduced wavevector k may represent a good quantum number.

In an impurity electronic transition the intensity of the zero-phonon band relative to the multi-phonon bands building on it, is a measure of the electron-phonon coupling strength. Specifically, it is usually considered to be a measure of the linear electron-phonon coupling strength. The usual linear coupling arises from the translational displacements of the equilibrium positions of the phonon oscillator coordinates between the two electronic states of the transition. Thus, the phonon intensity distribution is adequately treated in terms of the Franck-Condon principle. An alternative

mechanism for multi-phonon transitions arises through the dependence of the electronic transition moment on the phonon oscillator coordinates. We refer to the mechanism as phononic coupling in order to distinguish it from the Condon mechanism. To our knowledge, the importance of phononic coupling in impurity transitions has not been established experimentally, although it is probably minor relative to the Condon mechanism. This is by no means the case for the phonon structure associated with a zero-phonon exciton band.

The thermal broadening and shift of an impurity zero-phonon band is also a measure of the electron-phonon coupling strength. However, when anharmonic and nonadiabatic effects are negligible, both the broadening and shift arise through the quadratic electron-phonon coupling. Specifically, thermal broadening is usually considered to arise from the phonon analogue of the molecular Duschinsky effect.[36,37] The line shift is a consequence of the differences in the phonon frequencies between the two electronic states of the transition.

With regard to the thermal broadening and shift of impurity zero-phonon bands, two types of systems have been the principal subjects of previous workers. Perhaps the best characterized of these is the impurity ion/inorganic mixed crystal[61-63] in which the electron-phonon coupling is weak in contrast, for example, with F centers in alkali halides[64]

the impurity site in systems which exhibit several energetically different sites for the chemical impurity.[67-69] The first of the two systems chosen for this study is the 7000Å $^1B_1 \leftarrow {}^1A_1$ absorption system of azulene in naphthalene. The vibronic structure of this transition is well characterized and has recently been shown to exhibit several b_1 vibronic origins.[32] The second system is the 5600Å $^1B_1 \leftarrow {}^1A_1$ transition of 2-phenyl-1-monoazaazulene in p-terphenyl.[19] The absorption system exhibits twelve well resolved site origins with a maximum site splitting of 387 cm^{-1}. Thermal broadening data (for both systems) and line shift data for the latter system have been obtained over a temperature range of 4.2-28°K (ca. half the effective Debye temperature). The results of this investigation show that, within the harmonic approximation, the quadratic electron-phonon coupling is independent of the final vibron level of the transition. Therefore, the observation of a dependence of the zero-phonon band thermal band broadening on the final impurity vibron level of the electronic transition can be ascribed to system anharmonicity. More specifically, the intermolecular anharmonic terms of importance depend on both the phonon and vibron oscillator coordinates. From the outset one recognizes that certain of these "mixed" anharmonic terms lead to impurity vibron relaxation while others lead to a dependence of the adiabatic crystal potential energy for the phonon coordinates on the impurity vibron level. The latter terms predict a dependence

where the linear electron-phonon coupling is very strong. These systems are well understood in terms of the so-called Raman scattering of phonons by the impurity ion, and direct single phonon processes.[16,17] More recently, several papers have appeared dealing with the electron-phonon coupling associated with the electronic transitions of organic molecules in frozen paraffin (Shpolskii) matrices.[65,66] The analysis of band broadening and shift data for these systems has been done in terms of the McCumber theory employed for the inorganic ion/crystal systems. In particular, to our knowledge no previous attempt has been made to include in the theory a dependence of the thermal broadening and line shift on the impurity vibron level. In accordance with this, previous investigations of organic systems have either been confined to the origin band (zero-vibron level) of the electronic transition, or the tacit assumption made that there is no dependence of the broadening and shift on the impurity vibron level.

In this the first part of this work, we first consider the question of whether, in the adiabatic (with respect to the electrons and nuclei) and harmonic approximations, the thermal broadening and shift or, more generally, the spectral shape function of the zero-phonon band (due to electron-phonon coupling) should be independent of impurity vibron level within the final electronic state of the transition. We also consider the dependence of the electron-phonon interaction on

of the phonon frequencies and coordinates on the vibron state (the solid state analogue of gas-phase vibron-rotation interaction).

To date there has been no report in the literature on a molecular crystal system which exhibits anharmonic behavior in so far as zero-phonon band thermal broadening in an electronic spectrum is concerned. In this thesis data are presented for two mixed molecular crystal systems which exhibit a marked dependence of the zero-phonon band thermal broadening on the final impurity vibron level. They are: the 4500Å $^1B_1 \leftarrow {}^1A_1$ transition of 1,3-diazaazulene in naphthalene and the 3500Å $^1A_1 \leftarrow {}^1A_1$ transition of azulene in naphthalene.[3,10] The nature of the above vibron level dependence in these systems allows one to ascertain which type of mixed anharmonic term is of primary importance. Possible reasons why this anharmonicity is important for these two systems are considered.

We also report another, and unexpected, observation. In organic mixed crystals it is quite common to observe differing residual bandwidths for crystals of different histories. These variations may be as large as a factor of 2-3. We have measured variations of this magnitude for the thermal band broadening as well. In particular, we report measurements on the band broadening for the diazaazulene/naphthalene system where this effect is pronounced.

EXPERIMENTAL

Naphthalene (first fused with potassium) and p-terphenyl were both purified by zone refining (100 passes). Azulene, diazaazulene and phenylazaazulene were purified by sublimation under vacuum. Mixed crystals were then grown from the melt in a Bridgemann furnace. The optimum optical density for absorption band width measurements is about 0.5 and crystal concentrations were adjusted with this in mind. The weakest bands had O.D.'s of 0.2, and the strongest bands had O.D.'s of 0.7 at 4.2°K. The bulk concentrations of phenylazaazulene/terphenyl and diazaazulene/naphthalene were 5×10^{-4} mole/mole. For the azulene/naphthalene 7000Å absorption system we wished to make measurements on both the a_1 and b_1 vibronic bands. Since the most intense b_1 mode (at 1756 cm^{-1}) has only about 10% of the intensity of the allowed origin, it was necessary to use three crystals of azulene/naphthalene to obtain the appropriate optical densities for both spectra. A crystal of bulk concentration 10^{-5} mole/mole was used to study the a_1 fundamentals, and one of 10^{-3} mole/mole for the b_1 modes. A crystal of 10^{-4} mole/mole was used to compare the thermal broadenings of the 384 cm^{-1} (a_1) and 1756 cm^{-1} (b_1) fundamentals. The 10^{-5} mole/mole crystal was also used for azulene's 3500Å state. bc' faces, identified by conoscopic techniques, were cut from each crystal ingot. The

crystals were mounted on a brass plate in an Andonian Model MHD-3L-30N liquid helium cryostat.

Spectra were recorded in second order for the azulene/naphthalene 3500Å system, and in first order for the others using a Jarrell-Ash 1-m. Model 75-150 Czerny-Turner spectrometer operated in the photoelectric mode, with 10 μ slit widths. The maximum resolution of this spectrometer is 0.1Å in first order, which corresponds to 0.3 cm^{-1} at 5600Å. The continuum source was a tungsten-iodine lamp. Band positions were measured by superimposing on the spectra the emission lines of an Fe-Ne hollow cathode discharge lamp and measuring the absorption band positions from several nearby calibration lines. The maximum precision obtainable by this method is ±0.1 cm^{-1}. Band widths were measured at half peak height in terms of absorbance, from the spectral dispersion at the band. Scans over each band were repeated several times to eliminate errors arising from mechanical inconsistencies in the scan or chart drive.

All spectra were taken in polarized light. The temperature at the sample was measured with a Cryo-Cal germanium resistance thermometer (S/N 484) with a useful range of 2.8°K - 30°K, and a precision of ±0.1°K. Variation of the temperature was achieved by adjusting the flow rate of cold helium gas, entering through the bottom of the sample chamber, with the cryostat's No. 0-7 MH throttling system.

A 20 Ω heater, mounted below the sample chamber, heated the cold helium gas before its entry into the sample chamber, and was used to obtain fine adjustments of the temperature. Accurate measurement of the temperature at the sample is, of course, of major importance. To this end a 10 cm water filter was used to minimize heating of the sample by the continuum source, and the resistance thermometer was mounted on the sample support as close to the sample as possible.

THEORY

In the first part of this study we will employ the harmonic approximation in treating the system (impurity plus host molecules) vibrations. In contrast with earlier work, the Condon approximation is relaxed to introduce a dependence of the electronic transition moment on the vibration coordinates of the system. This is necessary because we wish to consider all possible electron-vibration coupling mechanisms, arising in the harmonic approximation, which can contribute to the temperature dependence of the spectral distributions of the zero-phonon vibron bands. In particular, we address the question of whether, in the harmonic approximation, the theory predicts that the variation in the width (center) of the zero-phonon band with T should be independent of vibron level within a given electronic state (final state of the impurity transition).

We start, in a familiar way, with the expansion of the potential energy of the ground electronic state, G, of the system in terms of the normal vibrational coordinates.

$$E_G(q,Q) = E_G(0,0) + \frac{1}{2}\sum_i \left(\frac{\partial^2 E_G}{\partial q_i^2}\right)_0 q_i^2 + \frac{1}{2}\sum_\alpha \left(\frac{\partial^2 E_G}{\partial Q_\alpha^2}\right)_0 Q_\alpha^2 \ . \qquad (1)$$

The q_i and Q_α are the system vibrons and phonons, respectively. One can assume that the coupling between the internal and external molecular motions and, also, the coupling between the

internal motions of the impurity and those of the host molecules have been taken into account. Attention is confined to systems in which the maximum phonon frequency, ω_M, is less than the minimum vibron frequency. Experimentally, this means restricting one's investigation of fundamental vibron levels to those with frequency > ω_M. With H_G the vibrational hamiltonian for the ground electronic state the vibrational hamiltonian for the system with the impurity molecule electronically excited is just

$$H_F = H_G + \sum_i A_i q_i + \sum_\alpha A_\alpha Q_\alpha + \frac{1}{2} \sum_{i,j} B_{ij} q_i q_j + \frac{1}{2} \sum_{\alpha,\beta} B_{\alpha,\beta} Q_\alpha Q_\beta + \sum_{\alpha,i} B_{\alpha i} q_i Q_\alpha \quad . \tag{2}$$

The linear terms describe the linear electron-vibration (vibron, phonon) coupling and the quadratic terms of quadratic electron-vibration coupling. To distinguish these types of couplings from those associated with the dependence of the electronic transition moment on the oscillator displacements we will adopt the convention of referring to the latter as vibronic or phononic coupling.

For the types of organic systems we consider and the temperature regime of the experiments, all the impurity transitions originate from the zero-point vibron level. Potentially, we have a large number of final state vibron levels corresponding to creation of one or more vibrons.

From the outset then, we realize that the terms, Equation 2, which must ultimately be responsible for the T-dependence of the widths and centers of the impurity zero-phonon vibron bands involve the phonon coordinates. Let $v' = \Sigma\, v_i'$ and $n' = \sum_\alpha n_\alpha'$ define the final vibron and phonon states of a transition and $n = \sum_\alpha n_\alpha$ define the initial phonon state. Then the probability of the absorption transition $v'n' \leftarrow 0n$ is, with the adiabatic approximation, proportional to

$$P_{v'n'\leftarrow 0n} \propto |\langle v'n'|\underset{\sim}{M}_{FG}(q,Q)|0n\rangle|^2 , \tag{3}$$

where

$$M_{FG}(q,Q) = \underset{\sim}{m}_{FG} + \sum_i \underset{\sim}{m}_i q_i + \sum_\alpha \underset{\sim}{m}_\alpha Q_\alpha . \tag{4}$$

In the expression for $\underset{\sim}{M}_{FG}$, the electronic transition moment, $\underset{\sim}{m}_{FG}$ is the Condon contribution (a constant). $\underset{\sim}{m}_i$ and $\underset{\sim}{m}_\alpha$ are the transition moments induced by a unit displacement of the oscillator coordinates q_i and Q_α, respectively. They arise through vibronic and phononic coupling. The quadratic and higher order dependences of $\underset{\sim}{M}_{FG}$ on the oscillator coordinates can be safely neglected, based on experimental molecular vibronic spectra.

It is appropriate now to define a zero-phonon transition as one in which the total number of phonons is conserved, i.e., $n = n'$. We note that it is the off-diagonal quadratic electron-phonon coupling which prevents a strict correlation between the ground and excited state phonon coordinates.

However, in the weak electron-phonon coupling limit (vide infra) it suffices to consider that only "off-diagonal" zero-phonon transitions, of the type $n_\alpha + 1$, $n_\beta - 1 \leftarrow n_\alpha$, n_β, contribute to the width of the zero-phonon band. There are two mechanisms, arising from Equation 2, which make these off-diagonal transitions allowed. However, as we will show, only one yields a Lorentzian band shape and is the off-diagonal quadratic electron-phonon coupling. The linear electron-phonon coupling is the second mechanisms, and does not lead to a Lorentzian profile.

Zero-Phonon Band Spectral Shape Function in the Linear Electron-Phonon Coupling and Adiabatic Approximations

As stated above the linear electron-phonon coupling contributes a non-Lorentzian component to the zero-phonon band profile. If its contribution to the zero-phonon band intensity is significant a temperature dependent asymmetry will be observed. To see this we must consider the spectral shape function for the transition to a vibron level v'. It is

$$G_{v'}(\omega) = \Big\langle \sum_{[n][n']} |\langle v'n'|\underset{\sim}{M}_{FG}|0n\rangle|^2 \delta(\omega-\omega_o - \sum_j v_j'\omega_j' - \sum_\alpha (n_\alpha'\omega_\alpha' - n_\alpha\omega_\alpha)) \Big\rangle_T \quad , \tag{5}$$

which, with Equation 4 becomes,

$$G_{v'}(\omega) = |\langle v'|\underset{\sim}{m}_{FG} + \sum_i \underset{\sim}{m}_i q_i|0\rangle|^2 \Big\langle \sum_{[n][n']} \sum |\langle n'|n\rangle|^2 \delta(\omega$$

$$- \sum_\alpha (n'_\alpha \omega'_\alpha - n_\alpha \omega_\alpha)) \Big\rangle_T \qquad (6)$$

$$+ |\langle v'|0\rangle|^2 \Big\langle \sum_{[n][n']} \sum |\langle n'|\sum_\alpha \underset{\sim}{m}_\alpha Q_\alpha|n\rangle|^2 \delta(\omega - \sum_\alpha (n'_\alpha \omega'_\alpha - n_\alpha \omega_\alpha)) \Big\rangle_T .$$

In Equation 5 ω_o is the pure electronic plus total zero-point energy difference between the states G and F. In Equation 6 $\omega_o + \sum_j v'_j \omega'_j$ has, for convenience, been set equal to zero. In both equations $\sum_{[n]}$ is over all possible initial phonon levels which must be thermally averaged. $\sum_{[n']}$ is over all possible final phonon levels subject to the condition $\sum_\alpha n'_\alpha = \sum_\alpha n_\alpha$.

An important simplification occurs in Equation 6 in the linear electron-phonon coupling approximation since the ground and excited state phonon frequencies are equal, i.e., $\omega_\alpha = \omega'_\alpha$ for every α. We first consider the contribution to $G_{v'}(\omega)$ from the diagonal zero-phonon transitions, $n_\alpha n_\beta \leftarrow n_\alpha n_\beta$ in the first thermally averaged term in Equation 6. We may assume the absence of local phonon modes[1] so that $|A_\alpha| \sim N^{-1/2}$, where

---

[1] The phonon density of states for organic crystals is generally a pseudo-continuum between 0 and $\omega_M \sim 100\text{-}150$ cm^{-1} so that impurity induced local modes would have $\omega > \omega_M$. In the temperature range we consider, thermal population of the local modes, were they to exist, is negligible.

N is the total number of phonon modes. Using excited state phonon wavefunctions $|n'\rangle$, correct to second order in the linear electron-phonon coupling, we find that

$$G^{d}_{v'}(\omega) = |\langle v'|\underset{\sim}{m}_{FG} + \sum_i \underset{\sim}{m}_i q_i|0\rangle|^2 \qquad (7)$$

$$x\Big\langle \sum_{[n]} \prod_\alpha (1 - a_\alpha^2 \gamma_\alpha (n_\alpha + {}^1/_2)) \Big\rangle_T \delta(\omega),$$

to order $^1/_N$. In Equation 7 $a_\alpha \omega_\alpha^2 = A_\alpha$ and $\gamma_\alpha = \omega_\alpha/\hbar$. Performing the thermal average one obtains

$$G^{d}_{v'}(\omega) = |\langle v'|\underset{\sim}{m}_{FG} + \sum_i \underset{\sim}{m}_i q_i|0\rangle|^2 \, e^{-S}\delta(\omega) \qquad (8)$$

where $S = \sum_\alpha a_\alpha^2 \gamma_\alpha (\langle n_\alpha \rangle_T + 1/2)$. $\langle n_\alpha \rangle_T$ is the thermal occupation number for mode α equal to $(\exp(\hbar\omega_\alpha/kT) - 1)^{-1}$. Thus the diagonal zero-phonon spectral distribution is a δ-function centered about $\omega=0$ for all T and <u>all</u> final vibron levels. As is well known, Equation 8 predicts that the zero-phonon band intensity is a sensitive function of the temperature.[18] By convention, if $\sum_\alpha a_\alpha^2 \gamma_\alpha/2 \ll 1$, the linear electron-phonon coupling is defined as weak. This situation arises experimentally when at low T the zero-phonon band intensity is much greater than the intensity of the one-phonon structure. More specifically, in the weak coupling limit the combined intensity of the zero-phonon band plus one-phonon structure should be static with T.

We turn our attention now to the spectral shape function arising from the class of most probable off-diagonal zero-phonon transitions of the type $n_\alpha + 1,\ n_\beta - 1 \leftarrow n_\alpha,\ n_\beta$. Such transitions are allowed through the linear electron-phonon coupling. We start by considering the contribution of these transitions to the first thermally averaged term in Equation 6. With

$$|\langle n_\alpha+1,\ n_\beta-1'|n_\alpha n_\beta\rangle|^2 = 4^{-1} \prod_{\substack{\sigma\neq \\ \alpha,\beta}} (1-a_\sigma^2\gamma_\sigma(n_\sigma+1/2)) \qquad (9)$$

$$\times\ \gamma_\alpha a_\alpha^2 \gamma_\beta a_\beta^2 n_\beta(n_\alpha+1)\ ,$$

we find that

$$G_{v'}^{od}(\omega) = 4^{-1}|\langle v'|\underset{\sim}{m}_{FG} + \sum_i \underset{\sim}{m}_i q_i|0\rangle|^2\ e^{-S} \qquad (10)$$

$$\times \int\int d\omega_\alpha d\omega_\beta g(\omega_\alpha)\gamma_\alpha a_\alpha^2 \gamma_\beta a_\beta^2 \langle n_\beta\rangle_T(\langle n_\alpha\rangle_T+1)\delta(\omega-[\omega_\alpha-\omega_\beta])\ ,$$

of

$$G_{v'}^{od}(\omega) \sim \int d\omega_\beta(\omega')g(\omega_\beta)\gamma_{\omega'}a_{\omega'}^2\gamma_\beta a_\beta^2\langle n_\beta\rangle_T(\langle n_{\omega'}\rangle_T + 1)\ , \qquad (11)$$

with $\omega' = \omega+\omega_\beta$ and $g(\omega)$ the phonon density of states. Integration in Equation 11 is appropriately limited depending on whether $\omega>0$ or $\omega<0$ (high or low energy side of the zero-phonon absorption band center).[1] A Lorentzian divergence at

[1]For the purposes of this treatment $G(\omega)$ will be considered to correspond to an absorption transition. This is not essential, and the results can be applied to emissive transitions by simply changing the appropriate energy conservation requirements. Also, when reference is made to the high energy and low energy sides of a zero-phonon band center this distinction should be noted.

$\omega = 0$ is clearly absent in Equation 11 and we conclude that the effect of the off-diagonal transitions would be to introduce a temperature dependent asymmetry to the zero-phonon band. Using the longwave approximation,[16] $a_\alpha = a\omega_\alpha^{-1}$, and a Debye density of states one can show that this asymmetry vanishes in the high T limit, $kT >> h\omega_D$. Moreover, at high T the off-diagonal transitions would lead to a linear tailing with $|\omega|$ which vanishes at $\omega = \omega_D$. In the low T limit the off-diagonal intensity on the low energy side of the zero-phonon line decreases rapidly (approx. exponentially) with increasing $|\omega|$. For the high energy wing, the intensity increases linearly for small $|\omega|$ but in a more complicated manner for larger $|\omega|$, reaching a maximum in close proximity to the one-phonon envelope maximum and decreasing to zero for $\omega = \omega_D$.

It would appear that in the weak linear electron-phonon coupling limit the contribution of the above off-diagonal transitions to the zero-phonon band intensity should be negligible since they may be viewed as two-phonon transitions which conserve the total number of phonons. However, when the two-phonon structure associated with the impurity spectrum is not weak relative to the one-phonon structure, these transitions could lead to a T-dependent high and low energy tailing of the zero-phonon band. Such tailing has been recently observed by Sapozhnikov[66] in some aromatic impurity Shpolskii matrix systems. He attributes the tailing to

anharmonic effects without considering the mechanism discussed above. However, it should be pointed out that the tailing is observed in a temperature region where Boltzmann population of initial low frequency excited vibron levels is no longer negligible.

With regards the last thermally averaged term in Equation 6, the linear electron-phonon coupling relaxes the forbiddeness of both the diagonal ($n_\alpha n_\beta \leftarrow n_\alpha n_\beta$) and off-diagonal transitions ($n_\alpha+1,\ n_\beta-1 \leftarrow n_\alpha n_\beta$). However, the spectral distribution for the diagonal transitions is still a δ-function centered about $\omega=0$ for all vibron levels. The off-diagonal transitions can be shown to lead to a spectral distribution which is not Lorentzian and is asymmetric. At the same time, though, the intensity contribution to the central zero-phonon peak is zero when one makes the assumption $\lim_{\omega_\alpha \to \omega_\beta} |\underset{\sim}{m}_\alpha - \underset{\sim}{m}_\beta| = 0$. It is worth emphasizing that the phononic coupling is a mechanism by which one-phonon transitions can occur. To our knowledge, this mechanism has not been invoked for any mixed molecular system. The question of how one could determine the importance of the phononic mechanism relative to the usual linear electron-phonon coupling mechanism is answered by Equation 6. That is, the phononic mechanism would be operative only for totally symmetric vibron levels $|v'\rangle$ which are Condon allowed.

In summary we conclude that, in the adiabatic and weak electron-phonon coupling approximations, each zero-phonon

vibron shape function is a δ-function centered at $\omega_o + \sum_j v_j'\omega_j'$.

When the linear electron-phonon coupling is no longer weak, the off-diagonal zero-phonon transitions can result in a T-dependent asymmetric shape function for the zero-phonon bands. However, in the linear electron-phonon coupling approximation the spectral shape functions for all vibron levels are identical at each temperature.

T-Dependence of the Widths and Centers of the Zero-Phonon Vibron Bands Arising from the Quadratic Electron-Vibration Coupling

One can readily prove that the spectral shape function for the off-diagonal zero-phonon transitions, $n_\alpha + 1$, $n_\beta - 1 \leftarrow n_\alpha n_\beta$, arising through the off-diagonal $B_{\alpha\beta}$ terms has a Lorentzian divergence at $\omega = 0$. At the same time one realizes that the "mixed" off-diagonal terms $B_{\alpha i}$ can also, in principle, contribute a Lorentzian component to the shape function of each zero-phonon vibron level. Furthermore, this component is dependent on the vibron level. However, as mentioned earlier, we specifically consider systems for which $\omega_i > \omega_M$ so that in a first order theory the $B_{\alpha i}$ terms will not contribute to the width of the zero-phonon bands. Contributions arise in higher order, but their inclusion is not appropriate in view of the fact we purposely neglect anharmonic contributions. In other words they should be treated on an

equal footing with the latter. Thus, we can immediately conclude that in the adiabatic harmonic approximation the temperature broadening of each and every zero-phonon vibron level is the same. The same is also true for the temperature dependent line shift.

With the neglect of the higher order contributions arising from $B_{\alpha i}$, the problem of determining the temperature dependence of the center and width of the zero-phonon band (Lorentzian) reduces to one which has been solved.[16,17] In the first order theory, the off-diagonal electron-phonon coupling is responsible for the T-dependence of the width of the Lorentzian distribution, while the diagonal quadratic coupling is responsible for the T-dependence of the band center. While the linear electron-phonon coupling contributes a thermally static term to the center of the zero-phonon band in second order it does not contribute a static term to the width.

The following familiar expressions have been used to fit our band broadening (ΔE) and band shift (δE) data for the 2-phenyl-1-monoazaazulene in p-terphenyl (5600Å) and azulene in naphthalene (7000Å) systems.

$$\Delta E(cm^{-1}) = \bar{\alpha} \left(T/T_D\right)^7 \int_0^{T_D/T} \frac{dx\, x^6\, e^x}{(e^x - 1)^2} \qquad (12)$$

$$\delta E(cm^{-1}) = \alpha \left(T/T_D\right)^4 \int_0^{T_D/T} \frac{dx\, x^3}{e^x - 1} \qquad (13)$$

where $x = \frac{h\omega}{kT}$. In the derivation of Equations 12 and 13 the longwave approximation is used for the quadratic electron-phonon coupling coefficients. In addition, a Debye density of states is employed, with $\omega_D(T_D)$ the Debye cut-off frequency (temperature).

T_D, $\bar{\alpha}$ and α are treated as adjustable parameters, and determined by fitting Equations 12 and 13 to the experimental data. T_D is the effective Debye temperature, and has a value particular to the system under study, and therefore cannot be obtained independently.

RESULTS AND DISCUSSION

Phenylmonoazaazulene in p-Terphenyl

The primary motivation for studying this system was the desire to determine the dependence of the band broadening and line shift parameters, α, $\bar{\alpha}$, T_D, on the site configuration of the impurity in an organic crystal. Measurements were confined to the lowest energy absorption system of PMAA, $^1B_1(\pi\pi^*) \leftarrow {}^1A_1$, which originates at $\sim$ 5600Å in p-terphenyl.[15] Analyses of the absorption and fluorescence spectra at 4.2°K have proven that PMAA occupied twelve energetically different sites in the lattice. This multiple site effect manifests itself in the optical spectra in the form of a clearly resolvable multiple structure. In absorption, the lowest energy (0_1) and highest energy (0_{12}) multiplet components of the zero-vibron band are separated by 387 cm^{-1}, cf. 4.2°K spectrum in Figure 36. 0_1-0_{12} are zero-phonon bands. Polarization measurements indicate that there is a considerable difference between the projections of the molecular axes onto the crystallographic axes of several sites. However, no structural information on the multiple sites is available. It is evident from the lower trace in Figure 36 that the linear electron-phonon coupling is weak for all twelve sites. Because of this and the fact that the multiplet bands are well resolved, the PMAA in p-terphenyl system is perfectly suited for the above studies.

In Figure 37 the total integrated intensity of the twelve zero-phonon origins is plotted for several temperatures. For a Debye density of states, the zero-phonon band intensity is predicted to follow an $\exp[-(T/T_D)^2]$ dependence in the low temperature limit.[65] The solid curve in Figure 37 is a fit of this function to the experimental data. It is necessary to consider the cumulative intensity of all twelve origins, since site equilibrations are decreasing or enhancing the intensities of individual origin bands. The solid curve fit to the data yields a first approximation for T_D which can be varied to fit the line shift and band broadening data for each zero-phonon origin. The value of T_D obtained from Figure 32 is 61±4°K.

The values of α and $\bar{\alpha}$ for the twelve zero-phonon origins are given in Table 24. Some representative curve fits to the data are given in Figures 38-40. It was found through curve fitting that a T_D of 60°K for both α and $\bar{\alpha}$ led to calculated curves for all site origins whose agreement with the experimental data could not be significantly improved by variation of T_D through one or two degrees. In fact, T_D's of 55°K and 65°K led to band broadening curves whose fits to the data are not as fine as those obtained with T_D = 60°K. Returning to Table 24, we note that the values of α for O_2, O_3 and O_7 are uncertain because of the scatter of the data, the result of a small line shift over the temperature range studied. O_3,

for instance, has a line shift of only 1.2 cm^{-1} at 27.6°K. This temperature range is equivalent, in units of the Debye temperature, to that used previously for both organic and inorganic band broadening and shift data. The largest line shift at this temperature is 4.5 cm^{-1} for O_{11}. No values of α are given for O_4 and O_5 because these bands essentially vanish for T>20°K, Figure 36. There is little doubt that their disappearance is due mainly to site equilibration[68] in which the O_4, O_6 sites are depopulated and, concomitantly, the O_{12} site populated, Figure 36. In viewing Figure 36 one should note that, because α is negative, the zero-phonon band centers shift to lower energy with increasing temperature. Finally, in Figure 41 we show a representative high temperature zero-phonon band spectral distribution, O_{11} (solid curve). The distribution is symmetric and close to Lorentzian. The crosses represent a Gaussian fit.

To begin our discussion of the data in Table 24, we note that the longwave and Debye density of states approximations employed in the derivation of Equations 12 and 13, lead to the prediction $\bar{\alpha} = CT_D^{-1}\alpha^2$, where C is a constant for a given host. Since we can say with certainty that $T_D(\alpha,\bar{\alpha})$, for the zero-phonon origins O_1, O_6, O_8-O_{12}, is the same, a comparison of $\alpha^2/\bar{\alpha}$ for these origins can be used to test the reasonableness of the above approximations. The values are given in the last column in Table 24 and agree within about

a factor of 2. Thus, the approximations appear not to be so severe that they cannot be usefully applied to organic systems. The fact that the Debye temperature does not vary significantly for the impurity sites, we find somewhat surprising. The maximum phonon frequency of p-terphenyl is ca. 120 cm^{-1} and it is clear that we are approximating a structured density of states with an effective Debye density of states with $\omega_D \sim \omega_M/2$. Apparently, each site is essentially coupling in a similar fashion with the "real" phonons, even though the multiplet splittings are very large for a mixed organic crystal. That we can use the same effective Debye temperature for all twelve origins is advantageous, since it allows direct comparison of the coupling strengths at each site in terms of a single parameter ($\bar{\alpha}$ or α). With regards the site dependence of $\bar{\alpha}$ we note that O_2 exhibits the lowest value, 45 cm^{-1}, while O_8 exhibits the largest value, 133 cm^{-1}, measured with certainty. Richards and Rice have found that there is no site dependence exhibited by $\bar{\alpha}$ in the anthracene/C_7 and 1,12-benzperylene/C_6 Shpolskii systems.[65] For these systems and others,[66] $\bar{\alpha}$ lies in the range 60-240 cm^{-1} (T_D = 144°K) so that PMAA/p-terphenyl is a mixed crystal system characterized by quadratic electron-phonon coupling which is as weak as that in most Shpolskii systems. More importantly, our results show that variations in $\alpha,\bar{\alpha}$ with impurity site in a given mixed crystal system can be as large as those between chemically different mixed

molecular systems. It is interesting to compare the one-phonon structures associated with O_2 and O_8. The phonon structures associated with O_1, O_2, O_3, O_7, O_8 and O_{10} are very similar and characterized by a single broad band displaced 28 ± 1 cm^{-1} from the zero-phonon line. Thus, the fact that the linear electron-phonon couplings for two sites are the same cannot be used to argue that their quadratic coupling parameters will be.

Dependence of Zero-Phonon Band Thermal Broadening on Vibron Level

It is not unusual to observe that the residual low T widths of different vibron levels in a given sharp line impurity electronic spectrum differ by a cm^{-1} or more. A clear example is the 906 cm^{-1} fundamental in the 3500Å absorption system of azulene in naphthalene. Its residual width is 3.9 cm^{-1} compared with the origin width of 1.3 cm^{-1}. Of course, comparisons of this type should be made with data from the same crystal. There are several mechanisms which can lead to these residual width variations, e.g., spectral conjestion between harmonic levels, inhomogeniety or strain broadening, nonadiabaticity and the vibron-phonon anharmonicity. The latter mechanism is responsible for vibron relaxation processes and the dependence of the phonon oscillator coordinates (frequencies) on vibron level. Vibron relaxation processes can be divided into two classes; those

which are static (T-independent) and those which are T-dependent (e.g., involving phonon emission). In large molecules like azulene where nonadiabatic decay processes are sufficiently fast to yield Lorentzian widths comparable with typical inhomogeniety widths of $\sim$1 cm^{-1}, the role of the medium should be minor.[70] Consequently, one does not expect the nonadiabatic decay rates to vary appreciably with temperature.

To our knowledge, no detailed T-dependent studies on the dependence of the zero-phonon band shape function on vibron level have been reported. Thus, the question of whether such studies can provide data on vibron-phonon anharmonic interactions is yet to be answered. Recall that, within the adiabatic harmonic approximation, the thermal broadening of the zero-phonon band (Lorentzian component) is independent of vibron level. Obviously this statement also applies when anharmonicity is taken into account, provided it depends only on phonon coordinates. In this section we report on the first of a number of studies designed to answer the above question.

We consider first the thermal broadening data for the 264 cm^{-1} totally symmetric fundamental of PMAA in p-terphenyl built on 0_1, 0_2 and 0_3, Figure 36. The data for 0_1 + 264 is plotted along with the theoretical curve (T_D = 60°K) in Figure 42. We find that $\bar{\alpha}(0_1 + 264)$ equals 100 cm^{-1} so that,

within experimental uncertainty, it is equal of $\bar{\alpha}(0_1)$. The same is also true for $0_2 + 264$ and $0_3 + 264$, i.e., $\bar{\alpha}(0_2) = \bar{\alpha}(0_2 + 264)$, etc. The residual widths of the three fundamentals are within ± 0.2 cm^{-1} of the widths of the corresponding origins. Studies on higher frequency fundamentals were not possible because of spectral conjestion due to the large number of multiplet origins.

We turn now to the thermal broadening data for a different mixed crystal system, azulene in naphthalene. The azulene absorption system we consider corresponds to the 7000Å $^1B_1(\pi\pi^*) \leftarrow {}^1A_1$ transition.[3] This system has recently been analyzed in great detail by Small and Kusserow[32] using a naphthalene host. A few of the bands in the azulene/naphthalene system exhibit a doublet structure which is barely resolvable. The doublet components have comparable intensities. However, the origin and 384(a_1), 1193(a_1) and 1388(a_1) cm^{-1} zero-phonon bands (fundamentals) appear as single peaks in regions which are not conjested. These bands, therefore, were chosen for study and found to have residual widths (4.2°K) of 2.0, 2.0, 2.5 and 3.7 cm^{-1} in a particular sample. At 4.2°K the origin and 384 cm^{-1} zero-phonon bands exhibit only slight asymmetry and are very close to Lorentzian (tailing more rapidly than Lorentzian in the wings). Hochstrasser and Li have previously studied the origin band and the deviation from Lorentzian behavior they observe[71] at 1.8°K appears similar to ours.

They ascribe the Lorentzian component to nonradiative decay of the 7000Å state. For the 1193 and 1388 cm^{-1} bands we observe somewhat greater deviations from a Lorentzian behavior, there being a larger Gaussian contribution. However, at the higher temperatures, T > 20°K, all four zero-phonon bands are Lorentzian. The thermal broadening data for these bands, along with the theoretical curve are shown in Figure 43. As before, the zero-phonon band intensity was plotted as a function of temperature to determine a first approximation to T_D. Through curve fitting we established that T_D = 60°K was optimum for all four zero-phonon bands. From Figure 43 we see that their coupling constants are equal to within the accuracy of our measurements, and $\bar{a}$ = 97 cm^{-1}.

It has recently been shown that the 7000Å $^1B_1 \leftarrow {}^1A_1$ system of azulene exhibits considerable vibronic coupling activity due to b_1 fundamental vibrations,[32] in addition to the progression forming a_1 fundamentals, such as 384, 1193 and 1388 cm^{-1}. In view of the fact that the a_1 fundamentals exhibit the same thermal broadening as the zero-vibron level it was decided to determine whether this is also true for the "vibronically active" modes. Two of the most intense b_1 fundamentals, 1362 and 1756 cm^{-1} (residual widths of 3.7 cm^{-1}) were chosen for study. The data is shown in Figure 44. The scatter of the data from the theoretical curve is low and both b_1 fundamentals are characterized by the same thermal broadening parameter, $\bar{a}$ = 76 cm^{-1}. Recall, however, that the

measurements of the a_1 and b_1 modes were made using different crystals to obtain the optimum intensities. Since we have no guarantee that the broadenings are independent of the particular crystal, the experiment was repeated for the weakest a_1 mode (384 cm^{-1}) and the strongest b_1 mode (1756 cm^{-1}) for an azulene/naphthalene crystal (10^{-4} mole/mole) that yielded optical densities for these bands of 0.5 and 0.2, respectively. The residual widths of the bands were 2.2 cm^{-1} (384) and 3.0 cm^{-1} (1756). The band broadenings were identical, and yielded the same coupling parameters as the a_1 modes in the 10^{-5} mole/mole crystal. On the basis of these observations we conclude that the 384, 1193 and 1388 cm^{-1} a_1 fundamentals and the 1362 and 1756 cm^{-1} b_1 fundamentals of azulene/naphthalene exhibit the same thermal broadening as the zero-vibron origin. The sensitivity of these broadenings, as well as the residual widths, to variations in the mixed crystal, is an important fact to bear in mind. However, the nature of the coupling, as described by the effective Debye temperature, is the same.

In summary, it is observed that the 264 cm^{-1} a_1 fundamental of PMAA in p-terphenyl and the 384, 1193, and 1388 cm^{-1} a_1 and, 1362 and 1756 b_1 fundamentals of azulene in naphthalene exhibit the same thermal broadening as the zero-vibron level.

It is clear that the above a_1 and b_1 vibron levels are not involved to any significant extent, in T-dependent

vibron-phonon anharmonic interactions. We note that the a_1 vibrations appear to be of the Condon type in contrast with the b_1 fundamentals which are vibronically induced. For the two other systems studied, however, there is a marked dependence of the zero-phonon band broadening on the final vibron level of the transition. To illustrate the contrast between the band broadenings of the azulene/naphthalene 3500Å and diazaazulene/naphthalene 4500Å absorption and of the azulene/naphthalene 7000Å and phenylazaazulene/p-terphenyl 5600Å absorptions, the results of the measurements on the first two systems are presented below, followed by a discussion of the theory necessary to explain their behavior.

The 3500Å $^1A_1 \leftarrow {}^1A_1$ Absorption System of Azulene in Naphthalene

This system in a naphthalene host crystal was first investigated by Sidman and McClure,[3] and has been the subject of a recent study by Lacey and coworkers.[10] The well-known properties of this state include its anomalous fluorescence,[3] the large extent to which absorption to it is vibronically induced by totally symmetric fundamentals,[10] and the strong medium dependence of its vibronic structure in absorption.[10] In contrast, the 7000Å $^1B_1 \leftarrow {}^1A_1$ absorption system of azulene is characterized by totally symmetric vibronic structure whose intensity distribution conforms to a Franck-Condon analysis[72] and does not exhibit a significant medium

dependence. The 7000Å system, however, is characterized by extensive b_1 vibronic activity which, in a naphthalene host, accounts for 15% of the oscillator strength.[32] Both states exhibit sharp line vibronic spectra in a naphthalene host and, thus, provide the rare opportunity of investigating the electron-phonon coupling for two states of a large molecule in a crystal medium. Above, we reported that the thermal broadening of the zero-phonon origin band (zero-vibron) was identical to that of the several a_1 and b_1 vibron fundamentals chosen for study. The thermal broadening parameters, $\bar{\alpha}$ and T_D, defined by the theoretical broadening expression[16-17]

$$\Delta E(cm^{-1}) = \bar{\alpha} \, (T/T_D)^7 \int_0^{T_D/T} \frac{dx \, x^6 \, e^x}{(e^x-1)^2} \qquad (14)$$

were determined as 97 cm^{-1} and 60°K, respectively. ΔE is the thermal broadening due to the quadratic off-diagonal electron-phonon coupling. T_D is the effective Debye temperature and $x = h\omega/kT$ with ω the phonon frequency. $\bar{\alpha}$ is related to the quadratic off-diagonal coupling coefficients which have been evaluated using the longwave approximation.[16] Its exact form is given in reference 17. Use of Equation 14 is justified when the zero-phonon band temperature dependent shape function is Lorentzian and the thermal broadening is independent of final impurity vibron level (i.e., anharmonic effects are negligible). As emphasized above, good agreement between the theoretical (Equation 14) and experimental

broadening curves does not necessarily mean that the longwave and Debye density of states approximations are valid. The parameters $\bar{\alpha}$ and T_D are, nevertheless, very useful for comparative studies of electron-phonon coupling strengths.

Turning now to the 3500Å absorption transition, we have measured the zero-phonon thermal broadening for the zero-vibron band (origin) and the a_1 vibron bands at 655, 669, 801, 854 cm^{-1} and the b_1 vibron fundamental at 695 cm^{-1}.[9,10] Unfortunately, spectral congestion to higher energy precludes study of other bands. The thermal broadenings of all the five vibron bands were identical (same crystal) and their spectral shapes Lorentzian at high T. Fitting the data to Equation 14 yielded coupling parameters of $\bar{\alpha}$ = 117 cm^{-1} and T_D = 60°K. The zero-vibron band, however, broadened more rapidly than the vibron bands and its data was fit with $\bar{\alpha}$ = 130 cm^{-1} and T_D = 50°K. The residual widths and coupling parameters are given in Table 25. In Figure 45 the band broadening data for the origin are plotted, along with the curve (solid) calculated from Equation 14. In Figure 46 the results are plotted for the 669 and 695 cm^{-1} vibron bands. Comparison of these two figures show that by 25°K the origin band broadening is approximately twice that of the vibron bands. From previous discussion on the applicability of Equation 14 it would appear to be contradictory for us to apply it to the experimental data for the 3500Å azulene system. We do so simply

because $\bar{\alpha}$ and T_D are useful indicators for the thermal broadening dependence on impurity vibron level.

The 4500Å $^1B_1 \leftarrow {}^1A_1$ Absorption System of 1,3-Diazaazulene in Naphthalene

The lowest energy absorption of 1,3-diazaazulene in naphthalene is the 4500Å, $^1B_1 \leftarrow {}^1A_1(\pi\pi^*)$ transition. This state, like the 3500Å state of azulene/naphthalene, exhibits considerable totally symmetric vibronic activity. There is sufficiently little spectral congestion that band broadening measurements could be made on several a_1 and b_1 vibron fundamentals. The results are given in Table 26, and in Figures 47 and 48. As with the azulene/naphthalene 3500Å transition, the origin band broadens more rapidly than any of the vibron fundamentals. However, there are marked differences between the broadening of the individual vibron bands as well. The experiment was repeated, using the same crystal (crystal 1) and the data for the origin band are plotted in Figure 47. The agreement of the two sets of data (crosses and circles) is very good, and data for the other bands were similarly reproducible. To preclude the possibility that the difference in band broadenings between the vibron bands was an artifact of the particular crystal used, a fresh crystal of diazaazulene was grown and the experiment repeated using two bc' sections cut from this ingot (crystals 2 and 3). The results for crystals 2 and 3 were identical within experimental

uncertainty and are shown in Figures 49-51 for crystal 2 and Table 26. The relative magnitudes of the band broadenings are the same as those observed previously (ΔE (origin) > ΔE (575) > ΔE (539)) but the absolute magnitudes have all increased. The dashed lines in Figures 49-51 are the broadening curves of Figure 47. The experiment using crystals 2 and 3 was repeated, and the results confirmed.

Anharmonicity in Electron-Phonon Coupling

The results in the previous section demonstrate that the harmonic level of approximation for the azulene/naphthalene 3500Å and diazaazulene/naphthalene 4500Å transitions is not adequate to explain the thermal broadenings. The values of $\bar{\alpha}$ and T_D determined for these systems, and listed in Tables 25 and 26, serve to indicate the extent of the inadequacy of the harmonic approximation. For the moment we put aside the problem of the thermal broadening dependence on sample history and consider the question first of how the anharmonicity for the system vibrations can be used to qualitatively explain the experimental data for a given sample. Our objective will be to consider the simplest model capable of doing this. The data show that: at sufficiently high T, the zero-phonon shape function for all bands is symmetric and very close to Lorentzian, Figures 52 and 53, and; the impurity vibron bands broaden less rapidly than the origin or zero-vibron band. The latter observation is

particularly informative because it means that those anharmonic terms which lead to impurity vibron relaxation cannot be responsible for the difference in behavior between the zero-vibron and vibron fundamental bands. These terms are in general composed of a static (T-independent) and T-dependent term. The latter, if important in the broadening mechanism, leads to the prediction that vibron bands should broaden more rapidly than the zero-vibron band.

To begin, we note that all absorption transitions in our experiments can be taken to originate from the zero-vibron level of the ground electronic state. Thus, the thermal broadening of the zero-phonon band due to ground state anharmonicity is the same for each and every final impurity vibron level. For simplicity we neglect this anharmonicity in what follows. With H_G the harmonic vibrational hamiltonian for the ground electronic state, G, we write the vibrational hamiltonian for the final electronic state as

$$H_F = H_G + V_1' + V_2' + V_3' + V_4' \qquad (15)$$

H_G is the sum of two hamiltonians, $h_G(P,Q)$ and $h_G(p',q')$. They are, respectively, the harmonic hamiltonians for the phonons and vibrons. P and p' are the momenta conjugate to the ground state oscillator coordinates Q and q'. V_1' and V_2' represent the linear and quadratic electron-vibration coupling for the system vibrations. V_3' and V_4' are the cubic

and quartic anharmonicities. The V''s are functions of the ground state coordinates q' and Q. Without loss of generality, we assume that the potential energy from $H_G(p',q')$ plus the terms in V_1' and V_2' dependent only on q (vibron coordinates), have been diagonalized to yield a new set of vibron oscillator coordinates, q. Then

$$H_F = h_G(P,Q) + h_F(p,q) + V_1 + V_2 + V_3 + V_4 , \tag{16}$$

where

$$h_F = T_q + \frac{1}{2} \sum_i B_{ii} q_i^2 . \tag{17}$$

T_q is the kinetic energy operator for the vibrons. The V terms are given by

$$V_1 = \sum_\alpha A_\alpha Q_\alpha , \tag{18a}$$

$$V_2 = \frac{1}{2} \sum_{\alpha,\beta} B_{\alpha\beta} Q_\alpha Q_\beta + \sum_{\alpha,i} B_{\alpha i} Q_\alpha q_i , \tag{18b}$$

$$V_3 = \frac{1}{2} \sum_{\alpha,\beta,i} D_{\alpha\beta i} Q_\alpha Q_\beta q_i + \frac{1}{2} \sum_{\alpha,i,j} D_{\alpha ij} Q_\alpha q_i q_j + .. , \tag{18c}$$

and

$$V_4 = \frac{1}{6} \sum_{\alpha\beta\gamma i} D_{\alpha\beta\gamma i} Q_\alpha Q_\beta Q_\gamma q_i + \frac{1}{6} \sum_{\alpha ijk} D_{\alpha ijk} Q_\alpha q_i q_i q_k + \frac{1}{4} \sum_{\substack{ij \\ \alpha\beta}} D_{\alpha\beta ij} Q_\alpha Q_\beta q_i q_j + ... \tag{18d}$$

The additional terms in Equations 18c and 18d are the anharmonicities which depend solely on either the vibron

coordinates or the phonon coordinates. They do not lead to a dependence of the impurity zero-phonon band broadening on final vibron level. We note that V_1, the linear electron-phonon coupling, is usually used to interpret multi-phonon transitions. The first term in V_2, the quadratic electron-phonon coupling, is responsible for the zero-phonon band shift and broadening (Lorentzian) in the harmonic approximation. The off-diagonal terms, $B_{\alpha\beta}$, give rise to Equation 1 when the longwave[16] and Debye density of states approximations are made.[17] As discussed above, the last term in V_2 does not contribute, in first order, to the broadening of a vibron band whose frequency is greater than ω_M. Since for naphthalene $\omega_M \sim 150$ cm^{-1},[73,74] this condition is met for the bands of azulene/naphthalene and diazaazulene/naphthalene.

We now solve the vibron problem (state F) by separating the fast (vibron) and slow (phonon) vibrational motions in a manner analogous to that used for the electron-nuclei problem.[75] That is, the vibron wavefunctions and energies are to depend parametrically on the phonon oscillator coordinates. For our purpose it is convenient to choose the vibron hamiltonian in the form

$$H_F(p,q,Q) = h_F(p,q) + \sum_{\alpha,i} B_{\alpha i} Q_\alpha q_i \qquad (19)$$

$$+ \frac{1}{2} \sum_{\alpha,i} D_{\alpha ii} Q_\alpha q_i^2 + \frac{1}{4} \sum_{\substack{i \\ \alpha,\beta}} D_{\alpha\beta ii} Q_\alpha Q_\beta q_i^2 \, .$$

In Equation 19 we have, for simplicity, omitted the anharmonic terms which depend solely on the vibron coordinates since they do not play a role in the thermal broadening. That is, the vibron levels in the ground state are not thermally populated in our experiments. The solutions to $h_F(p,q)\psi_v(q) = \varepsilon_v\psi_v(q)$ are known, $\varepsilon_v = \sum_i (v_i + 1/2)\hbar\omega_i$. Treating the last three terms in Equation 19 as perturbations one can show that the energies for $H_F(p,q,Q)$ are

$$\varepsilon_v(Q) = \sum_i \hbar\omega_i(v_i+1/2) + \frac{1}{2}\sum_{\alpha,i} D_{\alpha ii}\left(\frac{\hbar}{2\omega_i}\right)(2v_i+1)Q_\alpha + \frac{1}{4}\sum_{i\alpha\beta} D_{\alpha\beta ii}\left(\frac{\hbar}{2\omega_i}\right)(2v_i+1)Q_\alpha Q_\beta + \sum_{i\alpha\beta}\left(\frac{\hbar}{2\omega_i}\right)\left(\frac{B_{\alpha i}B_{\beta i}}{\hbar\omega_i}\right)Q_\alpha Q_\beta . \tag{20}$$

The second and third terms in this equation arise, in first order, from the anharmonic terms in Equation 19, while the last term arises, in second order, from the last term. $\varepsilon_v(Q)$ forms part of the potential energy for the phonon problem. We note that while the second and third terms in Equation 20 depend on the vibron quantum number, the last term does not. With Equation 20 we see how the <u>linear and quadratic electron-phonon coupling depend on the vibron level v</u>.

We now define the eigenfunctions of $H_F(p,q,Q)$, Equation 19, as $\psi_v^A(q,Q)$. The general solutions to the Schrödinger equation with H_F, Equation 16, can be written as

$$\Phi(q,Q) = \sum_v \psi_v^A(q,Q)\phi_v(Q) , \tag{21}$$

and, in a straightforward manner, can be shown to satisfy

$$[h_G(P,Q) + \varepsilon_v(Q) + \Lambda(Q) - E]\phi_v = \sum_{v' \neq v} \Lambda_{vv'}\phi_{v'} \ . \qquad (22)$$

In Equation 21, $h_G(P,Q)$ is the harmonic hamiltonian for the phonons in the ground electronic state, i.e.,

$$h_G(P,Q) = T_Q + \frac{1}{2} \sum_{\alpha} b_{\alpha\alpha} Q_\alpha^2 \ . \qquad (23)$$

$\Lambda(Q)$ is the sum of a harmonic term, Λ^h, and an anharmonic term, Λ^{an}.

$$\Lambda^h = \sum_{\alpha} A_\alpha Q_\alpha + \frac{1}{2} \sum_{\alpha,\beta} B_{\alpha\beta} Q_\alpha Q_\beta \qquad (24)$$

and

$$\Lambda^{an} = \frac{1}{3!} \sum_{\alpha\beta\gamma} D_{\alpha\beta\gamma} Q_\alpha Q_\beta Q_\gamma + \frac{1}{4!} \sum_{\alpha\beta\gamma\delta} D_{\alpha\beta\gamma\delta} Q_\alpha Q_\beta Q_\gamma Q_\delta \ . \qquad (25)$$

The phonon-vibron <u>nonadiabaticity</u> operator, $\Lambda_{vv'}$, is given by

$$\Lambda_{vv'} = - \langle \psi_v^A | V' | \psi_{v'}^A \rangle + h^2 \sum_{\alpha} \langle \psi_v^A | \frac{\partial \psi_{v'}^A}{\partial Q_\alpha} \partial/\partial Q_\alpha - \langle \psi_v^A | T_Q | \psi_{v'}^A \rangle \ , \qquad (26)$$

where

$$V' = \sum_{i=1}^{4} V_i - \sum_{i\alpha} D_{\alpha ii} q_i^2 Q_\alpha - \sum_{i\alpha\beta} D_{\alpha\beta ii} q_i^2 Q_\alpha Q_\beta - \sum_{\alpha,i} B_{\alpha i} Q_\alpha q_i \ . \qquad (27)$$

Thus, when $\Lambda_{vv'} = 0$ for every $v' \neq v$, the solutions to the vibron-phonon problem are adiabatic, that is

$$\Phi_{vn}(q,Q) = \psi_v^A(q,Q) \cdot \phi_{vn}(Q) \ , \qquad (28)$$

with the phonon wavefunctions, ϕ_{vn}, satisfying

$$[h_G(P,Q) + \epsilon_v(Q) + \Lambda(Q) - E]\phi_{vn} = 0 \ . \qquad (29)$$

In the adiabatic approximation the possibility of impurity vibron relaxation is not admitted.

Dependence of the Zero-Phonon Band Thermal Broadening on Anharmonicity

The nonadiabaticity operator, Equation 26, can give rise to a dependence of the zero-phonon thermal broadening on final impurity vibron level via vibron relaxation channels. However, as stated previously, their effect would be such as to have the excited vibron levels broadening more rapidly than the zero-vibron level. They cannot, therefore, be used to explain our experimental data. Apparently, the temperature dependent vibron relaxation band broadening is not competitive with the broadening due to the off-diagonal quadratic electron-phonon coupling in the mixed crystal system considered here. For this reason we do not consider the nonadiabatic terms any further. We are apparently left, therefore, with the terms in $\epsilon_v(Q)$, Equation 20, which depend on vibron quantum number as alone being capable of explaining the vibron level dependence observed for the thermal broadening. We may write the phonon hamiltonian for each vibron level, v, of the electronic state F in the form

$$h_{Fv}(P,Q) = h_G(p,Q) + \sum_{\alpha} Q_\alpha\{A_\alpha + A_\alpha^v\} + \sum_{\alpha,\beta} Q_\alpha Q_\beta\{B_{\alpha\beta} + B_{\alpha\beta}^v\}, \quad (30)$$

where from Equation 20,

$$A_\alpha^v = \sum_i \left(\frac{\hbar}{2\omega_i}\right) D_{\alpha ii}(2v_i+1) , \quad (31)$$

and

$$B_{\alpha\beta}^v = \sum_i \left[\left(\frac{\hbar}{2\omega_i}\right) D_{\alpha\beta ii}(2v_i+1) + \frac{B_{\alpha i}B_{\beta i}}{2\omega_i^2}\right] \quad (32)$$

h_{Fv} is harmonic in the phonon coordinates even though $D_{\alpha ii}$ and $D_{\alpha\beta ii}$ derive from cubic and quartic mixed anharmonic terms. We have neglected the cubic and quartic anharmonic terms, Λ^{an} (Equation 25), pure in the phonon coordinates since we have no data which would indicate that they are important. In any event, they do not lead to a vibron level dependence for the thermal broadening.

As shown above, the term linear in Q in Equation 30 can contribute to the zero-phonon band spectral shape function, but the contribution would not be Lorentzian. Based on our experimental line shapes, Figures 52 and 53, we may assume that the linear coupling does not significantly contribute to the thermal broadening in our systems. Thus, the off-diagonal quadratic terms, $(B_{\alpha\beta} + B_{\alpha\beta}^v)Q_\alpha Q_\beta$, which do lead to a temperature dependent Lorentzian profile, are taken as responsible for the zero-phonon band broadening. The coupling

coefficient $B^{v}_{\alpha\beta}$ ensures that the broadening will be vibron level dependent. The procedure for deriving the theoretical expression for the thermal broadening using the first order Fermi-Golden rule rate expression, with a perturbation of the form $Q_\alpha Q_\beta$, is a familiar one[17] and we simply give the result

$$\Delta E_v(cm^{-1}) = \hbar^{-3}c^{-1}\int_0^{\omega_M} d\omega\left(\frac{\hbar}{2\omega}\right)^2 g^2(\omega) \langle n_\omega\rangle_T(\langle n_\omega\rangle_T+1)\left|B_{\omega\omega}+B^{v}_{\omega\omega}\right|^2 . \tag{33}$$

$g(\omega)$ is the phonon density of states and $\langle n_\omega\rangle_T$ is the thermal occupation number for a phonon of circular frequency ω at temperature T, $\langle n_\omega\rangle_T = [\exp(h\omega/kT)-1]^{-1}$. Equation 33 reduces to Equation 14 if $B^{v}_{\omega\omega} = 0$, a Debye density of states is used and the longwave approximation employed for $B_{\omega\omega}$.[16-17]

Application of Equation 33 to our experimental data is not possible at this time because of our ignorance of the frequency dependence (ω) of the anharmonic coefficients $D_{\omega\omega ii}$ which arise in $B^{v}_{\omega\omega}$, Equation 32. We must assume also that the frequency dependence varies with vibron oscillator i. Another complication is the fact $B^{v}_{\omega\omega}$ for the zero-vibron level, v = 0, is nonzero due to the zero-point vibron motion. Nevertheless, with Equation 33, we are able to draw some conclusions. First, the frequency dependence of $B^{v}_{\omega\omega}$ is different from the frequency dependence of $B_{\omega\omega}$ (which is ω^2

in the longwave approximation). This follows since, for both the azulene/naphthalene (3500Å) and diazaazulene/naphthalene systems, T_D for the origin band differs from the T_D's for the vibron bands. In other words, when a Debye density of states is employed, the anharmonic contribution does not follow the T^7 (low T) and T^2 (high T) behavior of the harmonic contribution. Only the coupling coefficients, $\bar{a}$, should vary if $B_{\omega\omega}$ and $B^{v}_{\omega\omega}$ have the same frequency dependence. Second, since the vibron bands broaden less rapidly than the zero-vibron origin band, $B_{\omega\omega}$ and $B^{v}_{\omega\omega}$ destructively interfere, i.e., have opposite sign. This follows since the anharmonic terms make a greater contribution, $(2v + 1) = 3$, to a vibron fundamental level than to the zero-vibron level, $(2v + 1) = 1$. This suggests that the phonon frequencies <u>decrease</u> in going from the latter level to the former. Third, the magnitude of the anharmonic contribution is larger than one might expect for quartic terms. However, bear in mind that the anharmonic term, $B^{v}_{\omega\omega}$, was shown above to be <u>negligible</u> for the 7000Å azulene in naphthalene, and 5000Å phenylmono-azaazulene in p-terphenyl systems. At present, it is possible that the two systems considered here may prove to be anomalous in their thermal broadening properties.

If this were the case then, according to the theory above, the coefficients $D_{ii\alpha\beta} = \left(\frac{\partial^4 E_F}{\partial Q_\alpha Q_\beta \partial q_i^2}\right)_{q = Q = 0}$ must be

anomalously large. It is instructive to write this coefficient in the form

$$D_{ii\alpha\beta} = \left[\frac{\partial^2}{\partial Q_\alpha \partial Q_\beta}\left(\frac{\partial^2 E_F}{\partial q_i^2}\right)_{q=0}\right]_{Q=0} . \qquad (34)$$

Now $\left(\frac{\partial^2 E_F}{\partial q_i^2}\right)_{q=0}$ is the force constant for the vibron oscillator i whose value depends on the phonon configuration. The 3500Å and, to a lesser extent, 4500Å vibronic absorption systems of azulene and diazaazulene are known to be anomalous, in that the totally symmetric vibron structure (frequencies, intensities) is strongly dependent on medium. This is in contrast with the 7000Å and 5600Å absorption systems of azulene[32] and phenylmonoazaazulene.[19] The medium dependence is thought to arise because the fundamental frequencies of certain vibrons depend, through second order vibronic coupling, on the electronic state energies which, in turn, depend quite critically on the medium.[10] One can suggest, in view of this strong medium dependence, that the force constants, $\left(\frac{\partial^2 E_F}{\partial q_i^2}\right)_{q=0}$, for the two systems we consider here, are unusually sensitive to the phonon oscillator displacements, giving rise to large values for $D_{ii\alpha\beta}$. There is, however, one real difficulty with this explanation. It is that although the 500-700 cm^{-1} region of the diazaazulene absorption systems is very medium dependent, the 386, 876 and 904 cm^{-1} a_1 bands plus the b_1

vibron structure appear not to be.[44] From Figures 47 and 48 we see that these medium independent bands do, nevertheless, broaden differently from the origin band.

For the azulene/naphthalene 3500Å absorption, the region from 900-1000 cm^{-1} exhibits the strongest vibronic activity.[10] Unfortunately, this leads to a high decree of spectral congestion and makes band width measurements impossible, especially at the higher temperatures. Therefore, the fact that all of the lower frequency vibron bands measured exhibited the same broadening is not taken to mean that the broadenings of other levels might not differ. The band broadenings of the diazaazulene/naphthalene system support this. The 386, 575 and 876 cm^{-1} a_1 vibronic fundamentals exhibit identical thermal broadenings, as do the 1158 and 1457 cm^{-1} b_1 fundamentals, Table 26. However, there are differences in the broadenings of individual vibron levels as well, Figures 47 and 48.

To summarize this section, we have proposed that the dependence of the zero-phonon band thermal broadenings on vibron level reported here is due to the dependence of the phonon oscillator coordinates on vibron level, and not the vibron-phonon nonadiabaticity. To understand why the anharmonic interactions which lead to the vibron level dependence are large in certain systems but not in others will require further studies on a wider variety of systems.

Dependence of Thermal Broadening on Crystal Sample

Above, we reported that band broadening measurements of the 1756 cm^{-1} b_1 vibron fundamental of the 7000Å absorption system of azulene in naphthalene for two different crystals gave different values of the coupling constant $\bar{\alpha}$ (97 and 76 cm^{-1}) but the same value of T_D. This variation with crystal sample is small compared to that reported above for the diazaazulene in naphthalene system, Figures 49-51. For the 539 cm^{-1} band, Figure 50, the broadening for crystal 2 is more than twice that for crystal 1 even though the residual widths are nearly equal. Similar behavior is observed for the origin and 575 cm^{-1} bands, Table 26. Studies on other bands with crystal 2 were not performed. It is interesting that crystal 2, which is characterized by residual widths smaller than those of crystal 1, gives the greater thermal broadening. Presumably, the residual widths are, to a large measure, due to site inhomogeniety and strain. One possible reason for the dependence of the thermal broadening on crystal sample may be that the broadening is very sensitive to the defect structure of the impurity which undergoes sufficient variation from sample to sample. This is consistent with the data reported above on the phenylmonoazaazulene in p-terphenyl system which show that the variation in thermal band broadening and shift with impurity site is large.

Table 1. b polarized absorption spectrum, bc' face, of the 1,3-diazaazulene/naphthalene 4500Å transition

Band	ν,cm^{-1}	$\Delta\nu$	I/I(0,0)	Analysis	Error
1	22154		1	(0,0), O_1	
2	22194	40	.33	40, Lattice	
3	22210	56	.21	56, Lattice	
4	22224	70	.09	70, Lattice	
5	22236	82	.12	82, Lattice	
6	22248	94	.12	40 + 56, Lattice	+2
7	22256	102	.12	102, Lattice	
8	22315	160	.07	O_2(?)	
9	22354	200	.05	O_3(?)	
10	22418	264	.14	O_4	
11	22454	300		O_4 + 36, Lattice	
12	22464	310	.02		
13	22470	316		O_4 + 52, Lattice	
14	22540	386	.21	386, a_1	
15	22579	424	.05	386 + 40, Lattice	+2
16	22617	463	.02	386 + 82, Lattice	+5
17	22693	539	.27	539, a_1	
18	22719	565	.01		
19	22729	575	.38	575, a_1	
20	22750	596	.05	539 + 56, Lattice	-1
21	22769	615	.14	575 + 40, Lattice	0
22	22785	631	.07	575 + 56, Lattice	0

Table 1. (Continued)

Band	ν,cm^{-1}	$\Delta\nu$	I/I(0,0)	Analysis	Error
23	22827	673	.07		
24	22832	678	.52	678, a_1	
25	22837	683	.01		
26	22841	687	.10	fermi resonance w| 2x343	
27	22872	718	.11	678 + 40, Lattice	
28	22888	734		678 + 56, Lattice	
29	22915	761	.05	761	
30	22924	770	.07	2x386	(+2)
31	22949	795	.02		
32	22955	801	.02		
33	22970	816			
34	22986	832	.01		
35	22995	841	.01	575 + 264, 678 + 160	(-2)
36	23011	857	.01		
37	23030	876	.18	876, a_1	
38	23045	891	.07	fermi resonance	
39	23051	897	.07	fermi resonance	
40	23058	904	.15	904, a_1	
41	23076	922	.02	876 + 46, Lattice	
42	23084	930	.03	876 + 56, Lattice	
43	23098	944	.02	904 + 40, Lattice	
44	23104	950	.02		

Table 1. (Continued)

Band	ν,cm^{-1}	$\Delta\nu$	I/I(0,0)	Analysis	Error
45	23110	956	.07	956, a_1	
46	23151	996		956 + 40	0
47	23171	1017		956 + 56, Lattice	+5
48	23182	1028		956 + 70, Lattice	+2
49	23213	1059	.06	973 + 386	0
50	23216	1062	.02	678 + 386	+2
51	23222	1068	.15	2x539	
52	23250	1096	.21	1096, a_1	
53	23258	1104	.17	1104, a_1	
54	23262	1108	.11	1068 + 40, Lattice	0
55	23267	1113	.09	539 + 575 1059 + 56	+1 +2
56	23280	1126	.07	1068 + 56, Lattice	-2
57	23284	1130	.06	1059 + 72, Lattice	+1
58	23305	1151		1096 + 56 1068 + 82	+1 -1
59	23329	1175		1096 + 82 1104 + 70	+3 -1
60	23350	1196	.06	1104 + 93	+1
61	23365	1211	.10	539 + 678	+6
62	23385	1231	.02		
63	23388	1234	.03		
64	23399	1245	.06		
65	23415	1261	.03	876 + 386	+1

Table 1. (Continued)

Band	ν, cm^{-1}	$\Delta\nu$	I/I(0,0)	Analysis	Error
66	23421	1267	.03		
67	23444	1290	.01	904 + 386	0
68	23496	1341	.01	956 + 386	+1
69	23507	1353	.02	678 + 673	-2
70	23512	1358	.12	2x678	-2
71	23520	1366	.07	678 + 687	-1
72	23539	1385	.01		
73	23557	1403	.01		
74	23566	1412	.01		
75	23570	1416	sh	539 + 876	-1
76	23575	1421	.16	1421, a_1	
77	23577	1423	sh		
78		1443		539 + 904	0
79	23607	1453		876 + 575	-2
80	23610	1456		1068 + 386	-2
81	23628	1474	.07		
82	23634	1480	.03	904 + 575 1096 + 386	-1 +2
83	23644	1490	.03	1104 + 386	0
84	23652	1498	.01	956 + 539	-3
85	23663	1509		1421 + 82	-4
86	23674	1520			
87	23688	1534		956 + 575	-3

Table 1. (Continued)

Band	ν,cm^{-1}	$\Delta\nu$	I/I(0,0)	Analysis	Error
88	23692	1538		?	
89	23700	1546	.23	1546, a_1	
90	23713	1559	.06	678 + 876	-5
91	23722	1568			
92	23738	1584	.04	678 + 904	+2
93	23749	1595			
94	23761	1607			
95	23778	1624		Lattice	
96	23787	1633		1096 + 539	
97	23795	1641			
98	23802	1648	.06	1104 + 539	
99	23824	1670		575 + 1096	+1
100	23334	1680	.14	1104 + 575	-1
101	23840	1686			
102	23854	1700			
103	23868	1714	.06		
104	23894	1740	.02	2 x 678 + 386	+2
105	23903	1749		1068 + 678	-3
106	23909	1755	.06	2 x 876	-3
107	23932	1778	.09	1096 + 678	-4
108	23939	1785	.07	1104 + 678	-3
109	23943	1789		1068 + 678 + 40, Lattice	-3

Table 1. (Continued)

Band	ν,cm^{-1}	$\Delta\nu$	I/I(0,0)	Analysis	Error
110	23958	1804		1068 + 628 + 56, Lattice	-2
111	23962	1808	.02	2 x 904 1421 + 386	0 -1
112	23977	1823		1068 + 678 + 80	+3
113	24012	1858		956 + 904	+2
114	24028	1874			
115	24055	1901		2 x 678 + 539	-6
116	24068	1914	.01	2 x 956	-2
117	24084	1930	.03	1546 + 386	+2
118	24096	1942		1068 + 876	+2
119	24107	1953			
120	24112	1958	.02	1421 + 539	+4
121		1962			
122	24132	1978	.02	1096 + 876	-6
123	24153	1999	.03	1421 + 575 1096 + 904	+1 +1
124	24176	2022		1068 + 956	+2
125	24186	2032	.01	3 x 678	+2
126	24190	2036		673 + 678 + 687	+2
127	24197	2043		2 x 678 + 687	0
128	24216	2062	.01	1104 + 956	-2
129	24240	2086	.02	1546 + 539	-1
130	24255	2101	.05	1421 + 678	0

Table 1. (Continued)

Band	ν, cm^{-1}	$\Delta\nu$	I/I(0,0)	Analysis	Error
131	24275	2121	.07	1546 + 575	0
132	24290	2136		2 x 1068	0
133	24298	2144		2101 + 40	-3
134	24314	2160		1068 + 1096	+4
135	24324	2170		1068 + 1104	+2
136	24335	2181			
137	24353	2199		1096 + 1104	+1
138	24365	2211		2 x 1104	-3
139	24376	2222	.07	1546 + 678	+2
140	24400	2246			
141	24417	2263		2 x 678 + 904	-3
142	24454	2300		1421 + 876	-1
143	24468	2314			
144	24484	2330		1421 + 904	-5
145	24497	2343			
146	24518	2364			
147	24527	2373		956 + 1421	+4
148	24572	2418		1546 + 876	+4
149	24619	2465			
150	24644	2490		1421 + 1068	-1
151	24671	2517		1421 + 1096	0
152	24767	2613	.02	1068 + 1546	+1

Table 1. (Continued)

Band	ν, cm^{-1}	$\Delta\nu$	I/I(0,0)	Analysis	Error
153	24795	2641		1096 + 1546	+1
154	24806	2652		1104 + 1546	-2
155	24909	2755			
156	24937	2783		1104 + 1680	+1
157	24964	2810		876 + 1546 + 386	-2
158	25053	2899		2 x 678 + 1546	+3
159	25111	2957		876 + 1546 + 539	+4
160	25255	3101		876 + 678 + 1546	-1
161	25330	3176		2 x 876 + 1421	-3
162	25353	3199		1421 + 1096 + 678	-2
163	25374	3220			
164	25406	3252		876 + 956 + 1421	+1

Table 2. c' polarized absorption spectrum, bc' face, of the 1,3-diazaazulene/naphthalene 4500Å transition

Band	$\nu(cm^{-1})$	$\Delta\nu(cm^{-1})$	I/I(0,0)	Analysis	Error
1	22497	343	.024	343, b_1	
2	22666	512			
3	22670	516	.017	516, b_1	
4	23224	1070	.170	1070, b_1	
5	23262	1108	.036	1070 + 40, Lattice	0
6	23312	1158	.11	1158, b_1	
7	23351	1197	.023	1158 + 40	-1
8	23366	1212	.02	1158 + 54	
9	23376	1222		1158 + 64	
10	23387	1233	.041	1233, b_1	
11	23426	1272		1233 + 40	+1
12	23483	1329	.071	1329, b_1	
13	23513	1359		(2 x 678)	
14	23526	1372	.024	1329 + 40	-3
15	23565	1411		1068 + 343	0
16	23605	1451	sh	1070 + 386	+5
17	23611	1457	.115	1457, b_1	
18	23644	1490		1104 + 386	
19	23652	1498	.02	1457 + 40	-1
20	23663	1509		1457 + 56	+4
21	23698	1544	.053	1158 + 386, 1546, a_1	

Table 2. (Continued)

Band	$\nu(cm^{-1})$	$\Delta\nu(cm^{-1})$	I/I(0,0)	Analysis	Error
22	23731	1577			
23	23736	1582			
24	23743	1589			
25	23756	1602	.087	1602, b_1	
26	23772	1618	.011	1233 + 386	+1
27	23777	1623		1104 + 516	-3
28	23793	1639	.019	1602 + 40	+3
29	23804	1650	.02	Lattice	
30	23854	1700	.013	2 x 678 + 343	-1
31	23869	1715	.015	1329 + 386	0
32	23891	1737	sh		
33	23903	1749	.038	678 + 1070	-1
34	23909	1755		(2 x 876)	
35	23920	1766	.003	343 + 1421	+2
36	23939	1785		(1104 + 678)	
37	23956	1802		1068 + 386 + 343 904 + 386 + 516	-5 +4
38	23990	1836	.027	1158 + 678	0
39	23997	1843	.011	1457 + 386	0
40	24019	1865			
41	24057	1903			
42	24066	1912	.018	1233 + 678	-1

Table 2. (Continued)

Band	$\nu(cm^{-1})$	$\Delta\nu(cm^{-1})$	I/I(0,0)	Analysis	Error
43	24100	1946	.021	1070 + 876	0
44	24139	1985	.023	1602 + 386	+3
45	24163	2009	.014	1329 + 678	-2
46	24176	2022		1070 + 956	+4
47	24187	2033	.026	1158 + 876	+1
48	24216	2062	.011	1158 + 904 1546 + 516	0 0
49	24288	2134	.022	1457 + 678	+1
50	24307	2153		2 x 904 + 343	-2
51	24322	2168	.012	1096 + 1070	-2
52	24340	2186	.017	1233 + 956	+3
53	24360	2206	.027	1329 + 876	-1
54	24380	2226			
55	24410	2256	.035	1158 + 1096	-2
56	24418	2264	.017	1104 + 1158	-2
57	24435	2281	.013	956 + 1329 1602 + 678	+4 -1
58	24446	2292		1096 + 678 + 516	-2
59	24485	2331		1457 + 876 1233 + 1096	+2 -2
60	24507	2353		904 + 1457	+8
61	24544	2390		1068 + 1329	+7
62	24670	2516		2 x 678 + 1158	-2
63	24713	2559		1602 + 956	-1
64	24765	2611	.059	1070 + 1546	+5

Table 2. (Continued)

Band	$\nu(cm^{-1})$	$\Delta\nu(cm^{-1})$	I/I(0,0)	Analysis	Error
65	24807	2653		1233 + 1423	+3
66	24842	2688		2 x 678 + 1329	-3
67	24853	2699		1096 + 1602	-1
68	24933	2779		1233 + 1546	0
69	25027	2873		1329 + 1546	+2
70	25061	2907		1068 + 678 + 1158	-3
71	25086	2932		1546 + 876 + 516	+6
72	25149	2995		1104 + 1546 + 343	-2
73	25210	3056		1068 + 386 + 1602	0
74	25218	3064		1068 + 539 + 1457	0
75	25297	3144		1602 + 1546	+4

Table 3. The vibrational fundamentals of the 4500Å $^1B_1 \leftarrow {}^1A_1$ absorption spectrum of 1,3-diazaazulene

a_1			b_1		
NAPH[a]	DCB[b]	QAZ[c]	NAPH	DCB	QAZ
	357[d]	372			
386	382	384	343	339	344
539			516	515	515
575			1070	1066	1070
	644	660	1158	1156	1158
678	678	690	1233	1239	1233
761	719	734	1329	1319	1315
876	885	887	1457	1455	1460
904	900	906			
956	914	924	1602	1598	1590
1068[e]					
1096	1089	1091			
1104	1109	1103			
1421	1419	1415			
1546	1544	1546			
1680[e]					

[a]Naphthalene host.

[b]p-Dichlorobenzene host.

[c]Quinazoline host.

[d]Band positions in cm^{-1} displacement from the origin band.

[e]Not assigned as fundamentals, c.f. text.

Table 4. Unpolarized absorption spectrum of the 1,3-diazaazulene/p-dichlorobenzene 4500Å $^1B_1 \leftarrow {}^1A_1$ transition

Band	$\nu(cm^{-1})$	$\Delta\nu(cm^{-1})$	log I/I_o	Analysis	Error
1	22192	0	.85	(0,0)	
2	22233	41		41, Lattice	
3	22248	56		56, Lattice	
4	22273	82		82, Lattice	
5	22288	96		96, Lattice	
6	22302	110		110, Lattice	
7	22497	305			
8	22531	339	.02	339, b_1	
9	22549	357	.13	357, a_1	
10	22574	382	.10	382, a_1	
11	22707	515	.02	515, b_1	
12	22636	644	.22	644, a_1	
13	22864	672			
14	22870	678	.29	678, a_1	
15	22874	682		644 + 41, Lattice	+3
16	22882	690			
17	22911	719	.07	719, a_1	
18	23077	885	.05	885, a_1	
19	23092	900	.04	900, a_1	
20	23106	914	.11	914, a_1	
21	23193	1001	.05	644 + 357	0

Table 4. (Continued)

Band	$\nu(cm^{-1})$	$\Delta\nu(cm^{-1})$	log I/I_o	Analysis	Error
22	23217	1025	.02	644 + 382	+1
23	23227	1035	.08	678 + 357	0
24	23258	1066	.05	1066, b_1	
25	23281	1089	.04	1089, a_1	
26	23291	1099	.03	382 + 719	+2
27	23301	1109	.19	1109, a_1	
28	23348	1156	.07	1156, b_1	
29	23386	1194		1109 + 82, Lattice	-3
30	23431	1239		1239, b_1	
31	23511	1319	.06	1319, b_1	+3
32	23528	1336	.04	690 + 644	-2
33	23545	1353	.03		
34	23552	1360	.05	2 x 678	-4
35	23611	1419	.08	1419, a_1	
36	23647	1455	.07	1455, b_1	
37	23660	1468	.03	1109 + 357	-2
38	23683	1491	.03	1109 + 382	0
39	23731	1539	.02	1156 + 382	-1
40	23736	1544	.07	1544, a_1	
41	23753	1561	.02	678 + 885	+2
42	23784	1592		678 + 914	0
43	23790	1598	.11	1598, b_1	

Table 4. (Continued)

Band	$\nu(cm^{-1})$	$\Delta\nu(cm^{-1})$	log I/I_o	Analysis	Error
44	23798	1606		719 + 885	-2
45	23945	1753	.05	1109 + 644	0
46	23978	1786	.07	1109 + 678	+1
47	24290	2098	.03	1419 + 678	-1
48	24329	2137	.02	1455 + 678	-4
49	24415	2223	.03	1544 + 678	-1
50	24457	2265	.03	1109 + 1156	0

Table 5. Polarized absorption spectrum of 1,3-diazaazulene in quinazoline, z polarization, xz face

Band	$\nu(cm^{-1})$	$\Delta\nu(cm^{-1})$	I/I(0,0)	Analysis	Error
1	22540	0	1	(0,0)	
2	22569	29		29, Lattice	
3	22572	32		32, Lattice	
4	22582	42		42, Lattice	
5	22613	73		73, Lattice	
6	22632	92		92, Lattice	
7	22660	120		120, Lattice	
8	22695	155		multiplet	
9	22699	159		multiplet	
10	22884	344	.11	344, b_1	
11	22912	372	.09	372, a_1	
12	22924	384	.07	384, a_1	
13	23042	502	.03	344 + 159	±1
14	23055	515	.045	515, b_1	
15	23200	660	.54	660, a_1	
16	23211	671	.030	515 + 159	
17	23222	682	sh		
18	23225	685	sh	2 x 344	±3
19	23230	690	.11	690, a_1	
20	23243	703		660 + 42, Lattice	
21	23274	734	.10	734, a_1	

Table 5. (Continued)

Band	$\nu(cm^{-1})$	$\Delta\nu(cm^{-1})$	I/I(0,0)	Analysis	Error
22	23299	759		660 + 99, Lattice	
23	23361	821		660 + 159	-2
24	23387	847		690 + 159	+2
25	23427	887	.048	887, a_1	
26	23446	906	.073	906, a_1	
27	23464	924	.096	924, a_1	
28	23543	1003	.046	660 + 344	+1
29	23563	1023	.040		
30	23587	1047	.012	671 + 372	-4
31	23594	1054	.019	671 + 384	+1
32	23604	1064	sh	906 + 159	+1
33	23610	1070	.193	1070 (b_1)	
34	23615	1075	.035	734 + 344	+3
35	23622	1082	.060		
36	23631	1091	.183	1091 (a_1)	
37	23643	1103	.353	1103 (a_1)	
38	23675	1135	.01	1091 + 44, 1103 + 32, Lattice	
39	23684	1144	.01	1103 + 41, Lattice	
40	23698	1158	.127	1158 (b_1)	
41	23729	1187		1091 + 96, Lattice	
42	23749	1209	.019	690 + 515	-4
43	23762	1222	sh		

Table 5. (Continued)

Band	$\nu(cm^{-1})$	$\Delta\nu(cm^{-1})$	I/I(0,0)	Analysis	Error
44	23766	1226	.074	1070 + 159	+3
45	23773	1233	.100	1233, b_1	
46	23792	1252		1091 + 159	-2
47	23812	1272		924 + 344 1226 + 46 1233 + 39, Lattice	-4
48	23842	1302	sh	924 + 372 924 + 384	-6 +6
49	23855	1315	.147	1315 b_1	+2
50	23881	1341	.068		
51	23893	1353			
52	23921	1381	.110	2 x 690	-1
53	23926	1386	.025		
54	23934	1394	.025	1233 + 159	-2
55	23952	1412	.051	1070 + 344	+2
56	23955	1415	.089	1415, a_1	
57	23975	1435	.033	1091 + 344	
58	23991	1451		1070 + 384 1103 + 344	+3 -4
59	24000	1460	.268	1460, b_1	
60	24014	1474	.055	1103 + 372 1091 + 384	+1 +1
61	24030	1490	.040	1103 + 384	-3
62	24042	1502		1158 + 344	0
63	24054	1515	.061		

Table 5. (Continued)

Band	$\nu(cm^{-1})$	$\Delta\nu(cm^{-1})$	I/I(0,0)	Analysis	Error
64	24071	1531			
65	24086	1546	.073	1546, a_1	
				690 + 887	-1
				1233 + 344	-1
66	24118	1578	sh	1415 + 159	-4
67	24130	1590	.350	1590, b_1	
68	24140	1600	.053		
				1091 + 515	+1
69	24145	1605	.089	1233 + 372	0
				1103 + 515	0
				1233 + 384	-1
70	24158	1618	.115	1460 + 159	+1
71	24172	1632		1590 + 42	
72	24241	1701		1315 + 384	-2
73	24269	1729	.055	1070 + 660	+1
74	24283	1743	.139		+6
75	24297	1757	.072	1415 + 344	+2
76	24300	1760	.075	1103 + 660	+3
77	24332	1792		690 + 1103	+1
78	24358	1818		1158 + 660	0
				906 + 924	-1
				1158 + 671	-2
				1315 + 515	-1
79	24371	1831		1460 + 372	+1
80	24383	1843		1460 + 384	+1

Table 5. (Continued)

Band	$\nu(cm^{-1})$	$\Delta\nu(cm^{-1})$	I/I(0,0)	Analysis	Error
				1546 + 344	-2
				1158 + 734	0
81	24432	1892		1233 + 660	+1
82	24461	1921		1546 + 372	-3
				1590 + 344	
				1415 + 515	
83	24471	1931		1546 + 384	-1
				1226 + 734	
				1590 + 372	+4
84	24498	1958	.064	1070 + 887	-1
				1590 + 384	-1
				1315 + 660	0
85	24515	1975		1070 + 906	+1
86	24543	2003		1315 + 690	+2
87	24570	2030	.037	924 + 1103	-3
				1158 + 924	+6
88	24616	2076		1415 + 660	-1
				1590 + 515	+1
89	24644	2104		1415 + 690	+1
				887 + 1233	+3
90	24657	2117	.083	1460 + 660	+3
				1415 + 734	-2
				1226 + 924	-1
91	24691	2151		1460 + 690	-1
				1070 + 1103	-7
92	24720	2180		2 x 1091	+2
				1460 + 734	+2
93	24731	2191		1091 + 1103	+3
				2 x 1103	+3
				1546 + 660	+3
94	24743	2203		887 + 1315	-1

Table 5. (Continued)

Band	$\nu(cm^{-1})$	$\Delta\nu(cm^{-1})$	I/I(0,0)	Analysis	Error
				1091 + 1158	+3
				1315 + 924	-7
95	24786	2246	.180	1590 + 660	+4
				671 + 1890	
96	24799	2259		1103 + 1158	+2
				1546 + 734	+3
97	24817	2277		1590 + 690	+3
				1091 + 1233	+5
				1091 + 1226	-2
				1415 + 906	+2
98	24859	2319		1590 + 734	+5
99	24942	2402		1091 + 1315	+4
100	24979	2439			
101	25013	2473		1590 + 887	+4
				1091 + 1415	-3
102	25049	2509		1590 + 924	+5
103	25100	2560		1460 + 1103	+3

Table 6. Polarized absorption spectrum of 1,3-diazaazulene in quinazoline, x polarization, xz face

Band	$\nu(cm^{-1})$	$\Delta\nu(cm^{-1})$	Intensity	Analysis	Error
1	22540		0	(0,0)	
	[the origin is not observed in the "x" polarization]				
2	22884	344	.04	344, b_1	
3	23042	502	.03	344 + 159	+1
4	23055	515	.03	515, b_1	
5	23211	671	.04		+3
6	23543	1003	.02	660 + 344	+1
7	23585	1045	.02	372 + 671	-2
8	23596	1056	.01	384 + 671	-1
9	23608	1068	.16	1068, b_1	
10	23614	1074	sh		
11	23621	1081	.05	734 + 344	-3
12	23647	1107		1068 + 39, Lattice	
13	23652	1112		1068 + 44, Lattice	
14	23698	1158	.12	1158, b_1	
15	23748	1208	.03	690 + 515	-3
16	23761	1221	sh	1068 + 159	+6
17	23766	1226	.14	1226, b_1	
18	23772	1232	.04	887 + 344	-1
19	23804	1264		1226 + 38, Lattice	
20	23811	1271		1226 + 45, Lattice	
21	23825	1285			

Table 6. (Continued)

Band	$\nu(cm^{-1})$	$\Delta\nu(cm^{-1})$	Intensity	Analysis	Error
22	23855	1315	.16	1315, b_1	
23	23869	1329		660 + 671	+2
24	23891	1351		1315 + 36, Lattice	
25	23911	1371	.06		+1
26	23933	1393	.04		
27	23963	1423	.01	906 + 515	+2
28	23975	1435	.02	1091 + 344	0
29	23991	1451	sh	1068 + 384 1103 + 344	+1 -4
30	23999	1459	.15	1459, b_1	
31	24030	1490		1459 + 31, Lattice	
32	24039	1499		1459 + 40, Lattice	
33	24053	1513	.07		
34	24084	1544			
35	24105	1565			
36	24128	1588	.23	1588, b_1	
37	24138	1598	sh	1226 + 372	0
38	24143	1603	.06		
39	24156	1616	.15	1616, b_1	
40	24172	1632		Lattice	
41	24186	1646			
42	24213	1673			

Table 6. (Continued)

Band	$\nu(cm^{-1})$	$\Delta\nu(cm^{-1})$	Intensity	Analysis	Error
43	24240	1700	.04	1315 + 384	-1
44	24268	1728	.01	1068 + 660	0
45	24282	1742	.17		
46	24295	1755	.16		
47	24308	1768	.01		
48	24328	1788		Lattice	
49	24332	1792		1755 + 37, Lattice	
50	24356	1816		660 + 1158	+2
51	24372	1832		1459 + 372	-1
52	24386	1846			
53	24397	1857	.01		
54	24433	1893	.04	734 + 1158 1546 + 344	-1 -3
55	24469	1929	.01	1415 + 515	+1
56	24498	1958	.04	887 + 1068	-3
57	24515	1975	.04	906 + 1068 606 + 1315	-1 0
58	24543	2003	.03	384 + 1616 690 + 1315	-3 +2
59	24568	2028	.02		
60	24620	2080			
61	24642	2102			
62	24657	2117	0.4	1459 + 660	+2

Table 6. (Continued)

Band	$\nu(cm^{-1})$	$\Delta\nu(cm^{-1})$	Intensity	Analysis	Error
63	24714	2174			
64	24720	2180			
65	24784	2244			
66	24798	2258			
67	24817	2277			
68	24827	2287			
69	24861	2321			
70	24905	2365			
71	24942	2402		1091 + 1315	
72	24982	2442			
73	25013	2473			

Table 7. Unpolarized bc' fluorescence spectrum of 1,3-diazaazulene/naphthalene

Band	ν, cm^{-1}	$\Delta\nu$, cm^{-1}	I/I(0,0)	Analysis	Error
1	22154	0	1	(0,0)	
2	22117	37	.06	37, Lattice	
3	22098	56	.05	56, Lattice	
4	22073	81		81, Lattice	
5	22061	93	.01	93, Lattice	
6	21996	158	.002	multiplet	+4
7	21960	194			
8	21954	200	.002	multiplet	
9	21833	322	.003	332, b_2	
10	21805	349	.004	349, b_1	
11	21792	362			
12	21754	400			
13	21749	405	.06	405, a_1	
14	21710	444	.005	405 + 37	-2
15	21693	461		405 + 56, Lattice	0
16	21668	486		405 + 81, Lattice	0
17	21622	532	.02	532, b_1	
18	21569	585			
19	21551	603			
20	21535	619	.004		
21	21511	643	.008	(2 x 323)	

Table 7. (Continued)

Band	ν,cm^{-1}	$\Delta\nu$,cm^{-1}	I/I(0,0)	Analysis	Error
22	21458	696	.15	696, a_1	
23	21452	702	.05	(2 x 349) fermi resonance	
24	21424	730	.02	730, b_1	
25	21397	757	.007	696 + 56, Lattice	
26	21290	864			
27	21287	867	.007		
28	21284	870	.18	870, a_1	
29	21270	884	.004	349 + 532, f resonance w/ 870	+3
30	21247	907	.005	870 + 37, Lattice	0
31	21241	913	.01		
32	21232	922	.50	922, a_1	
33	21225	929	.005	870 + 56, Lattice	-3
34	21215	939			
35	21202	952	.03	952, a_1 (?)	
36	21194	960	.02	922 + 37, Lattice	-1
37	21174	980	.02	922 + 56, Lattice	-2
38	21152	1002	.08	1002, b_1	
39	21134	1020	.11	1020, b_1	
40	21113	1041		1002 + 37	0
41	21099	1055		1020 + 37	+2
42	21080	1074		1020 + 56	

Table 7. (Continued)

Band	ν,cm^{-1}	$\Delta\nu$,cm^{-1}	I/I(0,0)	Analysis	Error
43	21058	1096		Lattice	
44	21053	1101	.008	696 + 405	0
45	21048	1106	.07	1106, b_1	
46	21053	1119			
47	21022	1132			
48	21015	1139			
49	20954	1200	.04	1200, a_1	
50	20949	1205	.009		
51	20946	1208	.005		
52	20942	1212	.004		
53	20926	1228	.03	1228, a_1 (?)	
54	20918	1236		1200 + 37, Lattice	+1
55	20914	1240			
56	20911	1243		922 + 323	-2
57	20908	1246	.07	1246, a_1	
58	20899	1255		1200 + 56, Lattice	
59	20896	1258			
60	20888	1266	.01	1228 + 37, Lattice	-1
61	20875	1279	.008	870 + 405	-4
62	20863	1291		1200 + 93, Lattice	+2
63	20850	1304		1246 + 37, Lattice	
64	20838	1316			

Table 7. (Continued)

Band	ν,cm^{-1}	$\Delta\nu$,cm^{-1}	I/I(0,0)	Analysis	Error
65	20835	1319		1228 + 93, Lattice	+2
66	20827	1327	.15	1327, a_1	
67	20823	1331	.03	922 + 405	+4
68	20819	1335		1246 + 93, Lattice	+4
69	20813	1341		1020 + 323	+2
70	20805	1349		405 + 941	-3
71	20789	1365		1327 + 37, Lattice	-1
72	20769	1385	.007	1327 + 56, Lattice	-2
73	20757	1397	.02	2 x 696	-5
74	20751	1403		2 x 702	+1
75	20747	1407	.17	1407, a_1	
76	20733	1421	.004	1327 + 93, Lattice	-1
77	20726	1428	.004	1020 + 405	-3
78	20709	1445	.006	1407 + 37	-1
79	20697	1457	.003	922 + 532	-3
80	20689	1465	.005	1407 + 56	-2
81	20679	1475		941 + 532	-2
82	20670	1484			
83	20658	1496	.002		
84	20649	1505		922 + 579	-4
85	20643	1511		405 + 1106	0
86	20636	1518		2 x 760	

Table 7. (Continued)

Band	ν, cm^{-1}	$\Delta\nu$, cm^{-1}	I/I(0,0)	Analysis	Error
87	20629	1525		1200 + 323	
88	20613	1541	.01	1541, a_1 (?)	
89	20597	1557	.002		
90	20587	1567	.01	696 + 870	-1
91	20582	1572	.007	702 + 870	0
92	20565	1589	.002		
93	20557	1597	.024	1597, a_1	
94	20548	1606	.004	1200 + 405	-1
95	20543	1611	.004		
96	20536	1618	.039	696 + 922	0
97	20530	1624	.015	922 + 702	0
98	20522	1632	.002	1228 + 405	+1
99	20514	1640		696 + 941	
100	20503	1651		1246 + 405	0
101	20500	1654	.004	1618 + 37, Lattice	+1
102	20493	1661	.004		
103	20491	1663			
104	20487	1667			
105	20480	1674		1618 + 56, Lattice	0
106	20476	1678		349 + 1327	-2
107	20472	1682		922 + 760	0
108	20466	1688			

Table 7. (Continued)

Band	ν,cm^{-1}	$\Delta\nu$,cm^{-1}	I/I(0,0)	Analysis	Error
109	20457	1697	.004	1002 + 696	+1
110	20444	1710			
111	20439	1715	.005	1020 + 696	+1
112	20433	1721		1020 + 702	+1
113	20425	1729		1327 + 405	+3
114	20413	1741	.016	2 x 870	-1
115	20404	1750		1228 + 523	+1
116	20396	1758			
117	20390	1764		1002 + 760	-2
118	20386	1768		1246 + 523	+1
119	20376	1778		2 x 870 + 37	-1
120	20374	1780		760 + 1020	
121	20362	1793	.081	870 + 922	-1
122	20344	1810	.008	1407 + 405	+2
123	20331	1823	.003	952 + 870	-1
124	20323	1831	.002		
125	20310	1844	.11	2 x 922	0
126	20281	1873	.012	952 + 922	+1
127	20273	1881	.002	2 x 941	
128	20265	1889	.021	870 + 1020	+1
129	20260	1894	.003	1200 + 696	+2
130	20252	1902		1200 + 702	0

Table 7. (Continued)

Band	ν,cm^{-1}	$\Delta\nu$,cm^{-1}	I/I(0,0)	Analysis	Error
131	20232	1922	.023	1002 + 922	+2
132	20215	1939	.004	696 + 1246	+3
133	20213	1941	.029	1020 + 922	+1
134	20178	1976	.003	870 + 1106	0
135	20137	2017	.014		
136	20131	2023	.011	696 + 1327	0
137	20127	2027	.016	922 + 1106	+1
138	20087	2067	.006	1200 + 870	+3
139	20053	2101	.008	1407 + 696	+2
140	20048	2106	.007	1407 + 702	+3
141	20037	2117	.007	1246 + 870	-1
142	20034	2120	.011	1200 + 922	+2
143	20007	2147	.009	922 + 1228	+3
144	19991	2163	.020	922 + 1246	+5
145	19971	2183	.003	1240 + 941	+4
146	19960	2193	.017	922 + 1276	+5
147	19956	2198	.009	1327 + 870	-1
148	19910	2244	.042	2 x 922 + 405	+5
149	19904	2250	.009	1327 + 922	-1
150	19881	2273	.021	1407 + 870	+4
151	19826	2328	.050	1407 + 922	+1

Table 8. Unpolarized fluorescence spectrum of 1,3-diazaazulene/p-dichlorobenzene

Band	ν, cm^{-1}	$\Delta\nu$, cm^{-1}	I/I(0,0)	Analysis	Error
1	22192	0	1	(0,0)	
2	22149	43	.50	43, Lattice	
3	22104	88	.31	88, Lattice	
4	22094	98	.31	98, Lattice	
5	22081	111	.26	111, Lattice	
6	22061	131	.18	131, Lattice	
7	21987	205	.17	multiplet site	
8	21789	403	.19	403, a_1	
9	21658	534	.05		
10	21573	619	.08		
11	21497	695	.29	695, a_1	
12	21491	701	.21		
13	21464	728	.07		
14	21439	753	.08		
15	21320	872	.45	872, a_1	
16	21266	926	$\sim$2	926, a_1	
17	21246	946	.18	946, a_1	
18	21227	965	.09	Lattice	
19	21191	1001	.15	1001, b_1	
20	21167	1024	.60	1024, b_1	
21	21132	1060		Lattice	

Table 8. (Continued)

Band	ν,cm^{-1}	$\Delta\nu$,cm^{-1}	I/I(0,0)	Analysis	Error
22	21085	1107	.20	1107, b_1	
23	21053	1139	.05		
24	20997	1195	.09		
25	20989	1203	.14	1203, a_1	
26	20966	1226	.17	1226, a_1	
27	20953	1239	sh		
28	20949	1243	.19	1243, a_1	
29	20920	1272	.06	872 + 403	+3
30	20865	1327	.35	1327, a_1	
31	20861	1331	sh	926 + 403	-2
32	20819	1373	.07	Lattice	
33	20798	1394	.05	695 x 2	-4
34	20784	1408	.55	1408, a_1	
35	20778	1414	.08		
36	20767	1425	.04	1024 + 403	+2
37	20741	1451	.07	Lattice	
38	20715	1477	.04		
39	20653	1539	.05		
40	20646	1546	.04		
41	20593	1599	.09	1599, a_1	
42	20569	1623	.06	926 + 695	-2
43	20564	1628	.05	926 + 701	-1

Table 8. (Continued)

Band	ν,cm^{-1}	$\Delta\nu$,cm^{-1}	I/I(0,0)	Analysis	Error
44	20472	1720	.04	1024 + 695	-1
45	20447	1745	.03	2 x 872	-1
46	20392	1800	.13	926 + 872	-2
47	20379	1813	.03		
48	20338	1854	.20	2 x 926	-2
49	20314	1878	.05	926 + 946	-6
50	20296	1896	.05	872 + 1024	0
51	20264	1928	.03	926 + 1001	-1
52	20241	1951	.14	926 + 1024	-1
53	20170	2022	.03	695 + 1327	0
54	20155	2037	.03		

Table 9. Unpolarized xz fluorescence spectrum of 1,3-diazaazulene/quinazoline

Band	ν,cm^{-1}	$\Delta\nu$,cm^{-1}	Intensity	Analysis	Error
1	22706	-163		0_1	
2	22543	0		0_2	
3	22494	49		0_2 + 49, Lattice	
4	22464	79		0_2 + 79, Lattice	
5	22417	126			
6	22300	243	.06	0_1 + 407, a_1	-1
7	22136	407	.10	0_2 + 407, a_1	
8	22005	538	.13	0_1 + 701, a_1	0
9	21842	701	.24	0_2 + 701, a_1	
10	21836	707	.09	0_1 + 868, a_1	+2
11	21806	737	.06	0_2 + 701 + 36, Lattice	
12	21778	765	.41	0_1 + 926, a_1	+2
13	21743	800	.05	0_1 + 765 + 35, Lattice	
14	21675	868	.28	0_1 + 868, a_1	
15	22648	895	.18		
16	21628	915	.10	868 + 49, Lattice	+2
17	21617	926	.80	0_2 + 926, a_1	
18	21590	953	.16	953, a_1	
19	21578	965	.10	0_2 + 926 + 39, Lattice	
20	21535	1008	.17	0_2 + 1008, b_1	
21	21522	1021	.24	0_2 + 1021, b_1	

Table 9. (Continued)

Band	ν,cm^{-1}	$\Delta\nu$,cm^{-1}	Intensity	Analysis	Error
22	21486	1057	.06	O_2 + 1021 + 36, Lattice	
23	21472	1071	.04		
24	21460	1083	.08		
25	21426	1117	.14	O_2 + 1117, b_1	
26	21384	1159	.14	O_1 + 1323, a_1	-1
27	21342	1201	.09	O_2 + 1201, a_1	
28	21315	1228	.12	O_2 + 1228, a_1	
29	21296	1247	.22	O_2 + 1247, a_1	
30	21220	1323	.25	O_2 + 1323, a_1	
31	21178	1365	.10	O_2 + 1323 + 42, Lattice	
32	21133	1410	.24	O_2 + 1410, a_1	
33	21097	1446	.03	O_2 + 1410 + 36, Lattice	
34	20999	1544	.08	1544, a_1	
35	20949	1594	.07	1594, a_1	
36	20921	1622	.07	O_2 + 926 + 701	+5
37	20913	1630	.05	O_1 + 926 + 868	-1
38	20883	1660	.03		
39	20850	1693	.08	O_1 + 2 x 926	-4
40	20813	1730	.03	O_2 + 2 x 868	+6
41	20749	1794	.08	O_2 + 926 + 868	0
42	20692	1851	.17	O_2 + 2 x 926	+1
43	20665	1878	.04	O_2 + 926 + 953	+1

Table 9. (Continued)

Band	ν,cm^{-1}	$\Delta\nu$,cm^{-1}	Intensity	Analysis	Error
44	20651	1892	.07	O_2 + 868 + 1021	-3
45	20594	1949	.12	O_2 + 926 + 1021	-2
46	20462	2081	.04	O_1 + 926 + 1323	+5
47	20393	2150	.05	O_2 + 926 + 1228	+4
48	20371	2172	.09	O_2 + 926 + 1248	+2
49	20351	2192	.04	O_2 + 868 + 1323	-1
50	20322	2221	.06		
51	20294	2249	.10	O_2 + 926 + 1323	0
52	20273	2279	.06	O_2 + 1410 + 868	-1
53	20204	2338	.08	O_2 + 926 + 1410	-2
54	20176	2367	.06	O_2 + 1117 + 1248	-2
55	20155	2388	.05	O_1 + 2 x 926 + 701	+2

Table 10. The ground state fundamental vibrations of 1,3-diazaazulene

a_1					b_1				
NAPH	DCB	QAZ	IR	RAMAN	NAPH	DCB	QAZ	IR	RAMAN
405	403	407		410	349				355
696	695	701	690	696	532	534			538
870	872	868	870	870	730	728			760
922	926	926		920	1002	1001	1008		
952[a]	946	953		945					
1200	1203	1201	1195		1020	1024	1021	1030	1025
1228[a]	1226	1228	1230		1106	1107	1117	1115	
1246	1243	1247	1245	1245					
1327	1327	1323	1320						
1407	1408	1410	1405						
1541[a]	1543	1544	1535						
1597	1599	1594	1590						

[a]Assignment uncertain, c.f. text.

Table 11. Unpolarized phosphorescence spectrum of 1,3-diazaazulene/naphthalene

Band	$\nu(cm^{-1})$	$\Delta\nu(cm^{-1})$	I	Analysis	Error
1	19052	0	75	(0,0)	
2	19036	16	10	870 + 922 + 1327 fluorescence	-1
3	19031	22	5		
4	19016	36	31	(36) Lattice	
5	19009	43	10	2 x 870 + 1407 fluorescence	-2
6	18999	53	10		
7	18996	56	10		
8	18986	66	16	2 x 922 + 1327 fluorescence	-3
9	18980	73	11	3 x 922 + 405 fluorescence	+3
10	18963	89	5		
11	18957	95	30	870 + 922 + 1407 fluorescence	-2
12	18910	142	5		
13	18904	149	33	2 x 922 + 1407 fluorescence	-1
14	18898	155	9		
15	18874	179	27		
16	18858	194	5		
17	18852	200	6		
18	18837	216	8		
19	18824	228	5		

Table 11. (Continued)

Band	$\nu(cm^{-1})$	$\Delta\nu(cm^{-1})$	I	Analysis	Error
20	18815	237	3		
21	18806	246	6		
22	18770	282	3		
23	18764	288	6		
24	18735	317			
25	18729	323	80	323, a_1 or b_2	
26	18720	332	5		
27	18712	340	9	340, b_1	
27a	18703	349	7		
28	18693	359	7	323 + 36, Lattice	
29	18684	368	7		
30	18673	379	2	323 + 56, Lattice	
31	18652	400	6		
32	18647	405	5	405, a_1	
33	18638	414			
33a	18633	419			
34	18628	424	70	424, b_2 or a_2	
35	18588	464	16		
36	18584	468	16		
37	18582	470	16		
38	18567	485	16		
39	18555	497			

Table 11. (Continued)

Band	$\nu(cm^{-1})$	$\Delta\nu(cm^{-1})$	I	Analysis	Error
40	18529	523			
41	18520	532	23		
42	18516	537	10	3 x 922 + 870	+2
43	18504	548			
44	18503	549	19		
45	18499	553			
46	18475	577	3		
47	18473	579	43	579, a_2 or b_2	
48	18448	604	3		
49	18433	619	13		
50	18422	630	7		
51	18409	643	17	2 x 323	+3
52	18362	690	16		
53	18356	696	77	696, a_1	
54	18351	701	62		
55	18339	713	20		
56	18319	733	10		
57	18314	738	5		
58	18306	746	50	323 + 424	+1
59	18300	752	25		
60	18292	760	51	760, b_2	
61	18255	797	5		

Table 11. (Continued)

Band	$\nu(cm^{-1})$	$\Delta\nu(cm^{-1})$	I	Analysis	Error
62	18234	818	6		
63	18231	821	6		
66	18198	854	20		
67	18178	874	49	874, a_1	
68	18150	902	16	323 + 579	0
69	18144	908	6		
70	18129	923	19	923, a_1	
71	18115	937	45		
72	18111	941	60	941, a_2	
73	18099	953	15		
74	18081	971	55	971, b_2	
75	18074	978	16		
76	18056	996	47	996, b_1	
76a	18048	1004	13	424 + 579	-1
77	18045	1007	18		
78	18043	1009	31		
79	18030	1022	21	696 + 323	-3
80	18025	1027	35		
81	17956	1096	45		
82	17945	1107	30		
83	17932	1120	27	696 + 424	0
84	17868	1134	20	760 + 424	0

Table 11. (Continued)

Band	$\nu(cm^{-1})$	$\Delta\nu(cm^{-1})$	I	Analysis	Error
85	17845	1206	16		
86	17830	1222	17		
87	17825	1227	66	1227, a_1	
88	17810	1241	12		
89	17807	1245	55	1245, a_1	
90	17776	1276	57	1276, a_2	
91	17771	1281	28	579 + 701	-1
92	17759	1293	8	971 + 323	+1
93	17743	1309	18		
94	17728	1324	59	1324, a_1	
95	17720	1332	6		
96	17707	1345	12		
97	17703	1349	10	1027 + 323	+1
98	17668	1384	65	1384, b_2	
99	17656	1396	9	2 x 696	-4
100	17647	1405	35		
101	17645	1407	38		
102	17623	1429	12		
103	17604	1448	10		
104	17600	1452	32		
105	17598	1454	32	696 + 760	+2
106	17561	1491	7		

Table 11. (Continued)

Band	$\nu(cm^{-1})$	$\Delta\nu(cm^{-1})$	I	Analysis	Error
107	17557	1495	80	1495, b_2	
108	17539	1513	15		
109	17524	1528	40		
110	17511	1541	13		
111	17501	1548	7	323 + 1227	+2
112	17500	1552	14	971 + 579	-2
113	17496	1556	12		
114	17484	1568	22	323 + 1246	+1
115	17479	1573	10	374 + 696	-3
116	17462	1590	59		
117	17455	1597	64	1597, a_1	
118	17446	1606	16		
119	17440	1612	13		
120	17419	1633	30	874 + 760	+1
121	17415	1637	30	941 + 696	0
122	17411	1641	25	941 + 701	+1
123	17398	1652	26	1227 + 424	-1
124	17385	1667	15	971 + 696	0
125	17379	1673	14	971 + 701	-1
126	17370	1682	21		
127	17361	1691	16		
128	17355	1697	10	1276 + 424	+3

Table 11. (Continued)

Band	$\nu(cm^{-1})$	$\Delta\nu(cm^{-1})$	I	Analysis	Error
129	17342	1710	12	1384 + 323	-3
130	17326	1726	23	1027 + 696	-3

Table 12. Unpolarized phosphorescence spectrum of 1,3-diazaazulene/p-dichlorobenzene

Band	ν, cm^{-1}	$\Delta\nu, cm^{-1}$	I	Analysis	Error
1	18869	0	1	(0,0)	
2	18832	37	.31	37, Lattice	
3	18791	78	.16	78, Lattice	
4	18535	334	.25	334	
5	18350	519			
6	18304	565			
7	18266	603	.11		
8	18196	673	.03		
9	18179	690	.13	690, a_1	
10	18171	698	.06		
11	18165	713	.06	Lattice	
12	18107	762	.06		
13	18021	848			
14	17896	973			
15	17817	1052	.04		
16	17731	1138			
17	17690	1179			
18	17687	1182			
19	17678	1191			
20	17638	1231	.04		
21	17458	1411			

Table 12. (Continued)

Band	ν, cm^{-1}	$\Delta\nu, cm^{-1}$	I	Analysis	Error
22	17368	1501	.04	1501	
23	17275	1594	.05		
24	17268	1601	.11	1601, a_1	
25	17209	1660			
26	17205	1664			

Table 13. xz phosphorescence spectrum of 1,3-diazaazulene/quinazoline

Band	$\nu(cm^{-1})$	$\Delta\nu(cm^{-1})$	I/I(0,0)	Analysis	Error
1	19110		1		
2	18974	136	.04		
3	18916	194	.11		
4	18779	331	.16	331, b_1	
5	18683	427	.19		
6	18525	585	.09		
7	18410	700	.25	700, a_1	
8	18347	763	.07		
9	18222	888	.08		
10	18150	960	.04		
11	18129	981	.06		
12	18106	1004	.07	1004, b_1	
13	18085	1025	.06	1025, b_1	
14	18081	1029		700 + 331	+3
15	17983	1127		700 + 437	0
16	17878	1232	.06	1232, a_1	
17	17859	1251	.04	1251, a_1	
18	17830	1280	.08		
19	17781	1329	.07	1329, a_1	
20	17708	1402		2 x 700	+2
21	17697	1413	.10	1413, a_1	

Table 13. (Continued)

Band	$\nu(cm^{-1})$	$\Delta\nu(cm^{-1})$	I/I(0,0)	Analysis	Error
22	17669	1441			
23	17650	1460		700 + 763	+3
24	17604	1506	.28	1506	
25	17508	1602	.14		
26	17501	1609	.35		
27	17392	1718			
28	17339	1771	.18		
29	17321	1789	.09		
30	17314	1796			
31	17307	1803		1609 + 194	0
32	17260	1850	.07		
33	17219	1891	.06		
34	17174	1936	.10	1609 + 331	+4
35	17022	2088	.04	1506 + 585	+3
36	16934	2176	.10	1413 + 763	0

Table 14. Phosphorescence fundamentals of 1,3-diazaazulene

NAPH			DCB	QAZ	RAMAN	IR
$\Delta\nu(cm^{-1})$	I_b/I_c,	I_b/I_a	$\Delta\nu(cm^{-1})$	$\Delta\nu(cm^{-1})$	$\nu(cm^{-1})$	$\nu(cm^{-1})$
(0,0)	1.5	1				
323	1.4	1.7	334	331	310	
424	0.3	1		427	423	
579	0.4	1	603	585	550	
696 (a_1)	1.5	1	690	700		
760 (b_2)	0.4	1	762	763	760	770
874 (a_1)	1	1.5		888		
941 (a_2)	2	1.9		960	945	
971 (b_2)	1.2	2.6	973	981		970
996 (b_1)	1	1.7		1004		
1227 (a_1)	2	1.3	1231	1232		
1246 (a_1)	2	2.2		1252		
1276 (a_2)	0.9	1		1280		
1324 (a_1)	1.5	1.3		1329		
1384 (b_2)	1	0.8		1413		1390
1495 (b_2)	1.3	0.7	1501	1506		1505
1598 (a_1)	1.7	1	1601	1609		

Table 15. Vibronic coupling coefficients for the 4500Å $^1B_1 \leftarrow {}^1A_1$ absorption of diazaazulene/naphthalene

	f x10^4	C($S_1 \sim S_2$)		f x10^4	C($S_1 \sim S_4$)	C($S_1 \sim S_3$)
(0,0)	20.9		343	.5	170 cm^{-1}	390 cm^{-1}
386	4.5		516	.3	130	300
539	5.6	440 cm^{-1}	1070	3.0	420	940
575	7.9	520	1158	2.5	380	870
678	10.8		1233	.9	230	520
876	3.7		1329	1.5	290	670
904	2.7		1457	2.3	360	830
956	1.4		1602	2.0	340	770
1096	4.5					
1104	3.6					
1421	3.4					
1546	4.8					

Table 16. Vibronic coupling parameters for the 4500Å $^1B_1 \leftarrow {}^1A_1$ absorption of diazaazulene/p-dichlorobenzene

a_1	$f(\times 10^4)$	$C(S_1\text{-}S_2)$	b_1	$f(\times 10^4)$	$C(S_1 \sim S_4)$	$C(S_1 \sim S_3)$
(0,0)	22.4		343	.54	180 cm^{-1}	400 cm^{-1}
357	4.86	600	515	.54	180	400
382	4.73		1066	1.75	320	720
644	9.05	820	1156	.94	230	530
678	12.62		1319	2.03	340	780
			1455	3.11	420	960
888	1.77		1598	4.19	490	1110
900	.95					
924	4.59					
1089	1.89					
1109	6.89					
1419	2.30					
1544	2.43					

Table 17. a-polarized absorption spectrum of the 2-phenyl-1,3-diazaazulene/dibenzyl 4500Å $^1B_1 \leftarrow {}^1A_1$ transition

Band	$\nu(cm^{-1})$	$\Delta\nu(cm^{-1})$	I/I(0,0)	Analysis	Error
1	21812.3	-95		0_1	
2	21671.8	-36		0_2	
3	21891.9	-16		0_3	
4	21907.6		1	0_4	
5	21942.3	35	.27	Lattice	
6	22170.1	262	.54	262, a_1	
7	22203.2	296	.18	262 + 35	
8	22320.5	413	.04	413, a_1	
9	22357.6	450	.06	450, b_1	
10	22434.6	527	.17	2 x 262	-3
11	22464.8	557	.03	557, b_1	
12	22479.5	572	.04	572, a_1	
13	22534.6	627	.03	627, a_1	
14	22565.6	658	.05	658, a_1	
15	22581.4	674	.02	413 + 262	+1
16	22619.3	712	.03	262 + 450	0
17	22651.8	744			
18	22669.9	762			
19	22695.7	788	.02	3 x 262	-2
20	22741.9	834	.02	575 + 262	0
21	22796.0	888	.03	627 + 262	+1
22	22831.3	924	.02	658 + 262	-4

Table 17. (Continued)

Band	$\nu(cm^{-1})$	$\Delta\nu(cm^{-1})$	I/I(0,0)	Analysis	Error
23	22883.6	976		450 + 527	+1
24	22967.6	1060	.22	1060, b_1	
25	23003.4	1096	.27	1096, b_1	
26	23018.5	1111	.18	1111, a_1	
27	23051.9	1144		1111 + 35	+2
28	23084.0	1176	.05	1176, b_1	
29	23151.6	1244	.04	1244, b_1	
30	23184.8	1277	.06	1277, b_1	
31	23232.7	1325	.12	1060 + 262	-3
32	23268.6	1361	.16	1096 + 262	-3
33	23282.2	1375		1111 + 262	-2
34	23330.1	1422	.07	1422, a_1	
35	23349.5	1442	.03	1176 + 262	-4
36	23368.6	1461	.11	1461, b_1	
37	23409.4	1502	.02	1244 + 262	+4
38	23442.3	1535	.02	1277 + 262	+4
39	23465.2	1558		1111 + 450	+3
40	23499.5	1592		1060 + 527	-5
41	23531.2	1624		1096 + 527	-1
42	23546.2	1639		527 + 1111	-1
43	23594.3	1687		1422 + 262	-3
44	23631.5	1724	.07	1461 + 262	-1

Table 18. Vibronic coupling coefficients for the 4500Å $^1B_1 \leftarrow {}^1A_1$ absorption system of phenyldiazaazulene/dibenzyl

a_1	$fx10^4$	b_1	$fx10^4$	$C(S_1 \sim S_2)$	$C(S_1 \sim S_4)$
(0,0)	51.1	450	2.21	100	290
262	26.0	557	1.07	70	200
413	1.93	1060	8.19	195	560
572	2.00	1096	10.2	220	635
627	1.79	1176	1.92	95	270
658	2.66	1244	1.38	80	230
1111	9.42	1277	2.03	100	280
1422	3.82	1461	4.21	140	400

Table 19. Unpolarized bc' fluorescence spectrum of 2-phenyl-1,3-diazaazulene/dibenzyl

Band	$\nu(cm^{-1})$	$\Delta\nu(cm^{-1})$	I/I(0,0)	Analysis	Error
1	21908		1	(0,0)	
2	21631	277	.54	277, a_1	
3	21356	550	.17	2 x 277	
4	21250	658	.12	658, a_1	
5	21025	883	.04	883, a_1	
6	21978	930	.36	930, a_1	
7	20951	957	.12	957, a_1	
8	20881	1027		1027, b_1	
9	20777	1131		1131, b_1	
10	20751	1157	.03	883 + 277	3
11	20704	1204	.19	930 + 277	3
12	20672	1236	.08	957 + 277	2
13	20570	1338	.33	1338, a_1	
14	20517	1391	.21	1391, a_1	
15	20483	1425	.09	1425, a_1	
16	20424	1484	.05	550 + 930	4
17	20315	1593	.06	658 + 930	5
18	20289	1619	.18	1338 + 277	4
19	20238	1670	.13	1391 + 277	2
20	20208	1700	.04	1425 + 277	2
21	20045	1863	.05	2 x 930	3
22	20016	1892	.08	1338 + 550	4

Table 19. (Continued)

Band	$\nu(cm^{-1})$	$\Delta\nu(cm^{-1})$	I/I(0,0)	Analysis	Error
23	19964	1944	.03	1391 + 550	3
24	19908	2000	.03	1338 + 658	4
25	19855	2053	.02	1391 + 658	4
26	19772	2136	.03	2 x 930 + 277	1
27	19743	2165	.02	1338 + 550 + 277	0
28	19689	2219	.01	1391 + 550 + 277	1
29	19639	2269	.10	930 + 1338	1
30	19608	2300	.03	957 + 1338	5
31	19585	2323	.05	930 + 1391	2
32	19554	2354	.03	957 + 1391	6
33	19361	2547	.06	1338 + 277 + 930	2
34	19308	2600	.03	1391 + 277 + 930	2
35	19279	2629	.02	1425 + 277 + 930	3
36	19230	2678	.05	2 x 1338	2
37	19176	2732	.06	1338 + 1391	3

Table 20. Correlation of phenyldiazaazulene/dibenzyl and diazaazulene/naphthalene ground state fundamental frequencies

Phenyldiazaazulene/dibenzyl		Diazaazulene/naphthalene	
a_1	b_1	a_1	b_1
			349
277		405	
			532
658		696	
			730
883		870	
930		922	
957		952	
			1001
	1027		1024
	1131		1107
		1200	
		1228	
		1246	
1338		1327	
1391		1407	
1425		1541	
		1597	

Table 21. Unpolarized ab phosphorescence spectrum of 2-phenyl-1,3-diazaazulene/dibenzyl

Band	$\nu(cm^{-1})$	$\Delta\nu(cm^{-1})$	I	Analysis	Error
1	16853		10	0_1	
2	16822	31		0_1 + 31, Lattice	
3	16659	194	.28	0_2	
4	16590	263	.16		
5	16432	421	.77	421, f	
6	16421	432	.16		
7	16400	453		421 + 32, Lattice	
8	16258	595			
9	16235	618		421 + 194	-3
10	16213	640	.08		
11	16192	661	.80	661, a_1	
12	16161	692	.13	661 + 31, Lattice	
13	16125	728	.09		
14	16112	741	.19		
15	16093	760	.68	760, b_1	
16	16068	785		760 + 25, Lattice	
17	16052	801	.14		
18	15998	855			
19	15982	871	.28	871, f	
20	15894	959	.19	959, a_1	
21	15864	989		989, f	
22	15821	1032			

Table 21. (Continued)

Band	$\nu(cm^{-1})$	$\Delta\nu(cm^{-1})$	I	Analysis	Error
23	15769	1084	.08	661 + 421	-2
24	15732	1121	.09		
25	15684	1169			
26	15638	1215	.16	1215, f	
27	15570	1283			
28	15533	1320		2 x 661	+2
29	15507	1346			
30	15456	1397	.56	1397, a_1	
31	15430	1423		760 + 661	-2
32	15408	1445			
33	15395	1458			
34	15366	1487	.34	1487, f	
35	15352	1501	.44	1501, b_2	
36	15319	1534		871 + 661	
37	15263	1590	.86	1590, a_1	+2
38	15251	1602			
39	15235	1618		1590 + 28, Lattice	
40	15036	1817			

Table 22. Comparison of the diazaazulene/naphthalene 4500Å $^1B_1 \leftrightarrows {}^1A_1$ absorption and fluorescence fundamental frequencies.

Absorption		Fluorescence		
ν	I	ν	I	
(0,0)	1	(0,0)	1	
386	.21	405	.06	
539	.27	696	.15	
575	.38	870	.18	
678	.52	922	.50	
876	.18	1200	.04	
904	.13	1228	.03	a_1
956	.07	1246	.07	
1096	.21	1327	.15	
1104	.17	1407	.17	
1421	.16	1541	.01	
1546	.23	1597	.03	
343	.02	349	.01	
516	.01	532	.02	
1070	.14	1002	.08	
1158	.12	1020	.11	
1233	.04	1106	.07	b_1
1329	.07			
1457	.11			
1602	.10			

Table 23. Stark splitting results for diazaazulene/quinazoline 4500Å absorption spectrum

Band	$\Delta E_{1/2}(cm^{-1})^a$	$\frac{d\delta}{dE}(\frac{cm^{-1}}{Kv})^b$	$\lvert\Delta\mu\rvert$ (D)^c
(0,0)	2.45	0.475±.002	1.80
372	1.75	0.475±.003	1.80
384	2.25	0.453±.01	1.72
660	1.60	0.460±.002	1.74
734	1.90	0.477±.003	1.81

[a]Residual band width at 4.2°K.

[b]Slope of the splitting vs voltage curve.

[c]$|\Delta\mu|$ is calculated assuming $|\Delta\mu|$ of the origin band is 1.80 debye, the value found for diazaazulene/naphthalene.

Table 24. Thermal band broadening and band shift parameters for the 5600Å $^1B_1 \leftarrow {}^1A_1$ absorption system of phenylmonoazaazulene/p-terphenyl

Band	$\nu(cm^{-1})$ at 4.2°K	$\Delta E(cm^{-1})$ at 4.2°K*	$\alpha(cm^{-1})$	$\bar{\alpha}(cm^{-1})$	$\alpha^2/\bar{\alpha}$
0_1	17855.5 ± 0.1	1.0 ± .05	-47	104	21
0_1 + 264	18119	1.4		100	
0_2	17899.6	1.2	-16[a]	45	
0_2 + 264	18164	1.4		43	
0_3	17916.1	1.0	-17[a]	50	
0_3 + 264	18180	1.2		59	
0_4	18019.9	0.9	b	∿150[c]	
0_5	18042.8	3.3	b	∿200[c]	
0_6	18048.3	0.8	-48	87	26
0_7	18074.1	1.2	-42[a]	108	
0_8	18087.9	1.4	-69	133	35
0_9	18131.7	1.1	-61	89	42
0_{10}	18139.2	1.2	-68	108	43
0_{11}	18151.6	1.0	-66	81	54
0_{12}	18242.7	1.0	-66	96	45

[a]These values are approximate because of scatter of data.

[b]Insufficient data.

[c]Approximated from available data for T<20°K.

*Residual widths at 4.2°K, presumably due to inhomogeneity.

Table 25. Thermal band broadening parameters for the 3500Å $^1A_1(2) \leftarrow {}^1A_1(1)$ absorption system of azulene/naphthalene

Band	$\Delta E(cm^{-1})$, 4.2°K[a]	$\bar{\alpha}$, cm^{-1}	T_D,°K
(0,0)	1.4 cm^{-1}	130	50
655	1.4	117	60
669	1.5	117	60
695	1.5	117	60
801	2.0	117	60
854	3.0	117	60

[a]Residual width at half-peak intensity.

Table 26. Thermal band broadening parameters for the 4500Å $^1B_1 \leftarrow {}^1A_1$ absorption system of 1,3-diazaazulene/naphthalene

Band	Crystal 1			Crystal 2		
	$\Delta E(cm^{-1})$, 4.2°K[a]	$\bar{\alpha}$	T_D	$\Delta E(cm^{-1})$, 4.2°K[a]	$\bar{\alpha}$	T_D
(0,0)	2.3	91	50	1.9	140	50
386 cm^{-1} (a_1)	1.6	405	100	---[b]	---	---
539 (a_1)	4.0	62	65	3.8	163	65
575 (a_1)	3.0	405	100	2.6	256	65
876 (a_1)	3.4	405	100	---	---	---
904 (a_1)	1.9	195	75	---	---	---
1070 (b_1)	3.8	78	70	---	---	---
1158 (b_1)	2.5	140	70	---	---	---
1457 (b_1)	3.2	140	70	---	---	---

[a]Residual width at half-peak intensity.

[b]Not measured.

Figure 1. Energy level diagram and kinetic parameters for azulene.

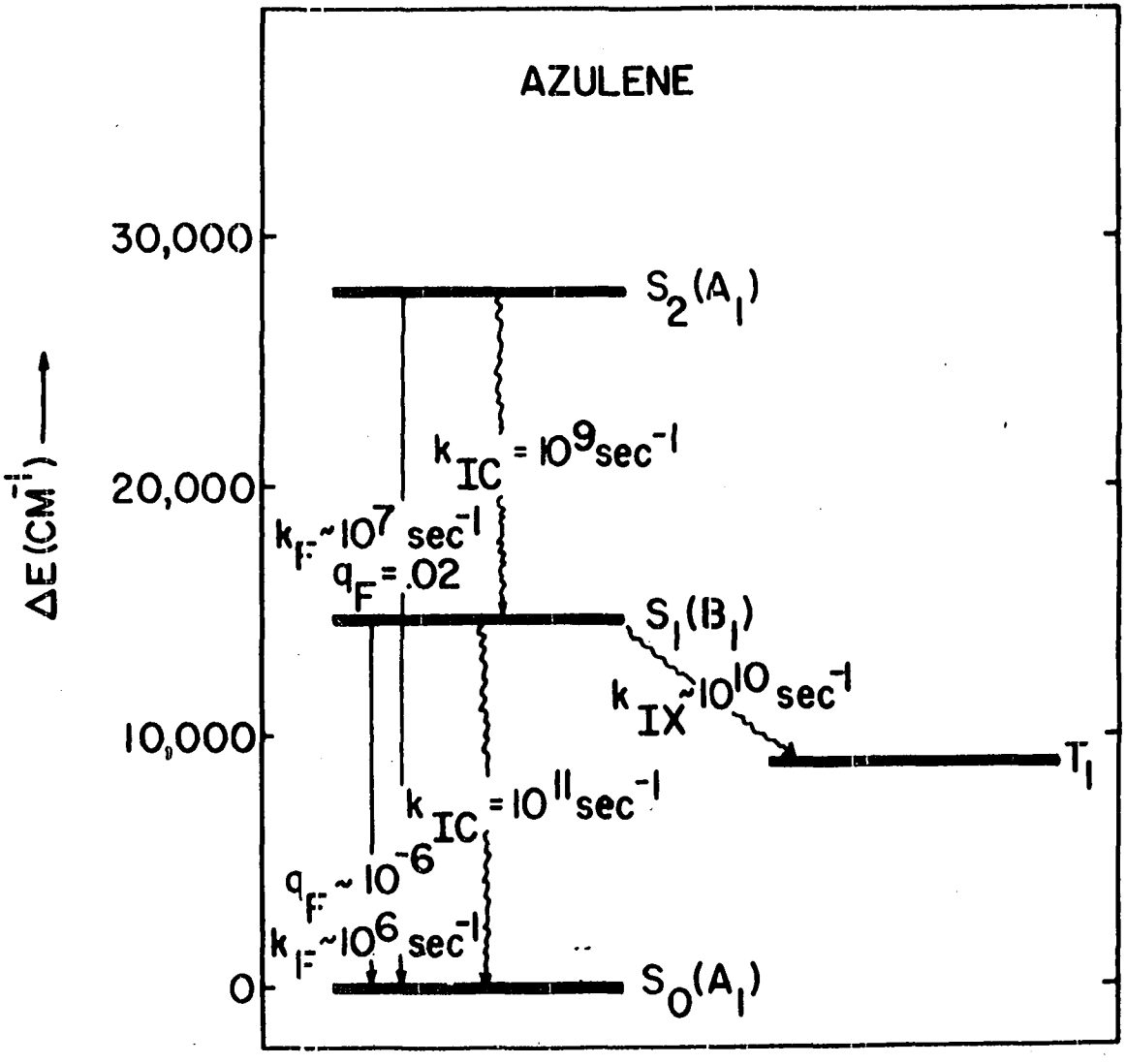
AZULENE
30,000
20,000
10,000
0
ΔE(CM⁻¹)
S2(A1)
S1(B1)
S0(A1)
T1
kIC = 10⁹sec⁻¹
kF ~ 10⁷ sec⁻¹
qF = .02
kIX ~ 10¹⁰ sec⁻¹
kIC = 10¹¹sec⁻¹
qF ~ 10⁻⁶
kF ~ 10⁶ sec⁻¹

Figure 2. Skeletal structure of 1,3-diazaazulene. The x axis transforms as the B_1 rep in point group C_{2v}.

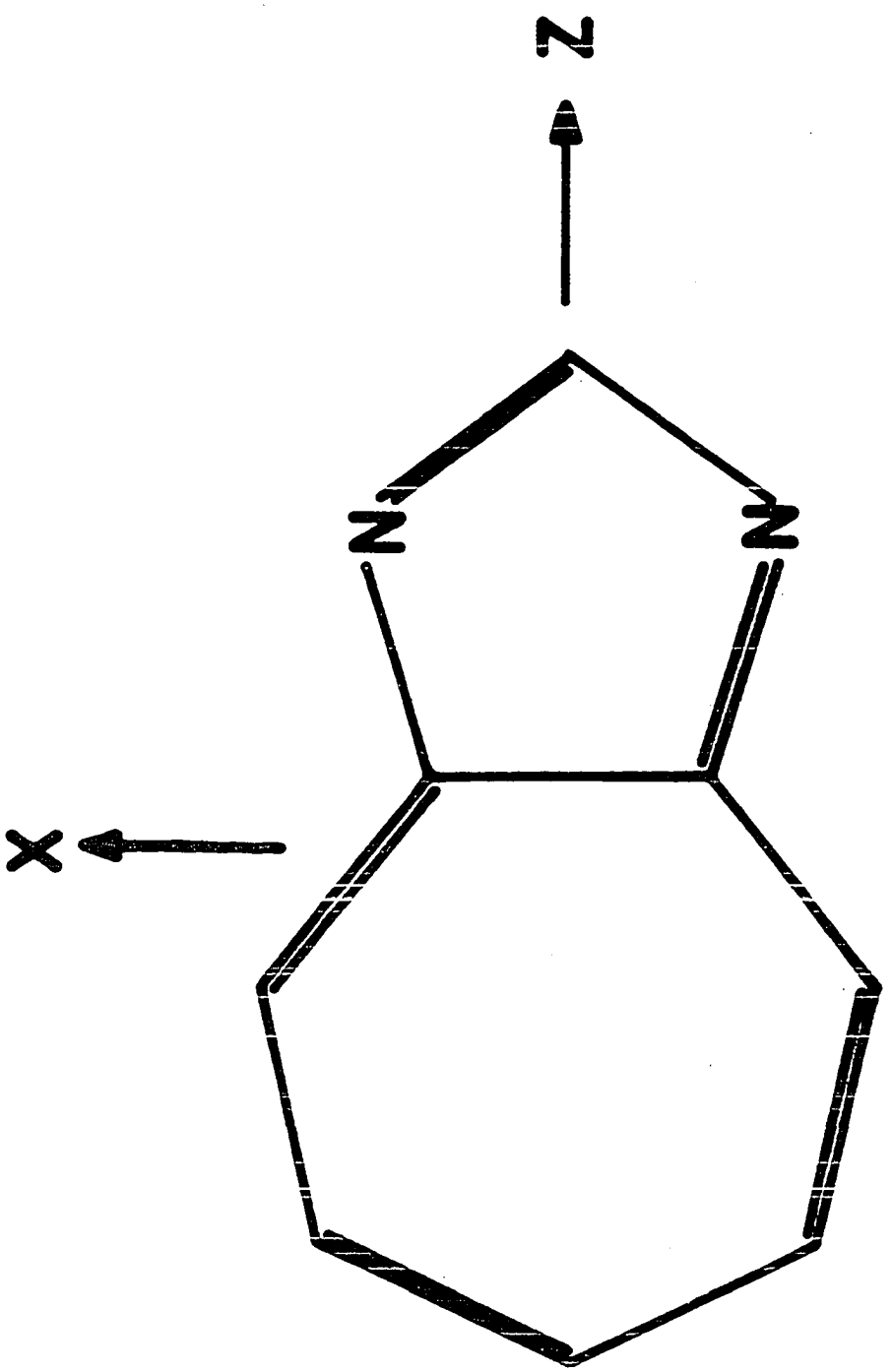
Z
N
N
X

Figure 3. ab polarized absorption spectra of the diazaazulene/naphthalene 4500Å $^1B_1 \leftarrow {}^1A_1(\pi\pi^*)$ transition (4.2°K). The upper trace is the b polarization.

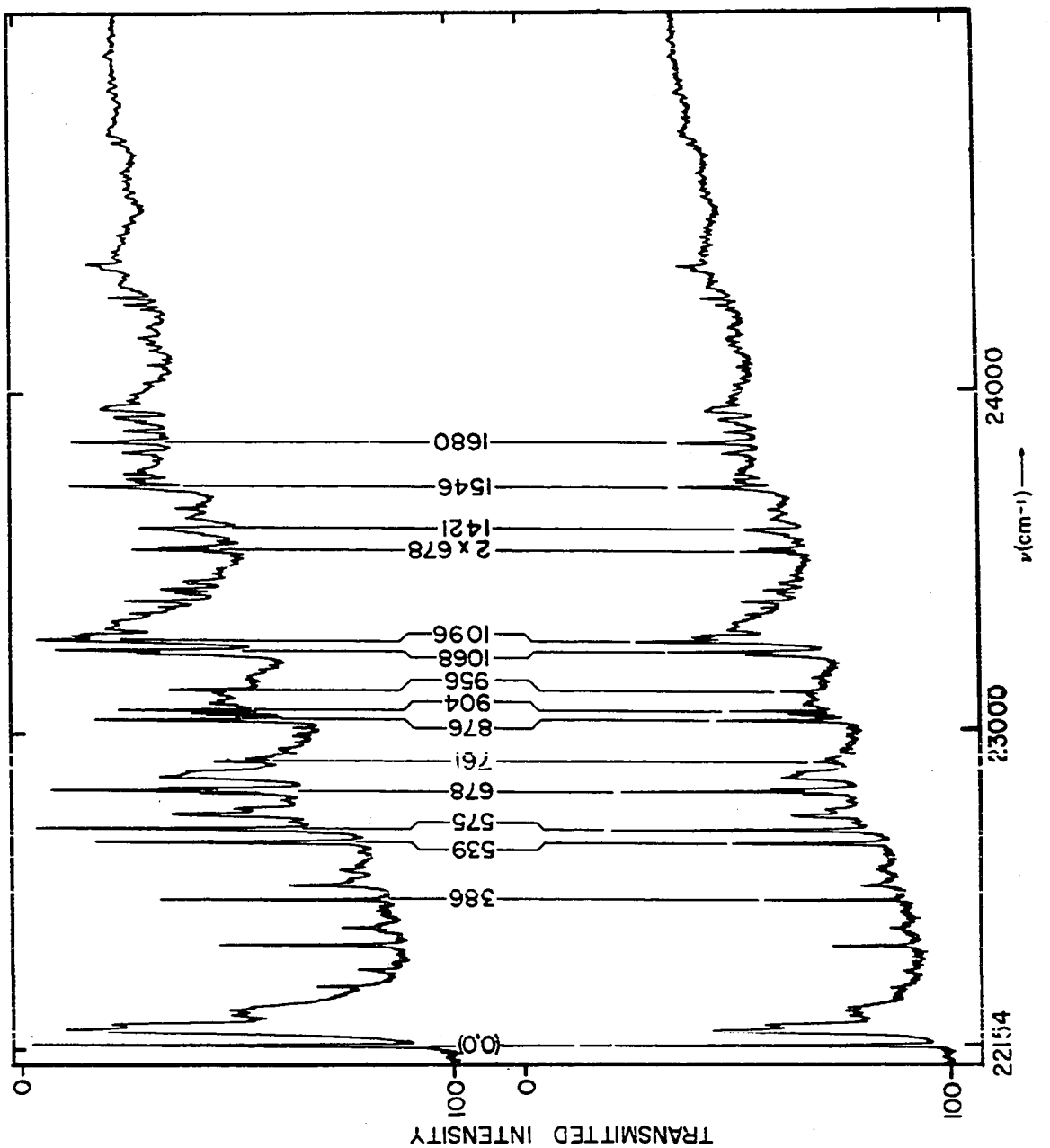
TRANSMITTED INTENSITY
100
0
100
0
22154
23000
24000
ν(cm⁻¹)
(0,0)
386
539
575
678
761
876
904
956
1068
1096
2 x 678
1421
1546
1680

Figure 4. bc' polarized absorption spectra of the diazaazulene/naphthalene 4500Å, $^1B_1 \leftarrow {}^1A_1(\pi\pi^*)$ transition (4.2°K). The upper trace is c'.

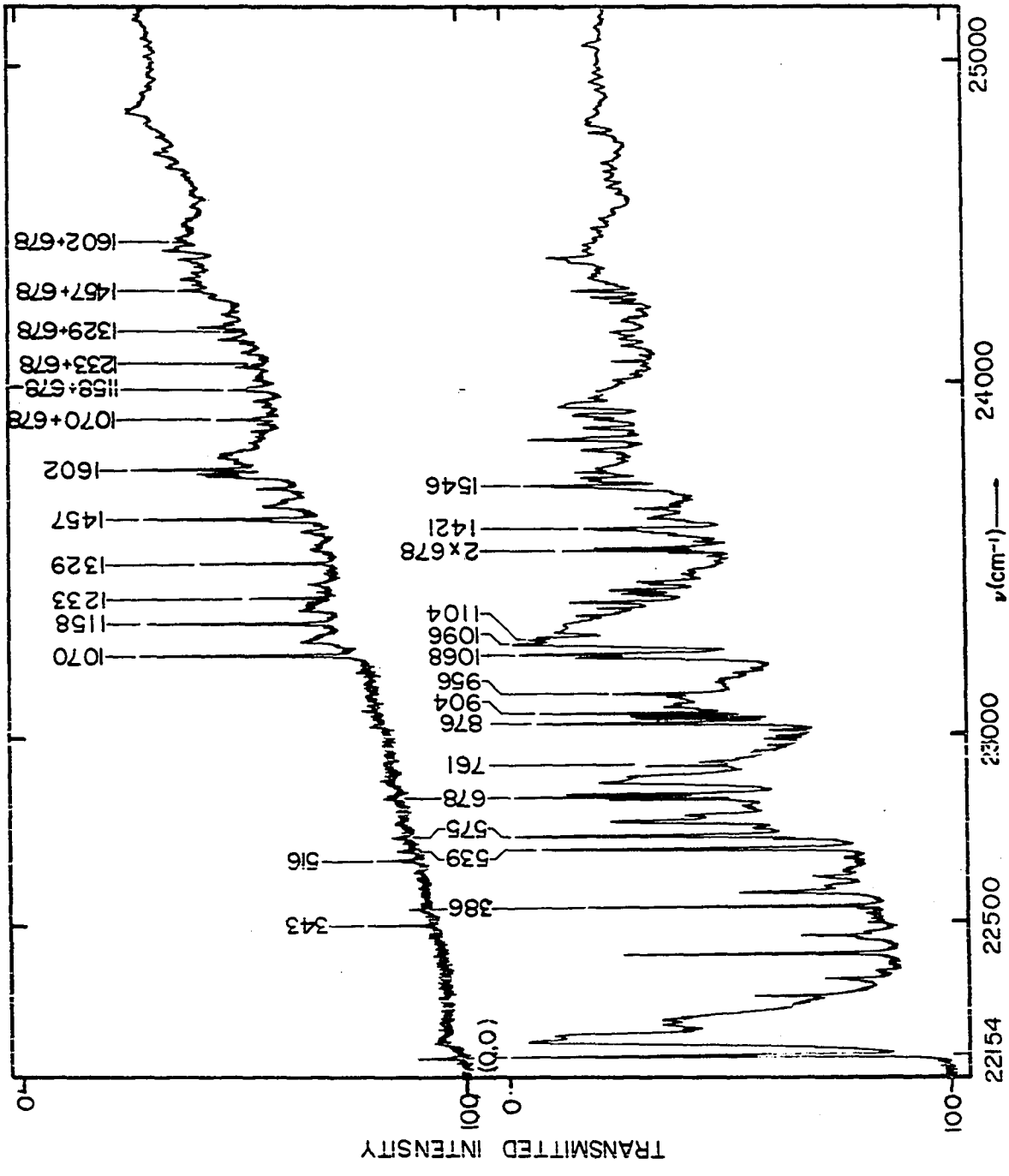
TRANSMITTED INTENSITY
0
100
0
100
22154
22500
23000
24000
25000
ν(cm⁻¹)
(0,0)
343
386
516
539
575
678
761
876
904
956
1068
1096
1104
1421
2x678
1546
1070
1158
1233
1329
1457
1602
1070+678
1158+678
1233+678
1329+678
1457+678
1602+678

Figure 5. bc' absorption spectra of the diazaazulene/naphthalene 4500Å $^1B_1 \leftarrow {}^1A_1$ transition (4.2°K). The polarization ratios of these spectra closely approximate the oriented gas ratios.

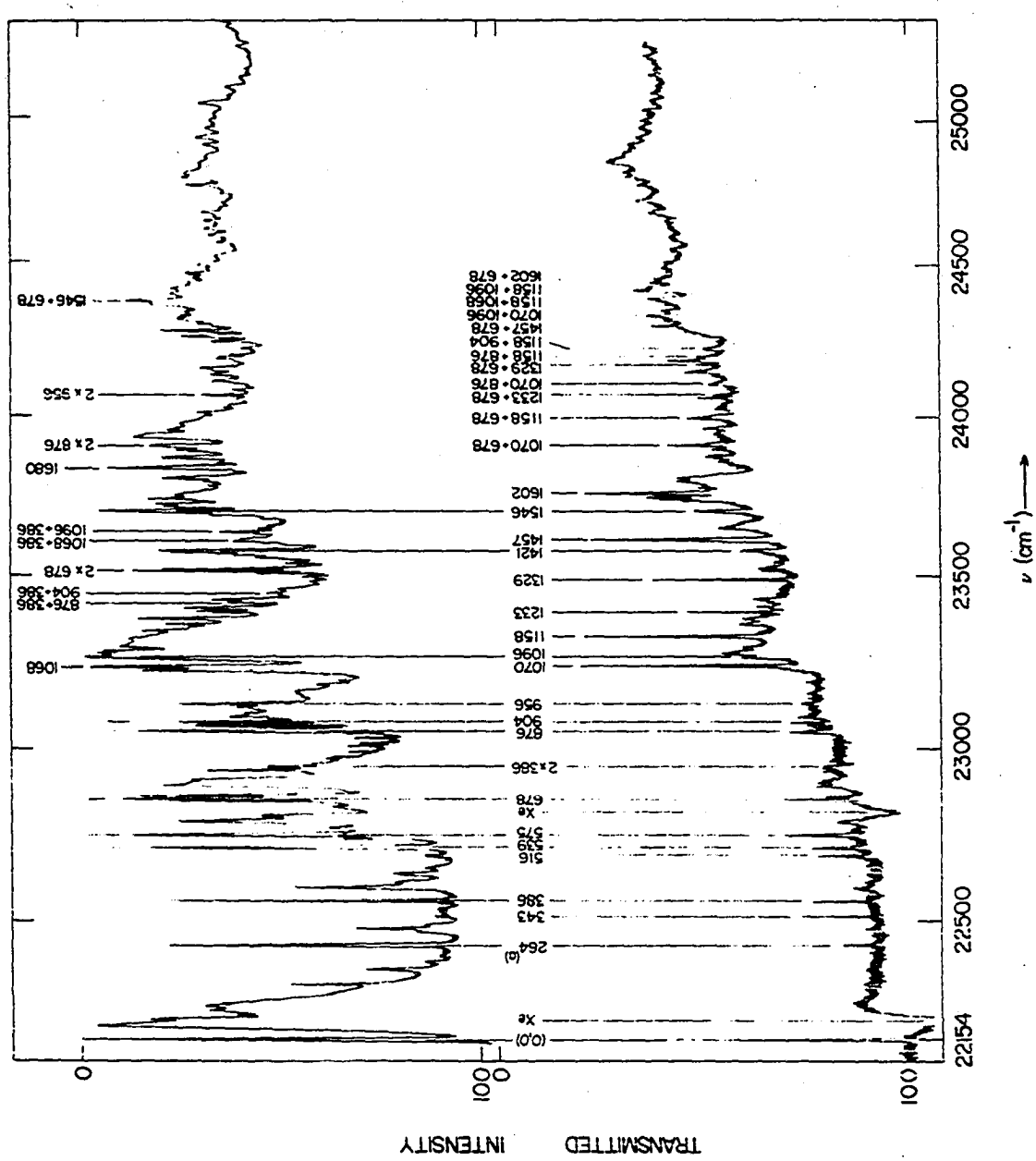
TRANSMITTED INTENSITY
0
100
100
22154
22500
23000
23500
24000
24500
25000
ν (cm⁻¹)
(0,0)
Xe
264(a)
343
386
516
539
573
Xe
678
2×386
876
904
956
1070
1096
1158
1233
1329
1421
1457
1546
1602
1070+678
1158+678
1233+678
1070+876
1329+678
1158+876
1158+904
1457+678
1070+1096
1158+1068
1158+1096
1602+678
1546+678
2×556
2×876
1680
1068
1096+386
1068+386
2×678
904+386
876+386

Figure 6. The absorption spectrum of the diazaazulene/ p-dichlorobenzene 4500Å, $^1B_1 \leftarrow {}^1A_1(\pi\pi^*)$ transition (4.2°K).

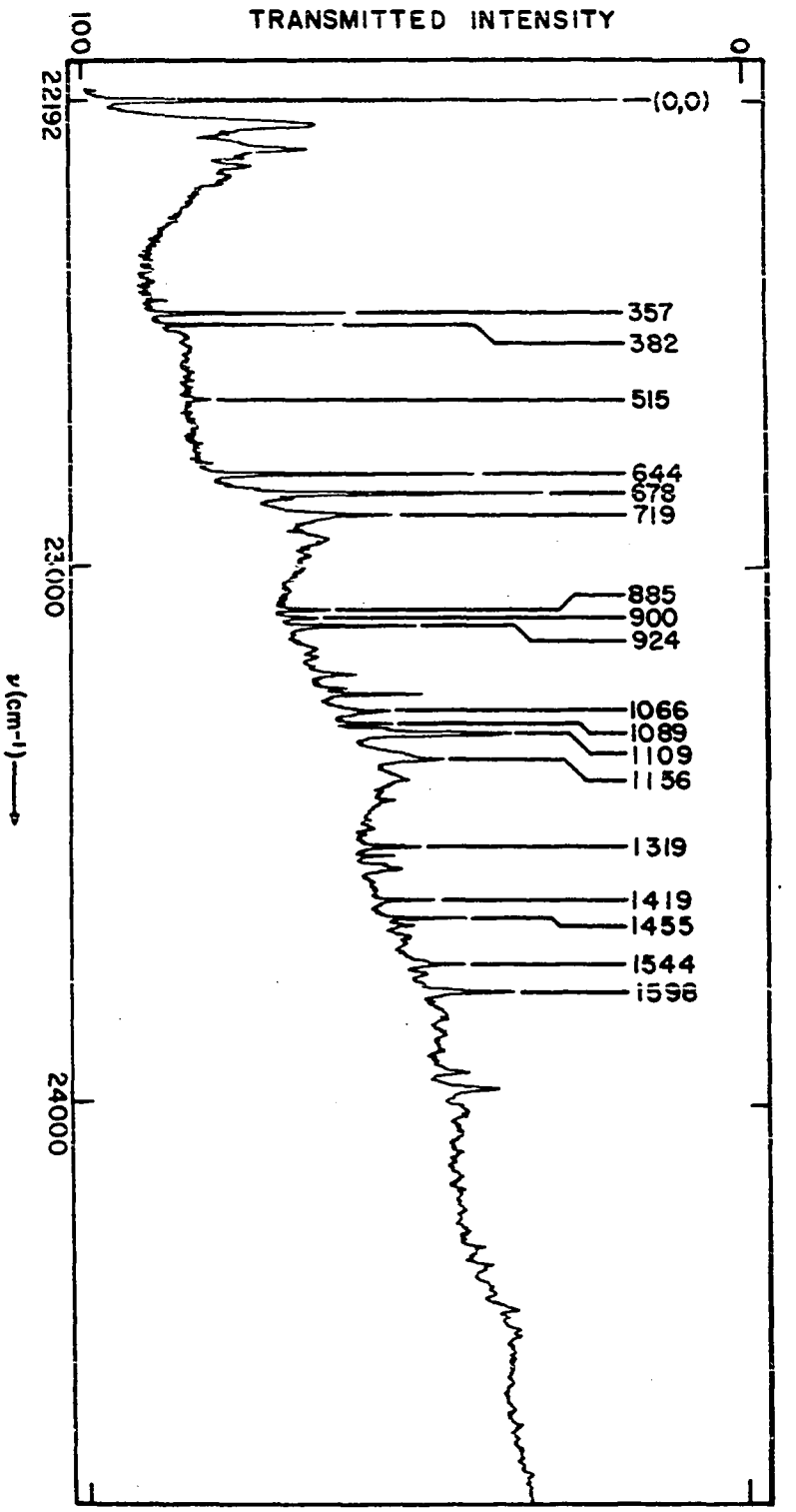
TRANSMITTED INTENSITY
100
0
22192
23000
24000
ν(cm⁻¹)
(0,0)
357
382
515
644
678
719
885
900
924
1066
1089
1109
1156
1319
1419
1455
1544
1596

Figure 7. The xz polarized absorption spectrum of the diazaazulene/quinazoline 4500Å, $^1B_1 \leftarrow {}^1A_1(\pi\pi^*)$ transition (4.2°K). The lower trace is z.

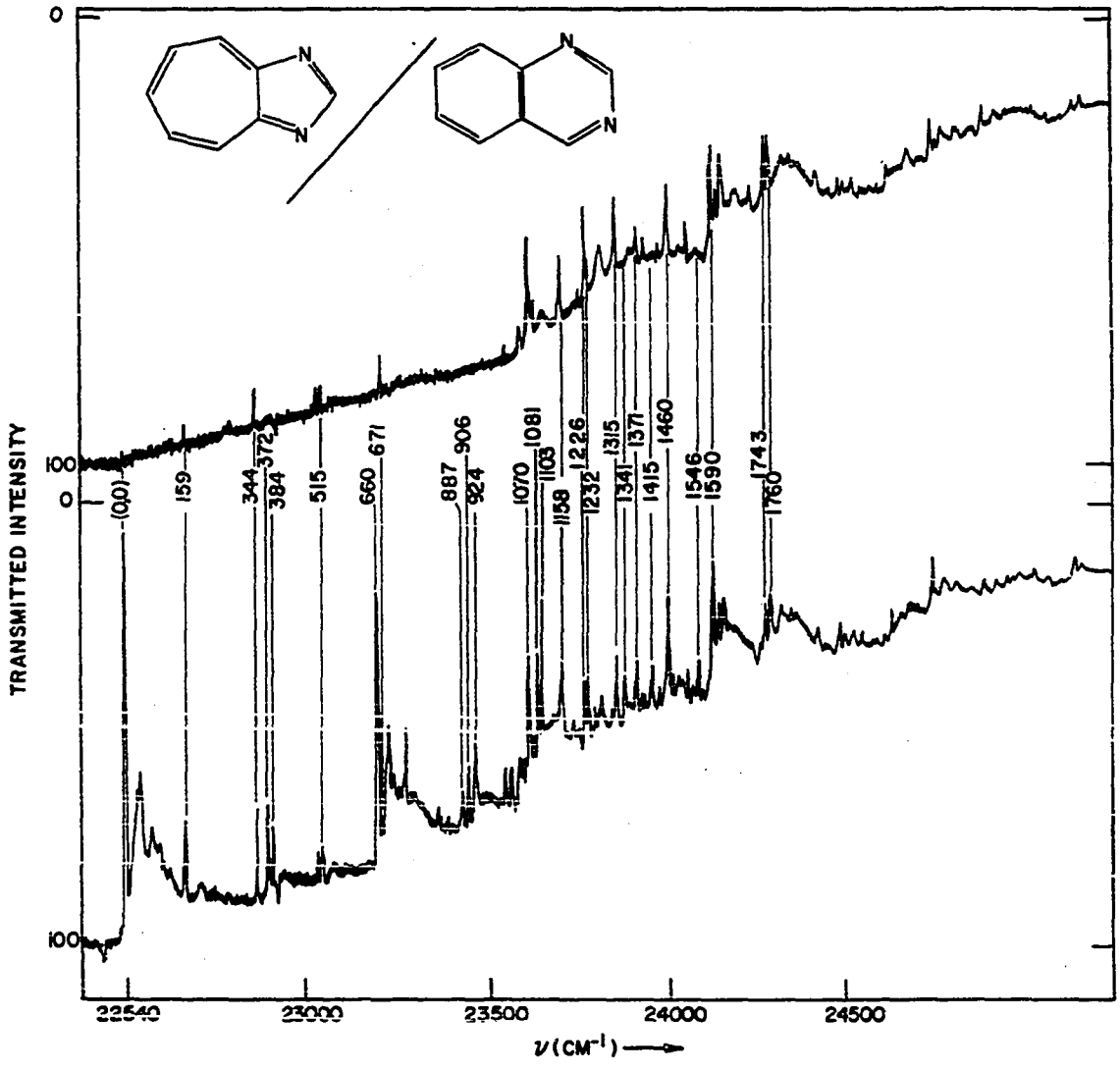
0
100
0
100
TRANSMITTED INTENSITY
(0,0)
159
344
372
384
515
660
671
887
906
924
1070
1081
1103
1158
1226
1232
1315
1341
1371
1415
1460
1546
1590
1743
1760
22540
23000
23500
24000
24500
ν(CM⁻¹)

Figure 8. The ab polarized $^1B_1 \rightarrow {}^1A_1(\pi\pi^*)$ fluorescence spectra of diazaazulene/naphthalene (4.2°K). The lower trace is the b polarization.

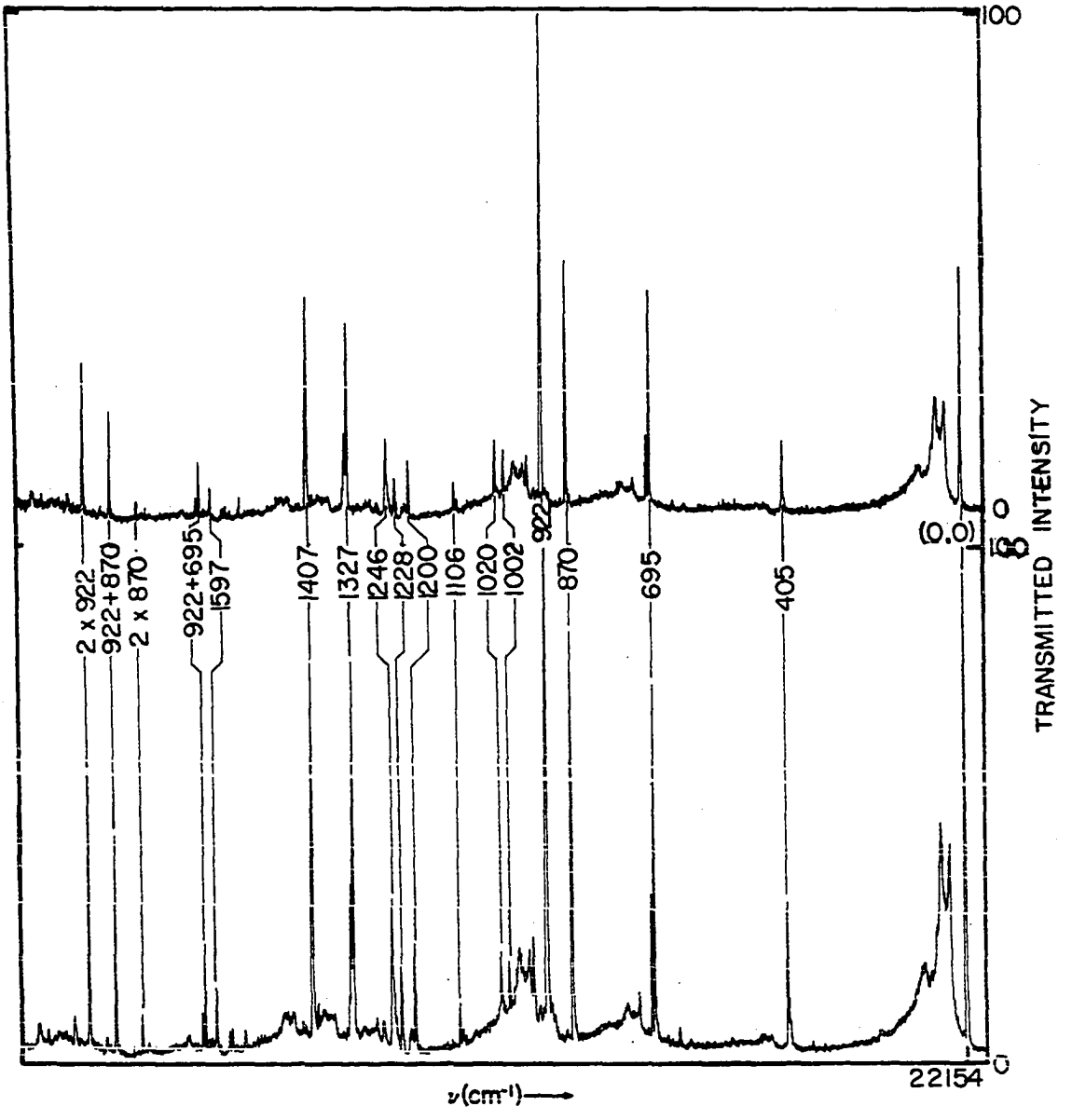
100
0
(0.0)
TRANSMITTED INTENSITY
2 x 922
922+870
2 x 870
922+695
1597
1407
1327
1246
1228
1200
1106
1020
1002
922
870
695
405
22154
ν(cm⁻¹)

Figure 9. The bc' polarized $^1B_1 \rightarrow {}^1A_1(\pi\pi^*)$ fluorescence spectra of diazaazulene/naphthalene (4.2°K). The lower trace is the b polarization.

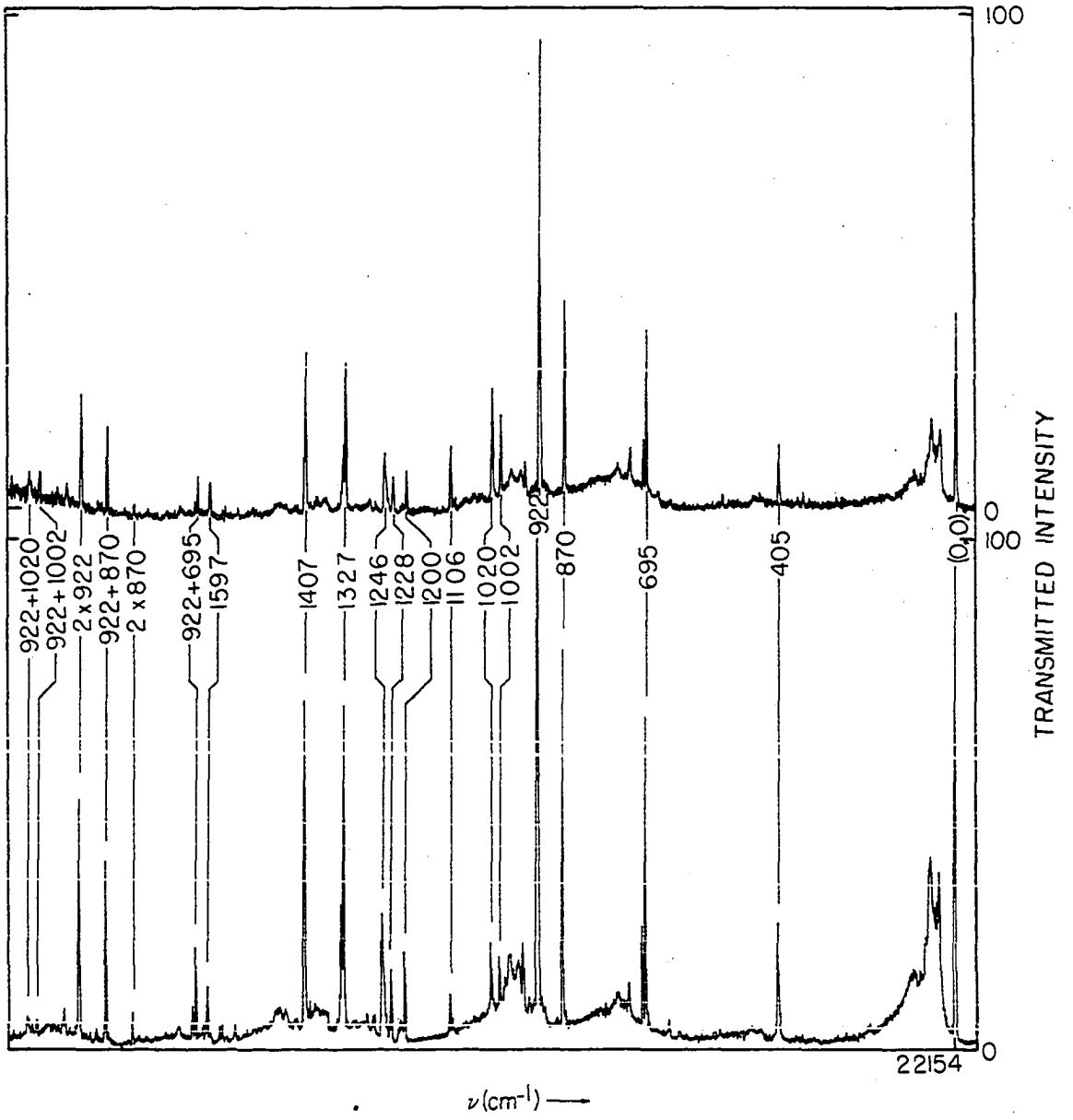
100
0
100
0
TRANSMITTED INTENSITY
22154
ν(cm⁻¹) ⟶
922+1020
922+1002
2×922
922+870
2×870
922+695
1597
1407
1327
1246
1228
1200
1106
1020
1002
922
870
695
405
(0,0)

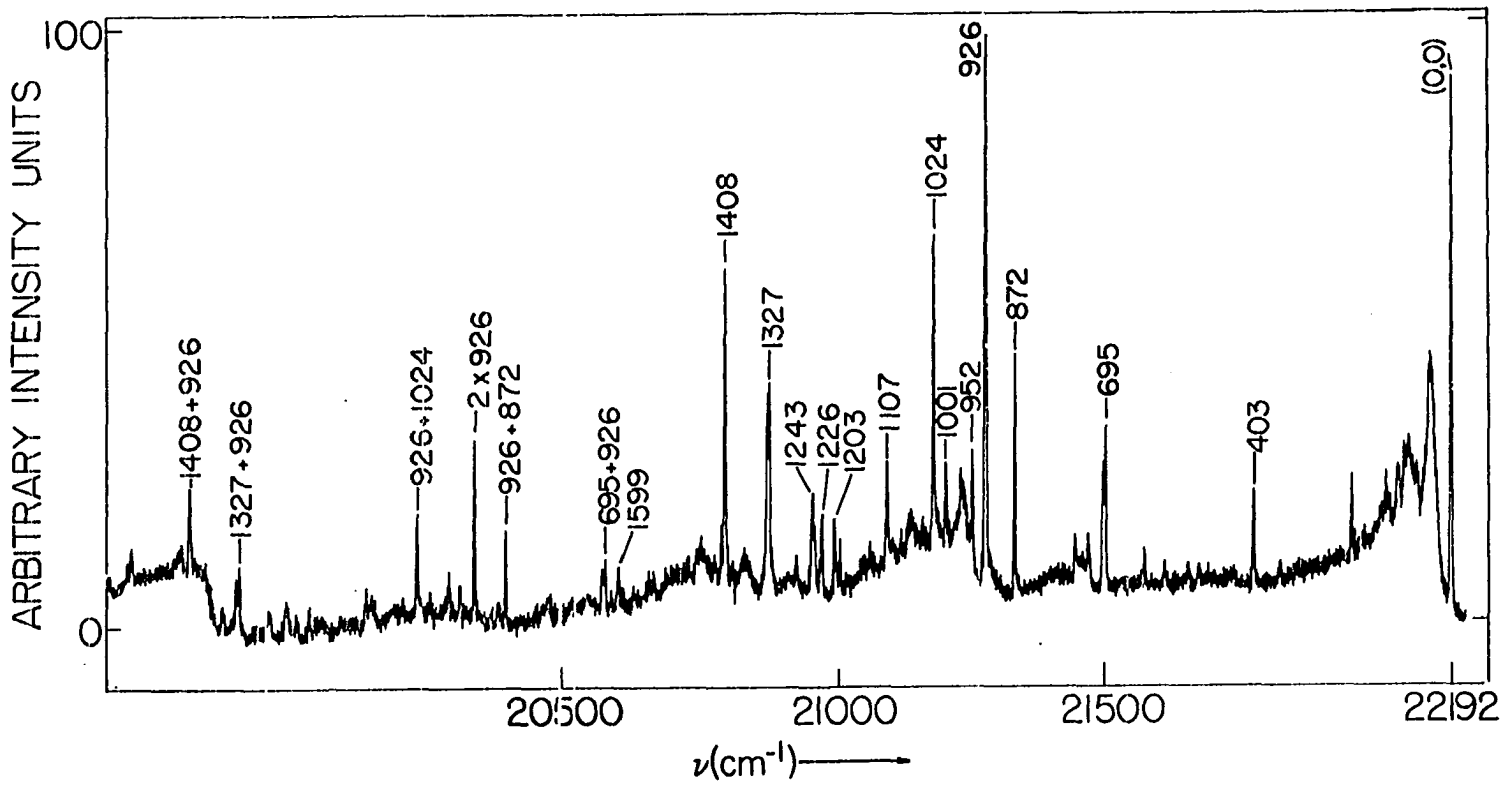

Figure 10. The 4500Å, $^1B_1 \rightarrow {}^1A_1(\pi\pi^*)$ fluorescence spectrum of diazaazulene/p-dichlorobenzene (4.2°K).

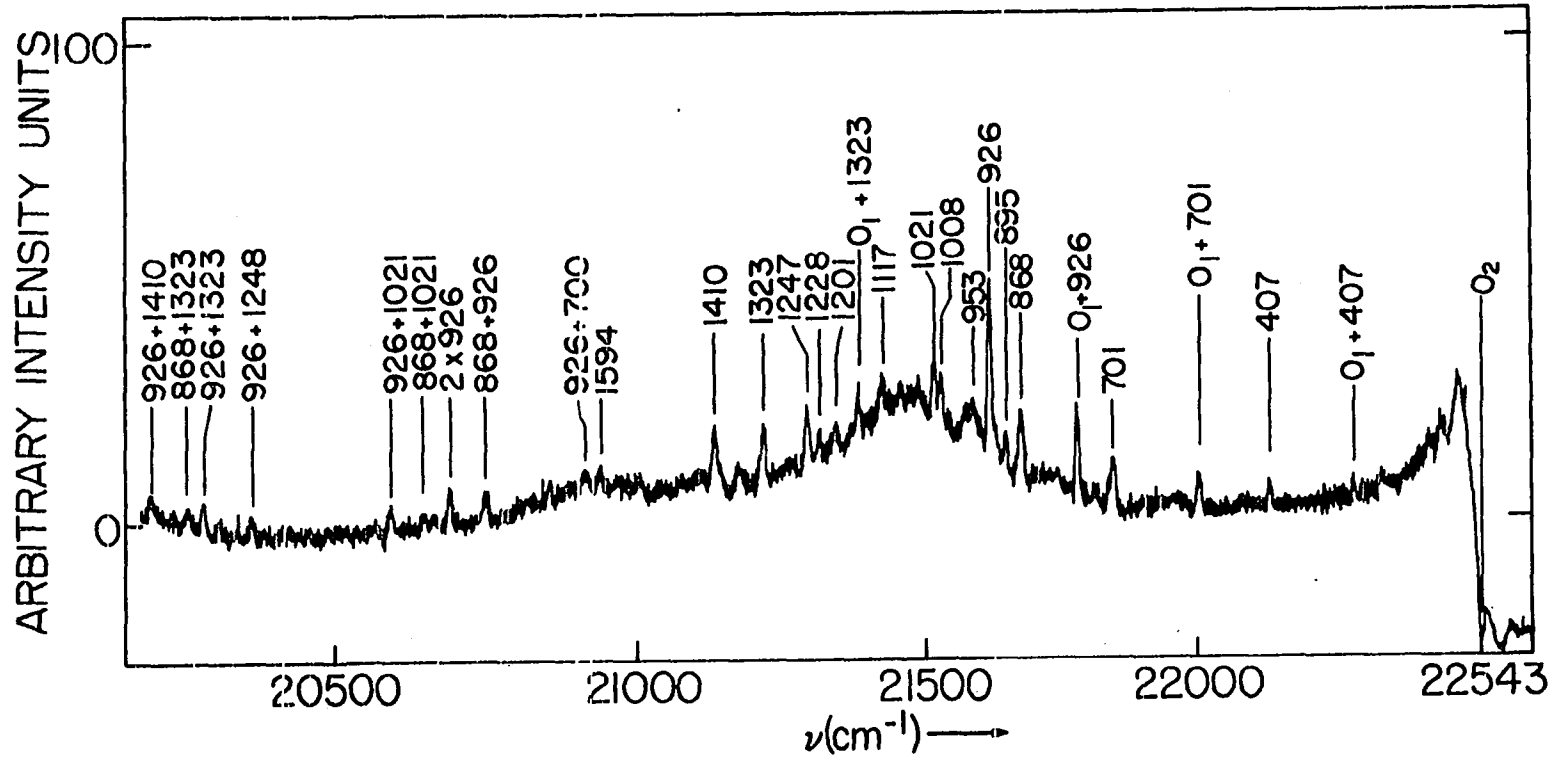

Figure 11. The $^1B_1 \rightarrow {}^1A_1(\pi\pi^*)$ fluorescence spectrum of diazaazulene/quinazoline (4.2°K).

Figure 12. The 5200Å ab polarized phosphorescence spectra of the diazaazulene/naphthalene $^3A_1 \rightarrow {}^1A_1$ transition (4.2°K).

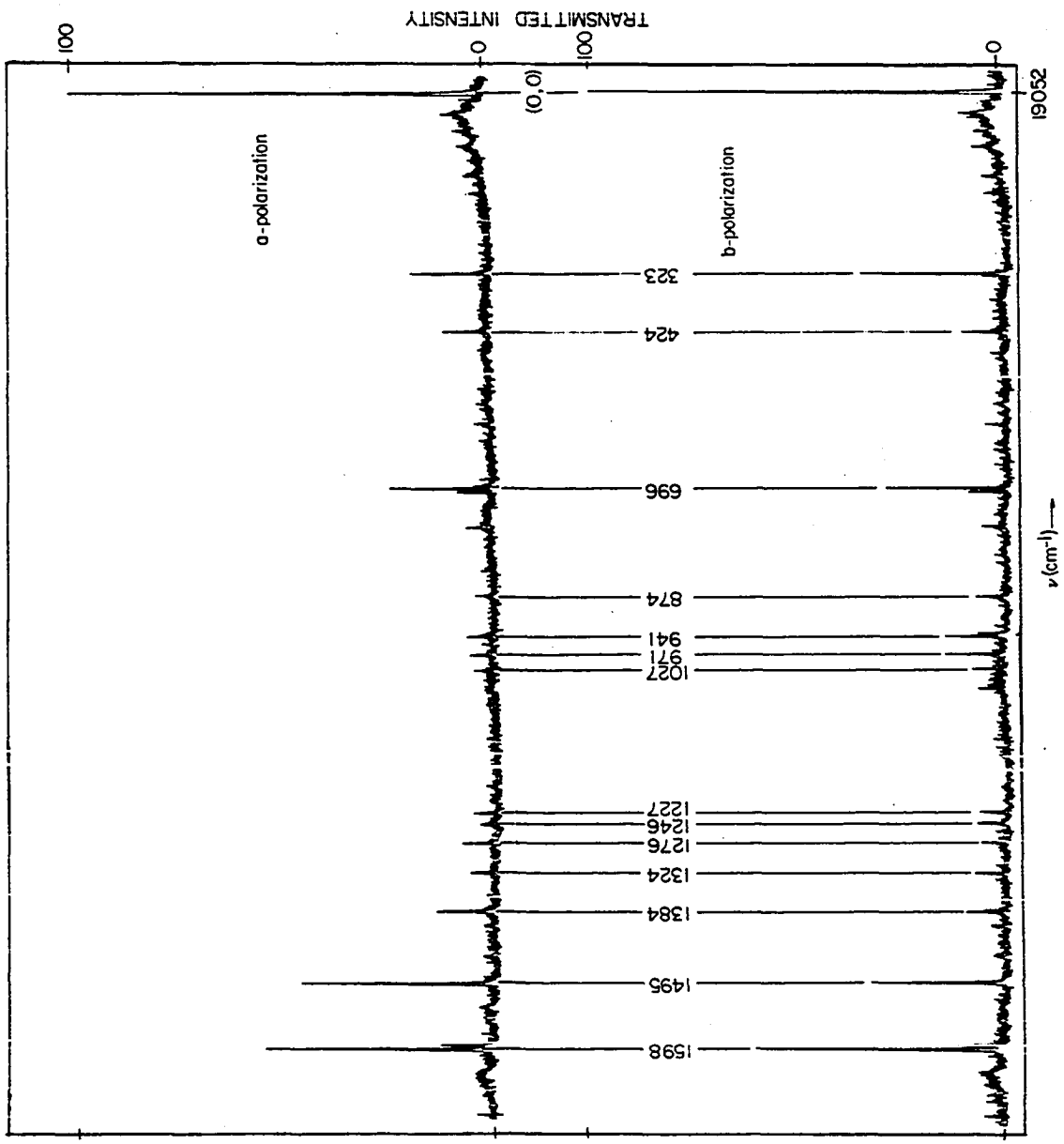
TRANSMITTED INTENSITY
100
0
100
0
(0,0)
19052
a-polarization
b-polarization
323
424
696
874
941
971
1027
1227
1246
1276
1324
1384
1495
1598
ν (cm⁻¹)

Figure 13. The bc' polarized phosphorescence spectra of the diazaazulene/naphthalene $^3A_1 \rightarrow {}^1A_1$ transition (4.2°K).

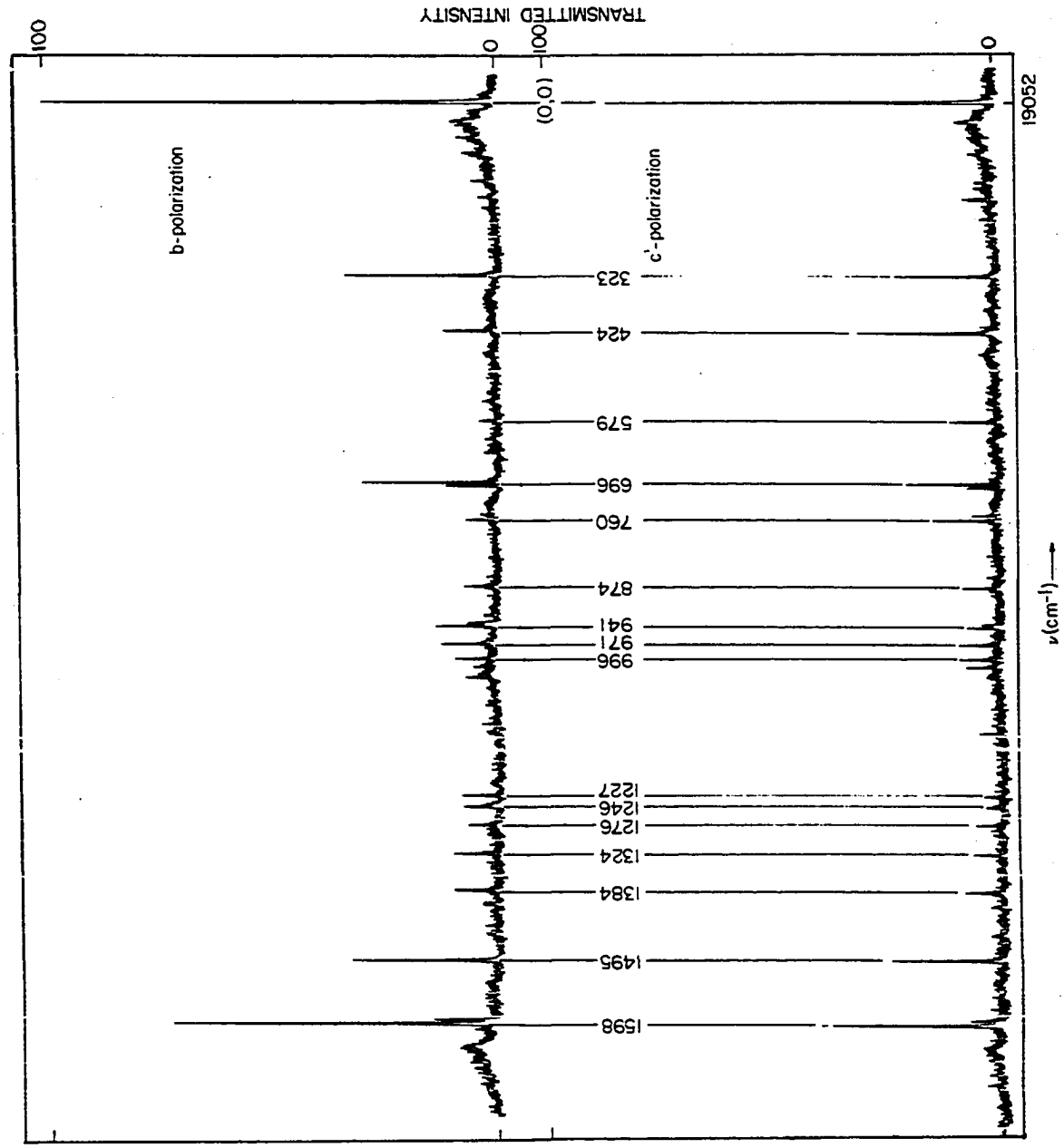
TRANSMITTED INTENSITY
100
0
100
0
(0,0)
19052
b-polarization
c'-polarization
323
424
579
696
760
874
941
971
996
1227
1246
1276
1324
1384
1495
1598
ν(cm⁻¹)

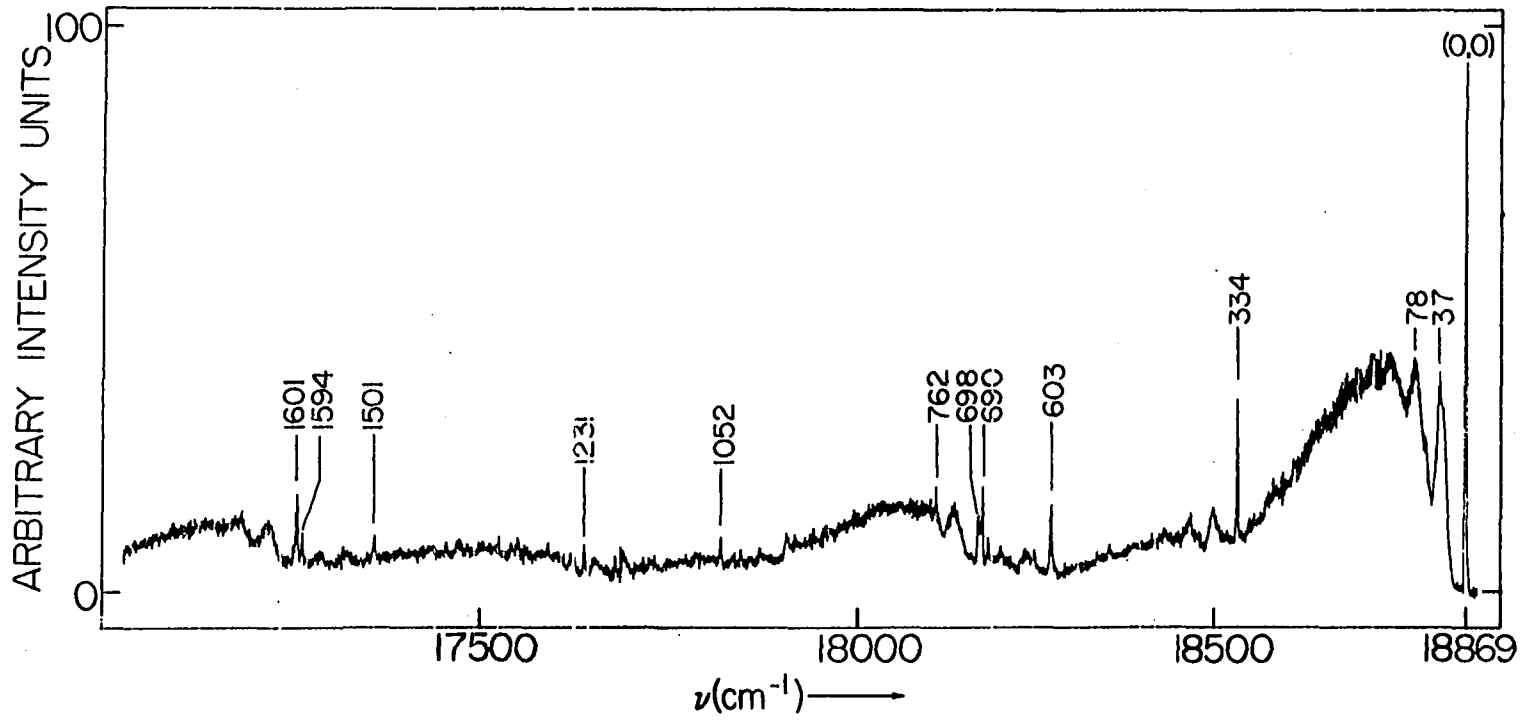

Figure 14. The 5200Å, $^3A_1 \rightarrow {}^1A_1$ phosphorescence spectrum of diazaazulene/p-dichlorobenzene (4.2°K).

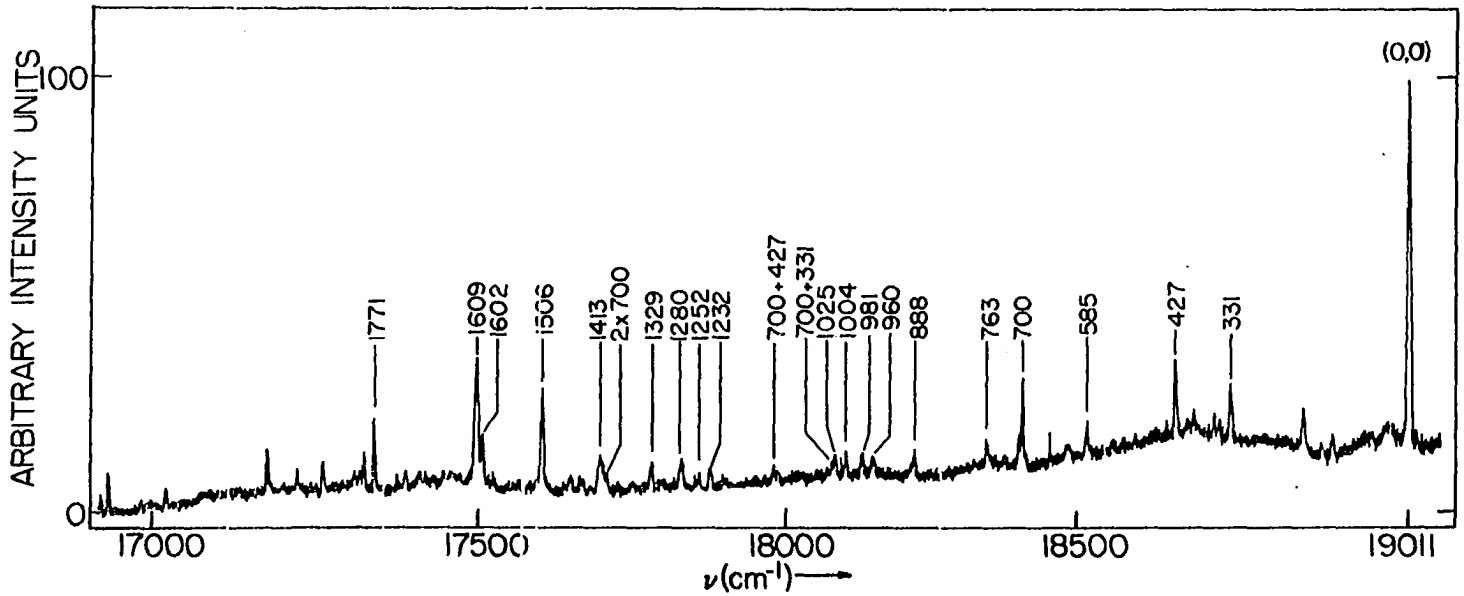

Figure 15. The 5200Å, $^3A_1 \rightarrow {}^1A_1$ phosphorescence spectrum of diazaazulene/quinazoline (4.2°K).

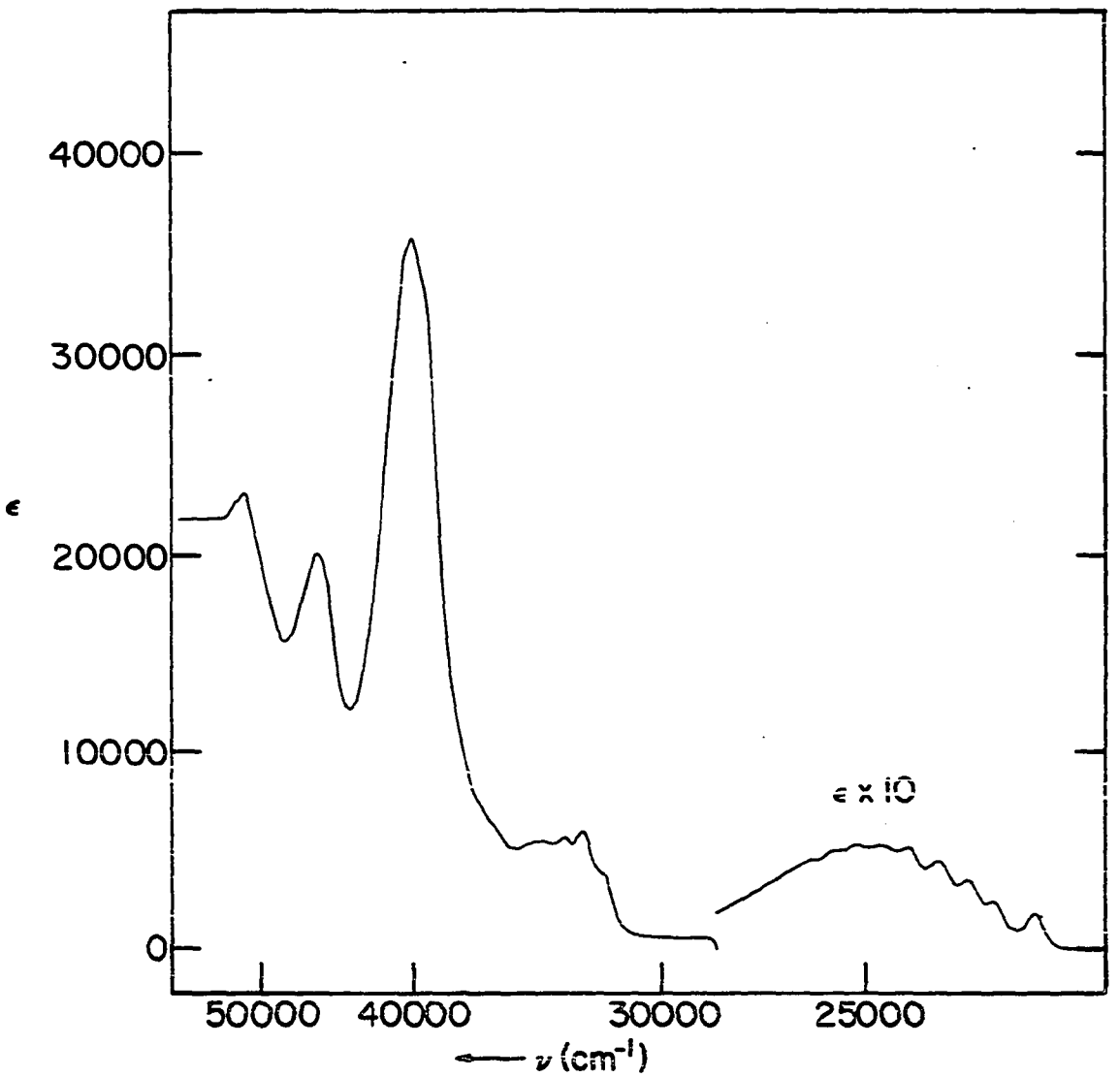

Figure 16. The room temperature spectrum of diazaazulene/methylcyclohexane.

Figure 17. The room temperature solution spectrum of azulene/cyclohexane.

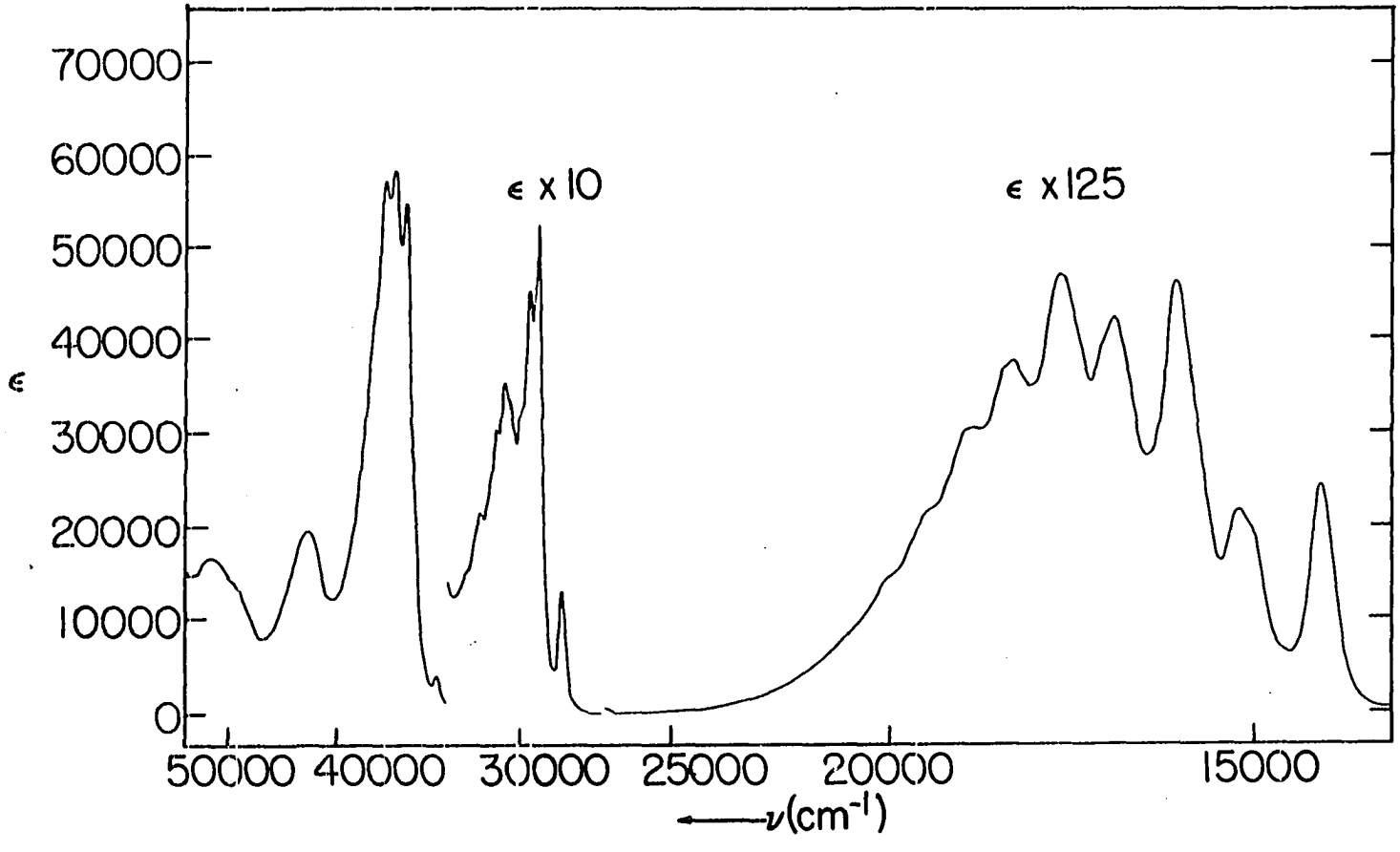
70000
60000
50000
40000
30000
20000
10000
0
ε
ε x 10
ε x 125
50000 40000 30000 25000 20000 15000
ν(cm⁻¹)

Figure 18. The polarized absorption spectra of the diazaazulene/naphthalene 3600Å $^1B_1 \leftarrow {}^1A_1$ transition (4.2°K).

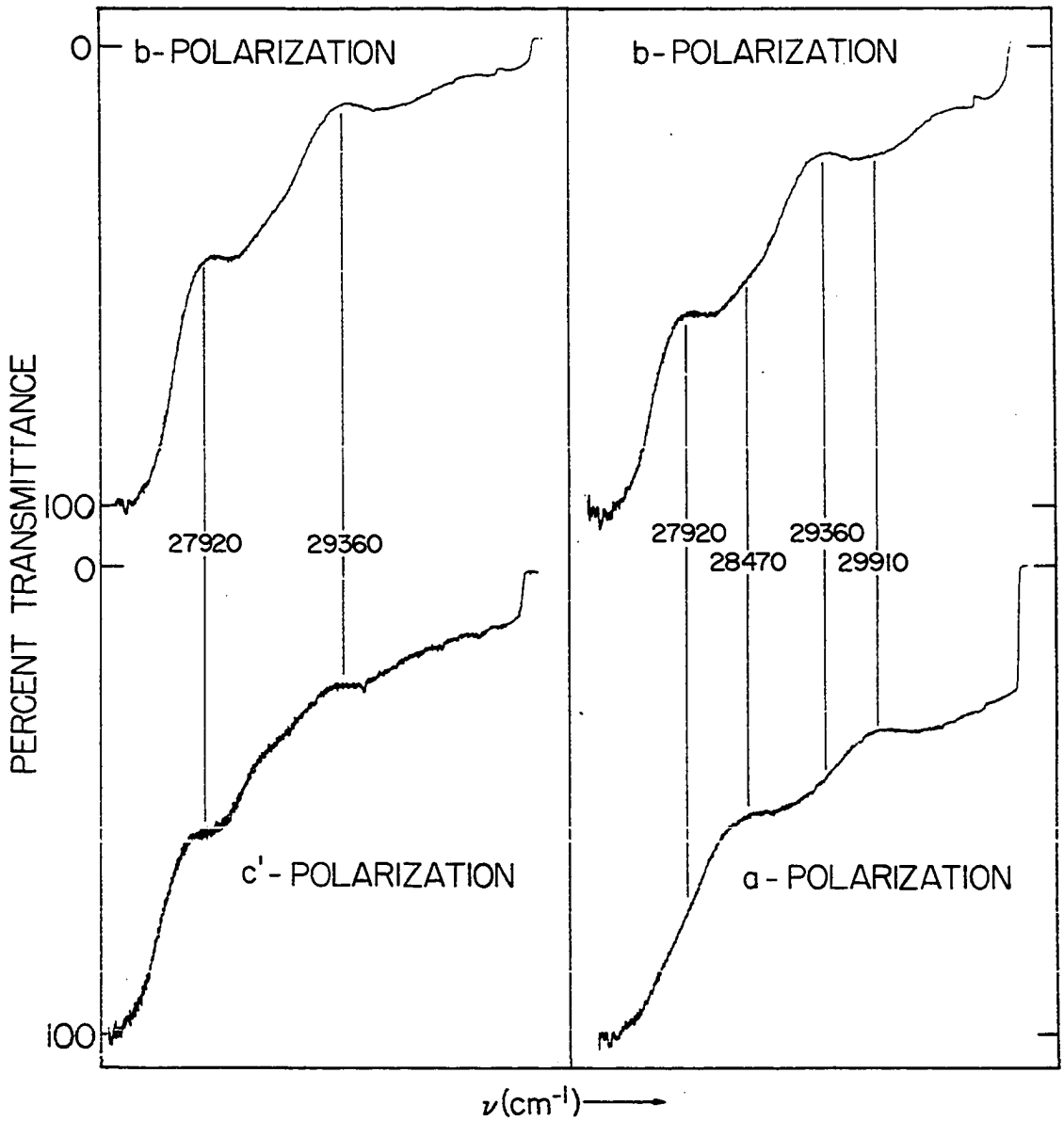
0
b-POLARIZATION
100
27920
29360
0
c'-POLARIZATION
100
PERCENT TRANSMITTANCE
b-POLARIZATION
27920
28470
29360
29910
a-POLARIZATION
ν(cm⁻¹)

Figure 19. The diazaazulene/p-dichlorobenzene 3250Å $^1B_1 \leftarrow {}^1A_1(\pi\pi^*)$ absorption spectrum (4.2°K).

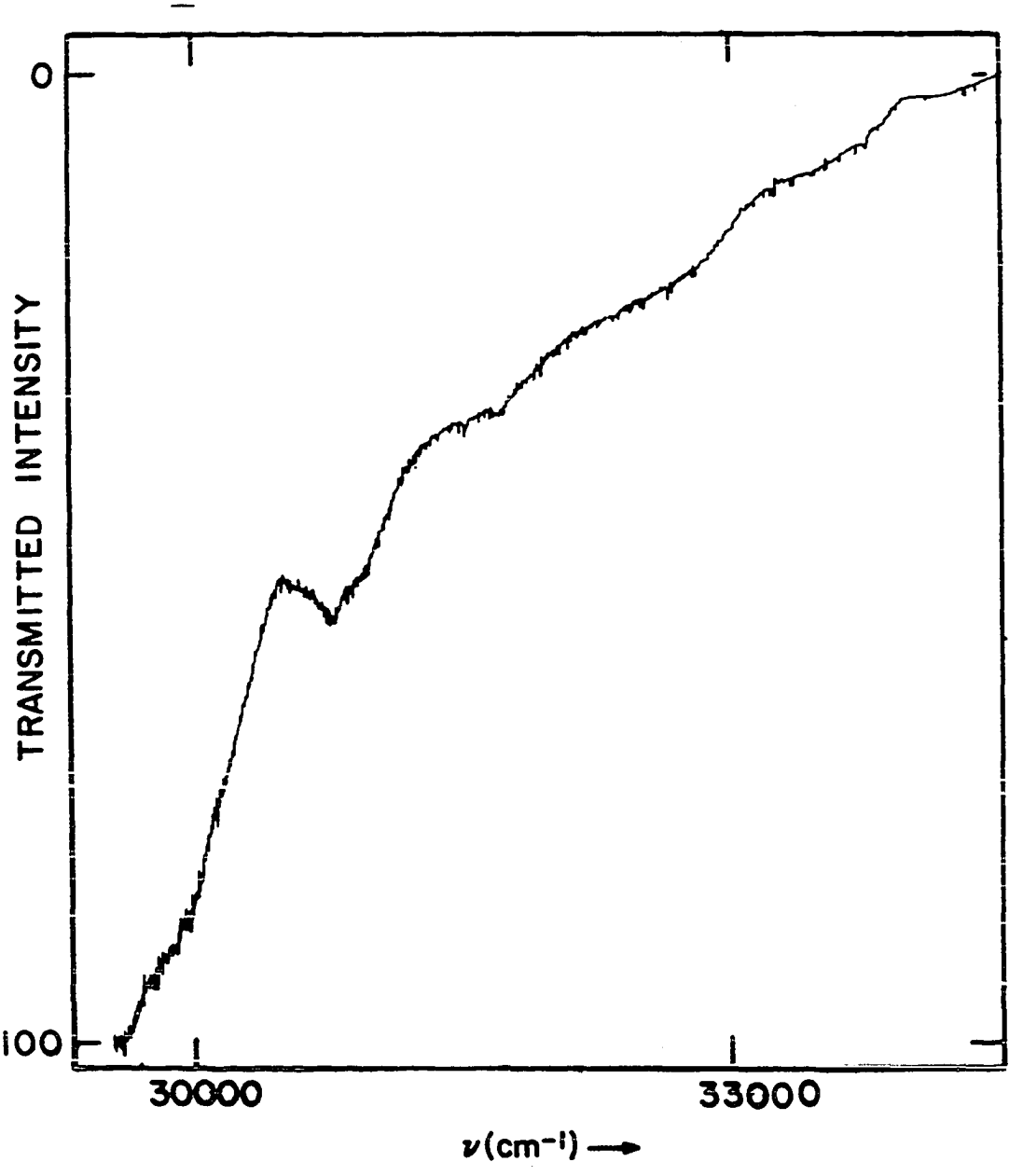
0
100
TRANSMITTED INTENSITY
30000
33000
ν(cm⁻¹) ⟶

Figure 20. The room temperature solution spectrum of 2-phenyl-1,3-diazaazulene/methyl-cyclohexane.

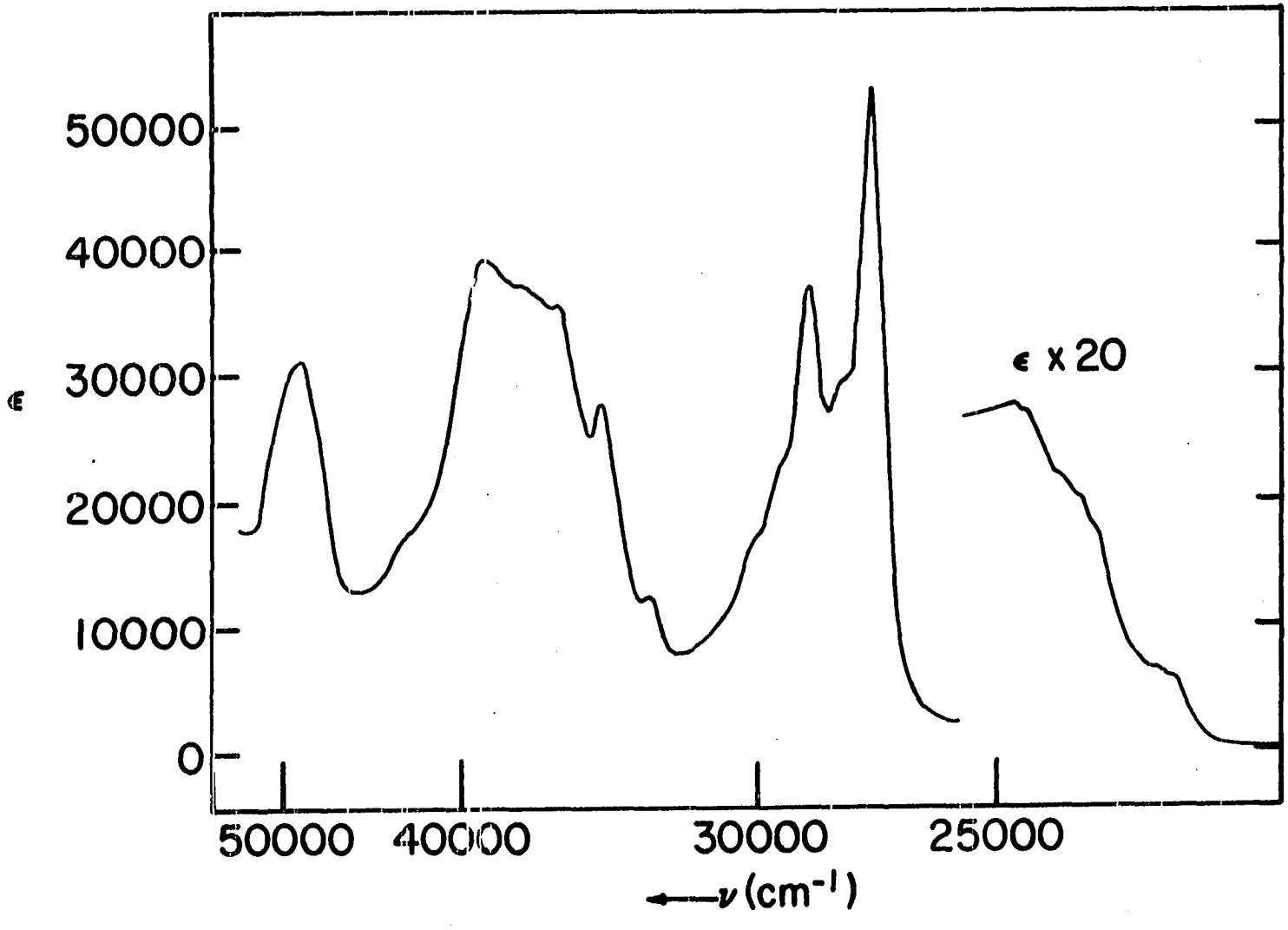
50000
40000
30000
20000
10000
0
ε
ε x 20
50000
40000
30000
25000
ν (cm⁻¹)

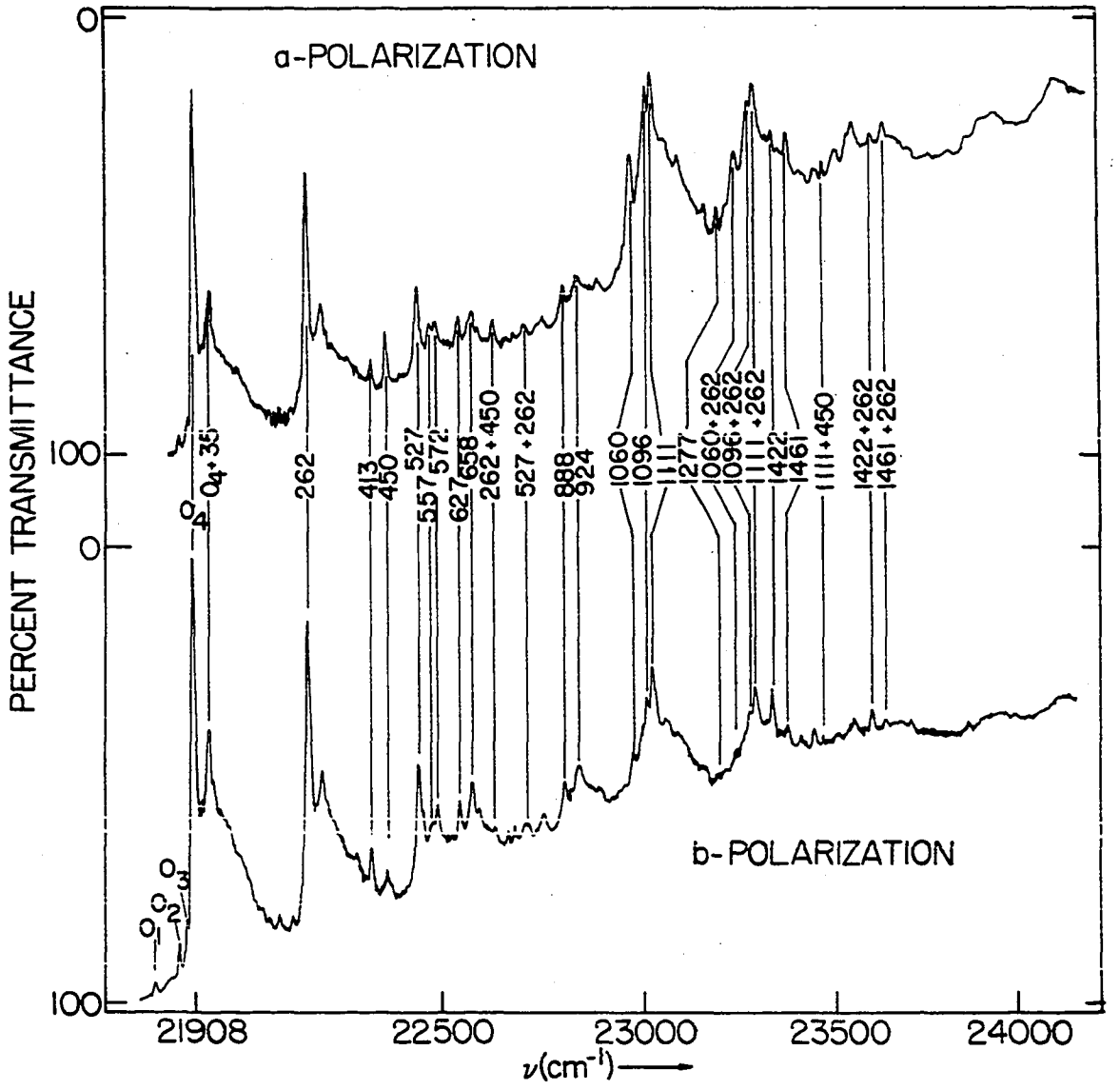

Figure 21. The ab polarized absorption spectra of the phenyldiazaazulene/dibenzyl, $^1B_1 \leftarrow {}^1A_1(\pi\pi^*)$ transition (4.2°K).

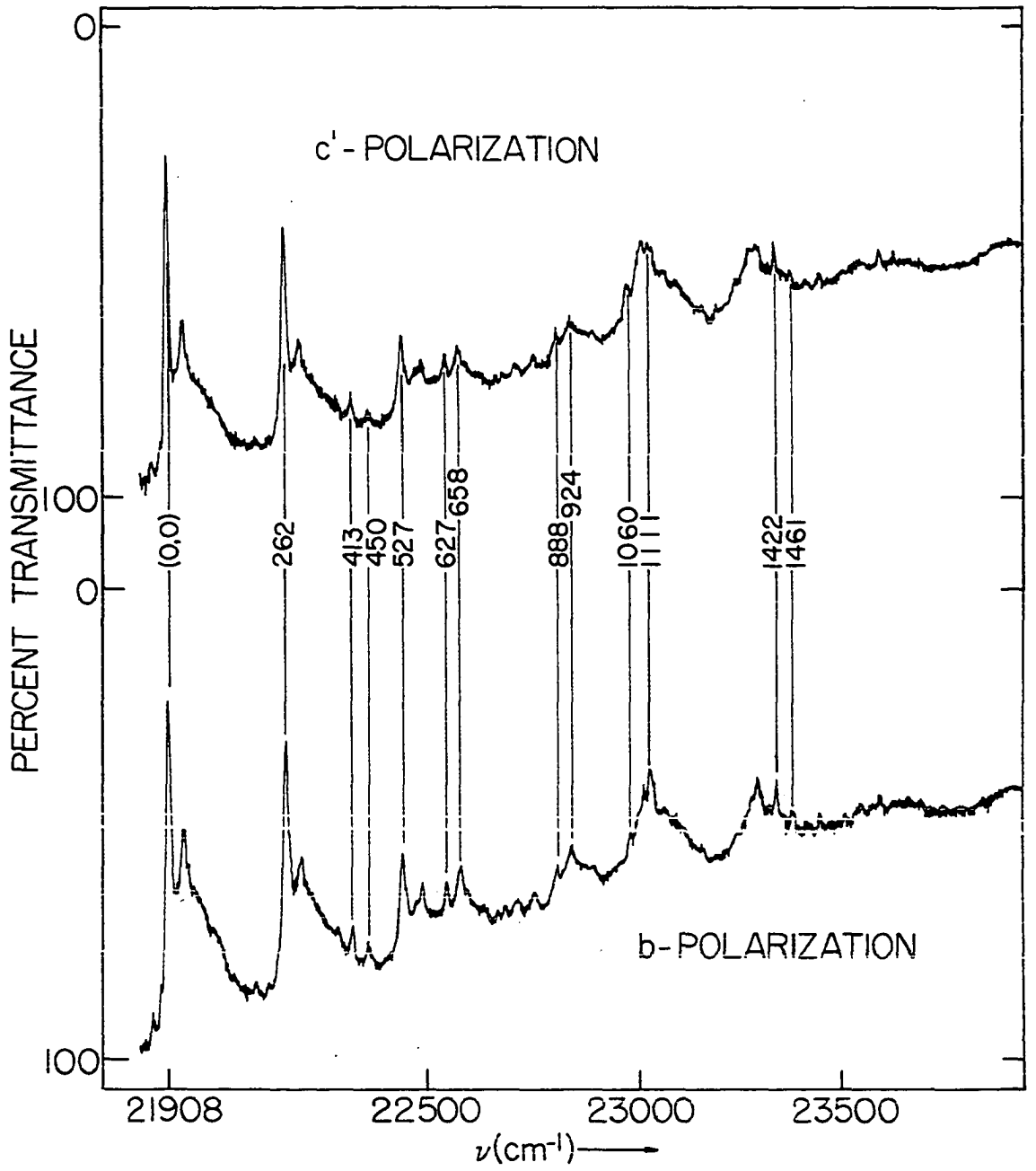

Figure 22. The bc' polarized absorption of the phenyldiazaazulene/dibenzyl, $^1B_1 \leftarrow {}^1A_1(\pi\pi^*)$ transition (4.2°K).

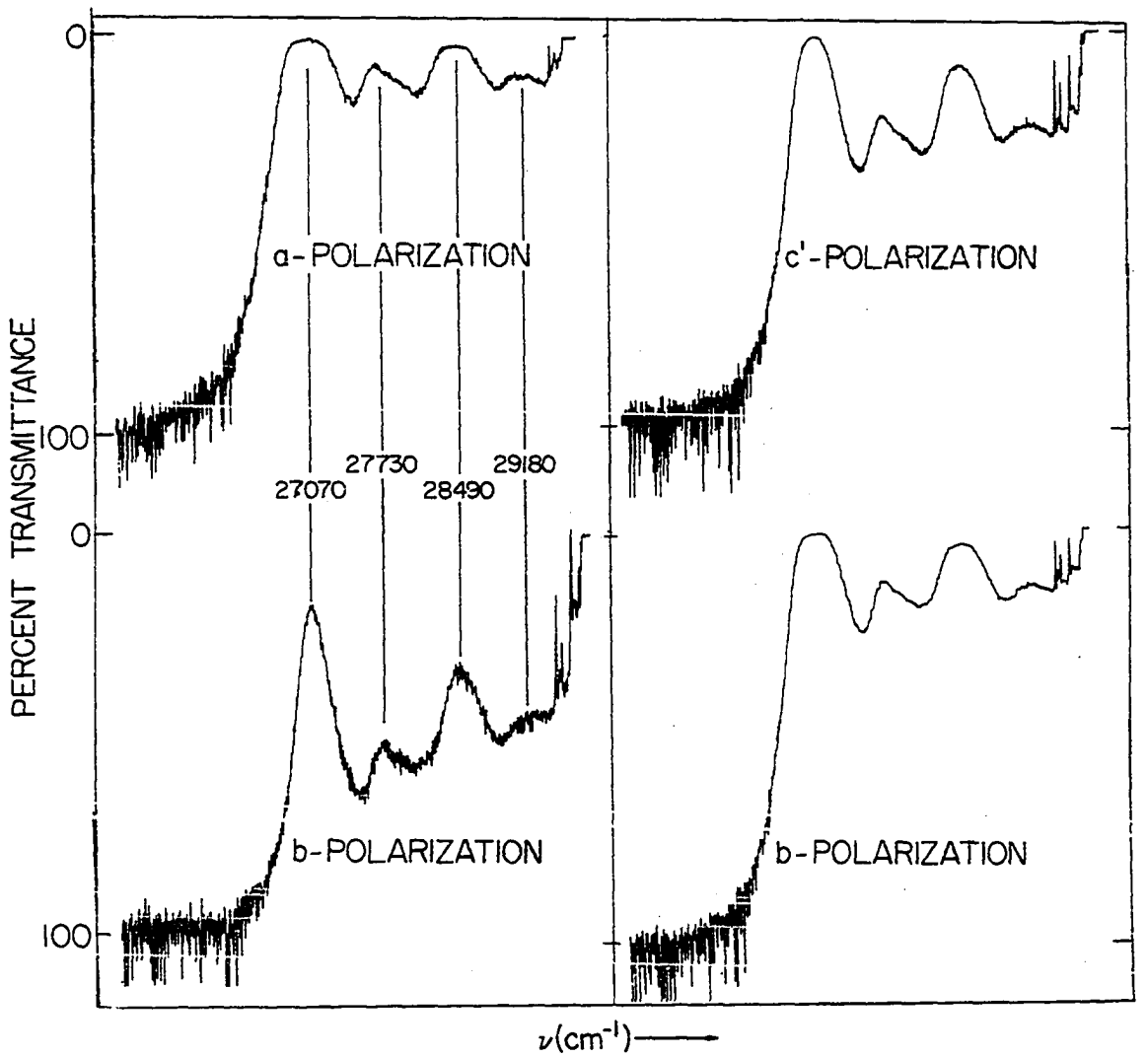

Figure 23. The 3800Å, $^1A_1 \leftarrow {}^1A_1(\pi\pi^*)$ absorption spectrum of phenyldiazaazulene/dibenzyl (4.2°K).

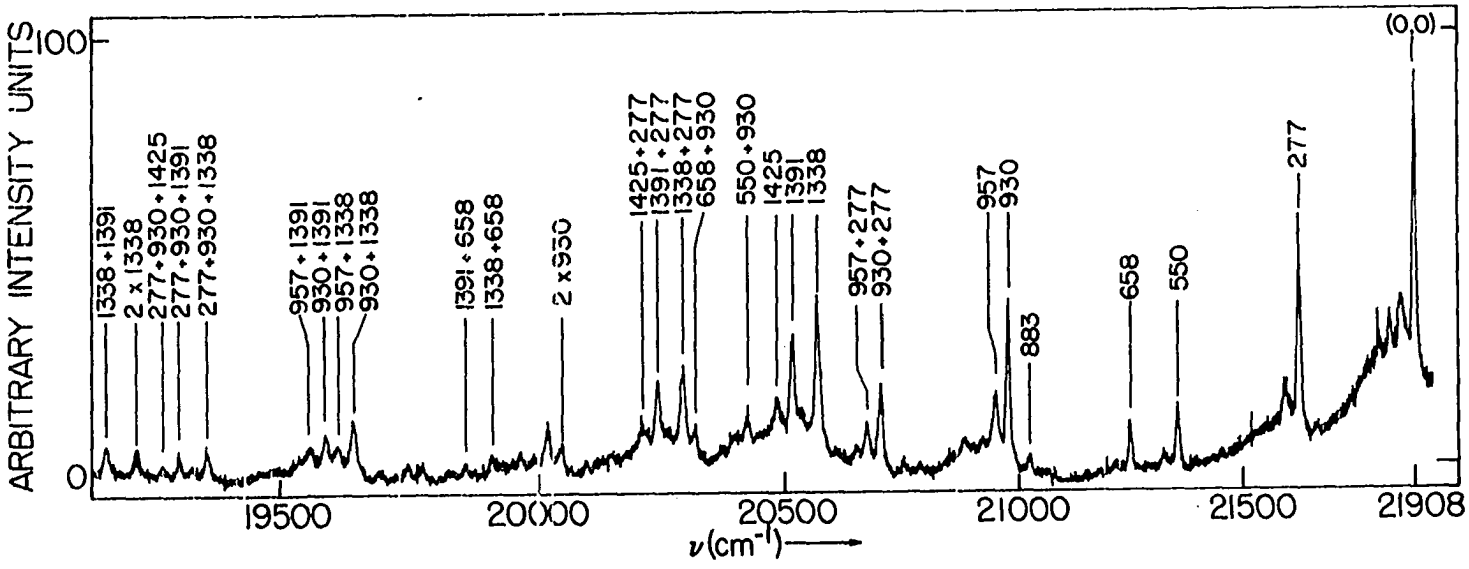

Figure 24. The 4500Å $^1B_1 \rightarrow {}^1A_1(\pi\pi^*)$ fluorescence spectrum of phenyldiazaazulene/dibenzyl (4.2°K).

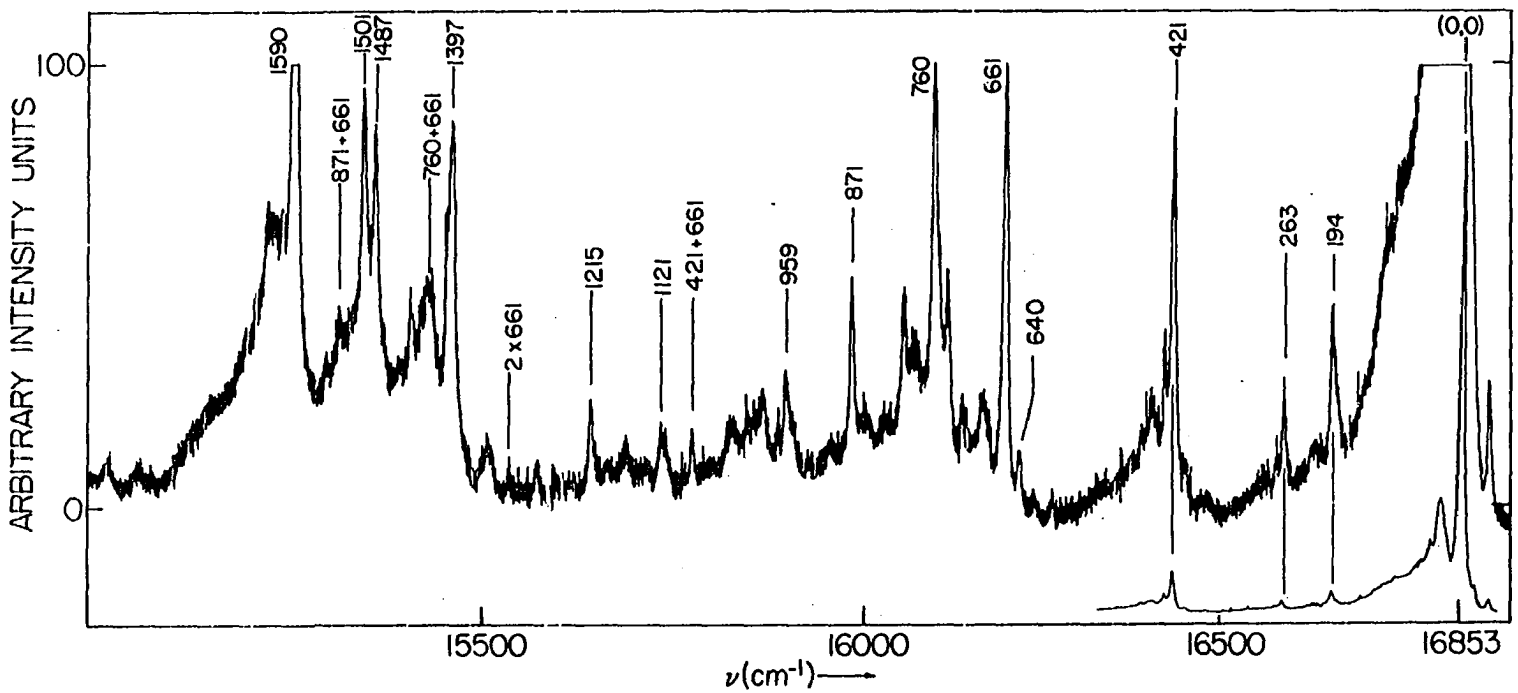

Figure 25. The 6000Å, $^3A_1 \rightarrow {}^1A_1(\pi\pi^*)$ phosphorescence spectrum of phenyldiazaazulene/dibenzyl (4.2°K). The origin in the upper trace is amplified off scale to demonstrate the vibronic band positions.

Figure 26. Correlation of the excited electronic states of azulene, 2-phenylazulene, and the azaazulenes.

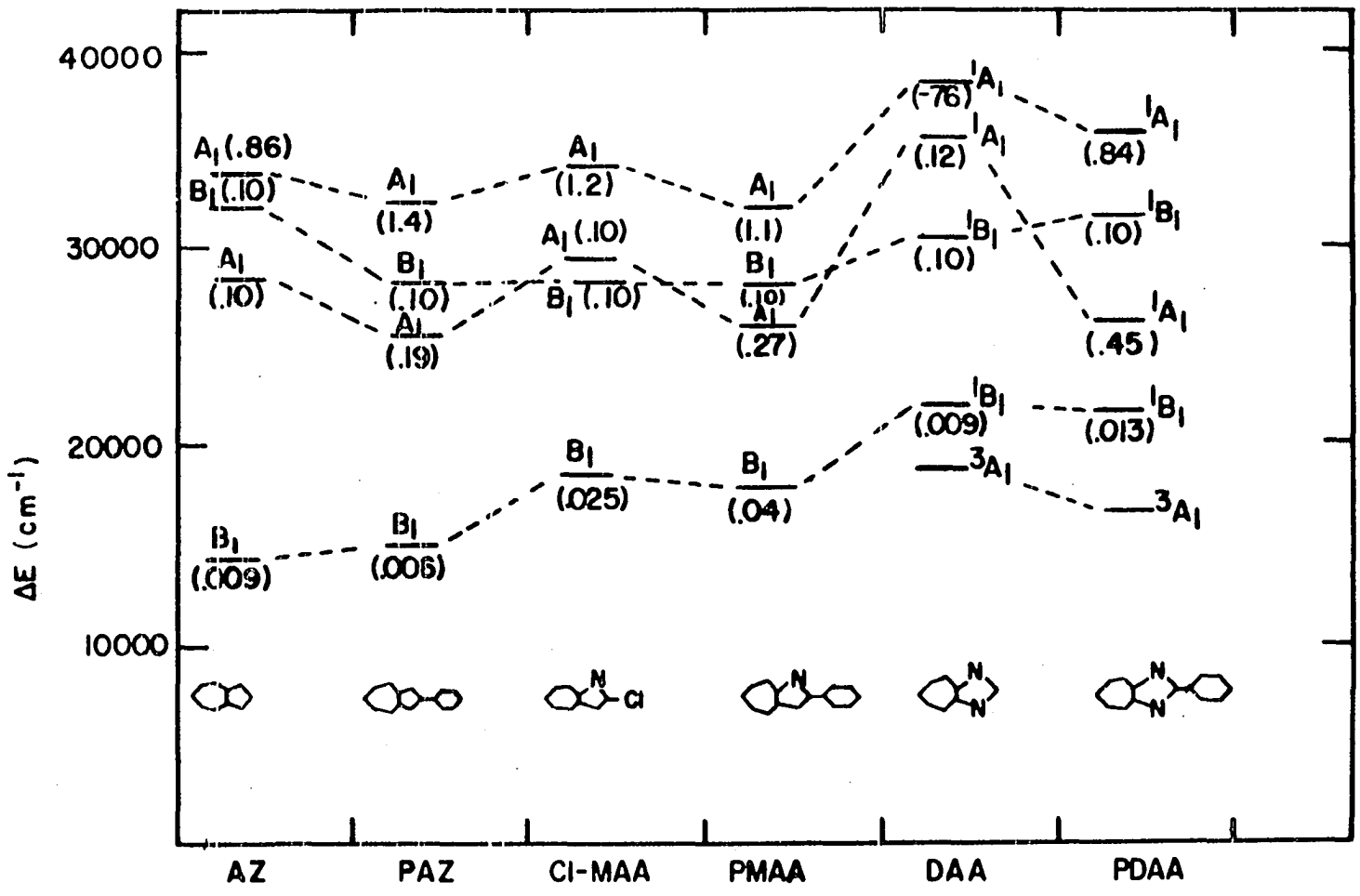
40000
30000
20000
10000
ΔE (cm⁻¹)
A1 (.86)
B1 (.10)
A1 (.10)
B1 (.009)
A1 (1.4)
B1 (.10)
A1 (.19)
B1 (.006)
A1 (1.2)
A1 (.10)
B1 (.10)
B1 (.025)
A1 (1.1)
B1 (.10)
A1 (.27)
B1 (.04)
1A1 (-76)
1A1 (.12)
1B1 (.10)
3A1
1B1 (.009)
1A1 (.84)
1B1 (.10)
1A1 (.45)
1B1 (.013)
3A1
Cl
N
N
N
AZ
PAZ
Cl-MAA
PMAA
DAA
PDAA

Figure 27. The room temperature solution spectrum of 2-phenylazulene/cyclohexane.

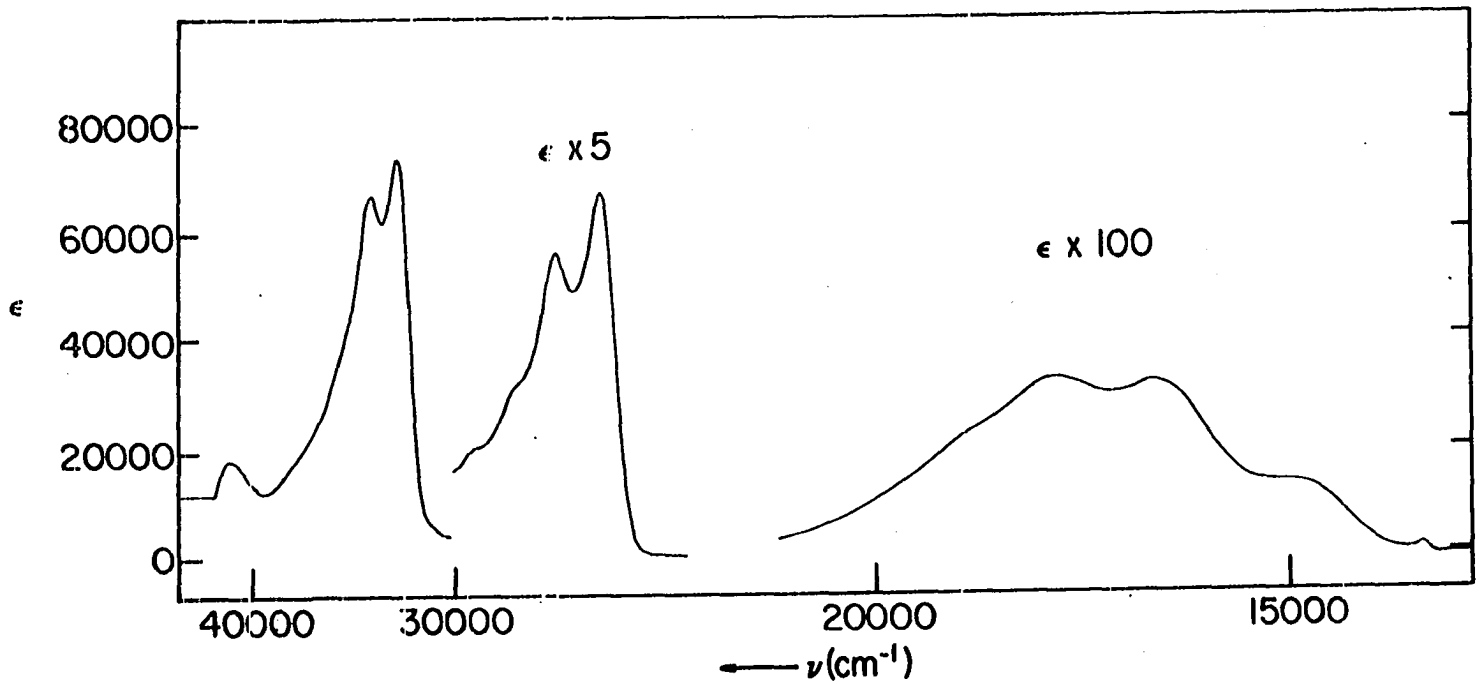
80000
60000
40000
20000
0
ε
ε x 5
ε x 100
40000
30000
20000
15000
ν(cm⁻¹)

Figure 28. The room temperature solution spectrum of 2-chloro-1-monoazaazulene/methylcyclohexane.

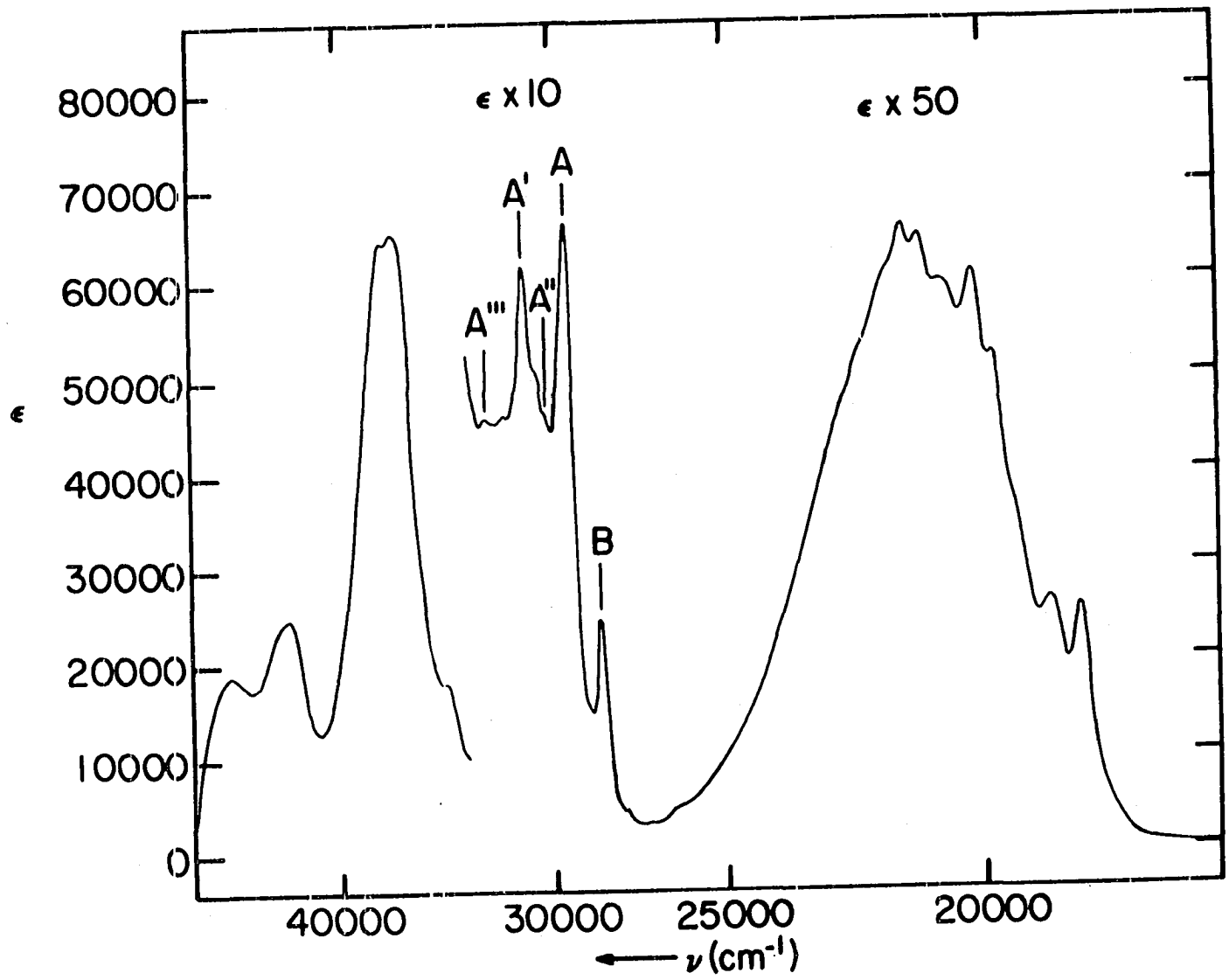
80000
70000
60000
50000
40000
30000
20000
10000
0
ε
ε x 10
ε x 50
A'''
A'
A''
A
B
40000
30000
25000
20000
ν (cm⁻¹)

Figure 29. The room temperature solution spectrum of 2-phenyl-1-monoazaazulene/methylcyclohexane.

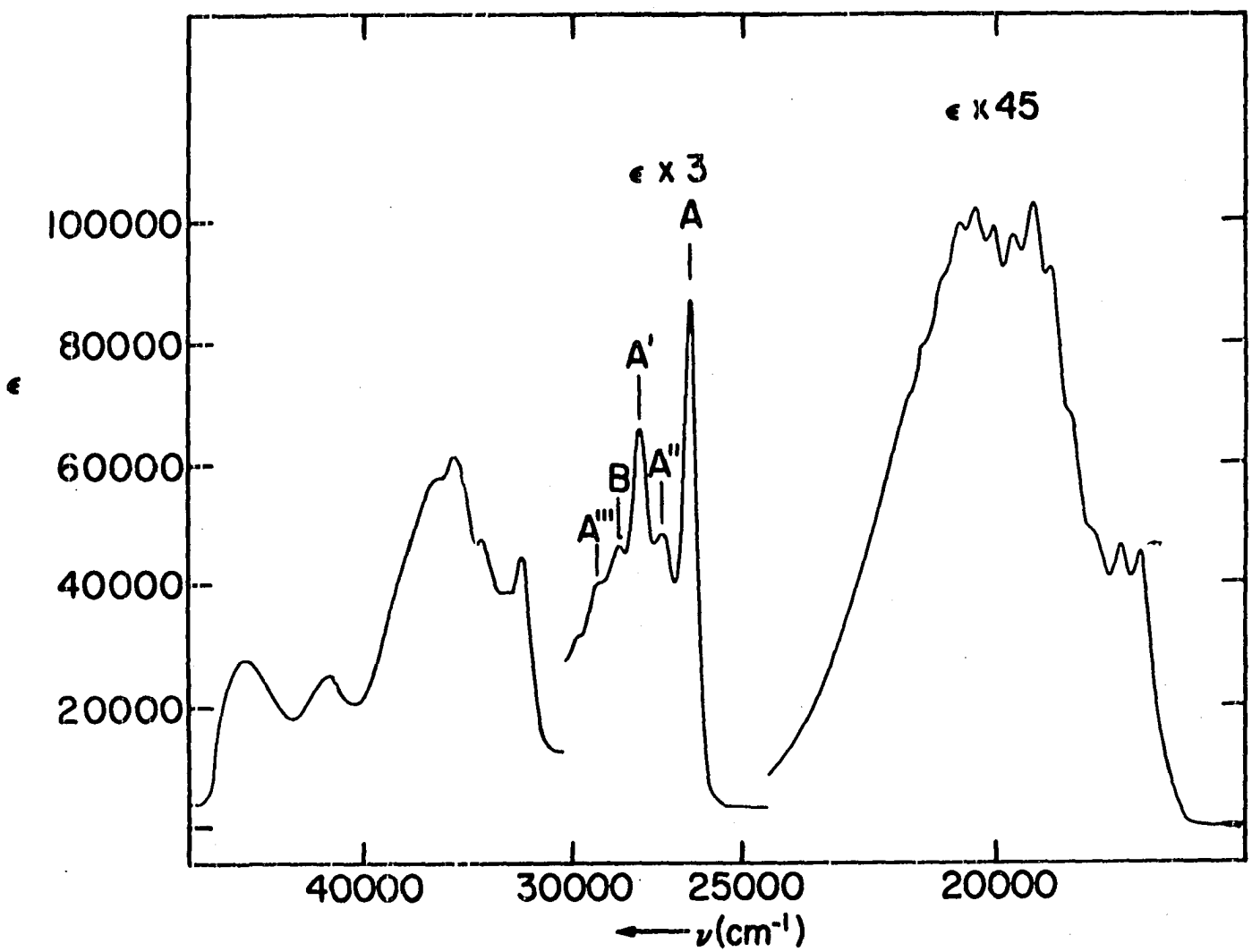
ε x 45
ε x 3
A
A'
A''
B
A'''
100000
80000
60000
40000
20000
ε
40000
30000
25000
20000
ν(cm⁻¹)

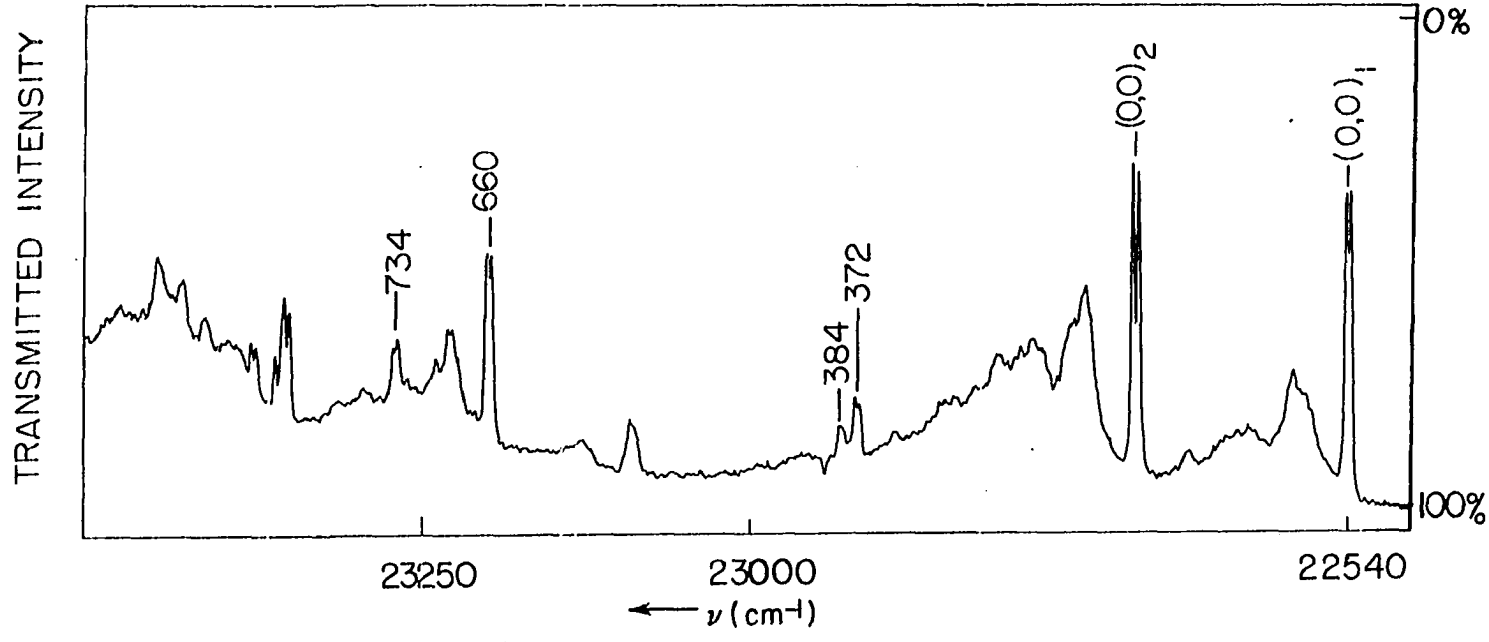

Figure 30. The electric field spectrum of diazaazulene/quinazoline, taken in low resolution. The applied field is about 10 kV/mm.

Figure 31. Stark splitting vs voltage curve for the origin band of the diazaazulene/ quinazoline 4500Å absorption. The crystal thickness is 1.6 mm.

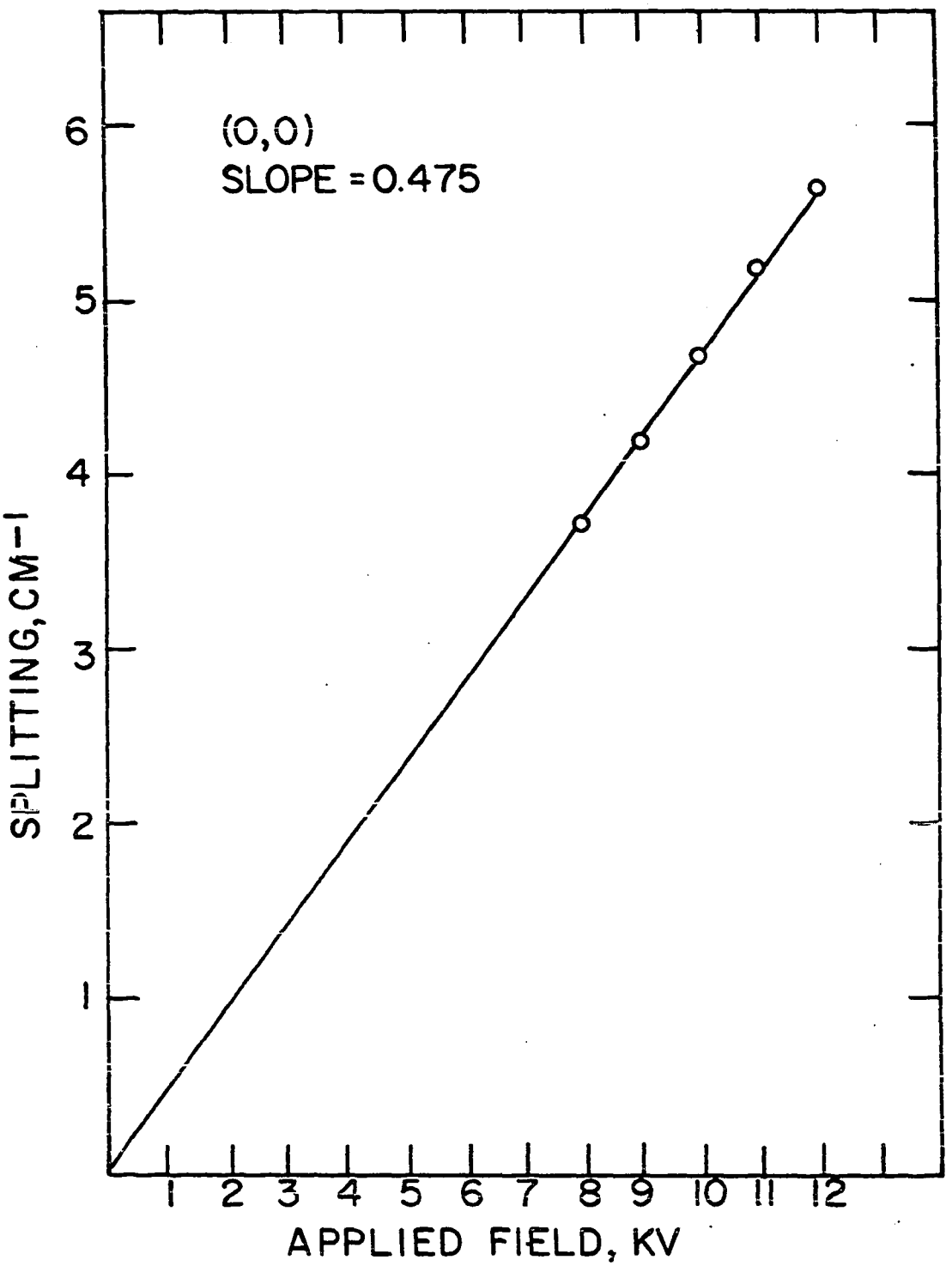
(0,0)
SLOPE = 0.475
SPLITTING, CM-1
APPLIED FIELD, KV
1
2
3
4
5
6
7
8
9
10
11
12

Figure 32. Stark splitting vs voltage curve for the 372 cm^{-1} band of the diazaazulene/quinazoline 4500Å absorption.

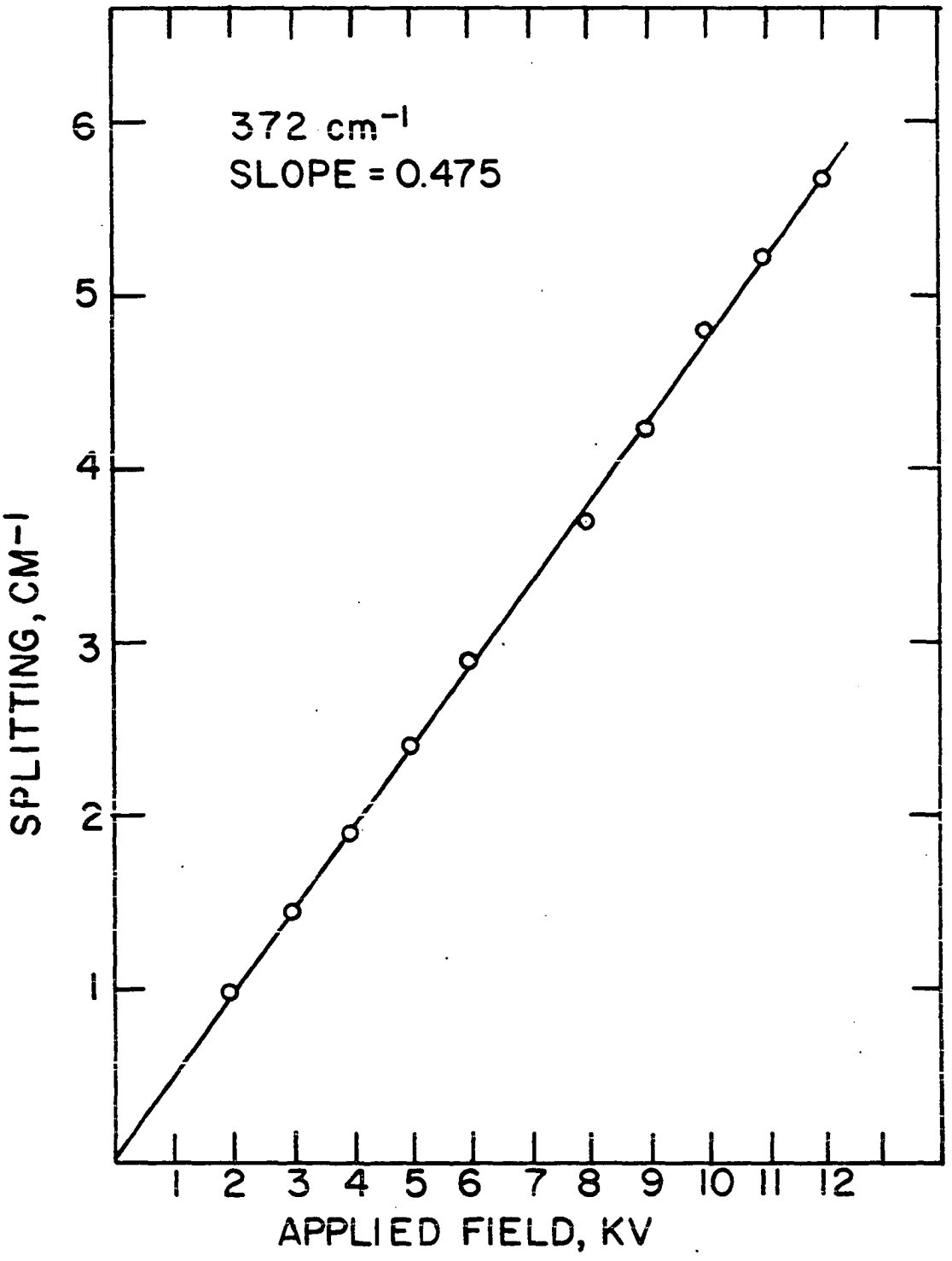
372 cm⁻¹
SLOPE = 0.475
SPLITTING, CM-1
APPLIED FIELD, KV
1
2
3
4
5
6
7
8
9
10
11
12

Figure 33. Stark splitting vs voltage curve for the 384 cm^{-1} band of the diazaazulene/ quinazoline 4500Å absorption.

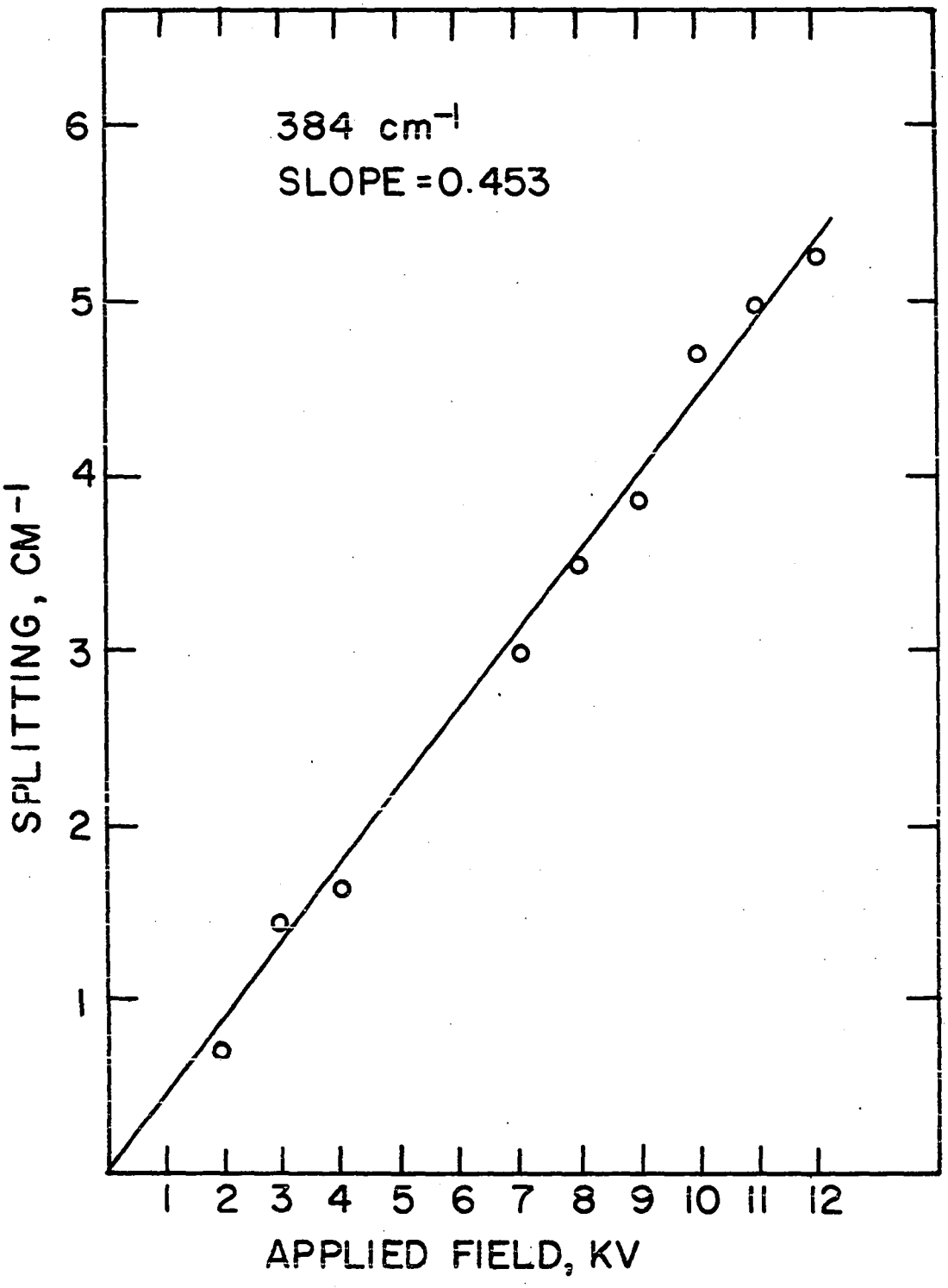
384 cm⁻¹
SLOPE = 0.453
SPLITTING, CM⁻¹
APPLIED FIELD, KV
1
2
3
4
5
6
7
8
9
10
11
12

Figure 34. Stark splitting vs voltage curve for the 660 cm^{-1} band of the diazaazulene/quinazoline 4500Å absorption.

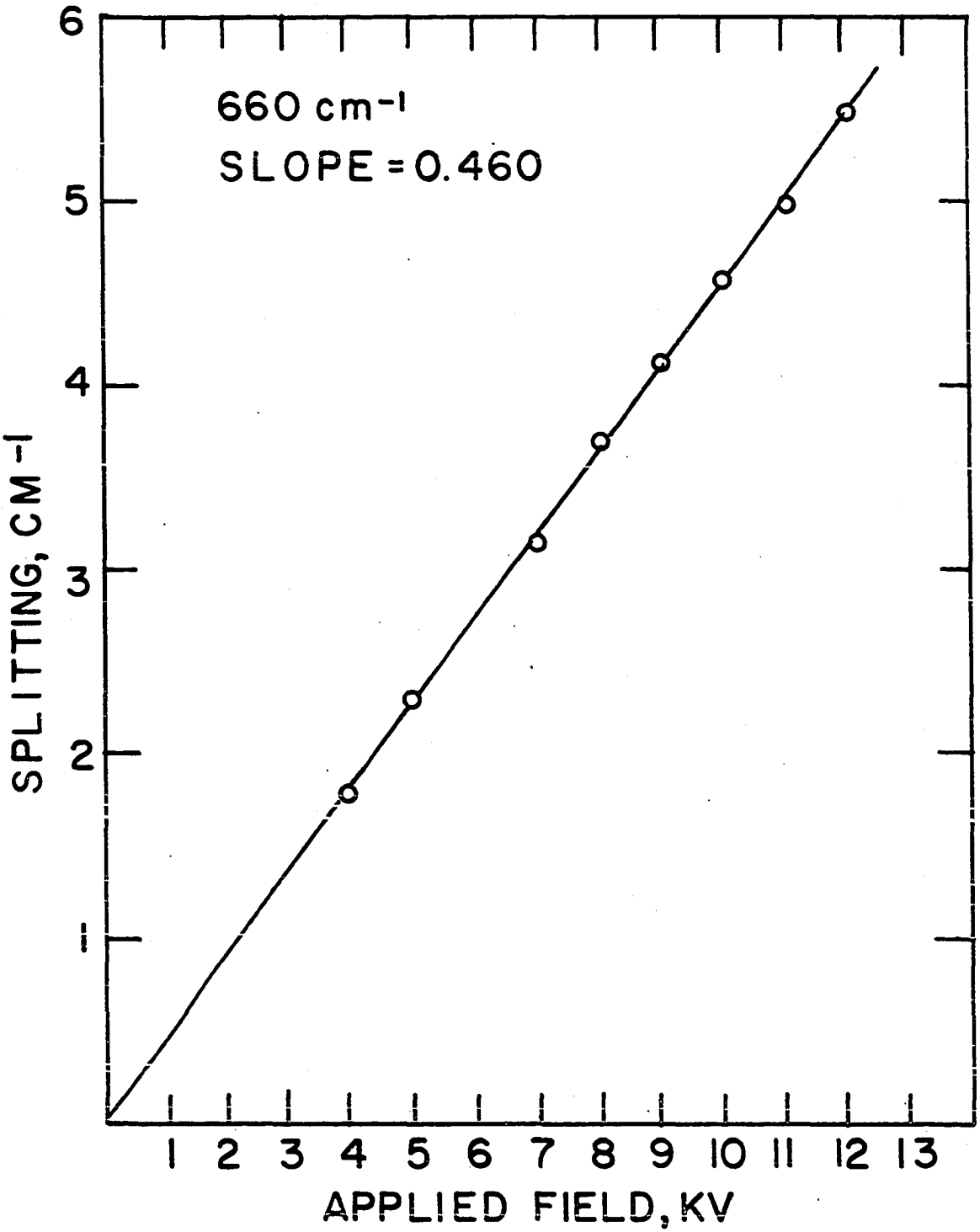
660 cm⁻¹
SLOPE = 0.460
SPLITTING, CM⁻¹
APPLIED FIELD, KV
6
5
4
3
2
1
1 2 3 4 5 6 7 8 9 10 11 12 13

Figure 35. Stark splitting vs voltage curve for the 734 cm^{-1} band of the diazaazulene/quinazoline 4500Å absorption.

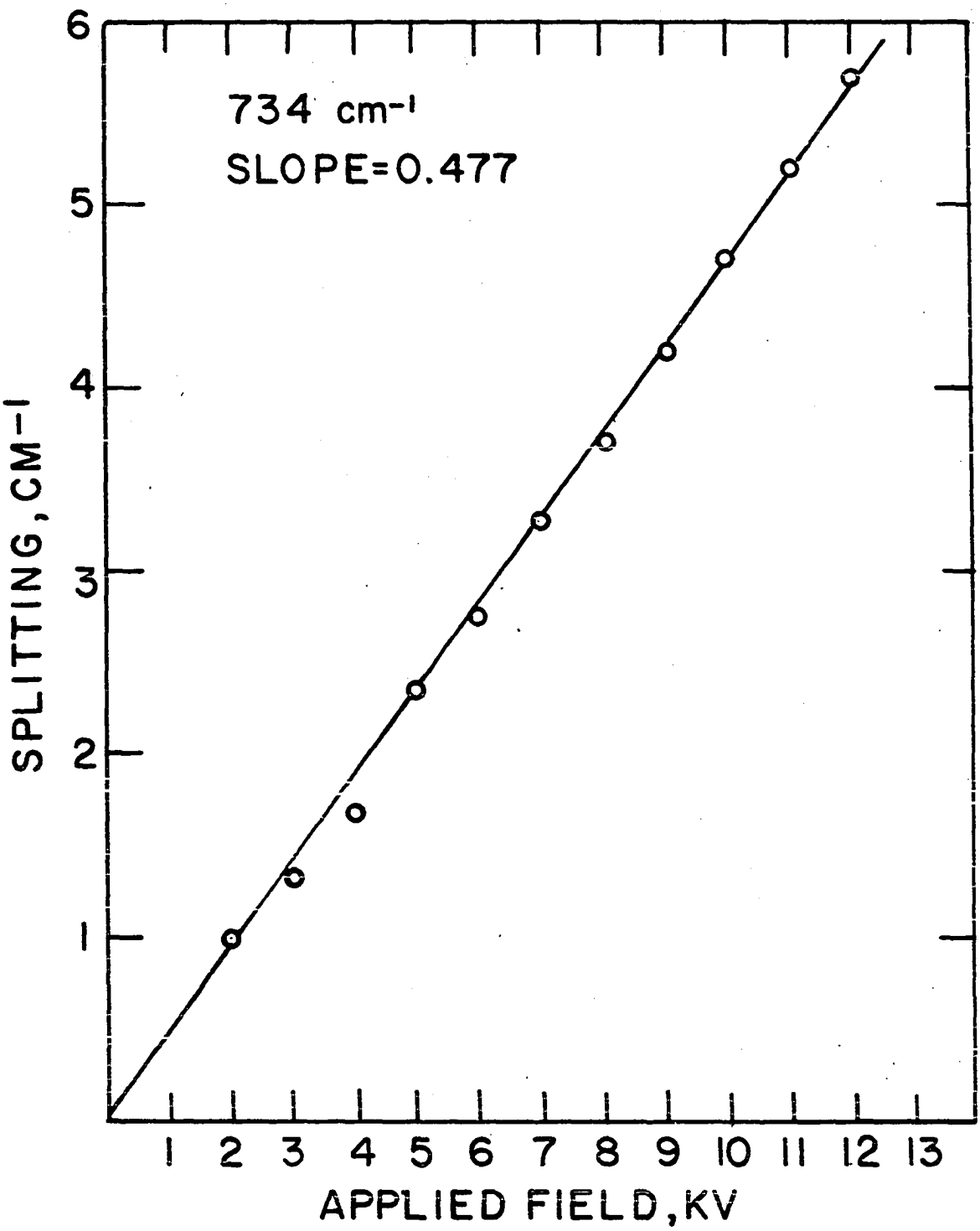
734 cm-1
SLOPE=0.477
SPLITTING, CM-1
APPLIED FIELD, KV
1
2
3
4
5
6
7
8
9
10
11
12
13

Figure 36. The origin region of the 5600Å absorption spectrum of phenylmonoazaazulene/ p-terphenyl at 4.2°K, 19.7°K and 25.0°K. The vertical lines indicate the band positions at 4.2°K, and demonstrate the red shift of the band positions with temperature.

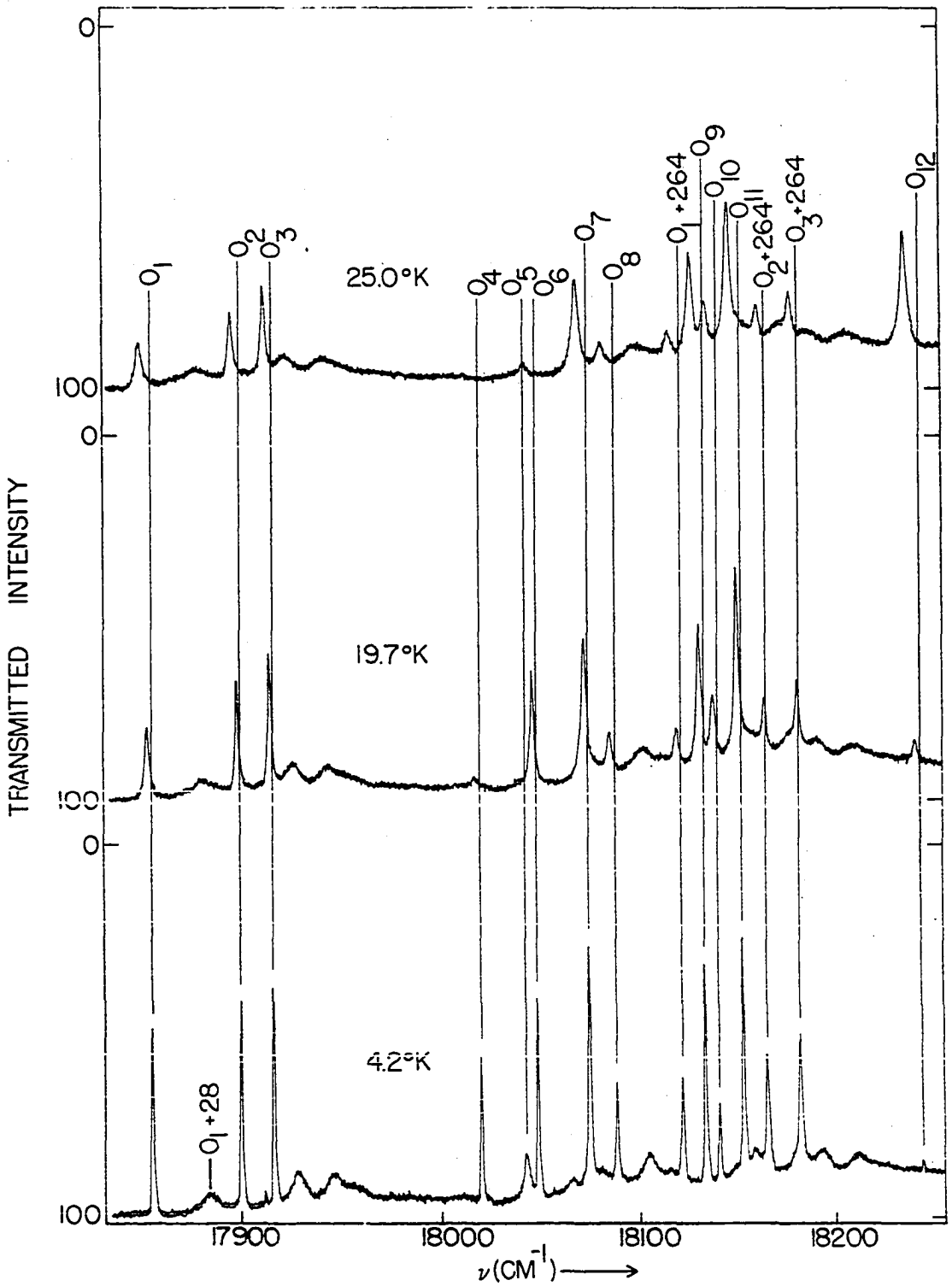
0
100
0
100
0
100
TRANSMITTED INTENSITY
25.0°K
19.7°K
4.2°K
0_1
0_2
0_3
0_4
0_5
0_6
0_7
0_8
0_1+264
0_9
0_{10}
0_{11}
0_2+264
0_3+264
0_{12}
0_1+28
17900
18000
18100
18200
$\nu(CM^{-1})$ ⟶

Figure 37. The total integrated intensity of all twelve zero-phonon origins *vs* temperature for phenylazaazulene/terphenyl. The solid line is the calculated intensity for T_D = 61°K, cf. text.

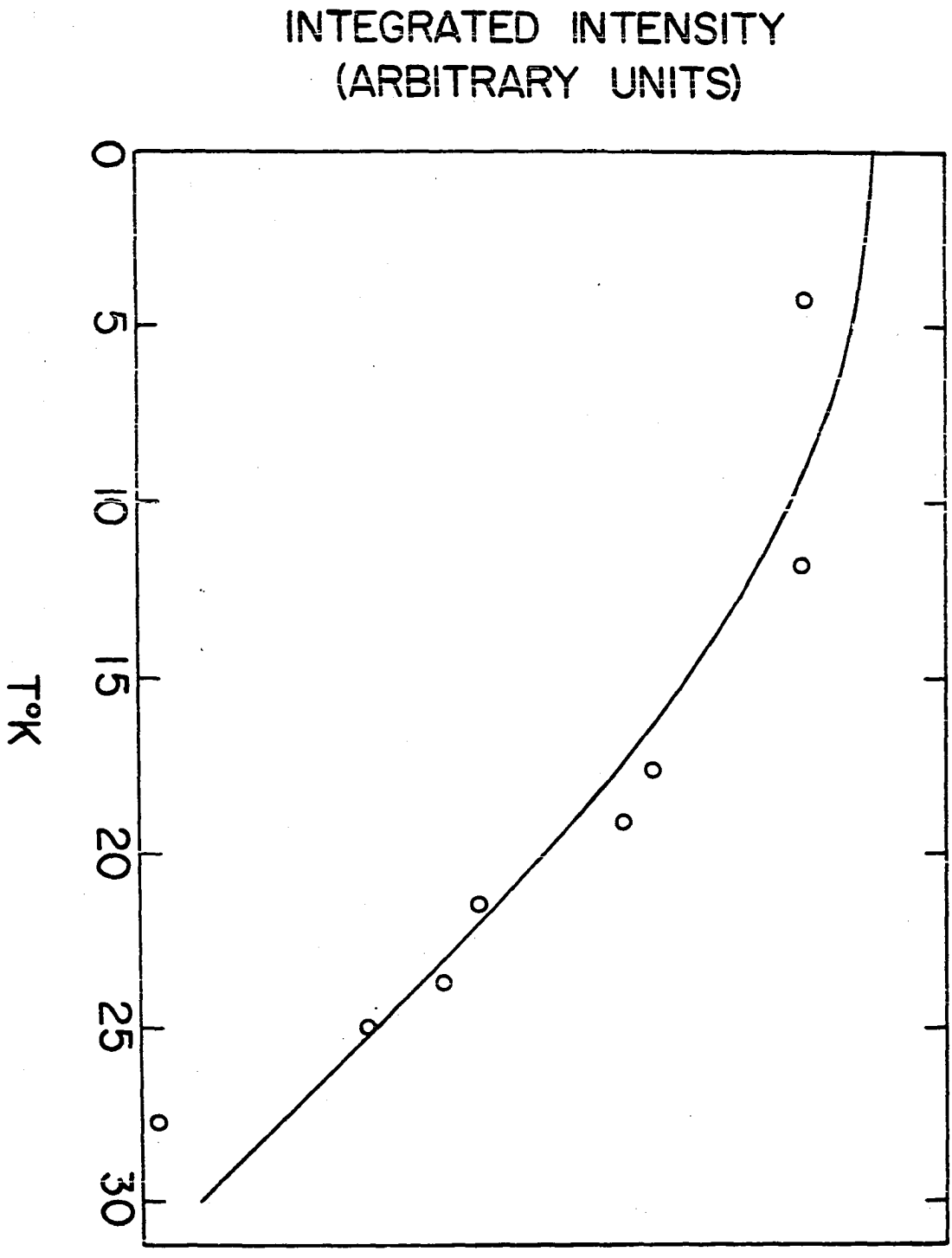
INTEGRATED INTENSITY
(ARBITRARY UNITS)
0
5
10
15
20
25
30
T°K

Figure 38. Band broadening (ΔE) vs temperature and band shift (δE) vs temperature for O_1. The solid lines are calculated using the coupling constants shown on the figure, with $T_D = 60°K$.

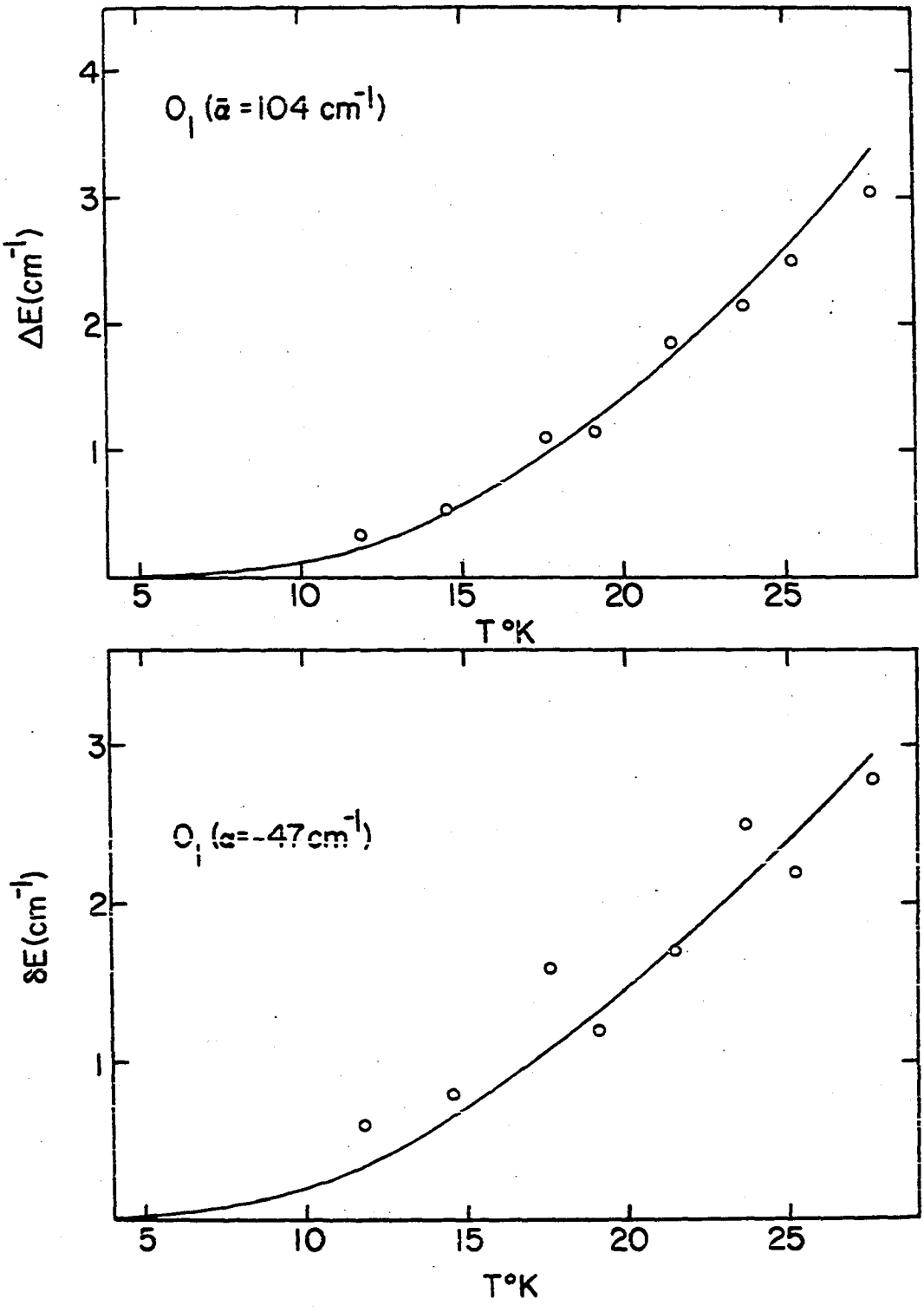
O_1 ($\bar{a}$ = 104 cm^{-1})
ΔE(cm^{-1})
T°K
O_1 ($\bar{a}$ = -47 cm^{-1})
δE(cm^{-1})
T°K

Figure 39. Band broadening (ΔE) vs temperature and band shift (δE) vs temperature for O_9. The solid lines are calculated using the coupling constants shown on the figure, with T_D = 60°K.

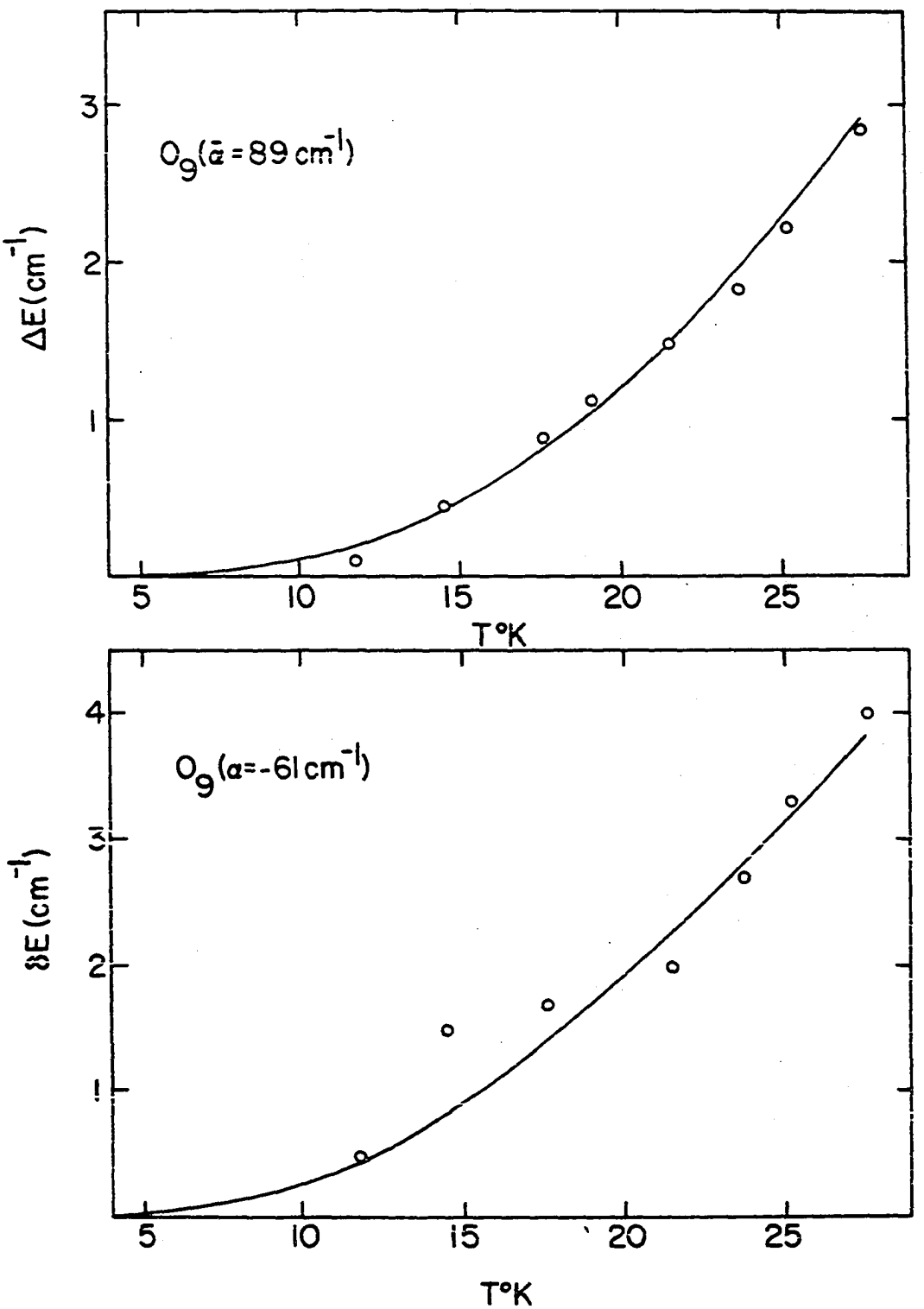
$O_9(\bar{\alpha} = 89\,cm^{-1})$
ΔE(cm⁻¹)
T°K
$O_9(\alpha = -61\,cm^{-1})$
δE(cm⁻¹)
T°K

Figure 40. Band broadening (ΔE) *vs* temperature and band shift (δE) *vs* temperature for O_{11}. The solid lines are calculated using the coupling constants shown on the figure, with $T_D = 60°K$.

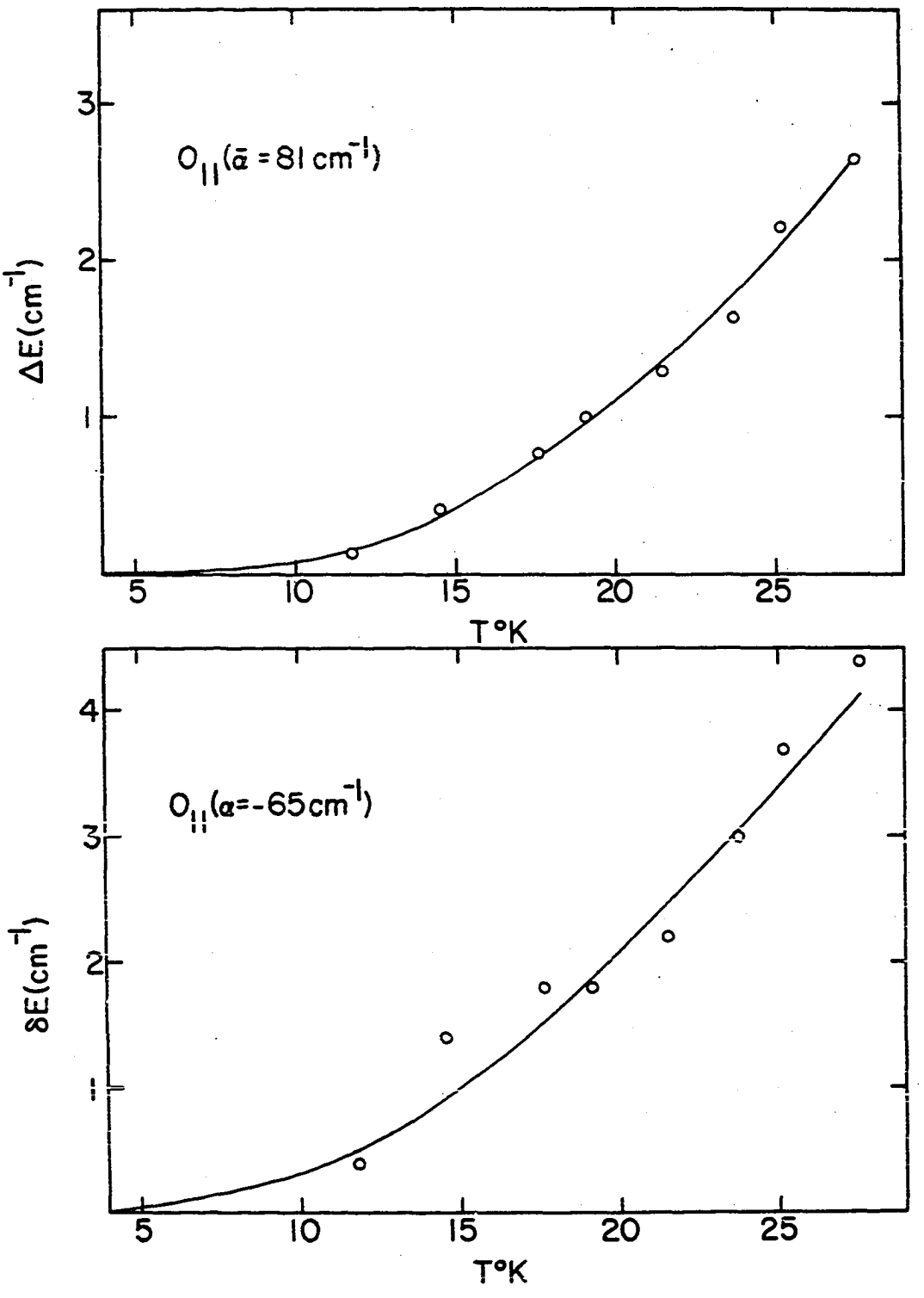
$O_{11}(\bar{\alpha} = 81\,cm^{-1})$
$\Delta E(cm^{-1})$
T°K
$O_{11}(\alpha = -65\,cm^{-1})$
$\delta E(cm^{-1})$
T°K

Figure 41. O_{11} of phenylazaazulene/terphenyl at 25°K. The solid line is the experimental band profile. Lorentzian (o) and Gaussian (x) band profiles having the appropriate half band width and intensity are also shown.

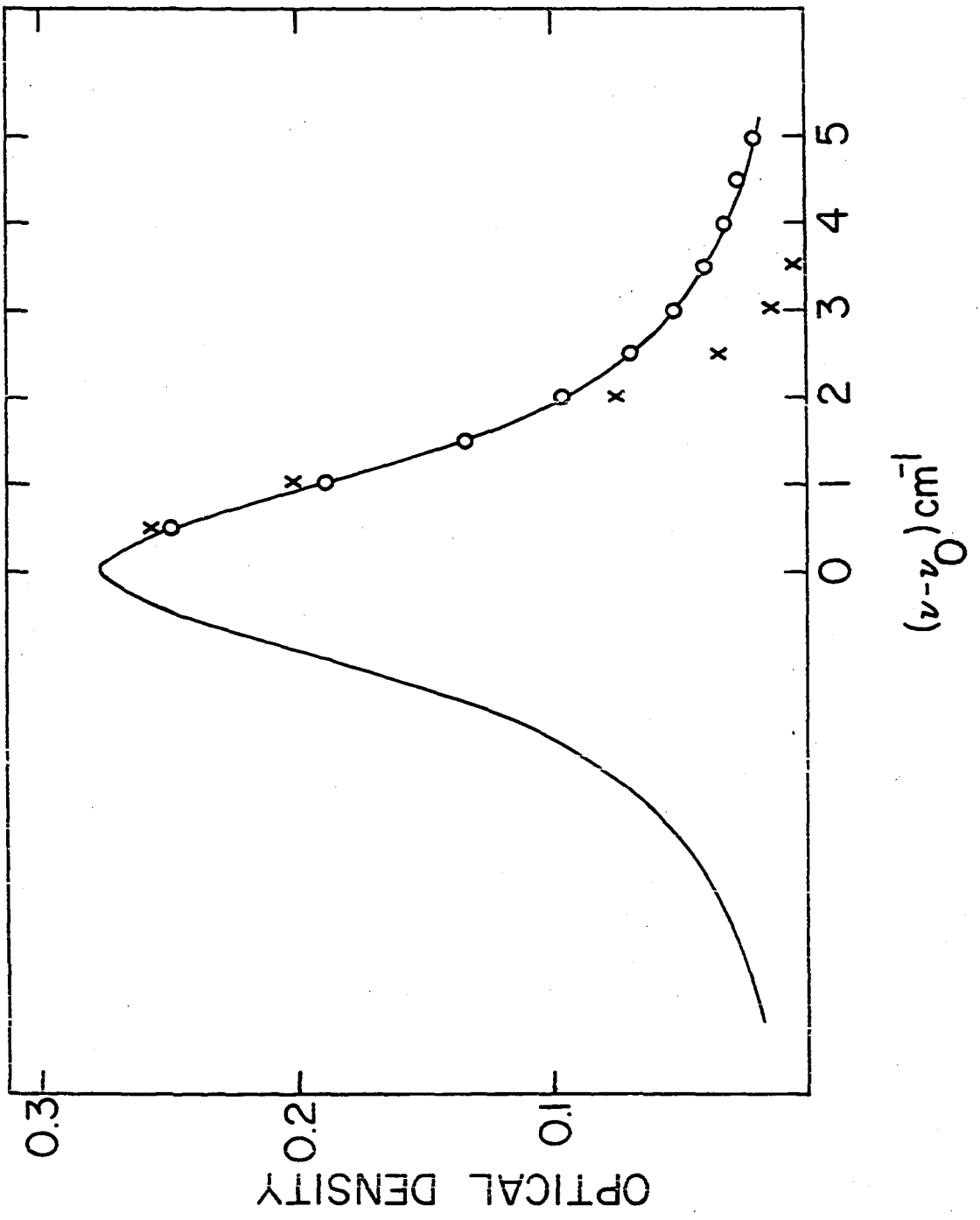
OPTICAL DENSITY
0.3
0.2
0.1
0
1
2
3
4
5
$(\nu-\nu_0)cm^{-1}$

Figure 42. Band broadening (ΔE) *vs* temperature for $0_1 + 264$ of phenylazaazulene/terphenyl. The solid line is the calculated curve for $\bar{\alpha} = 100\ cm^{-1}$, $T_D = 60°K$.

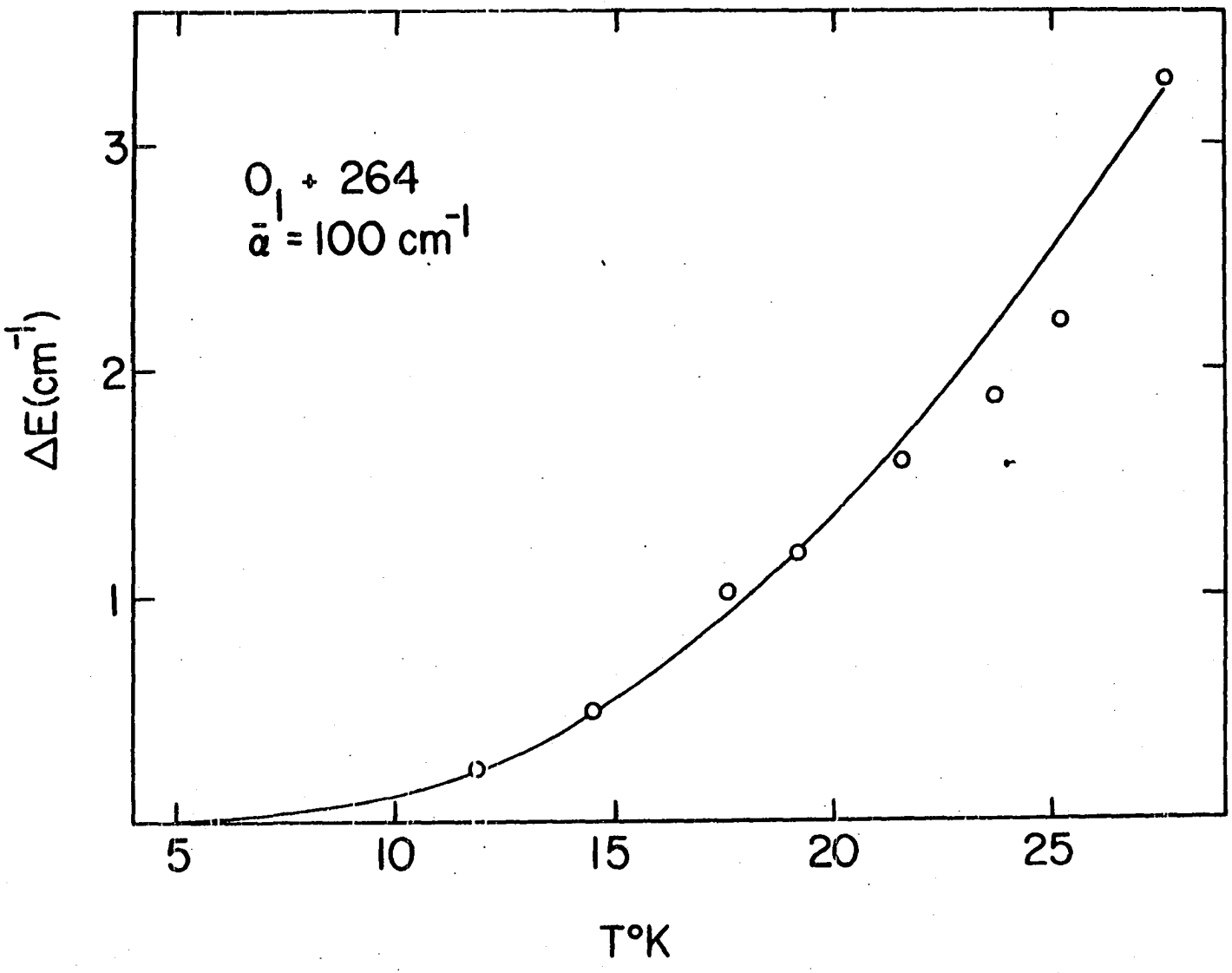
O_1 + 264
$\bar{\alpha}^1$ = 100 cm^{-1}
ΔE(cm^{-1})
3
2
1
5
10
15
20
25
T°K

Figure 43. Band broadening (ΔE) vs temperature for the origin band, and 384 cm^{-1}, 1193 cm^{-1}, and 1388 cm^{-1} a_1 vibronic fundamentals of azulene/naphthalene. The solid line is calculated from $\bar{\alpha}$ = 97 cm^{-1}, T_D = 60°K.

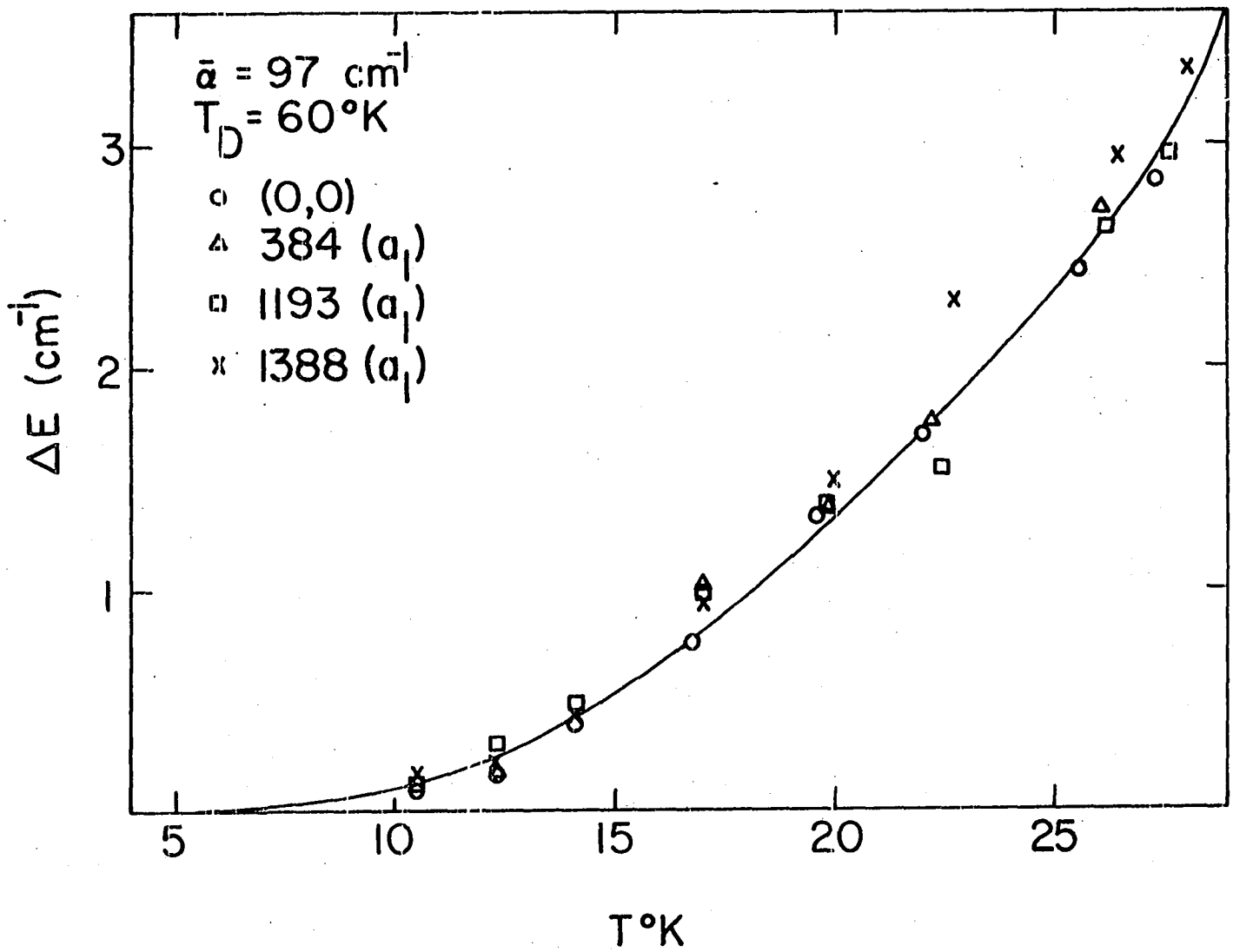
$\bar{\alpha}$ = 97 cm^{-1}
T_D = 60°K
(0,0)
384 (a_1)
1193 (a_1)
1388 (a_1)
ΔE (cm^{-1})
T°K
1
2
3
5
10
15
20
25

Figure 44. Band broadening (ΔE) *vs* temperature for the 1362 cm^{-1} and 1756 cm^{-1} b_1 fundamentals of azulene/naphthalene. The solid line is calculated from $\bar{\alpha}$ = 76 cm^{-1}, T_D = 60°K.

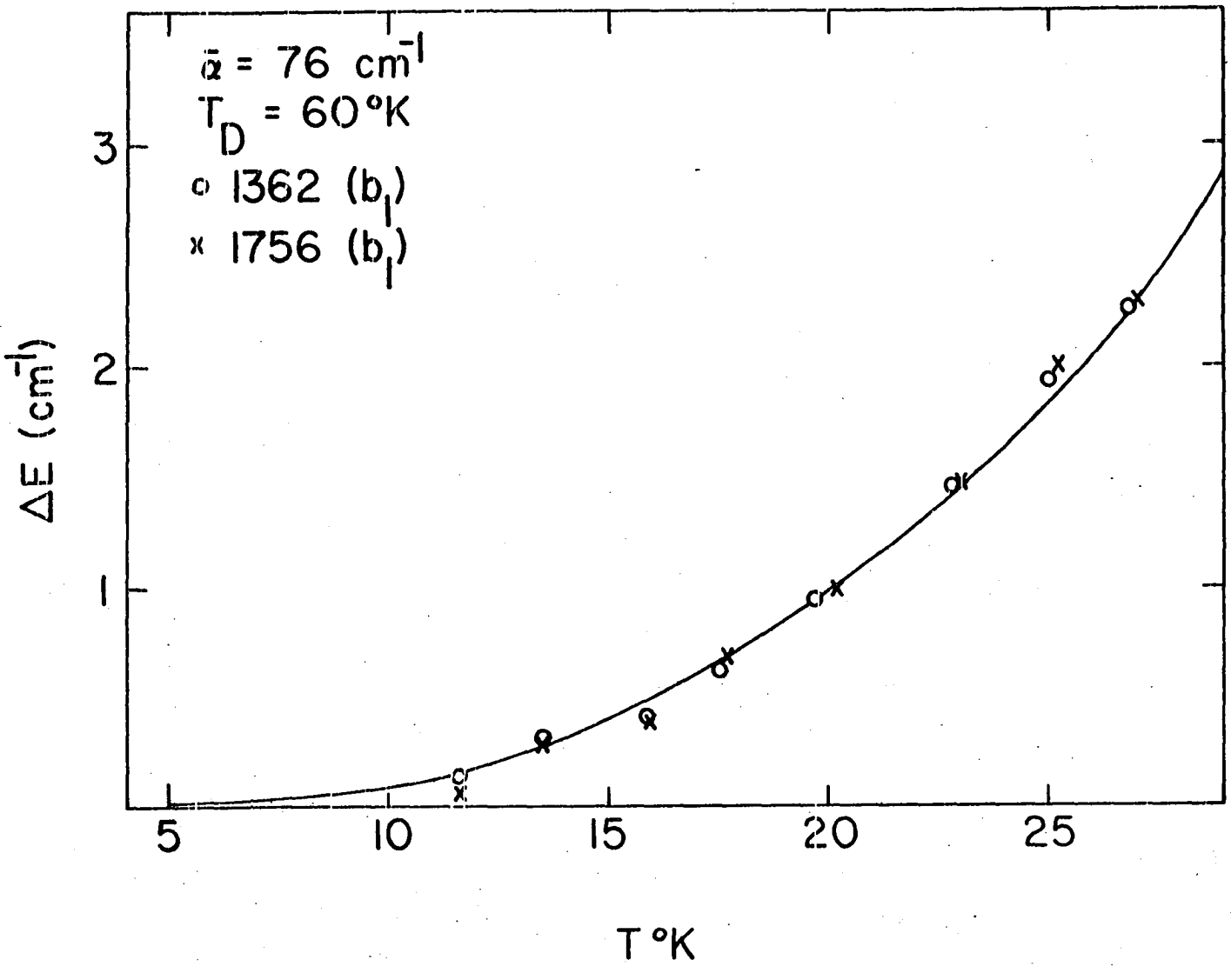
$\bar{\alpha}$ = 76 cm^{-1}
T_D = 60°K
o 1362 (b_1)
x 1756 (b_1)
ΔE (cm^{-1})
3
2
1
5
10
15
20
25
T °K

Figure 45. Thermal broadening of the origin vibron band, 3500Å absorption system of azulene in naphthalene.

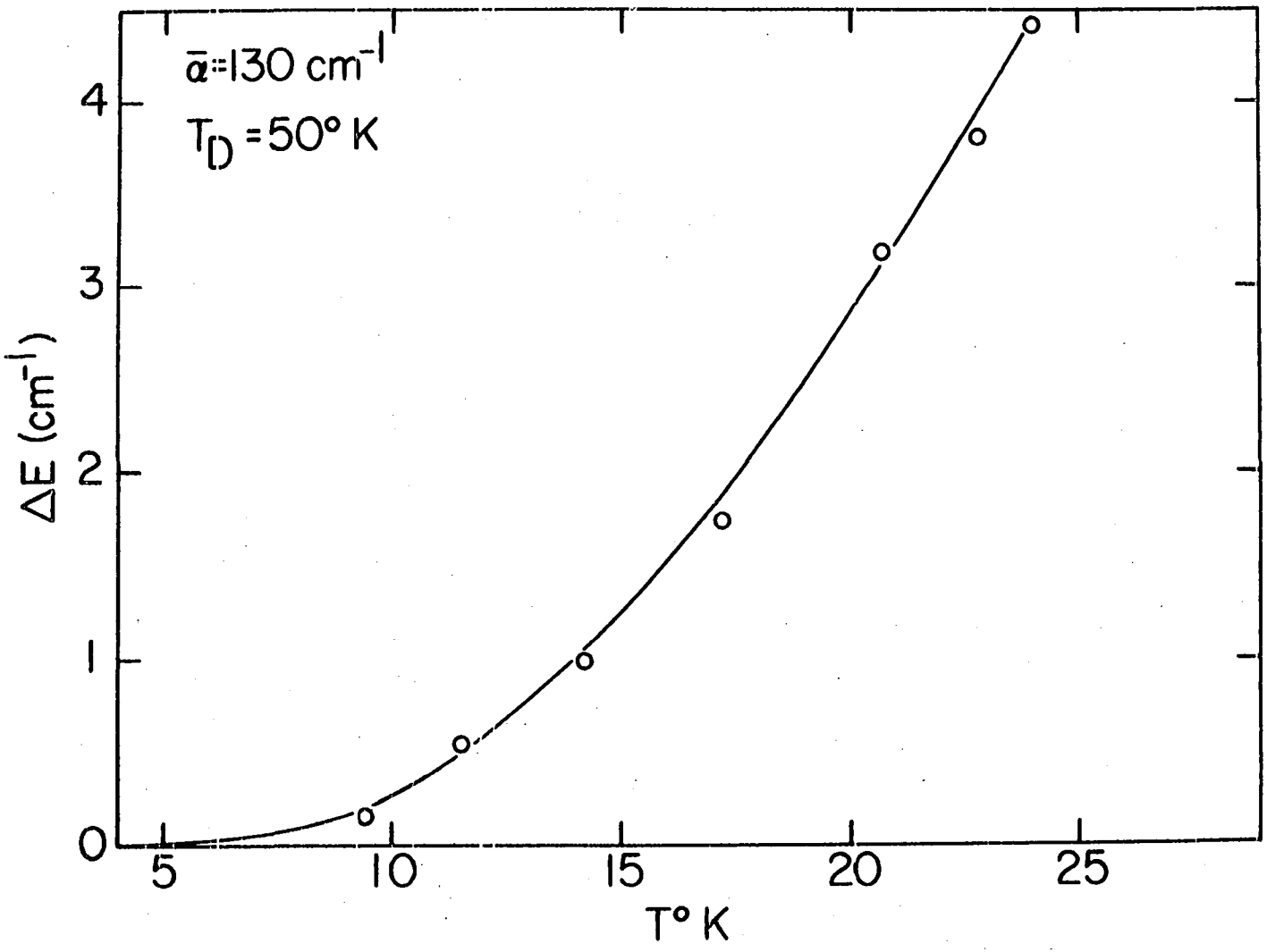
$\bar{\alpha}$=130 cm^{-1}
T_D = 50° K
ΔE (cm^{-1})
0
1
2
3
4
5
10
15
20
25
T° K

Figure 46. Thermal broadening of the 669 (a_1) and 695 (b_1) cm^{-1} vibron bands, 3500Å absorption system of azulene in naphthalene.

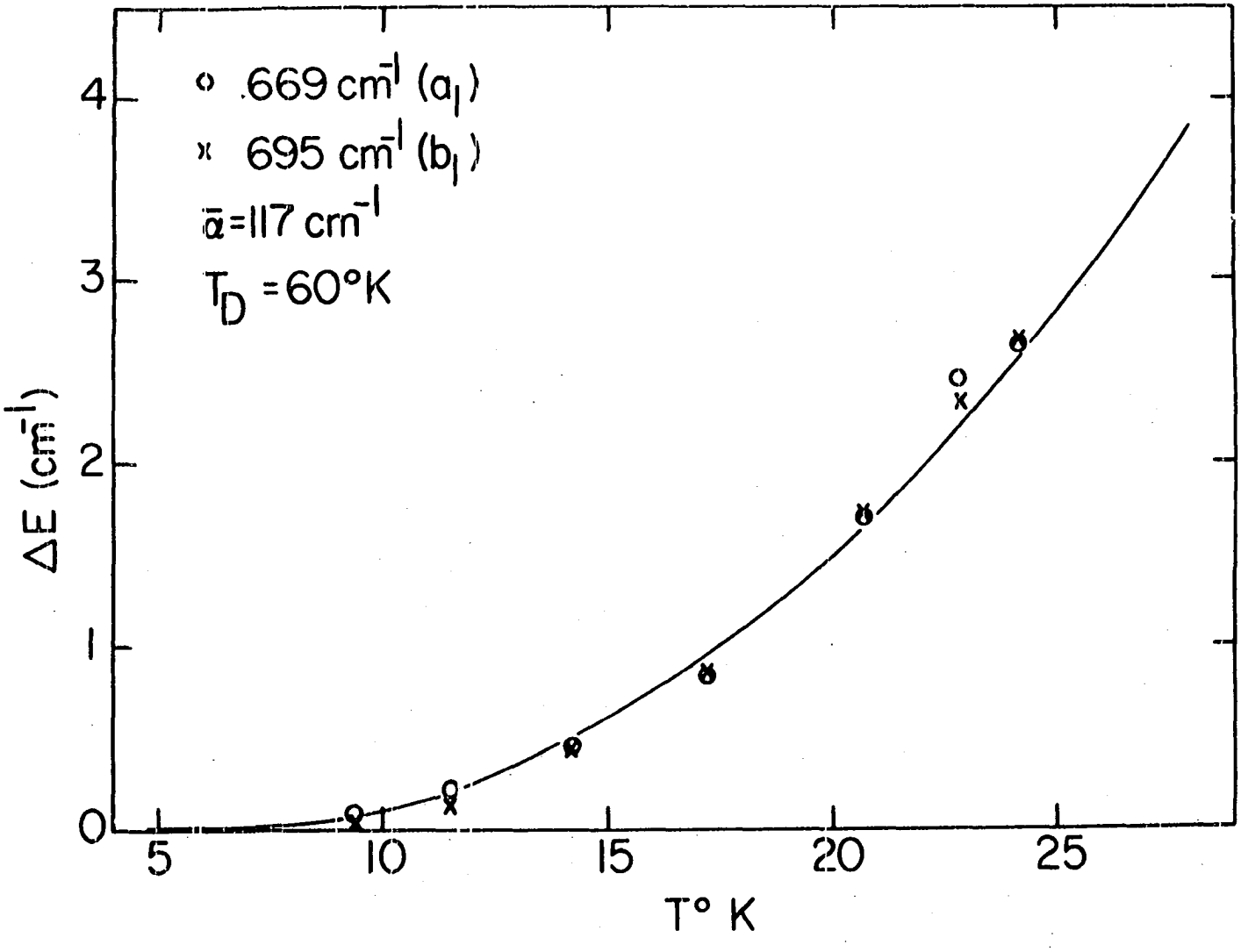
o .669 cm⁻¹ (a₁)
x 695 cm⁻¹ (b₁)
ᾱ=117 cm⁻¹
T_D =60°K
ΔE (cm⁻¹)
T° K
0
1
2
3
4
5
10
15
20
25

Figure 47. Thermal broadening of the origin, 539, 575 and 904 cm^{-1} vibron bands, 4500Å absorption system of 1,3-diazaazulene in naphthalene (crystal 1).

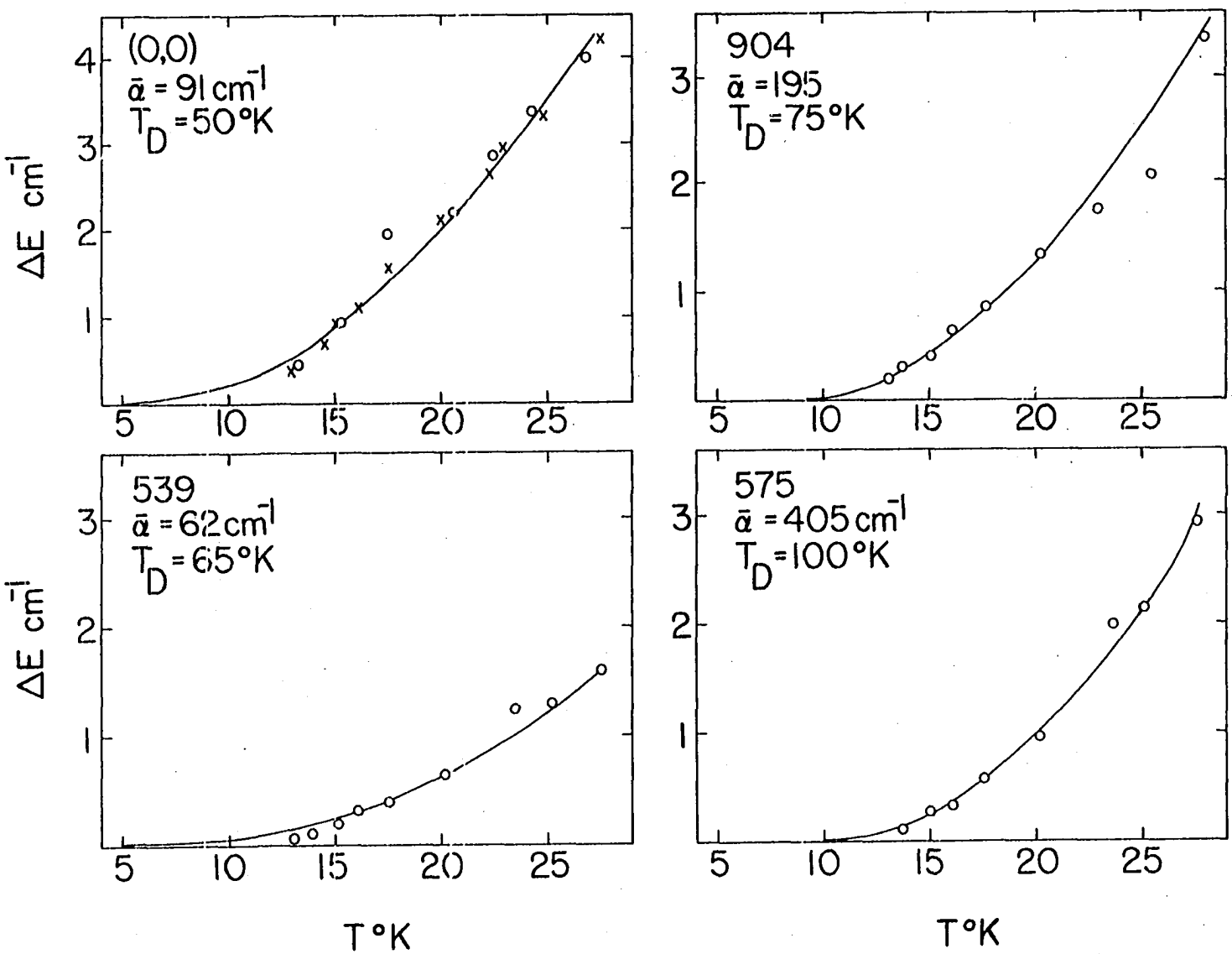
(0,0)
$\bar{\alpha}$ = 91 cm^{-1}
T_D = 50°K
904
$\bar{\alpha}$ = 195
T_D = 75°K
539
$\bar{\alpha}$ = 62 cm^{-1}
T_D = 65°K
575
$\bar{\alpha}$ = 405 cm^{-1}
T_D = 100°K
ΔE cm^{-1}
ΔE cm^{-1}
T°K
T°K

Figure 48. Thermal broadening of the 1070, 1158 and 1457 cm^{-1} b_1 vibron bands, 4500Å absorption system of 1,3-diazaazulene in naphthalene (crystal 1).

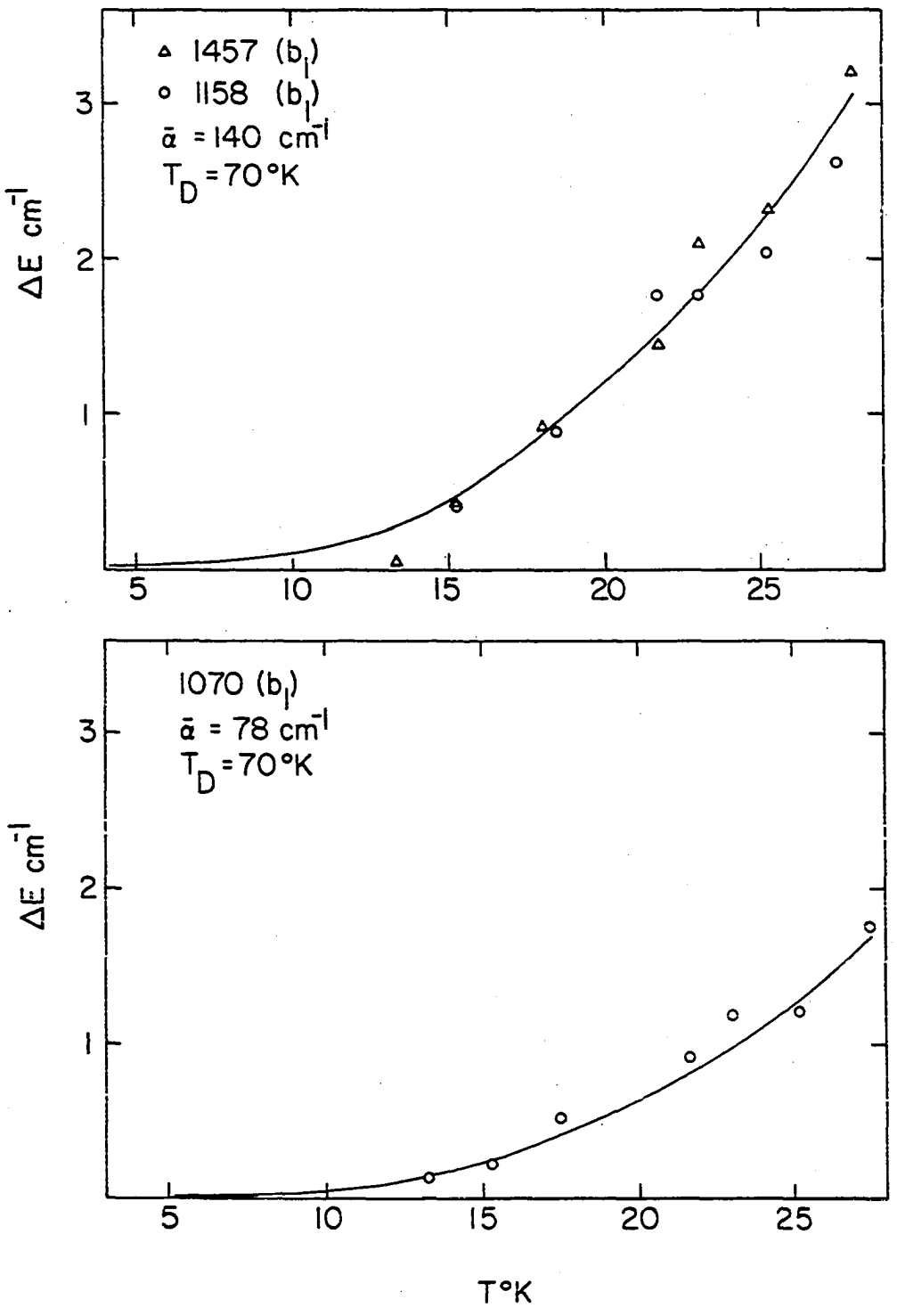
△ 1457 (b1)
○ 1158 (b1)
ᾱ = 140 cm⁻¹
TD = 70°K
ΔE cm⁻¹
1070 (b1)
ᾱ = 78 cm⁻¹
TD = 70°K
ΔE cm⁻¹
T°K

Figure 49. Thermal broadening of the origin band, 4500Å absorption system of 1,3-diazaazulene in naphthalene. Solid curve and experimental points (crystal 2); dashed curve (crystal 1, Figure 47).

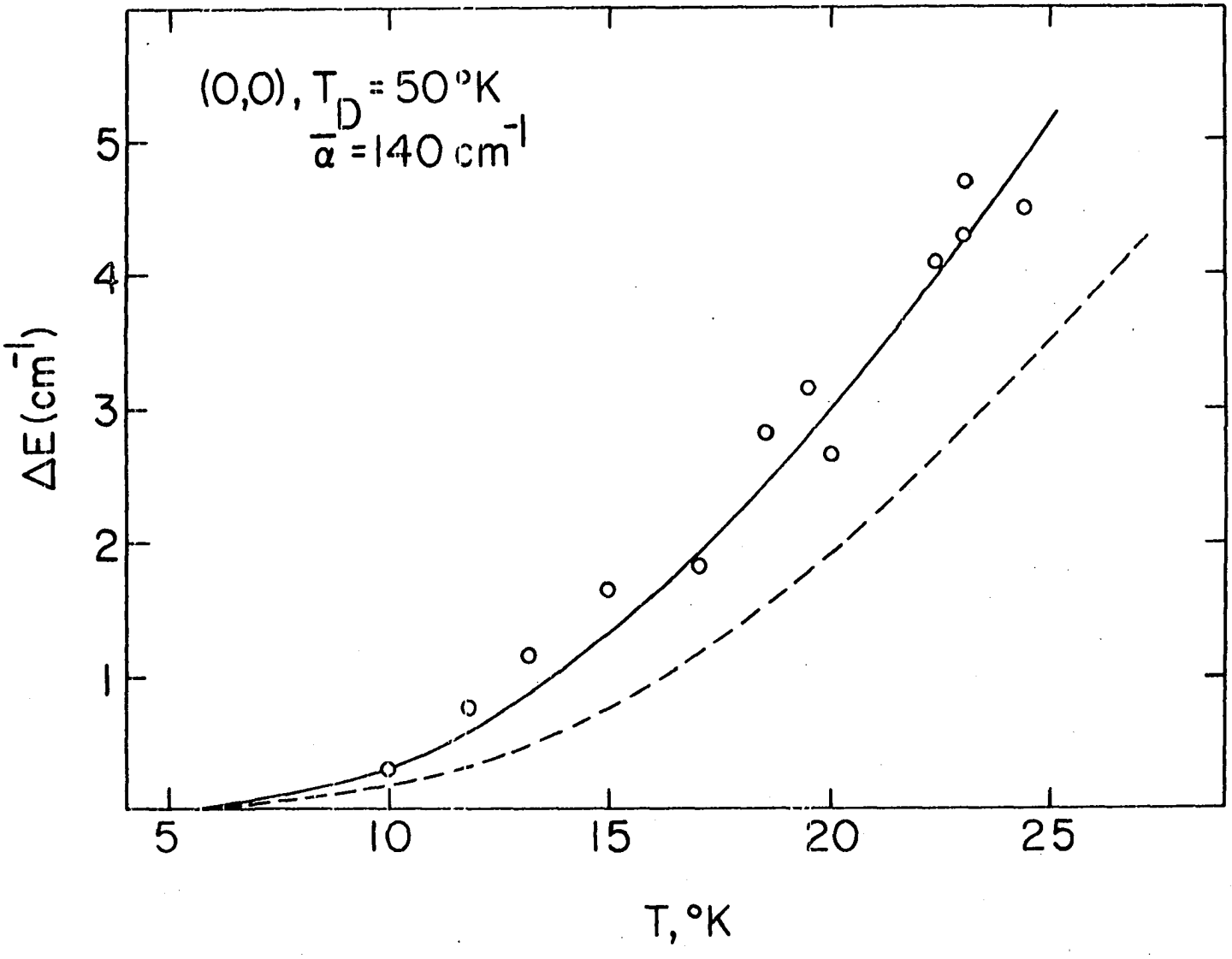
(0,0), T_D = 50°K
$\bar{\alpha}$ = 140 cm^{-1}
ΔE (cm^{-1})
1
2
3
4
5
5
10
15
20
25
T, °K

Figure 50. Thermal broadening of the 539 cm^{-1} vibron band, 4500Å absorption system of 1,3-diazaazulene in naphthalene. Solid curve and experimental points (crystal 2); dashed curve (crystal 1, Figure 47).

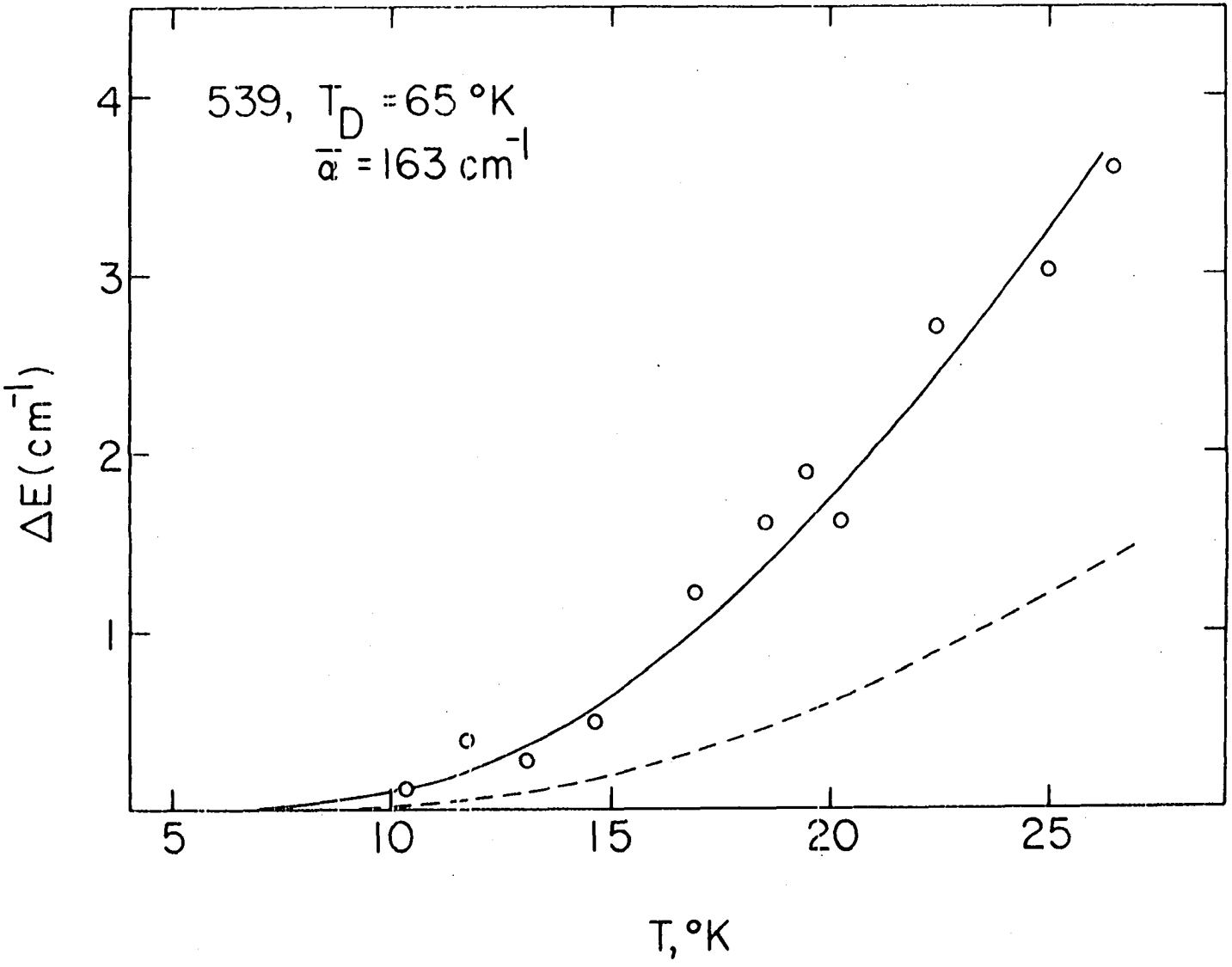
539, T_D = 65 °K
$\bar{\alpha}$ = 163 cm^{-1}
ΔE(cm^{-1})
T, °K
1
2
3
4
5
10
15
20
25

Figure 51. Thermal broadening of the 575 cm^{-1} vibron band, 4500Å absorption system of 1,3-diazaazulene in naphthalene. Solid curve and experimental points (crystal 2); dashed curve (crystal 1, Figure 47).

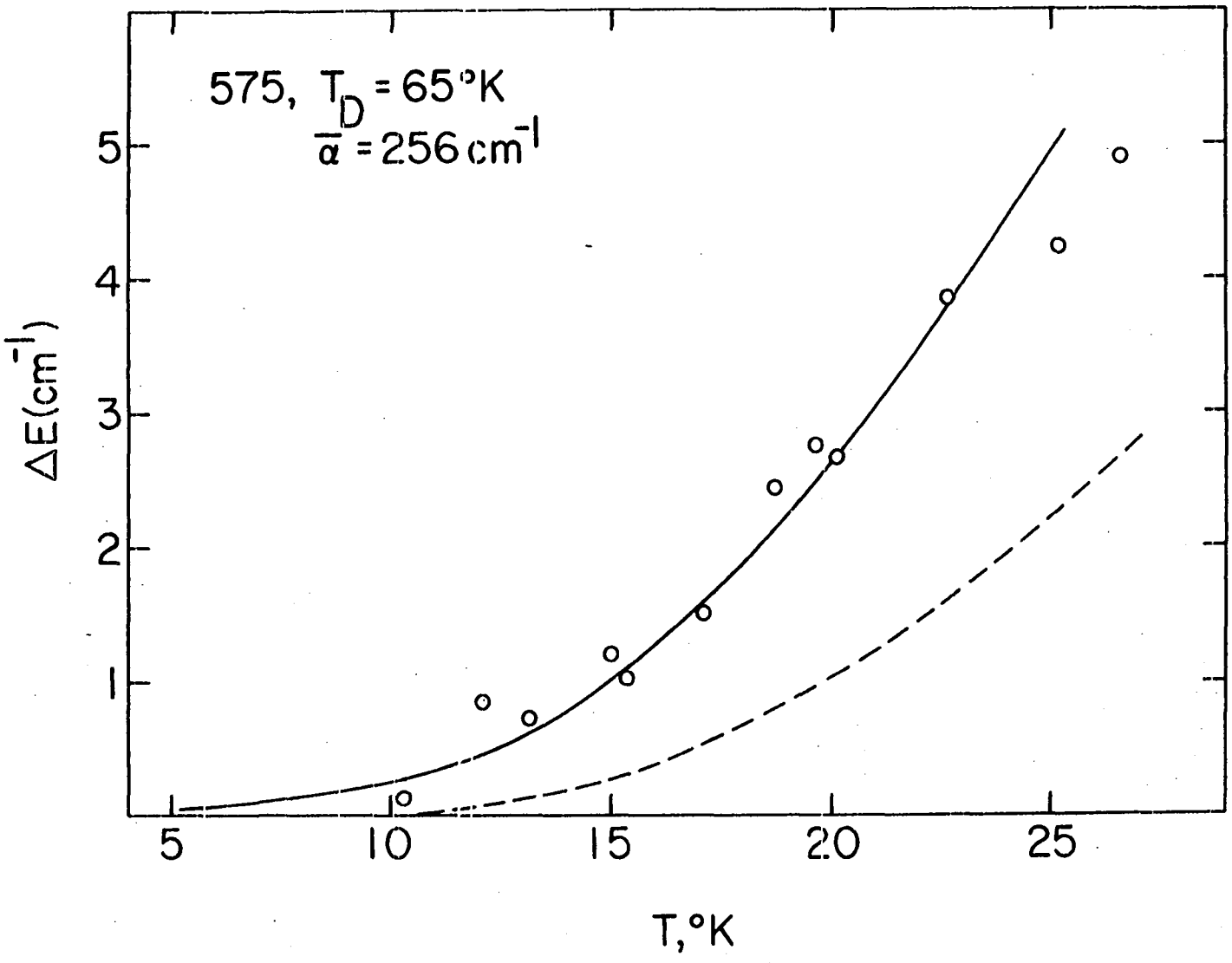
575, T_D = 65°K
$\bar{\alpha}$ = 256 cm^{-1}
ΔE(cm^{-1})
5
4
3
2
1
5
10
15
20
25
T,°K

Figure 52. Zero-phonon spectral shape function for the origin vibron band (27.3°K), 4500Å absorption system of 1,3-diazaazulene in naphthalene. Experimental (solid curve); crosses (Gaussian fit); circles (Lorentzian fit). The experimental curve has been redrawn with the ordinate linear in optical density, to better demonstrate the Lorentzian behavior (cf. Figure 53).

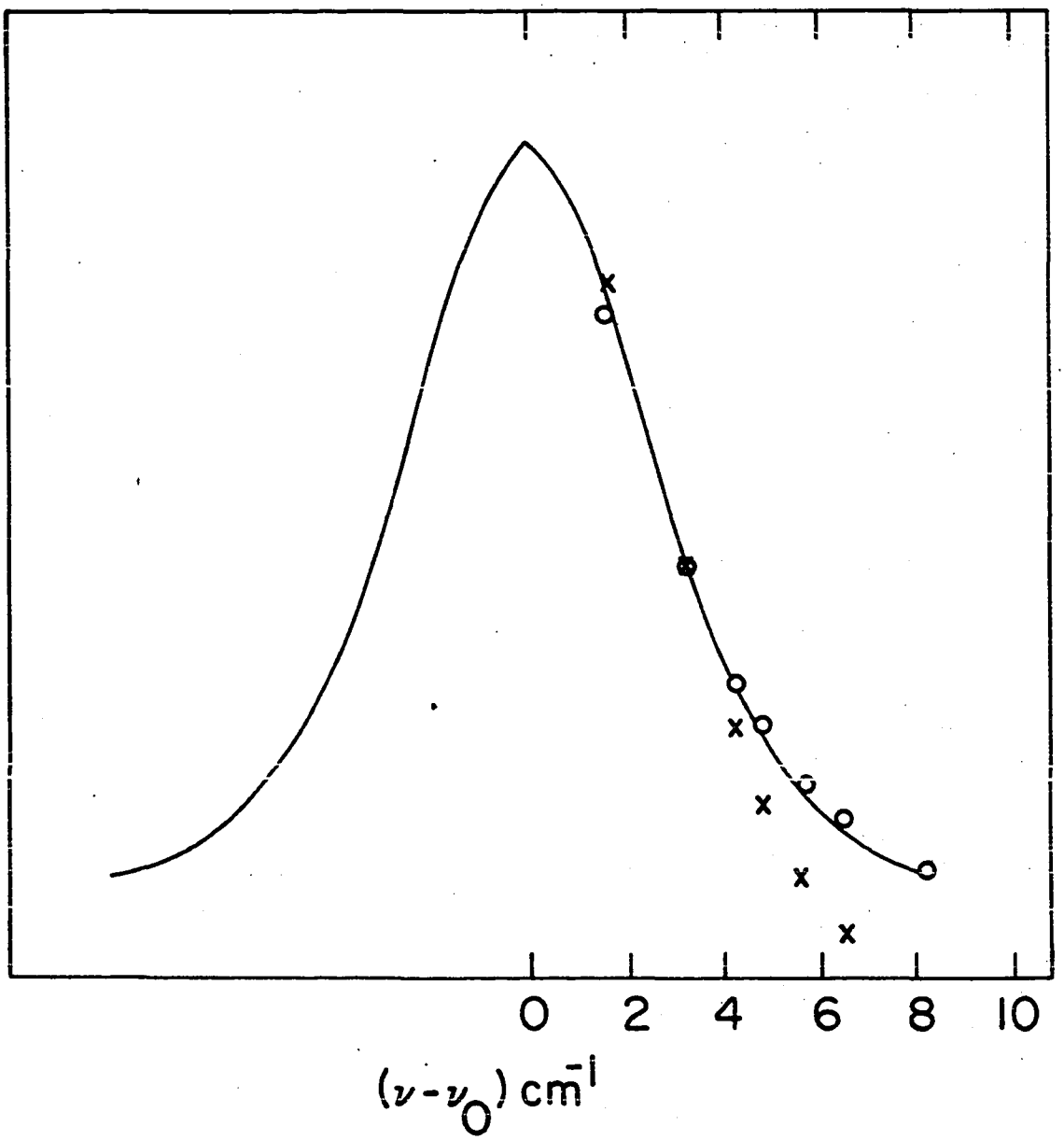
0
2
4
6
8
10
$(\nu-\nu_0)$ cm^{-1}

Figure 53. The zero-phonon origin band of the 1,3-diazaazulene in naphthalene 4500Å absorption at 20.3°K (experimental photoelectric tracing). The rising intensity on the high energy side of the zero-phonon band is the onset of the multi-phonon absorption.

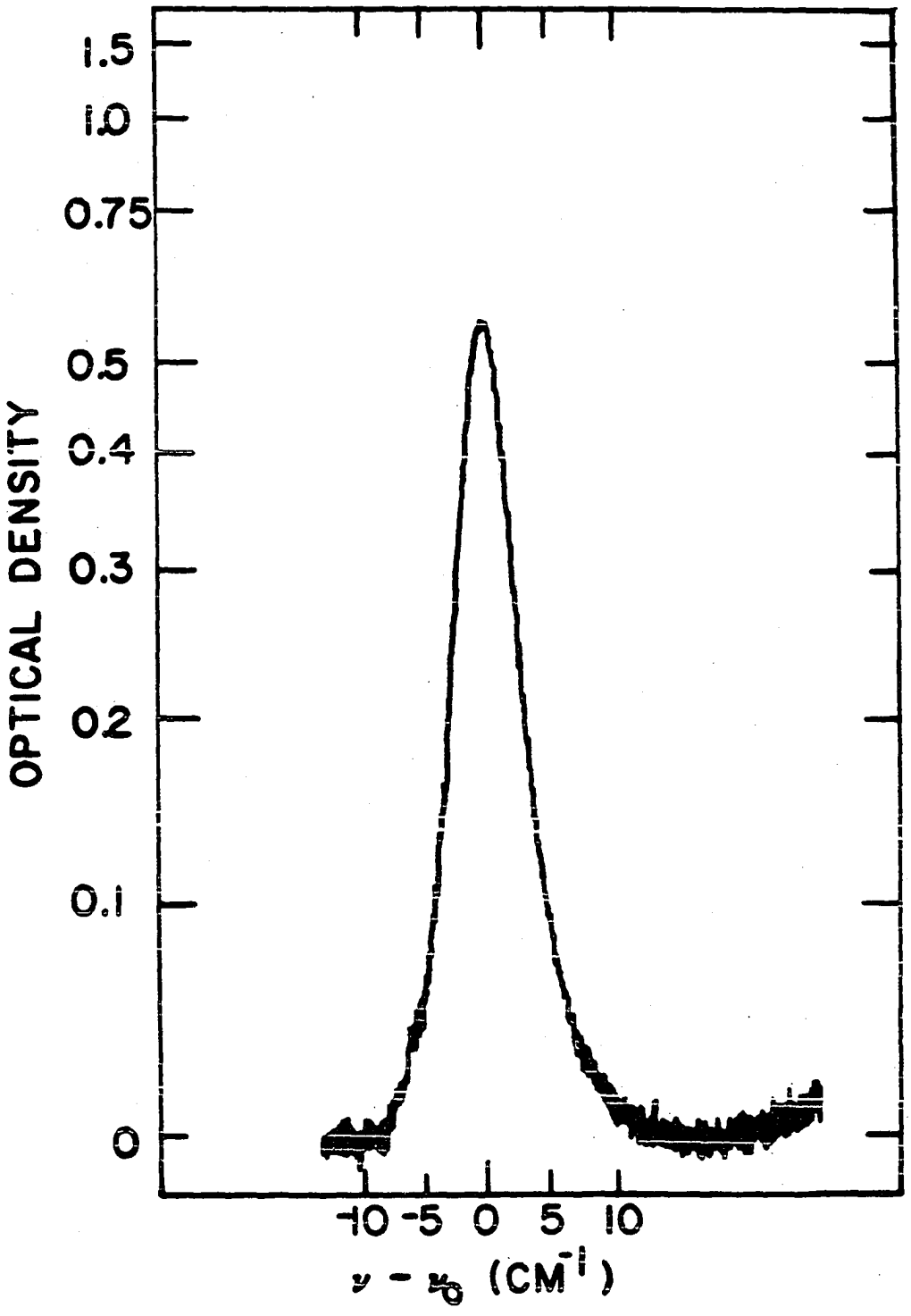
OPTICAL DENSITY
1.5
1.0
0.75
0.5
0.4
0.3
0.2
0.1
0
-10 -5 0 5 10
ν - ν0 (CM-1)

BIBLIOGRAPHY

1. M. Beer and H. C. Longuet-Higgins, J. Chem. Phys., 23, 1390 (1955).

2. M. S. Kasha, Discuss. Faraday Soc., 9, 14 (1950).

3. J. Sidman and D. S. McClure, J. Chem. Phys., 24, 757 (1956).

4. R. M. Hochstrasser and T-Y Li, J. Mol. Spec., 41, 297 (1972).

5. G. R. Hunt, E. F. McCoy and I. G. Ross, Aust. J. Chem., 18, 591 (1962).

6. G. W. Robinson and R. P. Forsch, J. Chem. Phys., 37, 1962 (1962); 38, 1187 (1962).

7. J. P. Byrne, E. F. McCoy and I. G. Ross, Aust. J. Chem., 18, 1589 (1965).

8. R. Engleman and J. Jortner, Mol. Phys., 18, 145 (1970).

9. A. R. Lacey, Ph.D. thesis, University of Sydney, 1972.

10. A. R. Lacey, E. F. McCoy and I. G. Ross, Chem. Phys. Lett., 21, 233 (1973).

11. P. M. Rentzepis, Chem. Phys. Lett., 3, 717 (1969).

12. P. M. Rentzepis, J. Jortner and R. P. Jones, Chem. Phys. Lett., 4, 599 (1970).

13. C. J. Marzzacco, Ph.D. thesis, University of Pennsylvania, 1968.

14. A. D. Jordan, Ph.D. thesis, University of Sydney, 1970.

15. K. K. Innes, J. P. Byrne and I. G. Ross, J. Mol. Spec., 22, 125 (1967).

16. R. H. Silsbee in Optical Properties of Solids, edited by S. Nudelman and S. S. Mitra (Plenum, New York, 1969), p. 607.

17. B. DiBartolo, Optical Interactions in Solids (Wiley, New York, 1968), p. 367.

18. K. K. Rebane, Impurity Spectra of Solids (Plenum, New York, 1970).

19. D. R. Eslinger, M.S. thesis, Iowa State University, 1973.

20. T. Nozoe, T. Mukai and I. Murata, J. Amer. Chem. Soc., 76, 3352 (1954).

21. E. E. Wahlstrom, Optical Crystallography (Wiley, New York, 1943).

22. A. N. Winchell, The Optical Properties of Organic Compounds (Academic Press, New York, 1954).

23. D.W.J. Cruickshank, Acta Cryst., 10, 504 (1957).

24. A. D. Jordan, Ph.D. thesis, University of Sydney, 1970.

25. L. W. Pickett, Proc. Roy. Soc. (London), 142, 333 (1933).

26. G. J. Small, J. Chem. Phys., 52, 656 (1970).

27. G. A. Jeffery, Proc. Roy. Soc., 188A, 222 (1947).

28. D.W.J. Cruickshank, Acta Cryst., 2, 65 (1949).

29. J. Trotter, Acta Cryst., 14, 1135 (1961).

30. G. J. Small, Ph.D. thesis, University of Pennsylvania, 1967.

31. E. Frasson, C. Garbuglio and S. Bezzi, Acta Cryst., 12, 126 (1959).

32. G. J. Small and S. Kusserow, J. Chem. Phys., 60, 1558 (1974).

33. R. G. Parr, D. P. Craig and J. G. Ross, J. Chem. Phys., 18, 1561 (1950).

34. D. S. McClure, J. Chem. Phys., 22, 1668 (1954).

35. G. Herzberg and E. Teller, Z. Physik. Chem., B21, 410 (1933).

36. F. Duschinsky, Acta Physiochim (URSS), 1, 551 (1937).

37. G. J. Small, J. Chem. Phys., 54, 3300 (1971).

38. B. Sharf and B. Hönig, Chem. Phys. Lett., 7, 132 (1970).

39. T. G. Pinter and G. L. Orr, VAMP, A Library of FORTRAN Programs for Solving the Vibrational Secular Equation for the Analysis of Polyatomic Molecules (National Technical Information Service, Springfield, 1973).

40. J. H. Schactschneider, Technical Report No. 231-64, Shell Development Co., Emeryville, California.

41. J. H. Schactschneider, Technical Report No. 57-65, Shell Development Co., Emeryville, California.

42. R. M. Hochstrasser, Molecular Aspects of Symmetry (Benjamin, New York, 1966), p. 327.

43. R. Pariser, J. Chem. Phys., 23, 1997 (1956).

44. F. P. Burke, G. J. Small, J. R. Braun and T-S Lin, Chem. Phys. Lett., 19, 574 (1973).

45. J. R. Braun, T-S Lin, F. P. Burke and G. J. Small, J. Chem. Phys., 59, 3595 (1973).

46. R. D. McAlpine, Ph.D. thesis, University of Pennsylvania, 1968.

47. J. Christie and D. P. Craig, unpublished results.

48. C. Manneback, Physica, 17, 1001 (1951).

49. J. R. Henderson, R. A. Willett, M. Muramoto and D. C. Richardson, Douglas Report SM-45807 (1964).

50. R. H. Dyck and D. S. McClure, J. Chem. Phys., 36, 2326 (1962).

51. S. J. Strickler and R. A. Berg, J. Chem. Phys., 37, 814 (1962).

52. J. B. Birks and D. J. Dyson, Proc. Roy. Soc. A275, 135 (1963).

53. G. J. Small, unpublished results.

54. G. L. Orr and G. J. Small, Chem. Phys. 2, 60 (1973).

55. G. L. Orr and G. J. Small, Chem. Phys. Lett., 21, 395 (1973).

56. R. M. Hochstrasser and Lewis J. Noe, J. Chem. Phys., 48, 514 (1968).

57. R. M. Hochstrasser, Accounts Chem. Res., 6, 263 (1973).

58. J. R. Braun, T-S Lin, F. P. Burke and G. J. Small, J. Chem. Phys., 59, 3595 (1973).

59. R. M. Hochstrasser and L. J. Noe, J. Chem. Phys., 50, 1684 (1969).

60. A. C. Vandenbroucke, R. W. King and J. G. Verkade, Rev. Sci. Instrum., 39, 558 (1968).

61. D. E. McCumber and M. D. Sturge, J. Appl. Phys., 34, 1682 (1963).

62. R. C. Powell, B. DiBartolo, B. Birang and C. S. Naiman, J. Appl. Phys., 38, 5113 (1967).

63. R. C. Powell, J. Appl. Phys., 39, 4517 (1968).

64. D. S. McClure, J. Chem. Phys., 36, 2757 (1962).

65. J. L. Richards and S. A. Rice, J. Chem. Phys., 54, 2014 (1971).

66. M. N. Sapozhnikov, Phys. Status Solidi, 56, 391 (1973).

67. R. M. Hochstrasser and G. J. Small, Chem. Commun., 5, 87 (1968).

68. R. M. Hochstrasser and G. J. Small, J. Chem. Phys., 48, 3612 (1968).

69. A. V. Solov'ov, Vkr. Fiz. Zh., 6, 56 (1961).

70. D. Huppert, J. Jortner and P. M. Rentzepis, J. Chem. Phys., 56, 4826 (1972).

71. R. M. Hochstrasser and T. Y. Li, J. Mol. Spec., 41, 297 (1972).

72. J. P. Byrne, E. F. McCoy and I. G. Ross, Aust. J. Chem., 18, 1589 (1965).

73. G. S. Pawley, Phys. Status Solidi, 20, 347 (1967).

74. P. N. Prasad, R. Kopelman and R. W. Ochs, J. Chem. Phys., 57, 5409 (1972).

75. A. S. Davydov, Quantum Mechanics (NEO Press, Ann Arbor, 1966), p. 254.

ACKNOWLEDGEMENT

A considerable portion of one's destiny is molded by those people with whom he is associated. While one must accept the ultimate responsibility for the realization of his objectives, it is manifestly obvious that they cannot be achieved without the assistance and encouragement of others. In appreciation of this, I extend my sincere gratitude to my colleagues in this research group and most especially to its mentor, Dr. Gerald J. Small, and wish them continued success in their every endeavor.

Finally, I am indebted for technical assistance to Dr. Clayton A. Swenson, Department of Physics, Iowa State University, for calibrating the germanium resistance thermometer used in the electron-phonon coupling experiments, and to Mr. Roger D. Clark for his assistance in performing the Stark experiments.